Two-phase flow properties upscaling in heterogeneous porous media

Jacques Franc

THÈSE

En vue de l'obtention du

DOCTORAT DE L'UNIVERSITÉ DE TOULOUSE

Délivré par :

Institut National Polytechnique de Toulouse (INP Toulouse)

Discipline ou spécialité :

Surfaces Interfaces Continentales Hydrologie

Présentée et soutenue par :

M. JACQUES FRANC

le jeudi 18 janvier 2018

Titre :

Mise à l'échelle des propriétés polyphasiques d'écoulement en milieux poreux hétérogènes

---

Ecole doctorale :

Sciences de l'Univers de l'Environnement et de l'Espace (SDUEE)

Unité de recherche :

Institut de Mécanique des Fluides de Toulouse (I.M.F.T.)

Directeur(s) de Thèse :

M. GERALD DEBENEST

Rapporteurs :

M. BRAHIM AMAZIANE, UNIVERSITE DE PAU ET DES PAYS DE L ADOUR

Mme MARGOT GERRITSEN, STANFORD UNIVERSITY

Membre(s) du jury :

M. SERGE GRATTON, INP TOULOUSE, Président

M. GERALD DEBENEST, INP TOULOUSE, Membre

M. LAURENT JEANNIN, STORENGY, Membre

M. RACHID ABABOU, INP TOULOUSE, Membre

M. ROLAND MASSON, UNIVERSITE DE NICE SOPHIA ANTIPOLIS, Membre

M. XAVIER VASSEUR, ISAE-SUPAERO, Membre

TWO PHASE FLOW PROPERTIES UPSCALING IN HETEROGENEOUS POROUS MEDIA

JACQUES FRANC

A DISSERTATION

PRESENTED TO THE UNIVERSITY

OF TOULOUSE IN CANDIDACY FOR THE DEGREE

OF DOCTOR OF FLUID MECHANICS

ADVISOR: GERALD DEBENEST

JANUARY, 18th 2018

Contexte :

La simulation d'écoulements polyphasiques souterrains est souvent utilisée dans les industries gazières ou pétrolières mais aussi pour l'étude des ressources en eau. Quand on s'attache à comprendre les phénomènes en jeu, les équations à l'échelle locale sont utilisées pour déterminer des tendances macroscopiques : c'est ce que l'on appelle la mise à l'échelle ou upscaling. Ainsi lorsqu'on parle d'écoulements souterrains, les équations de Navier-Stokes *upscalées* deviennent l'équation de Darcy à l'échelle macroscopique (*i.e.* l'échelle de plusieurs pores).

L'échelle de Darcy est toujours assez fine en comparaison de l'échelle mégascopique qui est celle du réservoir. L'échelle de Darcy sera considérée comme l'échelle fine et sera l'échelle de référence pour le second changement d'échelle : de l'échelle de Darcy à celle du réservoir.

Dans cette thèse, un code de simulation multiéchelle basé sur l'implémentation d'une méthode mixte hybride en formulation volumes finis a été développé. Contrairement aux méthodes classiques de changement d'échelle, qui visent à obtenir des lois macroscopiques, les méthodes multiéchelles gardent une trace, à la fois de l'échelle de Darcy et de l'échelle du réservoir. L'échelle fine, *i.e.* ici celle de Darcy, est couplée à l'échelle du réservoir via des deux étapes clés : l'étape d'*upgridding* et l'étape de *downgridding.* Ces deux étapes sont caractéristiques des méthodes multi-échelles. Dans la littérature des méthodes multi-grilles, elles peuvent être rapprochées respectivement des étapes de restriction et de prolongation. La méthode implémentée, la méthode mixte hybride multiéchelle volumes finis (*FV-MHMM),* s'appuie sur un *upgridding* qui repose sur la résolution de problèmes locaux (à l'échelle fine) sur un support réduit. Ce support est déduit de la superposition d'une discrétisation grossière sur la discrétisation fine originelle. Ces solutions forment alors un ensemble de fonctions de bases, incluant donc les phénomènes locaux dus aux hétérogénéités locales à la grande échelle. Ces fonctions de bases sont par la suite utilisées pour former un système global à la grande échelle dans lequel la continuité des flux est assurée par des multiplicateurs de Lagrange. Elles servent aussi à l'interpolation de la solution en pression à la grande échelle pour la petite échelle, formant ainsi l'approximation à la petite échelle de la pression par la méthode multiéchelle. Plusieurs schémas de pondération ont également été développés en

tant qu'étapes préalables à la résolution des problèmes locaux. Ils permettent d'obtenir des fonctions de base qui sont mieux adaptées à l'hétérogénéité sous-jacente et, par conséquent, améliorent la précision de la méthode. Une méthode de raffinement adaptatif basée sur un estimateur *a posteriori* est également présentée.

L'extension aux écoulements diphasiques est faite à l'aide d'un couplage faible séquentiel basé sur l'algorithme *IMplicit Pressure Explicit Saturation (IMPES).* L'équation elliptique en pression est résolue via l'algorithme multiéchelle puis couplée à l'équation hyperbolique en saturation discrétisée sur l'échelle fine. Un critère de mise-à-jour sélectif est aussi utilisé pour éviter la mise à jour des fonctions de base sur tout le domaine y compris dans les zones inactives. Cela permettra de gagner du temps CPU.

Les perspectives de ce travail sont nombreuses pour la meilleure compréhension des écoulements souterrains à la grande échelle. Notamment, la reformulation d'un tel algorithme pour en faire un préconditionneur efficace est en cours.

Context:

The underground multiphase flow simulations are used both in the gas and oil production and in the monitoring of water resources availability for groundwater hydrology studies. When trying to get a better understanding of the phenomenon, the local scale equations are upscaled to get macroscopic trends. In the groundwater hydrology field, the Navier-Stokes model equations are upscaled into the Darcy equations at the macroscopic scale (i.e. the scale of several pores).

The Darcy scale is still fine comparatively to the megascopic scale. However, this Darcy scale will be considered as the fine and reference scale for second upscaling from Darcy to reservoir scale.

In this thesis, a multiscale simulation code based on the implementation of a mixed hybrid multiscale algorithm into a finite volume formulation has been developed. Unlike the usual upscaling methods which aims to derive macroscopic laws, the multiscale algorithm are keeping track of both Darcy and reservoir scale. The fine scale, i.e. here the Darcy scale, is coupled to the reservoir scale through to main steps : the upgridding and the downgridding steps. These two steps are typical features of multiscale algorithm. In the Multigrid literature they correspond respectively to the restriction and prolongation steps. The implemented method, the Finite Volume Mixed Hybrid Multiscale Methods (FV-MHMM), uses an upgridding based on the solution of local (or fine scale) problem which support are decided by partitioning the fine scale by a coarse scale discretization. These solution will form a set of basis functions, which will include local phenomenon from the fine scale heterogeneities to the coarse scale. These basis functions are then used to assemble a global system in which the flux continuity is enforced thanks to Lagrange multipliers unknowns on the coarse scale. They are also used to interpolate the coarse scale pressure solution to the fine scale. Several weighting schemes have been introduced as preprocessing steps to the local problems in order to produce basis functions that better fit the underlying fine scale heterogeneities and, hence, improve the accuracy of the method. A method of adaptive refinement based on an a posteriori estimator have also been developed.

The transposition to the two phase flow model is made through a weakly sequential coupling based on an IMplicit Pressure Explicit Saturation (IMPES) algorithm. The elliptic pressure equation is solved with the multiscale algorithm and coupled with the hyperbolic saturation equation on the fine scale after the downgridding steps. A selective threshold-based criteria is also introduced to avoid updating of the basis functions on the whole domain and to select active area. This will spare CPU time.

The outlook are numerous to better understand the underground flow problem at a large scale. The adaptation of such an algorithm to make it an efficient preconditioner is one of the ongoing work.

Remerciements:

Les travaux décrits dans ce manuscrit ont été effectué et hébergé à l'Institut de Mécanique des Fluides de Toulouse (IMFT) dans le cadre d'une collaboration industrielle avec Storengy et ENGIE EPI. Je voudrais ici remercier les différentes entités ainsi que les personnes avec lesquelles j'ai eu la chance de travailler et d'échanger.

Mes premiers remerciements vont à mes encadrants de thèse : mon directeur de thèse Gérald Debenest ainsi que mon responsable industriel Laurent Jeannin (Storengy), pour leur disponibilité, leur investissement et leur complémentarité. Ils auront su orienter, guider et dynamiser mes travaux. Je remercie Laurent pour son investissement, son implication et ses nombreux conseils au cours des travaux ; un grand merci à Gérald pour sa confiance, ses discussions et pour m'avoir laissé une grande liberté au cours de la thèse. Je tiens également et tout particulièrement à remercier Roland Masson pour son accueil et sa disponibilité ainsi que pour son aide primordiale dans l'élaboration de ces travaux. Je veux aussi à remercier Rachid Ababou pour les discussions passionnées et passionnantes autour du/des changements d'échelles que nous avons eu. Je témoigne aussi ma reconnaissance à Michel Quintard et Patrick Egerman en tant que membres initiateurs du projet. Un merci tout particulier à Alain Bergeon et Franck Plouraboué pour leurs soutiens et conseils notamment dans les dernier instants.

Je remercie également M. Brahim Amaziane et Mme Margot Gerritsen pour avoir accepté de rapporter sur ce manuscrit. J'adresse aussi mes remerciements aux membres de mon jury et plus spécifiquement MM. Serge Gratton et Xavier Vasseur pour l'avoir présidé et en avoir fait partie.

J'aimerais renouveler mes remerciements à Mme. Margot Gerritsen pour m'avoir accueilli, guidée et conseillé au cours de mon échange à Stanford. Mes remerciements vont aussi à M. Matthias Cremon pour m'y avoir présenté et guidé, et M. Nicola Castelletto pour les échanges autour des méthodes multi-échelles. Un merci particulier à M. Cyprien Soulaine pour m'y avoir également reçu, mais aussi pour avoir initié, lors de sa période toulousaine, mes premiers pas au développement sous *OpenFOAM*.

Je salue les thésards et post-doc que j'ai eu l'occasion de côtoyer et avec qui j'ai pu échanger au cours de ces années. Mes remerciements vont également aux anciens thésards passés par GEMP, notamment Mauricio Duenas-Velasco et Paul Sapin pour leur bonne humeur communicative. Je tiens également à remercier Mme Suzy Bernard pour avoir su gérer toutes les inscriptions et démarches avec un enthousiasme inébranlable. J'ai également une pensée toute particulière pour Mme. Maryse André, qui a toujours été d'une grande aide et d'un grand soutien tant dans mes années d'ingénieur que dans mes après-midi de

thésard à l'ENSEEIHT. J'adresse également des remerciements nombreux et appuyés à Jules Dichamp et Pol Kennel pour les multiples pauses café et leurs discussions souvent inspirées et inspirantes.

Enfin, comment ne pas remercier mes deux collègues de bureau, Romain Guibert et Pierre Horgue, pour leurs idées, leurs conseils, leurs méthodes, leurs encouragements et leurs bonne humeur tout au long de la thèse. Un grand merci également à Ruddy Soeparno et Gregory Ehses pour leurs discussions tantôt footballistiques tantôt métaphysiques ainsi que leur grande adresse aux fléchettes. J'ai aussi une pensée particulaire pour Félix Collin-Bastiani malgré sa chance outrancière à monpetitgazon.

Je conclus ces remerciements par ceux adressés à ma famille et à mes amis, pour leur compréhension et leurs encouragements tout au long de ces années d'études : à mes parents, pour leur soutien infaillible et leur pondération aux moments de doute, à Camille et Lalo, pour leur bienveillance et leur aide à chaque fois renouvelées, à Christophe et Baptiste, Marie-Line et Hubert, pour leur support indéfectible et leur refuge stéphanois, à Fabien, Giuliano et Renan, pour leurs amitiés même aux quatre coins du globe. Enfin, le plus grand et l'ultime merci à Lucile, pour m'avoir soutenu, compris et accompagné malgré tous mes états, et pour l'infinité de ses attentions.

A Marinette et Marinette,

Contents

List of Tables

List of Figures

Introduction : écoulements polyphasiques dans les réservoirs, de l'échelle de Darcy à celle du réservoir

Les écoulements dans les réservoirs se retrouvent dans de nombreux domaines, de l'ingénierie pétrolière à la production de gaz en passant par l'étude de la pollution des sols par exemple. Les principales difficultés viennent de l'impossibilité d'observer tous les phénomènes mais aussi de la nature aléatoire du milieu qui rend difficile la conception de modèles physiques. Le phénomène de "coning" est ainsi un véritable problème dans l'extraction de gaz. Il apparaît souvent dans le cas de puits verticaux. Il est relié à l'arrivée d'eau dans les puits. Dès que l'eau apparaît au puits producteur, le puits est envahi et par conséquent, le débit de production de gaz chute radicalement. Pour prédire la survenue du "coning", on utilise la modélisation physique du réservoir mais ceci requiert d'obtenir des informations détaillées sur les propriétés de transport.

Ces propriétés peuvent être définies à plusieurs échelles, mais dans cette étude, nous en retiendrons trois :

- L'échelle du pore, où une description détaillée de l'espace occupé par le vide, le fluide et le solide peut être faite.

- L'échelle de Darcy ou géologique, où les propriétés de transport sont obtenues depuis l'échelle du pore.

- L'échelle du réservoir, où les propriétés de transport sont définies à l'aide d'un changement d'échelle depuis l'échelle de Darcy.

Il est possible de déterminer, en utilisant différentes techniques, des informations détaillées quant aux propriétés de transport à l'échelle géologique. Pour cela, on peut utiliser des données d'études sismographiques, des données de production (gaz, liquide) ou encore l'analyse

d'échantillons de roche du réservoir via la *Digital Rock Physics (DRP)*. Connaissant la perméabilité et la porosité, nous pouvons mieux interpréter le comportement de l'écoulement en le modélisant numériquement. Cependant, le nombre de données déterministes et accessibles est limité. Il est aussi important de savoir que, bien que les propriétés soient connues aux points de mesures, la nature aléatoire et hétérogène du sol implique qu'elles ne sont plus vraies dans le voisinage propre. Selon (Haldorsen et al., 1990), la description d'un réservoir tient à la fois d'observations (déterministes), de savoirs (géologie, sédimentologie) et d'hypothèses probabilistes (la composante stochastique). Les méthodes stochastiques sont principalement utilisées en raison d'un manque de détails dans la capture des propriétés de transport et des observations géologiques. Ces manques engendrent des modèles déterministes lacunaires incapables de décrire avec précision les écoulements. L'approche stochastique peut compléter ces données en générant une suite de modèles synthétiques équivalents qui reproduisent le comportement moyen observé.

Une fois le modèle de réservoir créé, il est utilisé avec les conditions limites associées au scénario étudié, en vue de prédire les écoulements *in situ* tels que ceux du gaz par exemple. En comparant les données de production aux résultats de simulation, on peut enrichir le modèle. L'*history matching* tout comme les problèmes inverses, sont utilisés et permettent de déterminer un meilleur candidat , en améliorant la description des propriétés de transport.

Le domaine doit maintenant être discrétisé pour y appliquer le modèle. Un premier essai pourrait être de le discrétiser à l'échelle géologique (cellule d'environ 1m) mais le nombre de cellules serait trop important pour être la base d'un calcul qui se voudrait efficace numériquement. Le temps nécessaire pour mener à bien les simulations serait si grand qu'il rendrait l'exploration de l'espace des paramètres irréalisable. Pour surmonter ce problème, il nous faut définir un modèle à l'échelle du réservoir. La taille typique des cellules serait alors de la centaine de mètres. Pour se faire, il faut transférer les propriétés de transport de l'échelle géologique à l'échelle du réservoir. C'est ce que l'on entend par *upscaling*. Grâce à différentes techniques, on peut déduire des propriétés équivalentes à l'échelle du réservoir en partant de celles utilisées à l'échelle géologique. L'*upscaling* regroupe alors plusieurs cellules de l'échelle géologique pour donner une valeur à la cellule grossière qu'elles constituent une fois réunies.

Cependant, en diminuant le nombre des cellules, le niveau d'erreur (mesuré en termes de données de production par exemple) s'en trouve augmenté. Il est aussi important de noter que le changement de discrétisation va engendrer une augmentation de la diffusion numérique (Sablok and Aziz, 2008).

Dans le cas monophasique, le problème d'*upscaling* est largement documenté. La question est alors : peut-on utiliser les méthodes monophasiques pour évaluer un écoulement dipha-

sique ? Comme le système d'équations est éloigné avec un couplage entre les équations de pression et de saturation, la tâche semble complexe voire impossible. D'autre part, traiter les hétérogénéités est également difficile car leur longueurs de corrélation définissent la taille du volume sur lequel l'*upscaling* doit être pratiqué. Les non-linéarités présentes dans le système d'équations (pression capillaire, perméabilités relatives) sont une difficulté de plus. Des hypothèses devront être faites pour rendre possible la résolution des problèmes de fermetures associés et réduisent alors la portée des résultats obtenus.

Ces travaux n'ont pas pour objectif d'étudier les méthodes d'*upscaling* physique ou les méthodes d'*upscaling* numérique. Ils concernent le développement d'une nouvelle approche multiéchelle qui construit un système à l'échelle macroscopique tout en gardant la trace de l'échelle géologique. L'échelle fine, *i.e.* ici l'échelle géologique, est couplée à l'échelle du réservoir à travers deux étapes clés : l'étape d'*upgridding* et l'étape de *downgridding.* Ces deux étapes sont caractéristiques des méthodes multiéchelles. La méthode implémentée, la méthode mixte hybride multiéchelle volumes finis (*FV-MHMM),* s'appuie sur un *upgridding* qui repose sur la résolution de problèmes locaux (à l'échelle fine) sur un support réduit. Ce support est déduit de la superposition d'une discrétisation grossière (à l'échelle du réservoir) sur la discrétisation fine originelle. Le *downgridding* utilise ensuite ces mêmes fonctions de bases pour prolonger la solution obtenue sur la discrétisation grossière vers la discrétisation fine. La construction de telles fonctions de bases permet d'incorporer plus de détails de l'hétérogénéité de l'échelle fine dans les opérations réalisées à l'échelle grossière.

Le chapitre 1 présente une revue de la littérature des méthodes d'*upscaling* physiques et numériques utilisées pour traiter les problèmes multiéchelles en ingénierie réservoir. Une attention particulière a été portée aux méthodes multiéchelles en formulation volumes finis.

Les chapitres 2 et 3 se concentrent sur les outils à l'échelle géologique. Le chapitre 2 développe une librairie en libre accès pour traiter les écoulements polyphasiques en milieux poreux. Elle est basée sur un couplage séquentiel des équations de pression/saturation, utilisant un algorithme *IMplicit Pressure Explicit Saturation (IMPES),* tout en profitant de la nature parallèle de la plateforme OpenFOAM. Il est alors possible d'envisager de traiter de grands domaines. Cependant, la stabilité de ce type de couplage est en question et doit être étudié. Le chapitre 3 s'attarde donc sur l'étude de trois critères de stabilité pour un tel algorithme en fonction des régimes d'écoulement envisagés (à dominante visqueuse, capillaire ou gravitaire). Le critère garantissant une simulation stable mais rapide est recherché.

Le chapitre 4 présente la méthode *FV-MHMM.* Après avoir évoqué la construction des systèmes d'équations à résoudre, on en vient rapidement à l'étude de convergence de cette méthode sur des cas tests particuliers. Même si elle s'avère efficace, dès que le milieu devient fortement hétérogène avec des variations de la longueur de corrélation des structures,

il est décidé d'adapter la méthode native. Plusieurs schémas de pondération sont alors introduits, agissant comme une adaptation préalable à la résolution des problèmes locaux dans l'optique de construire des fonctions de bases qui soient les plus cohérentes possibles avec l'hétérogénéité sous-jacente. Cela améliore grandement la précision de la méthode.

Le chapitre 5 compare à la *FV-MHMM* à deux autres méthodes multiéchelles volumes finis, *i.e.* la *Multiscale Finite Volume Method* (*MsFv*) et la *Multiscale Restriction Smoothed Basis Method* (*MsRSB*). En étudiant les résultats sur les coupes du cas SPE 10, leurs performances sont comparées.

Le chapitre 6 introduit un estimateur *a posteriori* à la base d'un processus de raffinement adaptatif des faces grossières. En effet, sa valeur nous renseigne sur la qualité de la solution approximée par la méthode multiéchelle aux faces grossières et donc sur le besoin d'un raffinement de la face ou non.

Enfin, une conclusion termine ce manuscrit permettant de donner aussi quelques perspectives à ce travail de thèse.

Haldorsen, H. H., Damsleth, E. et al. : 1990, Stochastic modeling (includes associated papers 21255 and 21299), *Journal of Petroleum Technology* **42**(04), 404–412.

Sablok, R. and Aziz, K. : 2008, Upscaling and discretization errors in reservoir simulation, *Petroleum Science and Technology* **26**(10-11), 1161–1186.

Introduction : multiphase flow in reservoirs, from Darcy to reservoir scale

Fluid flow in reservoirs concern many applications, from petroleum engineering togas production including pollution investigations for instance. The main difficulties come from the inability to observe all the phenomena but also to deal with the random nature of the medium which makes difficult to represent an accurate description of the physical models. The so-called "coning phenomenon" is a real problem in gas extraction, as it is related to the water breakthrough of water in wells. When the water appears at the producer well, the well is invaded and consequently, the production rate of gases decreases drastically. To overcome this issue, one can use reservoir modeling to predict this, but it will require information about the transport properties.

The transport properties could be defined at several relevant scales, but in this study, we will consider three of them :

- The pore scale, where a detailed image of void space, fluid and solid phases can be defined,
- The Darcy scale or geological scale, where transport properties determined on the pore scale,
- The reservoir scale, where the transport properties are defined using an upscaling procedure of the Darcy scale.

It is possible to determine, using several techniques, detailed information on the geological scale transport properties. One can use seismic data, well production or core samples analysis using Digital Rock Physics (DRP). Knowing permeability and porosity will lead to better understanding of the fluid flow behavior, using numerical modeling. However, the number of fixed and deterministic data is reduced. It is also important to notice that, even though the properties are known thanks to measurements in zones, the random nature of the geological physics makes the observations not relevant in the surrounding area. According to (Haldorsen et al., 1990), the reservoir description is a combination

of observations (deterministic), educated aiming (geology, sedimentology) and formalized guessing (the stochastic component). The stochastic methods are used mainly because of a lack of detail in the description of transport properties and geological observations. This incompleteness generates a poor deterministic model unable to describe with accuracy the flow paths. Stochastic approach could complement this, as it will generate a synthetic model, able to reproduce the average behavior observed.

Once this reservoir model generated, it is normally used with accurate boundary conditions, in order to predict the production of gases. Comparing production data, to the simulated one will allow to enhance the model used. History matching techniques such as inverse problem, are used and will lead to the choice of a best match in terms of transport properties used within the fluid flow model.

This numerical model will need discretization procedure of the whole domain. As a first step and on the geological scale, the number of cells will be large, as the cell dimensions are normally small (˜1 meter) compared to the whole reservoir size. The time spent on the calculations will then be large, and an exploration of the parameters (Boundary conditions, geology, ...) will be difficult to handle. To overcome this issue, we will try to define a new model at the reservoir scale. The typical length of the cells will be around 100 meters. To do so, we need to transfer the transport properties, from the fine geological scale to the reservoir scale. This is called the *upscaling* procedure. Thanks to different techniques, we can determine the cell properties at the reservoir scale thanks to fine scale properties. The upscaling will be done on several fine scale cells, determining the property of one larger cell at the reservoir scale. This will be an average behavior of the geological scale.

However, by decreasing the number of cells, we can increase the error level (measured in terms of production date for instance). This might be taken with care and the upscaling step is crucial in the definitions of large scale properties. Moreover, it is important to point out that changing the discretization by increasing the cell size will generate errors in terms of numerical dispersion (Sablok and Aziz, 2008).

In the single phase flow problem, the upscaling problem is fairly well understood. The question arising could be rephrased as: can we use a single phase flow upscaling to determine the multiphase flow behavior? As the system of equations is quite different with a strong coupling between pressure and saturations, this might be difficult to transpose directly the single phase flow knowledge. Also, dealing with heterogeneities and their correlation lengths can also be challenging as it will define the size of an elementary volume supporting the upscaling procedure. The non-linearities present in the system of equations (capillary pressure or relative permeability) are not easy to tackle. Some simplifications are then assumed to make the associated closure problems possible to solve, but it is really specific

to the method as the aim is to aggregate fine cells into larger ones, and then reproduce with accuracy the average behavior while crossing the scales.

This work aims to investigate neither the physical technique of upscaling nor the classical numerical upscaling but a new multiscale approach able to derive a macroscopic system of equations by keeping track of the geological and reservoir scales. The fine scale, *i.e.* here the geological scale, is coupled to the reservoir scale through to main steps : the *upgridding* and *downgridding* steps. These two steps are typical features of the multiscale algorithms. The implemented method, the Finite Volume Mixed Hybrid Multiscale Methods (*FV-MHMM*), uses an upgridding based on the solution of local (or fine scale) problem which support are decided by partitioning the fine scale by a coarse scale discretization. The *downgridding* step then uses this same basis function to prolong the coarse scale solution on the fine discretization. This basis function construction allows to include local phenomenon from the fine scale heterogeneities to the coarse scale.

The chapter 1 will present the literature analysis on different physical and numerical techniques used to treat the multiscale problem in reservoir engineering. A special focus will be done on current finite volume multiscale techniques.

The chapter 2 will focus on the geological scale, and the models developed using an open source toolbox. Based on an IMplicit Pressure Explicit Saturation (IMPES) algorithm, we take advantage of the parallel nature of the code, and then, it is possible to deal with large numerical systems. However,

the numerical stability of this sequential method implies strong limitations on the time step size, which may depend on the flow regime studied. Three stability criteria related to the IMPES method, that differ in their construction, are investigated. Their limitations and effects are studied in Chapter 3 in order to find the optimal one in the case of capillary, viscous or gravity dominated regimes.

The chapter 4 will introduce the *FV-MHMM*. After deriving the model equations of the algorithm, its convergence behavior is studied on simple test cases. Although it appears efficient in most of the configurations, when the permeability appears to be strongly heterogeneous with a varying correlation length of the heterogeneous features, the algorithm requires an adaptation. Several weighting schemes have been introduced as preprocessing steps to the local problems in order to produce basis functions that better fit the underlying fine scale heterogeneities and, hence, improve the accuracy of the method.

The chapter 5 will consider three of the main different multiscale finite volume methods, *i.e.* Multiscale Finite Volume Method (*MsFv*), Multiscale Restriction Smoothed Basis Method (*MsRSB*) and *FV-MHMM*. Based on 2D layers of the 10th SPE test case, we will cross compare the performance of each one.

The chapter 6 will consider an adaptation of the *FV-MHMM*. Two phase flow simulations are time consuming and will require understanding if a local refinement process could lead to a better description of the two phase flow. In this chapter, an *a posteriori* estimator method is developed and used to determine if adding degrees of freedom is necessary or not.

Finally, a conclusion part will follow. This will give rise to possible perspectives and new developments based on the *FV-MHMM*.

Haldorsen, H. H., Damsleth, E. et al.: 1990, Stochastic modeling (includes associated papers 21255 and 21299), *Journal of Petroleum Technology* **42**(04), 404–412.

Sablok, R. and Aziz, K.: 2008, Upscaling and discretization errors in reservoir simulation, *Petroleum Science and Technology* **26**(10-11), 1161–1186.

Chapter 1

Introduction : towards multiphase flow upscaling

Contents

Résumé en français :

Ce chapitre introductif concerne l'état de l'art en matière de changement d'échelle. Par la suite, le terme upscaling, signifiant mise à l'échelle des propriétés, sera aussi utilisé.

Il se décompose en deux parties, tout d'abord et historiquement plus anciens, les travaux sur l'upscaling monophasique (aussi dit saturé) sont abordés. Ensuite les méthodes adaptées ou étendues au modèle multiphasique sont évoquées avant de s'attarder sur le cas particulier des méthodes multi-échelle en formulation volumes finis. Cela constitue le cœur de cette étude et l'on reverra ce point plus en détail par la suite.

Pour aboutir à la modélisation à l'échelle d'un réservoir, un premier changement d'échelle est nécessaire : de l'échelle microscopique où l'écoulement du fluide autour d'une phase solide est modélisé par les équations de *Navier Stokes*. On s'attache à obtenir un comportement reliant débit et perte de charge : c'est la loi de *Darcy*. A l'échelle géologique, aussi dite de *Darcy*, on donc voit l'émergence de grandeurs moyennées telles que la porosité ou perméabilité qui traduisent la présence, à l'échelle locale, d'un solide qui affecte l'écoulement. Ce premier changement d'échelle a été fortement documenté dans la littérature.

Cependant, notre objectif porte plutôt sur un second changement d'échelle, c'est-à-dire celui de l'échelle géologique à celle du réservoir. Nous accepterons donc la loi de Darcy comme exacte et essaierons de construire des lois à l'échelle du réservoir capables de retranscrire ces comportements. Les premiers travaux ont porté sur le calcul de bornes à la valeur homogénéisée de la perméabilité dans le cas de distributions bi-modales de ses valeurs. Par la suite, la distinction entre méthodes déterministes et méthodes stochastiques d'upscaling est faite :

• les méthodes déterministes s'attachent à résoudre un problème sur un support connu et à interpréter les résultats en termes de comportement moyen. C'est le cas des méthodes de prise de moyenne, d'homogénéisation mais aussi des méthodes dites de "streamlines", des méthodes d'agrégation et de la théorie du milieu effectif, pour ne citer qu'une partie d'entre elles.

• Les méthodes stochastiques utilisent la statistique des champs de porosité et de perméabilité, afin de déterminer un modèle macroscopique permettant d'obtenir un comportement moyen satisfaisant.

Le passage au cas multiphasique, nécessite la définition de différents régimes d'écoulement traduisant l'action de la différence de viscosité, la présence et la nature des hétérogénéités. Le développement des méthodes se scinde alors en deux approches :

• D'une part, les approches physiques où l'on étudie l'inclusion et le dimensionnement de nouveaux termes permettant de traduire l'action des phénomènes de la petite échelle vers la

grande échelle. C'est notamment le cas des méthodes asymptotiques ou d'homogénéisation ainsi que celui de la prise de moyenne volumique.

• D'autre part, les approches numériques où l'on essaie par des simulations locales et simples d'en déduire des valeurs équivalentes par blocs à la plus grande échelle. On retrouve ces notions dans les nombreuses méthodes à Laplacien ainsi que dans le calcul des pseudo-fonctions. La renormalisation étendue aux écoulements à plusieurs phases s'y rattache également.

Enfin les méthodes multiéchelle permettent de conserver un couplage dynamique entre l'échelle géologique et l'échelle du réservoir. En effet, à l'image des méthodes numériques, elles simulent localement l'écoulement à l'échelle de *Darcy*. Cependant, plutôt que de construire des grandeurs équivalentes sur une gamme de paramètres, elles définissent leurs grandeurs équivalentes en conservant la petite échelle, traduisent à la petite échelle, l'effet de ses grandeurs équivalentes et les corrigent au besoin. Cette partie développe plus spécifiquement les méthodes volumes finis de cette famille (*MsFv*, *MsRSB*) auxquelles on peut ajouter la *Dual Mesh Method* même si elle n'est pas historiquement identifiée en tant que telle. On y trouvera également une présentation de la méthode *FV-MHMM* développée au cours de cette thèse.

This bibliographic synthesis browses the physics of upscaling in porous media and review as much dedicated methods as possible. If similar works for saturated flow are in widespread use and well documented, this is not the case for multiphase flow. Multiphase flow models adds indeed non-linearities to the heterogeneous distribution of permeabilities. The BROOKS and COREY or VAN GENUCHTEN models for relative permeabilities and capillary pressure are examples of such non-linearities. Upscaling such models is still an open question and is both physically (how to model non-linearities, how to solve this coupled non-linear system) and numerically challenging (how to speed up simulation and run it on a daily basis).

Underground flows define three main scales: the microscopic scale, which measures the pore throats and grains which are constituents of the porous medium, the DARCY scale, which measures the rock core plug which is extracted and analyzed in the laboratory and the reservoir scale, which measure moderated subdivision of the reservoir scale which can be handle by a computer running simulations.

The study focuses on upscaling which can be defined from the DARCY scale (hereafter referred to as local scale) to the reservoir scale (hereafter referred to as coarse scale). This second upscaling has to construct coarse scale equivalent properties from local scale petrophysical properties. It should be done without loss in accuracy as it is based on spatialized local scale properties. Before defining the DARCY scale hypothesis, it is worth mentioning that some recent works (Guibert, Horgue, Debenest and Quintard, 2015) adopt an integrated workflow for a two-step upscaling that then goes from microscopic to reservoir scale.

When dealing with a porous medium at the DARCY scale, the flow is described by averaging equations. Each element of volume consists in a two phase distribution of void invaded by fluid V_{void} and solid V_{solid}. This defines porosity ratio ϵ:

$$\epsilon = \frac{V_{void}}{V_{solid}} \tag{1.1}$$

An other similar definition is used when dealing with multiphase flow to define the saturation S_{α_i} of the phase α_i as the ratio between this phase's volume V_{α_i} and the sum of the constituents $\mathcal{E}(\alpha) = \{\alpha_1, \alpha_2, .., \alpha_n\}$,

$$S_{\alpha_i} = \frac{V_{\alpha_i}}{\sum\limits_{\alpha_j \in \mathcal{E}(\alpha)} V_{\alpha_j}}, \quad S_{\alpha_i} \in [0, 1] \tag{1.2}$$

For the two-phase flow model description, let us introduce a wetting phase denoted by w index and a non wetting phase denoted by n index. The mass conservation implies for a immiscible two-phase model that,

$$S_w + S_n = 1 \tag{1.3}$$

Assuming an incompressible, immiscible, two-phase flow, the mass conservation equation leads to:

$$\epsilon \frac{\partial S_{\alpha_i}}{\partial t} + \nabla \cdot (\mathbf{u}_{\alpha_\mathbf{i}}) = q_{\alpha_i} \quad \alpha_i \in \{w, n\}$$

introducing $\mathbf{u}_{\alpha_\mathbf{i}}$ as the superficial velocity and q_{α_i}as the source term associated with α_i phase, modeling injection or destruction of this phase.

In the generalized Darcy law (Muskat, 1949), the superficial velocities is derived to be ,

$$\mathbf{u}_{\alpha_\mathbf{i}} = -\boldsymbol{\lambda}_{\alpha_i}(\nabla p - \rho_{\alpha_i}\mathbf{g}) \tag{1.4}$$

where $\boldsymbol{\lambda}_{\alpha_i}$is the general mobility tensor, which for single phase flow is simply the element-wise ratio between the permeability tensor (which reduces to a scalar in isotropic medium) and the phase dynamic viscosity μ_{α_i}. For the two-phase flow of interest, this mobility includes the phase relative permeability $k_{r_{\alpha_i}}(S_{\alpha_i})$, which accounts for phase competition and friction in the throats, as relaxing prefactor, hence :

$$\boldsymbol{\lambda}_{\alpha_i} = \frac{\mathbf{K}}{\mu_{\alpha_i}} k_{r_{\alpha_i}}(S_{\alpha_i}). \tag{1.5}$$

Let us introduce here transmissivitty T_{α_i}, which is defined from mobility as :

$$\Phi_{\alpha_i} = T_{\alpha_i} \Delta p,$$
$$T_{\alpha_i} = \frac{\boldsymbol{\lambda}_{\alpha_i} A}{\delta x}.$$

The transmissivity is then defined as the product of the mobility by the crossed section area$\lambda_{\alpha_\mathbf{i}} A$ over a a short distance $\delta \boldsymbol{x}$.

The most used models for relative permeability have been introduced by Brooks and Corey (Brooks and Corey, 1964) and Van Genuchten (Van Genuchten, 1980). They both define a set of relative permeabilities and capillary pressures that are formulated to depend on one chosen phase's saturation S_{α_i}. For the two phase flow, the wetting saturation $S_w$is chosen.

The capillary pressure p_c are defined as the pressure difference between two phase pressure p_{α_i}, *e.g.* for two phase flow between p_n and p_w. At the Darcy scale, capillary pressure is

modeled as a function of reference saturation (Leverett, 1940). Hence, for two-phase flow :

$$p_c(S_w) = p_n - p_w$$

The capillary pressure values are dependent on the flow pattern and of the medium considered. These calibration factors are generally obtained thanks to experimentation on core plugs. Such a model gives us a closure equation for the multiphase system, which for a two-phase case then reads :

$$-\varepsilon\frac{\partial S_w}{\partial t} + \nabla\cdot\left(-\frac{\mathbf{K}k_{rn}\left(S_n\right)}{\mu_n}\left(\boldsymbol{\nabla}p_n - \rho_n\mathbf{g}\right)\right) = q_n \tag{1.6}$$

$$\varepsilon\frac{\partial S_w}{\partial t} + \nabla\cdot\left(-\frac{\mathbf{K}k_{rw}\left(S_w\right)}{\mu_w}\left(\boldsymbol{\nabla}p_n - \rho_w\mathbf{g} - \boldsymbol{\nabla}p_c(S_w)\right)\right) = q_w \tag{1.7}$$

Then summing Eq.1.6 and Eq.1.7 gives total conservation equation,

$$-\boldsymbol{\nabla}\cdot\left(\boldsymbol{\lambda_t}\boldsymbol{\nabla}p_n - (\boldsymbol{\lambda_w}\rho_w + \boldsymbol{\lambda_n}\rho_n)\mathbf{g} - \boldsymbol{\lambda_w}\boldsymbol{\nabla}p_c(S_w)\right) = q_w + q_n \tag{1.8}$$

with $\boldsymbol{\lambda_t} = \boldsymbol{\lambda_w} + \boldsymbol{\lambda_n}$ solved for the pair of unknowns (p_n, S_w).

Considering this model as the DARCY scale (or local scale) description of the flow, what will be its upscaled version ? The main challenge comes from the *non-linearities* that comes with the relative permeabilities and capillary pressure models. While the front is advancing, the local properties for transport are changing depending on the phase saturation. The feedback effects of these changes are included in the transport equations Eq.1.6 and Eq.1.7, which decides on saturation distribution. The solution to this *coupled* system of equation is then complex, as the main idea to gain convergence rate will be to use intensively refined grid in saturation front areas and high order scheme that will slow the simulations. This will make routinely use of simulations and stochastic workflows impossible with nowadays computers. The upscaling process is a mean to overcome this lock.

In the first part of this synthesis, the direct approach will be presented, explicitly derived coarse scale properties from fine scale's one. This includes the numerical methods which consist in gathering, grouping or agglomerating computational cells to lower the related CPU-cost. The equivalent properties are then obtained under the constraint of producing the same average values. This does not allow us to link them to intrinsic properties as they are depending on boundary conditions that are used in their calculation and on the sets of selected cells when dealing with locally adapted meshes.

This will be introduced by a quick review of the upscaling method for the saturated medium case as they have been the starting point for the multiphase flow upscaling methods. The second section will developed the proper multiphase flow technics. The last section is focused on an alternative: the multiscale methods which couple local and upscaled scale numerically.

1.1 Upscaling for saturated heterogeneous porous media

First of all, we try to determine the effective properties in the case of saturated flow in heterogeneous porous media. This part is based on the review (Renard and De Marsily, 1997). The main results are reminded. For further details, reader can refer to this reference.

When dealing with effective properties definition, two main approaches are available :

- Either solve the upscaling problem for a large enough number of different initial and boundary conditions, then derived an average flow behavior. This is the method chosen by *pseudo functions* methods. This introduces obvious sampling bias.
- Or make additional assumptions on the reservoir nature (periodicity, infinite medium) and on the initial and boundary conditions. This restrict theoretically the area of validity of the derived laws.

This last approach is the starting point of all analytically and theoretical upscaling methods; *e.g.* two-scale homogenization, asymptotic expansion, large scale volume averaging and perturbative stochastic methods (cf. (Fadili, 2001)).

In a first part, the usually used methods for upscaling heterogeneous saturated porous method are reviewed. This kind of methods are later used in two-phase flow upscaling considering a fixed saturation distribution.

1.1.1 Saturated flow

The steady state saturated flow case is described by DARCY equation(Henry, 1856). This is consistent with Eq.1.7 with $S_w = 1$ and $p_c = 0$. Giving up the phase index in the notations, this leads to:

$$\mathbf{u} = \frac{-\mathbf{K}(\mathbf{x})}{\mu}\boldsymbol{\nabla}[p + \rho\mathbf{g}\mathbf{z}] \tag{1.9}$$

In this equation, $\mathbf{K}(\mathbf{x})$ is of order 2, which varies in space. Considering an incompressible flow, the continuity equation can be written as:

$$\boldsymbol{\nabla} \cdot \mathbf{u} = 0 \tag{1.10}$$

Replacing Eq.1.9 in Eq.1.10 leads us to an *elliptic diffusion equation :*

$$\boldsymbol{\nabla} \cdot \left(\frac{-\mathbf{K}(\mathbf{x})}{\mu} \boldsymbol{\nabla} [p + \rho \mathbf{g} \mathbf{z}] \right) = 0 \tag{1.11}$$

The upscaling process defines a macroscopic law, which describes mean flux variations with respect to a mean pressure gradient variations. A key step is then to define an equivalent permeability (or homogenized, or effective depending on the methods used), which reproduces the best the correlation between the mean flux and the averaged pressure gradient.

Using the *equivalent* permeability is to derive a constant permeability tensor $\mathbf{K}$, whose reproduces the same average flow properties as the heterogeneous medium it replaces. A strict equivalence between local and upscaled medium is impossible, though some criteria can be scoped to defined *equivalence*:

- *Flow equivalent:* At the domain boundary, the flow should be the same as for the locally heterogeneous medium(Cardwell Jr et al., 1945).

- *Energy criteria:* The viscous energy dissipated should be the same in the upscaled and heterogeneous medium(Matheron, 1967). This energy E is defined as :

$$E = -\boldsymbol{\nabla} \left(\frac{p}{\rho ||\mathbf{g}||} \right) \cdot \mathbf{u} \tag{1.12}$$

This is important to notice that these two criteria are strictly identical in the case of periodic boundary conditions. They are the physically bound , even if for different boundary conditions, the theoretical equivalence proof is still an open question.(cf. (Bøe, 1994))

Using the *effective* permeability, one can define is an intrinsic properties of the considered medium, independent of the boundary value problem. In the review (Renard and De Marsily, 1997), this properties is extensively defined. The methods to determine it are sort into two main branches:

- *Stochastic methods,* as in (Matheron, 1967)

- *Homogenized equations methods,* as in (Quintard and Whitaker, 1994)

The resulting tensor for the effective permeability is a symmetric, positive-definite second order tensor. In most of the case, it is hard to derive this tensor as the required conditions

are strict regarding the scale at which they can be verified. Then a weaker versions of these methods construct *upscaled* permeability or *block* permeability.

Recently, (Guibert, Horgue, Debenest and Quintard, 2015) tests several methods to derived the *effective* permeability in an infinite medium. An optimization method with the equivalent medium approach allows to find a symmetric, positive-definite tensor as much independent from boundary condition as possible. Due to computational limitations, this methods can nowadays still not be apply to full 3D model. Nonetheless, the authors don't prove the equivalence between the derived tensor and the *effective* permeability.

In the following part, we will refer to *equivalent* permeability, without any mention to *effective* permeability. The reader has to keep in mind that it then depend on the boundary condition used in its derivation.

1.1.2 Literature results

Methods ranging from different bounds definition to the physical upscaling methods including analytic and theoretical methods are described in what follows. For further details, readers can refer to (Renard and De Marsily, 1997; Kruel Romeu, 1994).

Bounds to permeability values

From Wiener bounds to Carwell and Parsons bounds For 1D flow case, Wiener proved that homogenized permeability for saturated medium , is bounded by its harmonic mean, $\mu_H(K)$, and its arithmetical mean, $\mu_A(K)$. The former case is reached when dealing with flow orthogonally directed with respect to the layers. The last case is reached then the flow is directed along the layers.

$$\mu_H(K) < K_{eff} < \mu_A(K) \tag{1.13}$$

This inequality also referred to as fundamental inequality, is always valid.

(Cardwell Jr et al., 1945) generalized this result to multidimensional flow, deriving an inequality that uses a combination of Wiener bounds (cf. Fig.1.1)

A review of the computational steps can be found in (Fadili, 2001).

Other bounds for isotropic media For isotropic bi-modal medium, some inequalities that bound *equivalent* permeability can be found in (Matheron, 1968; Hashin and Shtrikman, 1963). These bi-modal medium are composed of $f_1$part of permeability K_1 and f_2 part of permeability K_2. Depending on the partition factors (f_1, f_2), three cases give three inequality:

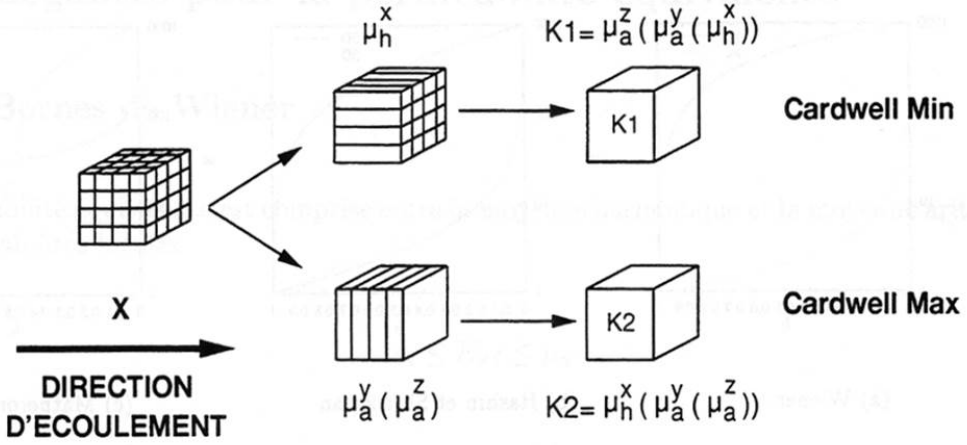

Figure 1.1: Carwell and Parsons' bounds (Cardwell Jr et al., 1945)

$$\begin{cases} f_1 > 0.5 & \Rightarrow K_{eff} \geq K_{ac}, K_{eff} \leq K_m \\ f_1 < 0.5 & \Rightarrow K_{eff} \leq K_{ac}, K_{eff} \geq K_m \\ f_1 = 0.5 & \Rightarrow K_{eff} = \sqrt{k_1 k_2} \end{cases} \tag{1.14}$$

with:

$$K_{ac} = \frac{1}{2}\left[(f_2 - f_1)(k_2 - k_1) + \sqrt{(f_2 - f_1)^2(k_2 - k_1)^2 + 4k_2k_1}\right]$$

and,

$$K_m(f_1 \geq 0.5) = \frac{f_2k_2k_1 + f_1\mu_a\sqrt{k_1(2\mu_a - k_1)}}{f_2m^* + f_1\sqrt{k_1(2\mu_a - k_1)}}$$

$$K_m(f_1 \leq 0.5) = k_1k_2\frac{f_1\mu_a + f_2\sqrt{k_2(2m^* - k_2)}}{f_1k_1k_2 + f_2m^*\sqrt{k_2(2m^* - k_2)}}$$

using the following definitions:

$$m^* = f_2k_1 + f_1k_2$$

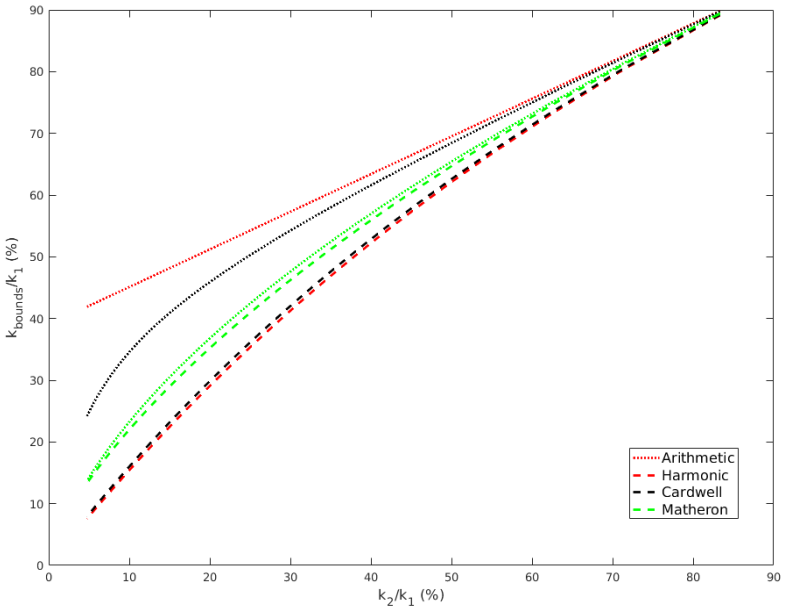

Figure 1.2: Illustration of effective permeability bounds on simple 2D bi-modal distribution with $f_1 = 0.39$

$$\mu_a = f_1 k_1 + f_2 k_2$$

Using sphere composed theoretical medium, in which inner shell permeability is denoted K_{in} and outer shell permeability is denoted K_{out}. According to (Hashin and Shtrikman, 1963), the *efficient* permeability is then bounded as:

$$\mu_a - \frac{f_1 f_2 (k_2 - k_1)^2}{(D - f_1)k_1 + f_1 k_2} \leq K_{eff} \leq \mu_a - \frac{f_1 f_2 (k_2 - k_1)^2}{(D - f_2)k_2 + f_2 k_1} \tag{1.15}$$

with D the number of dimension.

When comparing bounds, as remind in (Renard and De Marsily, 1997), Eq.1.13 and Eq.1.15 are almost identical. The bounds from Eq.1.14 define a narrower range (cf. Fig. 1.2). Nonetheless, these bounds systems are very similar to each other. In reservoir engineering, they provide fast estimates of the *equivalent* permeability knowing locally the detailed map of heterogeneous permeability values.

Other bounds including anisotropic effect (Ababou, 1996) or power laws of the mean values (Journel et al., 1986) have also been derived to extend validity scope of the above mentioned laws.

Deterministic methods

Solution to diffusion equation

Analytic solution In the steady sate flow configuration, DARCY equation Eq.1.9 can be solved analytically. In the case of flow in layered medium, it can be verified that arithmetic mean K_A if the *effective* permeability while the harmonic mean K_H is the value when flow is orthogonal to layers. Let us consider a bi-modal permeability distribution of tensor $\mathbf{K}_0$ and $\mathbf{K}_1$ respectively of fraction f_0 and f_1. It is then found (Quintard and Whitaker, 1987) that:

$$\mathbf{K}_{eff,x} = f_0\mathbf{K}_0 + f_1\mathbf{K}_1 + \frac{f_0 f_1 (\mathbf{K}_0 - \mathbf{K}_1).\begin{pmatrix} 1 & 0 \\ 0 & 0 \end{pmatrix}.(\mathbf{K}_1 - \mathbf{K}_0)}{\begin{pmatrix} 1 \\ 0 \end{pmatrix}.(f_0\mathbf{K}_0 + f_1\mathbf{K}_1).\begin{pmatrix} 1 \\ 0 \end{pmatrix}} \tag{1.16}$$

Numerical solution In more complex cases, the solution cannot be analytically derived anymore and requires numerical approximation of Eq.1.9. According to (Renard and De Marsily, 1997), the methods can be split according to their local to global level.In the local methods, a difference can be made according to the type of boundary conditions:

- *permeameter conditions*, which gives directional permeability value. This is inferred from the lab experiments. Numerically, a head loss is applied along a direction while the others are considered as walls. Then the direction is switched. It provides us with diagonally dominant permeability tensor.

- *periodic conditions,* which ensures symmetry of the found *effective* permeability tensor, moreover, it will respect equivalence criteria.

Other types of boundary conditions are used, but they do not guarantee the symmetry of the permeability tensor (see (Guibert, Horgue, Debenest and Quintard, 2015)). The generic use on real media without any intrinsic periodicity has to be discussed. The method and the type of boundary condition are sensible parameters of the value of the upscaled tensor, as it can even be shown on homogeneous media.

The non-local methods are also used(White et al., 1987). It consists in simulating over the local domain but also on the global domain with different boundary conditions. It constructs then small scale velocities by averaging global velocities with respect to the area crossed at the local domain boundaries. From it, and using identification, an upscaled tensor can be inferred block by block, which may not be symmetric.

Later works starting from this method have tried to restrain the *global* area to the more or less expanded neighborhood of the local area to upscale (see (Gomez-Hernandez and Journel, 1990; Holden and Lia, 1992)). This allows to reduce the computational cost of this upscaled tensor.

Percolation theory results The percolation theory has first been used in (Guyon et al., 1984) and extended by (Berkowitz and Balberg, 1993) to the concept of porous media.

The percolation is the study of flow around impermeable media. If the volume fraction of impermeable media is too high, the liquid flowing will not reach the other end of the medium. This transition is called *percolation transition* and defined a *percolation threshold,* n_c. Considering n as the fraction of impermeable elements, in the narrow of percolation threshold, it can be derived :

$$\begin{cases} n < n_c, & K_{eff} = 0 \\ n > n_c & K_{eff} = A(n - n_c)^{\mu} \end{cases} \tag{1.17}$$

with μ which depends on number of spatial dimension used. A and n_c depends on the poral geometry.

Effective medium theory We can find this theory under several names, but the methodology remains the same for all the studies reported hereafter.

The main idea is to replace the heterogeneous media, composed with blocks of constant permeability values, by a unique block of permeability K_{EMT} in a surrounding media with an unknown permeability value. Then, the boundary conditions are far from the effective medium. So, it is possible to assume that the variations of charge and velocity will not influence the conditions around the block on which the upscaling process is performed.

For instance, (Dagan, 1979) has determined an exact expression of the effective permeability. This result has been generalized by (Dagan, 1982) and (Poley, 1988) for ellipsoids. The determined permeability is then a tensor. More recently, (Guibert, Horgue, Debenest and Quintard, 2015) have used the effective medium theory to determine a symmetric tensor for locally disordered media using direct numerical simulation and optimization.

Renormalization The renormalization technique reaches exactly the same principle of the recursive aggregation. It is usually associated with the work of (King, 1989). Starting from an initial grid with 2^{nD} cells, D is the space dimension, we aggregate cells to obtain a $2^{(n-1)D}$ cells domain. The equivalent permeability is obtained using different techniques and this recursive cell aggregation is stopped when the desired size of the domain is reached.

To estimate the aggregated permeability, there is no exact solution. (King, 1989) used the analogy with electric network and using successive star/triangle transformations, an equivalent permeability can be found for aggregates.

Several other methods could be used. In the literature, we can find examples where renormalization technique is done by the use of numerical simulations. Then, we obtain a complete description of the flow (see (Nœtinger, 2000)) and an equivalent tensor of permeability. In the case where 2D meshes are used, (Le Floch et al., 1999) proposed to aggregate 2 blocks by the use of an harmonic mean of the permeability. In this case, we have to keep in mind that the orientation of the upscaling process could lead to different values of the equivalent permeability in each block.

Streamlines The streamline method is really intuitive. It involves a simple calculation along a tube of current of the head loss induced by the porous medium. For instance, (Fayers and Hewett, 1992) apply this technique to determine the effective permeability for a clay/sand medium.

They obtain the following result :

$$K_{eff} = \frac{(1 - F_s)H^2}{N_s \sum_{i=1}^{N_s} \frac{1}{S_i S_{ei}}} \tag{1.18}$$

Where F_s is the fraction of clay inclusions, N_s is the number of streamlines on which we perform the calculations, H the width of the formation, S_i the length of the i^{th} streamline, and S_{ei} the length weighted by the permeability of the layer.

Laplacian Methods Another type of approaches are the Laplacian methods. They are constructed using simulation on a *local support* discretized at the fine scale in a more or less extended coarse scale neighborhood of the area to upscale. The trade-off here will be the independence of the local boundary conditions of the simulation versus the size of the local support (and hence the computational cost). These methods can then be classified into three levels regarding the definition of their *local supports* (cf. Fig 1.3):

- The *global methods* (Holden and Nielsen, 2000) will consider the whole domain, including boundary condition (reported in Fig. 1.3(a)). They will then apply an optimization using the $L_2 - norm$ error to construct the equivalent permeability K_{eq} per zone , which better reproduce the fine scale flow behavior.

- The *local* (Gautier et al., 1999) and *extended local methods*(Chen and Durlofsky, 2006) will include the immediate coarse scale neighbors or the coarse scale immediate

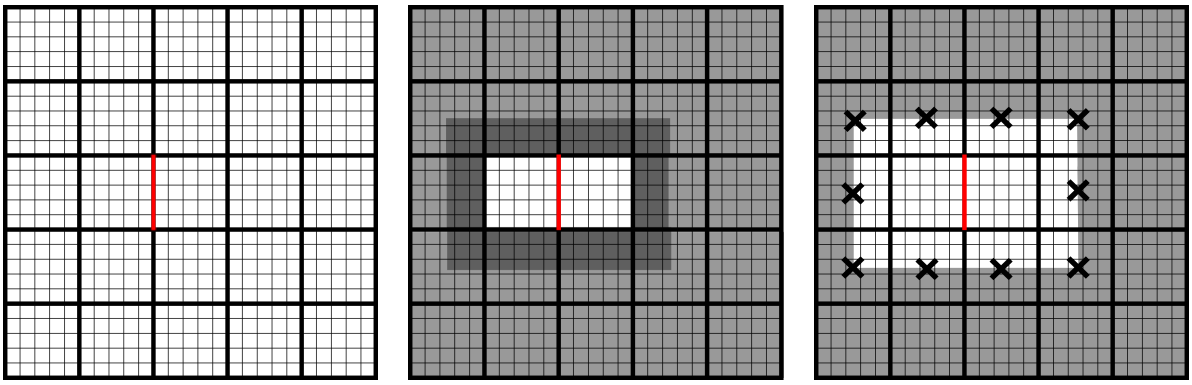

(a) Global methods

(b) Local methods or Extended local methods

(c) Extended Local Global methods

Figure 1.3: Different support definition. White areas represent parts of the fine discretized domain considered as *local domain*. The red coarse face is the area to upscale. On (a) the whole domain is considered as *a local domain*. On (b), *local domain* is considered as the white area (Local methods) or white and dark grey area (extended local). On (c), interpolated coarse pressures (bold crosses) are used to enhance the boundary condition to apply to the extended local domain.

neighbors plus the nearest coarse scale neighbors (reported in Fig. 1.3(b)). The extension of the neighborhood allows to include more details on the fine scale flow at the boundary of the *local support,* and hence, they are less dependent on the local simulation boundary condition.

- The *local global methods*, which will iterate between the *local domain* and the global coarse scale (as reported in Fig. 1.3(c)). On the local support, the equivalent permeability K_{eq} is calculated and, on the coarse scale, using these equivalent permeabilities K_{eq}, a coarse scale pressure field is defined and its interpolated values on the boundaries of the local domain are used to enhance the boundary condition. The iterations stop when these coarse scale pressures do not vary anymore.

These local-global methods have been improved and adapted further. For instance, (Gerritsen and Lambers, 2008) add a mesh adaptation approach in the area to upscale in order to refine the mesh in the zones where gradients are too stiff to be upscalable. This refinement tends to the fine grid discretization and hence excludes these zones of the upscaling process. Another enhancement is developed in (Chen et al., 2010), which extend these local-global methods to multi-point stencil while constraining the monoticity of the solution.

Homogenized equation and upscaling In this part, we find three main methods :

1. Homogenization(Bourgeat, 1984),

2. Volume Averaging Theory(Quintard and Whitaker, 1987),

3. Moments Method(Kitanidis, 1988).

Those three methods allow to treat the upscaling process. They all treat rigorously the mathematical problem. Their common goals are to determine the parameters of the macroscopic equations starting from the microscopic description. In all of them, the spatial periodicity assumption is used. This allows to reduce the problem on a *Representative Elementary Volume* (REV) on which periodic boundary conditions will be used. This periodicity assumption and the arbitrary use of periodic boundary conditions reduce the generality of the solution; anyhow, this does not allow to treat disordered natural media (Guibert, Horgue, Debenest and Quintard, 2015). However, if the property evaluation is done at the larger scale where an upscaled permeability could be defined, it will become *Boundary Condition Independent*. So, defining a periodicity on the geometrical frontiers will not change anything neither to the mathematical nor the results.

The second assumption needed is the *separation of length scales*. The media on which we determine the effective properties might be small regarding the whole domain. This allows the macroscale system of equations to be written by assuming some approximations on term related to the macro scale derivatives. Then, once the problem is simplified, it is needed to solve some closure problems. In the following we will assess the different effective tensors thanks to the closure variable resolutions. In order to present them, we will firstly start back from the definition of the initial problem in pressure, and then write the equation at the larger scale. The final aim is to determine the macroscopic law by relating an average flux to an average pressure gradient. We will denote F, the local flux. We have :

$$\langle F \rangle = - < \frac{-K_s}{\mu} \nabla p > \approx \frac{-K_{se}}{\mu} \nabla < p > \tag{1.19}$$

According to what we have written previously, we need to determine an equivalent permeability K_{se} which will connect the average flux $\langle F \rangle$ to the average head loss$< p >$.

The initial problem is the fluctuation of the permeability field, which is a random variable. If we decompose the permeability field and pressure between mean values, $< X >$, and fluctuation values, X', such as :

$$\ln(K_s) =< Y > +y' \tag{1.20}$$

$$p =< p > +p^{'} \tag{1.21}$$

Inserting these expressions in Eq.1.19, we obtain :

$$\langle F \rangle = \frac{-K_G}{\mu} \left[\nabla < p > + < y' \nabla p^{'} > \right] \tag{1.22}$$

with K_G, the geometric mean of K_{se}, such as $K_G = e^{<Y>}$.

In this equation Eq.1.22, it is important to notice that we approximate the exponential to order one. However, this average flux shows the term $< y' \nabla p^{'} >$, we will need to estimate as a function of the average values of the macroscale problem.

In all the three methods, it is necessary to perform this *closure step*. It will take different forms but the final aim remains the same. We will rely this fluctuation term with the average pressure gradient. Then, we recover a DARCY's law at the larger scale. In (Fadili, 2001), the reader could find a summary of the main results of the upscaling and homogenization techniques. For each of them, it is given the form of the obtained permeability tensor with an associated closure problem. Let us have a look on the main results given using a simple formula.

Theory of homogenization (Bourgeat et al., 1988) and asymptotic development (Saez et al., 1989) The theory of homogenization proposed an homogenized permeability such as :

$$K_{se} = < K_s > + < \nabla.(K_s \nabla \mathbf{b}) > \tag{1.23}$$

with **b,** the closure variable, solution of the associated closure problem written in the following form :

$$\nabla_y.(K_s \nabla_y \mathbf{b}) = -\nabla_y K_s \tag{1.24}$$

with $y \in REV(K_s)$ of length L and periodicity condition on a unit cell, $\mathbf{b}(x + L) = \mathbf{b}(x)$, adding a null average value constraint$< \mathbf{b} >= 0$ to close the problem.

Large scale volume averaging (Quintard and Whitaker, 1987, 1988) Starting from the same closure problem, the large scale volume averaging proposed the following homogenized value for permeability:

$$K_{se} = f1K_1 + f_2K_2 + (K_2 - K_1)\frac{1}{V}\int_{\Gamma_{12}} \mathbf{n}_{12}.\mathbf{b}\, dS \tag{1.25}$$

with f_1, f_2,the volume fractions of the media 1 and 2 considered in the unit cell, and **b,** the closure variable, solution of *Bourgeat* problem (Eq.1.23).

Momentum methods (Kitanidis, 1988) Introducing the wave vector $\mathbf{k}$ and using Fourier analysis, the momentum theory derive such an homogenized permeability :

$$K_{se} = K_G \left\{ \left(1 + \frac{\sigma^2}{2} \right) \delta_{ij} - \int_{R^D} \frac{k_i k_j}{\mathbf{k}.\mathbf{k}} S_{yy}(\mathbf{k}) dk \right\} \tag{1.26}$$

with respectively σ and $S_{yy}(\mathbf{k})$, the standard deviation of the permeability field and the spectral density of the log-permeabiliy.

Stochastic methods

To address the random features of the reservoir properties, stochastic methods have been used to obtain average behavior at the large scale. In this sense, these methods do not differ, for the purpose, from deterministic approaches. However, equations with deterministic properties are not solved. We will rather solve the equations of the flow in terms of statistical properties (porosity, permeability) while describing as best the parameters of interest that are pressure and velocity.

Stochastic methods can be described in three main families: the spectral methods (Gelhar, 1977; Dagan, 1982); the perturbative methods (Sagar, 1978; Winter et al., 1984) and the Monte Carlo methods (Freeze, 1975; De Marsily, 1986).

We will not here describe each method and the results obtained. However, the main results will be resumed, referring the reader to the references. Initially, analytical work focused on simple media; then, they have been generalized taking into account the possible anisotropy of the medium under consideration.

First, (Matheron, 1967)demonstrated that the effective permeability could be expressed in the following form:

$$K_{eff} = exp\left[E(\ln\, K_s)\right] = K_G \tag{1.27}$$

with K_G, the geometric mean, $E(X)$, the expectation of X. The permeability and its inverse must be random functions having the same distributions of probability. Moreover, these functions are invariant by a 90° rotation. This is particularly true for an isotropic log-normal medium, or a binary checkerboard (in value of K_s) for example. In order to generalize, (Matheron, 1967) stresses that for a radial flow, the harmonic mean K_H, at long distance, should be suitable.

(Matheron, 1967) also generalized the previous result by first approximating the effective permeability according to:

$$K_{eff} = K_A^{(D-1)/D} K_H^{1/D} \tag{1.28}$$

using K_A, the arithmetic mean of the distributed permeability K_s.

In 3 dimensions, and for a log-normal distribution, the preceding formula becomes :

$$K_{eff} = K_G exp\left[\sigma^2_{ln\,K}\left(\frac{1}{2} - \frac{1}{D}\right)\right] K_A^{1/D} \tag{1.29}$$

with, $\sigma^2_{\ln K}$the variance of the logarithm of the permeability. This is the Matheron's conjecture (Matheron, 1967).

This result has been examined and extended by a number of studies, in particular (Noetinger, 1994) which shows that the equation 1.29 applies even for an uncorrelated, isotropic, log-normal medium. He proposed rewriting the equation in the following form:

$$K_{eff} =< K^{1-(2/D)} >^{[1-(2/D)]^{-1}} \tag{1.30}$$

The equation Eq.1.29 has been tested by many authors, for varied distributions, with varying lengths of correlation. This demonstrates the robustness of Matheron's conjecture, making a consistent basis for stochastic upscaling.

As a generalization to anisotropic media, we can rely on the work of (Gelhar and Axness, 1983) which, in the case of media with main axes, find the following result:

$$(K_{eff})_{ii} = K_G exp\,(\frac{\sigma^2}{2}\,[1 - g_{ii}]) \tag{1.31}$$

with $g_{ii} = \int \frac{k_i}{\mathbf{k}.\mathbf{k}} S_{yy}(\mathbf{k})\,dk$, $\sum_{i=1,3} g_{ii} = 1$, k_i the local wave vector component in direction i and l_i the correlation length in direction i. (Ababou, 1994) proposes a simplification and an extrapolation of this result for anisotropic media. Then, the effective permeability is expressed in the following way:

$$(K_{eff})_{ii} = K_G exp\,(\frac{\sigma^2}{2}\left[1 - \frac{2}{d}\frac{l_H}{l_i}\right]) \tag{1.32}$$

with $l_H = (\frac{1}{D}\sum_{j=1}^{D} l_j^{-1})^{-1}$where $l_j$is the correlation length in the direction j.

Higher order development have been proposed, and the reader may refer to (Renard and De Marsily, 1997).

In the literature,(Rubin and Gómez-Hernández, 1990) are the first to study the problem of block permeabilityK_b using the stochastic approach. They obtain the expressions of the expectation $E(K_b)$, the covariance of the block permeability C_{K_b} and the cross-variance $C_{K_b,ln\,K_s}$ between the block permeability and the local permeability, based on the permeability distribution function. If the first work was done under simplifying assumptions such as infinite medium, uniform flow and weak variance of the $\sigma(\ln k)$, anisotropy effects on block permeability were also investigated. (Fenton and Griffiths, 1993) studies particularly

the effects of the ratio of block sizes in all the directions of the space and notes that this effect is maximal when the block size is of the order of the correlation length. Finally, in the case of anisotropic media (Gomez-Hernandez and Journel, 1990), it is suggested to use numerical computation (resolution of the diffusion equation) to calculate the permeability tensors between the blocks. These permeabilities are used to estimate the expectation, the covariance of the transmissivity, and the crossed covariance (Hernandez, 1991).

In the case of the single phase flow upscaling, the strategy to be adopted depends on the desired result and the fineness of the data to qualify the reservoir. Although computational performances have evolved greatly in recent years, they do not yet solve a problem of flow in a heterogeneous porous medium on a local scale.Nowadays, we are limited to resolutions of the order of one billion points using domain decomposition methods (Horgue, Guibert, Gross, Creux and Debenest, 2015) or via Lattices Boltzmann (LBM) methods (Mattila et al., 2016). However, they do not address a direct solution to the megascopic problem of interest, namely, prediction of flow in an underground reservoir. At best, they inform about the local properties to be introduced in the blocks for a DARCY scale simulation. So what can a reservoir engineer do dealing with this problem?

If one is looking for simple and fast estimators, the bounds will be preferred. They can be used quickly and are well documented even for heterogeneous and anisotropic media. Nevertheless, as soon as one wishes to obtain more precision of the calculation, one will be confronted with choices. No method seems to give more accurate or more acceptable results than the others. Rather, it will be necessary to estimate biases in the measurement of methods. Is the permeability effective or equivalent? Is the periodized medium an acceptable choice for the sample being worked on ?

All the points discussed above allow to feed the discussion in a case that is simplified (*i.e.* saturated flow).

Now, we will see in more detail the problem of upscaling unsaturated flows for a more complex system of equations to solve and attempt to group and classify existing methods.

1.2 Multiphase flow upscaling in heterogeneous media

In this section, we return to the initial formulation of the system of equations Eq.1.4 for two phase flow, described in the introduction to the chapter. The latter emphasizes non-linearities that do not allow the upscaling process to cross the scales. Simple scalant models can not be defined *a priori*.

In a first step, we will describe the various flow regimes. Then, we will come to the usual methods of upscaling and some results obtained in reservoir engineering for these particular regimes.

1.2.1 Flow regime

If it is possible to describe multiphase flow in porous media using the system of equations, it is also interesting to class them by main phenomena involved. The different regimes are strongly dependent on the properties (density and viscosity) but also on the underlying porous media heterogeneities (spatially distributed permeability field).

Dealing with heterogeneous permeability field and immiscible fluids, instabilities related to viscous fingering could appear (see (Horgue, Soulaine, Franc, Guibert and Debenest, 2015)) and this will deform the saturation front. Here, we try to characterize the front development and we will try to correctly describe this front location when the upscaling process will be done. In order to categorize the different regimes, one could refer to the study of (Lenormand et al., 1996).

1. When the viscous effects are negligible (mobility ratio $M = \frac{\mu_w}{\mu_n}$ close to one) and the correlation lengths are small compared to the total length of the reservoir, the regime will be *macro-dispersive* at the larger scale. This will be the dominant effect and the saturation front will spread.

2. If the injected fluid is more mobile than the one initially present in the reservoir, and if the correlation lengths are small compared to the dimensions of the reservoir, the regime will be possibly unstable. This will generate an instability in the front displacement. The perturbations of the local permeability field amplify the *viscous instability*. This could lead to digits as reported in (Horgue, Soulaine, Franc, Guibert and Debenest, 2015). The form, length and numbers of digits depend both on the mesh and on the numerical scheme.

3. If correlation lengths are large compared with the dimensions of the medium, preferentially oriented along one direction, and viscous effects negligible, the flow will be governed by the underlying heterogeneity. This could generate *channeling effects*.

(Lenormand et al., 1996) summarizes by proposing a diagram, classifying the different phenomena. Using an equation in which three parameters appear, M for mobility ratio, H for Heterogeneity and D for Dispersion. The reader could refer to his paper or (Artus, 2003) for more details.

Our objective is clearly to determine the physical methods when dealing with the upscaling process. However, the model proposed by *Lenormand* demonstrates an important fact: the physics is modified when the upscaling process is done. According to the values of some key parameters at the fine scale (viscosity ratio, structure of the permeability field, flow velocity), we will converge, at the larger scale, on different flow regimes, well predicted by the different MHD parameters. It will be crucial to describe with accuracy the main phenomena involved and the order of magnitude of each of then, when the upscaling process is done.

This review seems to bring out the broad classes of approaches allowing the description of the multiphase transport phenomena at the larger scale. We can classify these into two main groups :

- *Deterministic approach*: this class will include the asymptotic development (or two scales homogenization) and the volume averaging method. Both require to solve a closure problem (differential or integro-differential) on a periodic medium representative of an elementary volume.

- *Stochastic approach*: this includes the theory of homogenization in a probabilistic framework and the stochastic perturbative method.

Subsequently, all these methods will be described and the main results inherent in the use of the techniques will be detailed.

1.2.2 Deterministic methods

First, we will describe the work related to this class of scaling method. These can lead to large-scale descriptions with additional terms, and require the resolution of associated problems.

Asymptotic development or homogenization at two scales

The implementation of this technique requires the identification of two scales: a macroscopic scale L and a scale on which the local fluctuations of the variables are based, denoted l.

The assumption of scale separation will result in the independence of the spatial variables. Generally, we put, $\varepsilon = \frac{l}{L}$.

In the case of the two phase flow problem, characterized by non-linearities, the linearization of relative permeabilities and capillary pressures will be necessary. The formalism becomes rather cumbersome (see (Saez et al., 1989)).

Another problem is the definition of the scale ratio. If the latter tends to zero ($\varepsilon \to 0$), as it is the case in ((Bourgeat et al., 1988)), the capillary forces become dominant. If dynamic effects are to be studied and heterogeneity or gravity taken into account, the scale ratio should be thresholded. This method is used by various authors in the literature, see for instance, (Hou et al., 2006).

Volume Averaging Method

In the context of the Volume Averaging Theory, the most notable bibliographic reference is the work of (Quintard and Whitaker, 1988). They start from a reservoir consisting of a binary media, commonly denoted as a "two region model" in the literature. This medium is assumed to be periodic and therefore a representative elementary volume (REV) can be defined. This is consistent with the assumptions of the homogenization method described above.

In a series of papers and studies, they study two cases:

1. The *capillary equilibrium*, the flow is then quasi-static,

2. The *non-equilibrium* with gravity effects, taking into account the effects of average gradients of macroscopic quantities (pressures and velocities) and of the gravity.

For quasi-static flows, (Quintard and Whitaker, 1988) obtained homogenized permeabilities formally identical to those obtained by these same authors for saturated flows in single-phase cases. In this configuration, if the regions of the two-phase medium are subscripted by 1 and 2 indexes and considering α the fluid phase index as introduced above, we have:

$$\boldsymbol{\lambda}_\alpha^* = f_1 \boldsymbol{\lambda}_\alpha^1 + f_2 \boldsymbol{\lambda}_\alpha^2 + (\boldsymbol{\lambda}_\alpha^1 - \boldsymbol{\lambda}_\alpha^2) \frac{1}{V} \int_{\Gamma_{12}} \mathbf{b}_{\alpha 1} . \mathbf{n}_{12} dA_{12}, \quad \text{with } \alpha = w, n \tag{1.33}$$

Where (f_1, f_2) are the respective fractions of the two regions, $\mathbf{n_{12}}$ the normal vector to A_{12}, the surface separating them. The vectors $\mathbf{b}$ are the solutions of similar differential problems. These are called the closure variables commonly encountered in the problems of upscaling (see (Whitaker, 1998) for instance).

In this case, (Quintard and Whitaker, 1999) point out that these results show that the relative macroscopic permeability takes on a tensor form. The macroscopic capillary pressure curves are flow dependent, in particular to the mean gradients of potentials $\nabla < p_\alpha >$.

In the general case, they obtain the following macroscopic capillary pressure curve:

$$
\begin{aligned}
p_c^* =& < p_n > - < p_w > \\
&+ \nabla < p_n > . \frac{1}{V} \int_V (y + \mathbf{b}_n) dy - \nabla < p_w > . \frac{1}{V} \int_V (y + \mathbf{b}_w) dy \\
&+ (\rho_{\mathrm{n}} - \rho_{\mathrm{w}}) \mathbf{g} . \frac{1}{V} \int_V y dy
\end{aligned}
\tag{1.34}
$$

with y a point of REV, the vectors $\mathbf{b}_{\alpha,\alpha=w,n}$ being the closure variables of the associated problems and $\nabla < p_\alpha >$, are gradients of mean pressure of the fluids.

For quasi-static flows, the gradients of mean pressure potentials are assumed to be negligible. If, moreover, the flow is horizontal (or if the fluids are of the same densities), the mean capillary pressure is reduced to:

$$
p_c^* =< p_n > - < p_w > \tag{1.35}
$$

In this case, the definition of mean pressures as volume average of local pressure (identical definition as the pseudo functions, see section 1.2.5) can give a non zero macroscopic capillary pressure even if locally, there is no capillary pressure. The comparison between the method of upscaling and pseudo-function is discussed in the article by (Quintard and Whitaker, 1999).

The upscaling methods and in particular the Volume Averaging theory often finds a limit in the linearization process. In the absence of linearity, it is necessary to keep a fine description or to take heuristic formulations on the largest scale. It should be noted that resolutions taking into account dynamic effects are possible using this upscaling method. Non-local time approaches for mass transport in porous media exist in the context of mass transport and reactive systems. They remain to be developed for heterogeneous problems including various operators (diffusive or convective).

1.2.3 Stochastic methods

The stochastic approach of flows in heterogeneous porous media has been widely developed since the early work of (Freeze, 1975). It stems from the impossibility of describing the heterogeneity of natural environments in a deterministic way. The parameters of the medium such as the permeability or porosity are then considered as random variables characterized by a statistical spatial structure. The flow equations must therefore be solved in terms of statistical properties (mean, variance, covariance) of the parameters of interest (pressure, velocity, saturation).

This approach serves two purposes. First, it provides an average large-scale equation in the medium without needing a deterministic description of the underlying heterogeneity. It also allows for uncertainty about prediction to be assessed without systematic testing of all possible scenarios. Such an approach is able to give an answer to the problems posed by the emergence of stochastic reservoir modeling techniques.

If the approach can be simplified in the single phase case or two phase flow with a decoupling between pressure and saturation, the standard case of two phase flows is much more complex. Then, the velocity field implicitly depends on the saturation field *via* the relative permeability terms in the generalized DARCY's law (Eq.1.4). In the non-stationary configuration, which is generally the case in the problem treated, the velocity field will therefore evolve with the injection of the fluid phase in the medium. The correlations terms between the different time-dependent variables will appear.

In the case of stochastic upscaling methods for two phase flow, two approaches can be distinguished, the *Eulerian approach* and the *Lagrangian approach.*

Lagrangian framework

In this approach, a major hypothesis is made, namely the independence of the total velocity field from the saturation. Thanks to this assumption, the current lines remain fixed over the time and followed the streamlines. This allows to work with a Lagrangian approach for the study of the saturation evolution, while keeping a Eulerian calculation of the velocity covariances. Therefore, we can decouple the study into two independent problems: on one hand, the 1D displacements of the two immiscible fluids along the current lines (Lagrangian description), and on the other hand the multidimensional description of the velocity field governed by the boundary conditions but also by the geostatistical properties of the permeability field (Eulerian description). In the case of a semi-infinite medium and in stationary regime, the theory of (Rubin and Gómez-Hernández, 1990) makes it possible to find an analytical expression of the Eulerian velocity covariances, but in the general case, numerical resolution is required.

These works lead to estimate a front region spreading continuously over the time, exactly in the same way as the spreading of a passive tracer dispersion in a heterogeneous porous medium. This spreading is a dispersion effect due to the heterogeneity, each point of the front region sampling different velocities during the displacement. It is not surprising that this theory predicts a front region behaving like a passive tracer. As the viscous coupling has been neglected in the calculations, everything happens at the front as if the injected liquid was a tracer, although it moves at a slightly higher speed (see analytical development in Appendix A of (Artus, 2003)).

Eulerian framework

In the PhD of (Artus, 2003), by using the example of a fluid drainage by the injection of another fluid, preferentially in 1D situation, one can obtain an equation governing the saturation equation in heterogeneous medium.

Considering the heterogeneity of the permeability field, this induces heterogeneities in the pressure fields, velocities and saturations. Each variable is decomposed into an average value and a perturbation,as $x = \bar{x} + \delta x$. These quantities are regionalized random values.

(Artus, 2003)obtains an average saturation equation Eq.1.36. In the following saturation function $S(\mathbf{x},t)$ and velocity $\mathbf{u}(\mathbf{x},t)$, are simply denoted by S and $\mathbf{u}$ for the sake of clarity.

$$\epsilon\frac{\partial\overline{S}}{\partial t} + \nabla.(\overline{f}(\overline{S})\overline{\mathbf{u}}) + \nabla.(\overline{f}'(\overline{S})\overline{\delta S\delta\mathbf{u}}) \tag{1.36}$$
$$+\frac{1}{2}\boldsymbol{\nabla}\cdot(\overline{f}''(\overline{S})\overline{\delta S\delta S}\overline{\mathbf{u}}) = 0\ \forall(\mathbf{x},t)\in\Omega\times\mathbb{R}^+$$

with $\bar{f}(\bar{S})$, the mean fractional flow and $\bar{f}'(\bar{S})$, $\bar{f}''(\bar{S})$, its first and second derivative.

Using the local equation and subtracting the previous average equation, we obtain the perturbation equation for the saturation. Thus, we can determine the expression of$\overline{\delta S(\mathbf{x},t)\delta S(\mathbf{x},t)}$ and of $\overline{\delta S(\mathbf{x},t)\delta\mathbf{u}(\mathbf{x},t)}$.

The resolution of such a system involves equations governing the moments of the random variables considered. This system has been solved numerically for single phase flow (Graham and McLaughlin, 1989). The two phase flow case must be done using simplifying assumptions (velocity independent from the saturation for instance) given the problem complexity to be treated.

It should be noticed that (Langlo and Espedal, 1994) have reduced this system to a simple macrodispersion equation. The Independence of the flow field to the saturation allows to estimate the covariance terms of velocity $\overline{\delta\mathbf{u}(\mathbf{x},t)\delta\mathbf{u}(\mathbf{x},t)}$. They obtain the following equation :

$$\epsilon\frac{\partial\overline{S}}{\partial t} + \nabla.(\overline{f}(\overline{S})\overline{\mathbf{u}}) + \nabla.(\mathbf{D}\nabla\overline{S}) = 0\ \forall(\mathbf{x},t)\in\Omega\times\mathbb{R}^+ \tag{1.37}$$

The dispersion tensor $\mathbf{D}(\mathbf{x},t)$, in the preceding equation, can be expressed using the results of (Rubin and Gómez-Hernández, 1990) for the single phase case. Assuming that the field $Y = ln(K)$ has an exponential covariance function of variance σ_Y^2 and an integral length I, we obtain the result of (Langlo and Espedal, 1994):

$$\mathbf{D}_{ij}(\mathbf{x},t) = \delta_{ij}(\overline{f'}(\overline{S}(\mathbf{x},t))^2 U\sigma_Y^2 I\alpha_{ij}(t) \tag{1.38}$$

with U, the mean filtration velocity and$\alpha_{ij}(t)$ the components of the dispersivity tensor. Even if the components are time-dependent, they are established when several correlation lengths have been traveled. Then, the dispersive regime is a linear function of the heterogeneity index $\sigma_Y^2 I$ also depending on the distance.

However, and both in the Eulerian or Lagrangian case, these methodologies do not allow us to trace the different flow regimes(Artus, 2003). The Lagrangian approach predicts the dynamics of the saturation front spreading in the same way that of the passive tracer because the flow takes place along fixed current lines. In the Eulerian case, the conclusion is exactly the same. The macrodispersion term obtained will control the spreading of the the saturation profile, but it will not reproduce, as would the flow will do on the fine mesh, a true front. Simplifications are then too large and do not allow to reproduce the expected flow regimes(Lenormand and Fenwick, 1998).

Finally, this stochastic scaling process highlights the presence of additional terms in the descriptions, which are due to the local heterogeneity, but also at the order in which the perturbative analysis is truncated. This is also found in deterministic methods, and these will be described in the next section.

1.2.4 Generalized upscaled system : unexplored dependencies ?

An important element in the deterministic upscaling (volume averaging method, homogenization) is the appearance of additional terms modifying the form of the equation at the larger scale. The average saturation profiles can not be captured by large-scale equations identically to those of the DARCY scale.

In the particular case of multiphase flows, if the regime is not purely convective, there are macrodispersion phenomena for saturation (see previous section Sec. 1.2.3 , for instance). This is reported by several authors in the literature and with different upscaling methods. Far from extensive listing, we will just describe the differences between the initial DARCY scale equations and the macroscopic description involving new terms (terms of exchange, macrodispersion).

Similarly, the convective term can be transformed in a complex way during the upscaling process while it is trivial on the fine scale: one would then be tempted to calibrate the average profiles by a macrodispersion coefficient depending on time and/or distance, without taking into account a change of the large-scale fractional flow (Lenormand et al., 1996). The description of the large-scale flow must therefore be reformulated in order to take into account the physical processes which govern the evolution of the average saturation profiles.

(Lenormand et al., 1996) also proposes to use a dispersion term at the larger scale in the transport equation of saturation. This dispersion is dependent on the permeability field statistics. It will be dependent both on space and time, and also on the saturation fields evolution.

This is consistent with the work of (Panfilov and Floriat, 2004) but also from (Langlo and Espedal, 1994). These studies demonstrate that the saturation transport equation has a non-linear hydrodynamic dispersion term in saturation but also modifies the mean velocity. In addition, it is even shown that the one-dimensional flow does not reduce the dispersion tensor to be 1D and it remains completely 3D.

In the simplified case in which the velocity field does not depend on the saturation, we can use the results of the single phase case (Rubin and Gómez-Hernández, 1990) to find an analytical formulation of different covariance terms of velocities and saturations. Thus, the general transport equation is of the same type as (Lenormand et al., 1996).

(Quintard and Whitaker, 1988)and(Ahmadi and Quintard, 1996) also mention additional terms in the description of upscaled multiphase flow equations in heterogeneous media. These terms are derived from inter-phase exchanges but also from the distribution of active and inactive phases for flow. The distribution of these phases may vary over time. The larger scale equations are always dependent on the saturation field (modification of the active phases spatial distribution), but also on the average pressure gradients between phases.

To solve this complex problem, the authors make several simplifying assumptions. The closure problems assume the existence of a medium on which periodic boundary conditions are imposed. The most restrictive assumption comes from the quasi-static regime. We can not then generalize these results for media in which the behavior of the system is controlled, throughout the domain, by various time scales. Dynamics and gravitational effects are also ignored in these closure problems.

Finally, this is to be linked to the empirical work of (Durlofsky et al., 1997). It considers a two flow in heterogeneous medium with a non uniform background, using a single set of relative permeability $k_r(S_w)$. In this study, they propose to use the following method to compute the coarse grid flow by determining $\overline{\lambda}(\overline{S}, \sigma_S, \sigma_{uS}, \sigma_p)$ instead of $\overline{\lambda}(\overline{S})$. For this purpose, they assume the dependence of the relative permeability on the large scale, not only on the average saturation but also on the correlations between the saturation and velocity field, suggesting the appearance of the σ_S, σ_{uS} but alsoσ_p. Even if this meets the aim of the the pseudo-functions (described below), this method seems less sensitive to the changes in initial and boundary conditions. However, it requires a fine grid simulation, but this should be replaced by a rough grid estimator, favoring more general methods of upscaling.

Finally, whether mathematically or empirically, the conclusion remains the same: the nonlinear two phase model (Muskat, 1949) does not cross the scales without modifying the larger scale equations and some additional terms appear. We will now review the numerical methods for upscaling. They allow to reduce the numerical effort while proposing to possibly mix the scales between them in order to preserve a predictability of the flow.

1.2.5 Engineering methods for relative permeabilities construction

The numerical methods developed for homogenization are generally adaptations of the methods used for single phase flow. However, there are some specific methods, such as the pseudo-functions, which are only relative to multiphase flows. Subsequently, we will describe them in a concise manner, not forgetting to remind the other methods available in the literature.

Static pseudo

Early beginning and starting point The relative permeabilities or capillary pressures obtained on a coarse scale are called "*pseudos*" in order to differentiate them from models obtained with laboratory experiments and used at the fine scale. In the case of pseudo-functions, we consider that the equations do not change, unlike the case of a more "physical" upscaling. It is possible to take into account the heterogeneities of the lower scale and/or the numerical dispersion due to the mesh coarsening. The role of pseudo-functions is to determine the averaged output flow rates of a coarse block for each phase flowing in the system. These pseudo-functions take into account heterogeneities and variations in pressure and saturation at the lower scale. Pseudo-function methods are widely used when dealing with numerical upscaling process.

The origin of these methods can be found in (Stiles et al., 1949). A "layer-cake" reservoir made of homogeneous layers is the support for upscaling process. Inter layers exchanges, but also gravity and capillary effects, are neglected. The layers are ordered with increasing permeability values, which makes it possible to make a vertical aggregation, and thus, to reduce the number of meshes. At each time and at any point, one can calculate an average saturation over the thickness of the medium, which depends on the number of strata already invaded, as well as effective relative permeability curves for the medium (curves of *pseudo*-relative permeabilities). The later study of (Dykstra and Parsons, 1950)extends this work to the cases of fluids with different viscosities. These models are easy to implement and and easy to use. They are robust and predictive when the exchange between layers remains

weak. In the case of the vertical equilibrium, we can find a set of works that we present in the next section.

Vertical equilibria At first, we must remind the following assumption in order to study the vertical equilibrium case: in the direction normal to the base of the reservoir, the viscous forces are dominated by the capillary and/or the gravity forces. In this case, fluids that move faster vertically than in the horizontal direction are segregated. In this case, the 3D problem is reduced to a 2D one. This does not express the absence of displacement following the z-direction but rather a maximum flow in a 2D plane, as the fluids are in hydrostatic equilibrium under the action of gravity and capillarity. According to (Dake, 1983), besides the fact that the problem becomes independent on the initial and boundary conditions, the conditions allowing the existence of this vertical equilibrium are:

- Low vertical reservoir extension,
- High permeability layers in the vertical direction,
- Low lateral velocities,
- Important gravity and capillary effects,
- Negligible viscous effects.

We can distinguish three preferential situations of the vertical equilibrium which are found many times in the literature. These are reported below along with their associated pseudos.They are reported in a simplified way in the figure 1.4 which is inspired by the representations of (Ahmadi, 1992).

- Gravitational equilibrium

This case is fairly simple to describe. The fluid distribution follows a bimodal distribution, with a small capillary transition zone compared to the height of the reservoir. Average saturations are estimated on the section of the reservoir. Firstly, the average saturation by segregation is calculated.

$$S_w^* = \int_0^h \varepsilon(z) S_w(z) dz / \int_0^h \varepsilon(z) dz \tag{1.39}$$

So, if the absolute permeability is isotropic in the $x - y$ plane, pseudo-functions are calculated by averaging over the height of the reservoir according to :

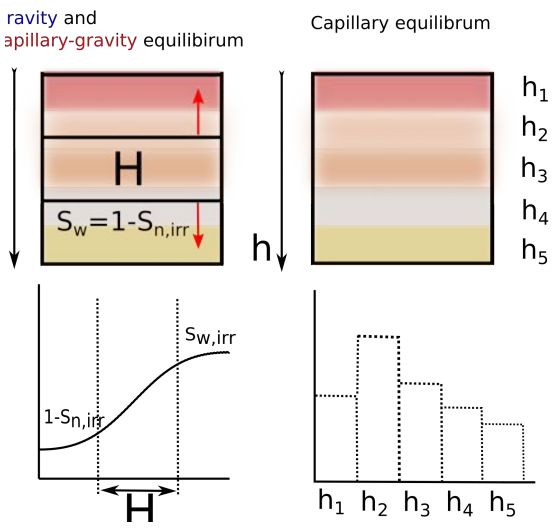

Figure 1.4: Simplified representation of the different equilibrium cases according to (Ahmadi, 1992)

$$k^*_{r,\alpha} = \int_0^h K_h(z) kr_\alpha(z) dz / \int_0^h K_h(z) dz \quad \alpha = w, n \tag{1.40}$$

Where, K_h is the vertical permeability. This result has been generalized to anisotropic medium(Coats et al., 1967) and 3D reservoir(Killough et al., 1979).

- Capillary equilibrium

This situation is described by (Yokoyama et al., 1981) and (Dake, 1983). Gravity forces are low and the capillary pressure is uniform over the thickness of the reservoir. The saturation values of the different layers will depend on the capillary pressure curves of each layer. Saturation jumps are then observed between the layers. In order to estimate the pseudo-curves of relative permeabilities and capillary pressures, we proceed according to a simple algorithm Alg.1.1.

- Capillary-gravity equilibrium

This case is described in the literature by (Coats et al., 1967) or (Killough et al., 1979). The capillary and gravitational forces are of the same order of magnitude in the vertical direction of the reservoir. Compared to the gravity equilibrium, a thickening of the capillary zone is observed in the figure Fig. 1.4. This explains why this case is treated in the same way than the capillary equilibrium case.

The set of equilibrium methods are often related to a more general care, namely the "steady state" or quasi-static methods. We have chosen to describe them because they are

Algorithm 1.1 Determination of capillary pressure curves in the case of capillary equilibrium.

1. Determine an arbitrary saturation in one of the layer of the reservoir,
2. Calculate the capillary pressure from the saturation thanks to the capillary curve in the chosen layer,
3. Since the capillary pressure is uniform over the height, deduce the saturations in the other layers are deduced by using the capillary pressure curve p_c relative to each of the layers,
4. Average saturations and relative permeabilities,
5. Repeat steps 1-4 for varying degrees of saturation, and construct curves of pseudo-relative permeabilities and pseudo-capillary pressure.

related to physical effects and to forces comparison. The quasi-static case assumes that the temporal variation of saturation will be null, so they are much more general than the previous cases of equilibrium. We describe them below.

Quasi-static For the time being, we have studied cases where the equilibria were determined by the relationships between the dominant effects. If one is in a case where the saturation of a block does not vary in time, i.e. $\frac{\partial S}{\partial t} = 0$, then one is in a so-called quasi-static situation.

In this case, the temporal derivatives of the system of initial equations disappear. We obtain two decoupled equations:

$$\nabla \cdot (\lambda_n (\nabla p_n - \rho_n \mathbf{g})) = q_n \tag{1.41}$$

$$\nabla \cdot (\lambda_w (\nabla p_w - \rho_w \mathbf{g})) = q_w \tag{1.42}$$

Relative permeabilities can be calculated by solving a single-phase problem per phase. The fractional flux is constant over time, which is a consequence of the quasi-static hypothesis.

In this case, the fractional flow f_w is constant, and if the viscous effects are predominant, it depends only on the mobility of each phase. It is written:

$$f_w = \frac{\frac{kr_w}{\mu_w}}{\frac{kr_n}{\mu_n} + \frac{kr_w}{\mu_w}} \tag{1.43}$$

The saturations are then calculated by inverting this flux function, $S_w = f_w(S_w)^{-1}$. However, if capillary effects dominate, fluids tend to move faster in areas with high permeability. This can generate a large dispersion in the saturation front (Artus and Noetinger, 2004). These same authors study the behavior of the saturation front given the variable mobility ratioM_f.

$$M_f = \frac{\mu_w k_{r,n}(S_f) + \mu_n k_{r,w}(S_f)}{\mu_w k_{r,n}(S_{irr}) + \mu_n k_{r,w}(S_{irr})} = \frac{\lambda_t(S_f)}{\lambda_t(S_{irr})} \tag{1.44}$$

S_f represents saturation at the front, S_{irr}, irreducible saturation of water, and therefore λ_t, the total mobility. In this case, according to (Artus and Noetinger, 2004), two cases branches:

1. If $M_f > 1$, the case is stable, a stationary front exists and is set up for weakly heterogeneous environments. The viscous effects will compete with the perturbative effects of heterogeneity. (Artus, 2003) deals with this case using a stochastic model and obtains a full upscaled description.

2. If $M_f < 1$, the front is unstable and the phenomenon is amplified.

Dynamic pseudo

We use the notion of dynamic flow when the methods allowing the implementation of static or vertical equilibrium solutions are no longer usable. In this case, this can be due to high flow rates, but also because of a strong anisotropy in the reservoir. Simulations should be carried out on the fine grid in order to obtain averaged properties using the averaged values of the fine grid, hence it requires a prior fine grid simulation on the whole reservoir.

These type of methods were first introduced by (Jacks et al., 1973) and generalized by (Kyte et al., 1975) while taking into account numerical dispersion. The first question is to ask what this method brings. (Pickup et al., 2005)describe some of the benefits in their study:

- The simulation on a fine grid will make it possible to better represent the saturation field conforming to what will be observed in a real reservoir model. The description of the model is indeed correct, provided that correct boundary conditions are used.

- The dispersion of the front and its spreading due to heterogeneities of the transport properties are taken into account.

- The dispersion due to mesh coarsening can be controlled, unlike in the static pseudo functions case.

Two major approaches will be distinguished in the literature in order to determine the relative pseudo-permeabilities dependent to the averaged saturation.

1. A first method consists in defining the average pressure gradients on the coarse mesh. Thus, introducing them into the generalized DARCY's law on the coarse scale, one can determine the pseudo relative permeability laws and thus be sure to conserve the fluxes from the fine grid to the coarse grid. This is described by various authors (see (Jacks et al., 1973; Kyte et al., 1975)).

2. A second method consists in estimating the pseudo-fractional flows on the coarse grid and then to determine the relative permeabilities using these coarse fluxes. Then, fluxes are preserved from the fine grid towards the coarse mesh (see (Stone et al., 1991; Hewett and Behrens, 1991)).

Then, we use these numerically constructed functions to perform simulations on coarse meshes representing our reservoir model.

(Stone et al., 1991) is very critical in its review of previous work on pseudo functions, in particular as the first dynamic pseudo can lead to negative transmissivity. He suggests abandoning the use of pressure potentials in calculations and initiates the use of fractional flows. This opens the way to new methods. For example (Guzman et al., 1996) propose a potential-weighted flux-based method. (Hewett and Yamada, 1997) present a 3D, semi-analytical method that does not require the full calculation of the streamlines. Even if this method considers a two-phase system, the streamlines are estimated by making only one single-phase simulation, which greatly simplifies the approach and reduces the associated numerical effort. The single-phase transmissivity of each segment of the current tube is first determined from the results of a single phase flow resolution. Now, that we have described the main studies using or developing the use of pseudo-functions, we will study the constraints and validity of these methods.

Assumptions and validity of pseudo

As for static pseudo functions, (Jonoud and Jackson, 2008) demonstrated that the validity domains of each upscaling method (upscaling where viscous or capillary effects may be dominant) could be determined. In conjunction with empirical thresholds determined during their study, three dimensionless numbers are defined to determine the ratios of capillary and viscous forces. Two of them are always required: the ratio of the mobilities to the end-points, and the ratio between the longitudinal Péclet (based on the viscous flow ratio by the capillary forces) of the most conductive layer and the less conductive. In conjunction with empirical

thresholds determined during their study, these numbers give domains of validity for the use of models where viscous or capillary effects dominate. However, it should be recalled that no dynamic effect can be captured by this method in a robust manner. Moreover, the authors have developed their estimators for simplified geometries (multi-layered systems) and concede that the heterogeneity will not allow them to generalize to more complex reservoirs. More recently, more sophisticated (Wu, 2013) and regionalized decomposition methods have been developed in order to achieve a numerically efficient upscaling without losing information about local heterogeneity and its effects on flow.

Dynamic pseudo-functions are effective properties that can only provide correct results for the particular fine-grid situation and the boundary conditions for which they were calculated. Complex initial conditions, intermittent and unsteady injection phenomena, the addition of new wells or, more generally, the phenomenon of hysteresis are some of the limits to the method. A different set of relative permeabilities is then assigned to each coarse block, for each direction of flow. In contrast to the vertical equilibrium methods, dynamic pseudo-functions depend on external factors. Their main defects are summarized by (Pickup and Stephen, 2000): these methods are costly because of the necessity to perform a lot of two phase flow simulations on the fine mesh blocks in order to generalize their use at the larger scale and in numerous different situations. However, (Barker et al., 1997) propose to bypass the generation of a set of pseudo functions for each of the fine mesh blocks by grouping these blocks into "rock types". Several zones of the reservoir, each one being continuous, having the same petrophysical properties as well as the same production behavior, will be attributed the same "rock type". A "rock type" can be defined by static data (permeability, porosity) and/or by dynamic data (relative permeability and capillary pressure curves). According to (Gholami et al., 2009) one can define a "rock type" upscaled according to the distribution of the "rock types" present in the fine model. The method is all the more effective when a rock type is dominant in the reservoir studied. In their review of pseudo functions methods, (Barker et al., 1997) emphasize the lack of tools to judge whether two sets of pseudos are close enough to be treated in the same way. The use of "rock types" could be a criterion for limiting the number of pseudo functions to be determined. The pseudo function calculations in inactive zones, where flow is non-existent, is also unnecessary. Finally, the regeneration of pseudos, in the case of a sensitivity study, must be avoided. This avoids too expensive calculations and the use of a quantity of memory, necessary for the storage of the pseudos, to be too large. This question again highlights the problem of choosing the size of coarse blocks and the choice of fine simulations to generate the required nicks. The inadequacy of relative permeabilities on a large scale is emphasized by (Artus, 2003). The use of the same equations on fine scale and coarse scale is problematic. It is difficult to reproduce within a

coarse block a saturating front representative of the heterogeneities underlying the fine scale. From this perspective, (Durlofsky et al., 1997) proposes to use relative permeability curves that no longer depend only on saturations, but on the variance in saturation and covariance in speed /saturation, among others. This technique makes it possible to generalize the pseudo functions and to reduce the dependence on a particular situation.

Each structural, boundary conditions, geometrical modification could therefore lead to perform a new calculation on the fine mesh to determine the new pseudo functions. The method should be used with caution and the exploitation of the pseudo functions obtained in order to generalize calculations on a coarse mesh will be hazardous. Nevertheless, some of these troubles are discussed in the literature. It is noteworthy that some works(Zhang et al., 2008) allow more realistic wells and boundary conditions to be taken into account in order to preserve the fine structures of the flow. The coarse medium generated can then better reproduce the flows observed at the fine scale. However, this remains dependent on the configurations in which the models are constructed and therefore on the position of the wells and the geometric heterogeneity.

1.2.6 Other methods

Some other methods not mentioned above have been developed or adapted from saturated flow. This section aims to describe briefly their principles and limits.

Renormalization

(King et al., 1993) extend the single phase flow technique of renormalization to the unsaturated cases. The main assumptions of the method are:

- Capillary pressure equal to zero : $p_c = 0$.
- No gravity effects, the flow remains horizontal.

In this case, it is necessary to adopt a slightly different formulation of the problem, as we have seen only a fractional flow formulation. Starting from the Buckley-Leverett model (Buckley and Leverett, 1942), we can exhibit the fluxes of each fluid fraction transported.

Taking the mass balance equation, and adding the saturation constraint, we obtain the expression of a total flux denoted Φ_t satisfying the following system of equations:

$$\begin{aligned} \mathbf{u}_t &= -\left[\lambda_w(S_w)\nabla p_w + \lambda_n(S_w)\nabla p_n\right], \\ \boldsymbol{\nabla}\cdot\mathbf{u}_t &= 0 \end{aligned} \tag{1.45}$$

If one takes up the generalized DARCY equations (Muskat, 1949), the flow of the wetting phase can then be expressed as a function of the total flux:

$$\Phi_w = \frac{\lambda_w}{\lambda_t}\Phi_t + \lambda_t \nabla \left[p_c + (\rho_n - \rho_w)\mathbf{g}z\right] \tag{1.46}$$

Some basic manipulation later, we obtain the fractional flow f_w:

$$f_w = \frac{\Phi_w \Phi_t}{||\Phi_t||^2} = \frac{\lambda_w}{\lambda_t} + \lambda_t \frac{\nabla \left[p_c + (\rho_n - \rho_w)\mathbf{g}z\right] \phi_t}{||\Phi_t||^2} \tag{1.47}$$

Including the total mass conservation of immiscible flow, the wetting phase mass conservation equation can then be rewritten:

$$\epsilon \frac{\partial S_w}{\partial t} + \Phi_t \nabla f_w = 0 \tag{1.48}$$

(King et al., 1993) but also (Hansen et al., 1997) demonstrate that it is possible to apply the renormalization method developed for single phase flow by (King, 1989). It is then necessary to replace the intrinsic permeability by the total mobility λ_t, which corresponds to the intrinsic permeability weighted by a mobility term.

MHD methods and derivatives

(Lenormand et al., 1996; Lenormand and Fenwick, 1998) approach the homogenization of the transient two phase flow problem in terms of average saturation profiles and not in terms of effective permeabilities. By performing streamline simulations, they determine the coarse structure of the reservoir by detecting heterogeneities at the large scale. They characterize the subgrid flow using a coefficient of dispersivity. A transport equation for the average saturation at the advection/dispersion scale is then obtained. The advective and dispersive fluxes are estimated from the saturation profile.

Aggregation methods

The method of mesh aggregation aims to perform several steps of gathering certain fine meshes cells in particular zones of the reservoir into coarser cells. On the other hand, we can also free ourselves from the contrasts related to regular Cartesian meshes by using more elaborate meshes corresponding to the geologic features or to the physics of the flows (Aziz et al., 1993).

This method of aggregation was initiated by (Durlofsky, Jones and Milliken, 1997) (see Fig. 1.5).

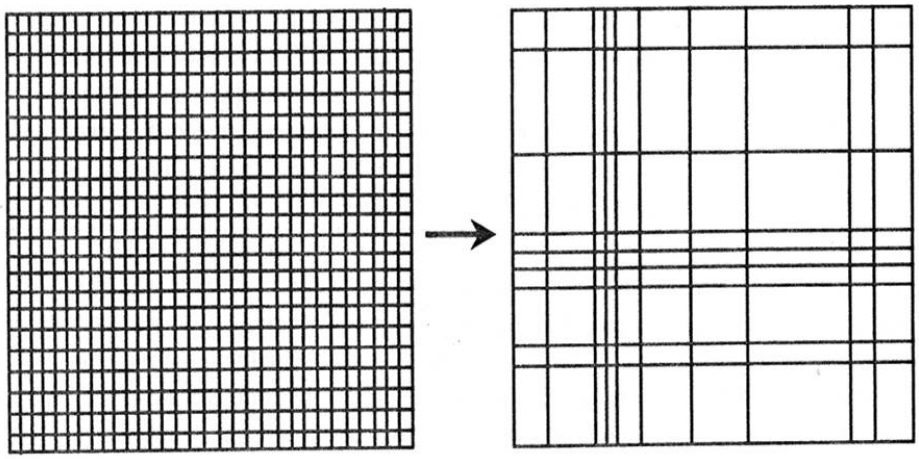

Figure 1.5: Aggregation non uniform from Durlofsky (Durlofsky, Jones and Milliken, 1997)

They reproduce the results of the homogenization of (Bourgeat et al., 1988; Saez et al., 1989). The upscaling process concerns only the saturated flow permeability which is homogenized, starting from the same system of equation (Eqs. 1.45;1.48) as mentioned in Sec. 1.2.6.

The model used by (Durlofsky, Jones and Milliken, 1997) is reminiscent of the type methods of currents developed initially in the 1990's by (Thiele, 1994; Thiele et al., 1996; Lenormand, 1995; Lenormand and Wang, 1995; Hewett and Yamada, 1997; Portella et al., 1997). We adapt the mesh to the reservoir heterogeneity by making the hypothesis that the multiphase flows follow the preferential paths of saturated flow case(Van Meurs, 1956).

The main problem of these methods consists in correctly estimating and conserving the fluxes in the reservoir (Ponting, 1989; Peaceman et al., 1996) using mesh-based schemes. Another possible trouble is that the construction of the initial mesh is based on static considerations, without paying attention to the possible structures generated by the two phase transport.

To partially avoid these biases, (Prevost et al., 2002) use the current tubes method. The pressure is solved on a fine mesh in order to identify the zones in which the observed fluxes are large and other zones considered more *stagnant*. The mesh will be built on these single

phase flow considerations, by refining the so-called *fast* zones and by roughly aggregating the so-called *stagnant* zones.

The dynamic behavior could be treated using adaptive meshes. However, they remain difficult to control and there is a tendency to highly refine the unstable zones and thus to create or amplify unstable phenomena such as viscous digitation. The initial gain in number of cells is then lost. This is consistent with observations in other applications such as dissolution in porous media (Luo et al., 2015).

According to (Artus and Noetinger, 2004), it is then no longer necessary to find the results of the fine grid. Then, the non-uniform aggregation method becomes an attractive method, and its possible adaptation must be studied more physically to determine the areas to be refined.

Aggregation methods leads us to another type of upscaling methods : the multiscale methods. Following the idea that has been used in deriving the Algebraic Multigrid Algorithm, a partitioning of a fine grid, on which lies the fine scale properties such as permeability, by a coarse grid, on which the elliptic pressure equation Eq.1.4 is solved, is defined. It allows to overcome the insoluble question of fine scale detail inclusion in the upscale model. It indeed constructs a dynamically communicating fine to coarse to fine scale model.

1.3 Towards numerical multiscale methods

The latest increase in computing power goes with an increase in the level detail that goes with geophysical model. It then requires always more CPU power and memory capacity to include these small scale data in the whole reservoir simulation. The upscaling of some of these data is then needed to make them manageable on a desktop computer and to make the simulations stochastically repeatable.

Several methods have been developed to upscale the *elliptic pressure* equation Eq.1.4, while the *hyperbolic transport/saturation* equation Eq.1.7 is kept on the local scale (also referred to as fine scale).

These methods can be split whether they have a *finite volume* formulation or *a finite element* formulation.

The finite element multiscale originated from the work on the *Multiscale Finite Element Method(MsFEM)(Hou and Wu, 1997).* Then it has been extended(Chen and Hou, 2003b) and completed(Aarnes, 2004; Efendiev et al., 2013). *Numerical Subgrid Methods(NSub)(Arbogast, 2000, 2002a)* adopt a different approach decomposing pressure into a mean component on the coarse scale and its subscale variation on the fine scale. On the finite volume part,

the *Multiscale Finite volume (MsFv)(Jenny et al., 2003)* has been first derived inspired by the *MsFEM*(Hou and Wu, 1997). It constructs local basis functions as well and obtain an *interpolation* operator to deduce from a coarse scale system a fine scale approximated solution. Later developments lead to the *Multiscale Restriction Smoothed Basis (MsRSB) (Møyner and Lie, 2016)* that use overlapping region and Jacobi iteration to get smooth and globally conservative basis functions. During this thesis, an alternate approach has been proposed. The *Finite Volume Mixed Hybrid Multiscale Method(FvMHMM) (Franc et al., 2017)* has also been adapted from finite element formulation (Harder et al., 2013b, 2015). It uses Lagrange multipliers that can be regarded as coarse fluxes to ensure flux continuity at coarse scale.

A key point in multiscale methods for multiphase flow application is to construct a fine-scale pressure approximation, which is both globally and locally conservative. The finite volume methods are intrinsically locally conservative while finite element methods use mixed elements to achieve that. Further details are provided in the following section for the finite volume methods.

1.3.1 *Dual Mesh Methods* (DMM)

Core method

The *dual mesh method (Verdiere and Vignal, 1998)* can be included retrospectively in the finite volume formulated multiscale methods. It weakly couples saturation and pressure equations constructing pressure system for inversion on the coarse grid and updating explicitly saturation distribution on the fine grid in an IMPES-like manner (Sheldon et al., 1959). It defines two key steps to go from the fine grid to the coarse grid, *upgridding,* and from the coarse grid to the fine grid, *downgridding.* The former allows to define an equivalent transmissivitty from fine scale details of the heterogeneities. The latter provides distribution function of the coarse flux on the fine scale faces. Several couple of *downgridding/upgridding* methods can be then tested. Two of them are detailed in the following part, Pressure Solved Method (PSM)(Gautier et al., 1999)/transmissivitty weighting and Adaptive Local Global/flux weighting(Babaei and King, 2012).

PSM/Transmissivity weighting The PSM method solves a Poisson equation with permeameter boundary conditions. As mentioned in 1.1.2, the test is conducted along each direction to construct an upscaled permeability tensor. Following the same idea, a gravity-driven equivalent permeability can be constructed imposing homogeneous boundary condition and a gravity source term.(Audigane and Blunt, 2004)

The transmissivity weighting distribution function assumes that the flow will follow fine scale permeability distribution in the vicinity of the coarse faces of the coarse cell considered. This will the ease the flow in highly permeable region and hinder it in the barrier zone. This is a limited assumption that can fail if an small inclusion happen to lay next to a coarse cell.

In spite of its shortcomings, this couple of methods keep the overhead computational cost low.

ALG/flux weighting A new couple of downgridding/upgridding is tested. It uses a ALG (Chen and Durlofsky, 2006) method for upgridding the permeability. That is to say, it consider a more extended area around the considered coarse cell ("jacket zone") and imposed computed pressure in these area as boundary conditions. The algorithm iterates then until found permeability is consistent with boundary conditions. It constitutes a more accurate way of upgridding

Fluxes that appears in the ALG steps are later reused to construct the distribution function on the downgridding step.

1.3.2 *Multiscale finite volume* (MsFv)

Core method

The *Multiscale Finite Volume(Jenny et al., 2003)* method is build on the construction of a *primal* coarse grid, denoted M_H, and its *dual* staggered grid, denoted $\widetilde{M}_H$, on which basis functions will be evaluated (cf. Fig. 1.6). These basis functions $\Phi_K^{\widetilde{K}}$ help estimating an equivalent transmissivity and therefore assembling the coarse scale *elliptic* system. In order to partitioned the problem into a collection of problems on coarse cell's support, a *localization assumption* is made that is written as:

$$\boldsymbol{\nabla}_{||} \cdot \mathbf{u} = 0, \qquad on\ \partial\tilde{K}. \tag{1.49}$$

The first step is then to build the basis functions$\Phi_K^{\widetilde{K}}$, $K \in M_{\widetilde{K}}$ on each dual coarse cell $\widetilde{K} \in \widetilde{M}_H$, where $M_{\widetilde{K}}$ stands for the set of primal coarse cells that sharing the vertex $\mathbf{x}_{\widetilde{K}}$. For each $\widetilde{K} \in \widetilde{M}_H$, the basis function $\Phi_K^{\widetilde{K}}$, $K \in M_{\widetilde{K}}$ are solution of the following equations set on the dual coarse cell $\widetilde{K}$ with value $\delta_{K,L}$ at the vertices $\mathbf{x}_L$, $L \in M_{\widetilde{K}}$ of the dual coarse cell $\widetilde{K}$:

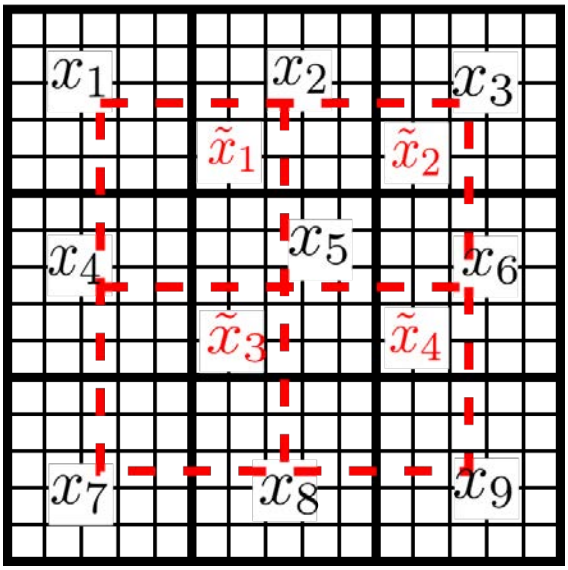

Figure 1.6: MsFv: primal mesh(solid lines) and dual mesh(dashed lines).

$$\begin{cases} \nabla \cdot \frac{-\mathbf{K}(\mathbf{x})}{\mu} \nabla \Phi_K^{\widetilde{K}} & = 0 \qquad in\ \widetilde{K}, \\ \nabla_\perp \cdot \frac{-\mathbf{K}(\mathbf{x})}{\mu} \nabla \Phi_K^{\widetilde{K}} & = 0 \qquad on\ \partial\widetilde{K}, \\ \Phi_K^{\widetilde{K}}(\mathbf{x}_L) & = \delta_{K,L}, \quad L \in M_{\widetilde{K}}. \end{cases} \tag{1.50}$$

Once these basis function $\Phi_K^{\widetilde{K}}$ obtained, they form an interpolator operator that is called *prolongation operator* in multigrid literature. An example of a basis function is represented on Fig. 1.8(a). Once these basis functions are computed, the approximate fine scale pressure $p^{msfv}(x)$ is interpolated as a linear combination of the primal coarse cell pressures as follows

$$p(\mathbf{x}) \approx p^{msfv}(\mathbf{x}) = \sum_{K \in M_H} \bar{p}_K \left[\sum_{\widetilde{K} \in \widetilde{M}_K} \Phi_K^{\widetilde{K}}(\mathbf{x}) \right] \tag{1.51}$$

and the primal coarse cell pressures$\bar{p}_K, K \in M_H$ are obtained from the conservation equation in each primal coarse cell K defining the set of linear coarse scale equations.

For transport or two-phase flow application, the reconstruction of mass conservative fine fluxes is essential. In order to ensure that, a post processing steps is designed. Once the approximate multiscale pressure obtained $p^{msfv}(\mathbf{x})$, small fluxes $q(\mathbf{x})$ across the *dual* coarse cells boundaries are computed and cast in a source term f'. Then the approximate multiscale pressure is corrected solving the following system on each $\widetilde{K} \in \widetilde{M}_H$:

$$\begin{cases} -\boldsymbol{\nabla}\cdot(\frac{\mathbf{K(x)}}{\mu}\boldsymbol{\nabla}p) & = f' \\ f' & = \frac{\int_{\partial\tilde{K}} q d\sigma}{\int_{\tilde{K}} dx} \end{cases} \tag{1.52}$$

Following these steps, the reconstructed pressure field is both divergence free and consistent with basis functions.

Correction functions formulation

A second kind of basis function is then introduced (Lunati and Jenny, 2008; Jenny and Lunati, 2009) to deal with non-homogeneous term in the equation Eq.1.9. These are called *correction functions* and denoted $\Phi_*^{\tilde{K}}$. In the same way as the *basis functions*, they are obtained on the dual coarse grid $\widetilde{M}_H$ for homogeneous boundary condition and considering the source term f. The system to solve is then written :

$$\begin{cases} \boldsymbol{\nabla}\cdot\frac{-\mathbf{K(x)}}{\mu}\boldsymbol{\nabla}\Phi_*^{\widetilde{K}} & = f \qquad in\ \widetilde{K}, \\ \boldsymbol{\nabla}_\perp\cdot\frac{-\mathbf{K(x)}}{\mu}\boldsymbol{\nabla}\Phi_*^{\widetilde{K}} & = 0 \qquad on\ \partial\widetilde{K}, \\ \Phi_*^{\widetilde{K}}(\mathbf{x}_L) & = 0, \quad L \in M_{\widetilde{K}}. \end{cases} \tag{1.53}$$

Then the reconstruction step is modified to include these new terms :

$$p(\mathbf{x}) \approx p^{msfv}(\mathbf{x}) = \sum_{K\in M_H} \bar{p}_K \left[\sum_{\widetilde{K}\in\widetilde{M}_K} \Phi_K^{\widetilde{K}}(\mathbf{x})\right] + \sum_{\widetilde{K}\in\widetilde{M}_H} \Phi_*^{\widetilde{K}}(\mathbf{x}) \tag{1.54}$$

Iterative formulation

The iterative MsFv (*i-MsFv*)(Hajibeygi et al., 2008) is based on the iterative improvement of this localization assumption Eq.1.55 added to the use of a smoothing operator on the approximated multiscale pressure of Eq.1.54 (*e.g.* line-relaxation operator). Let introduce a weaker boundary condition for Eq.1.53 such as :

$$r^{\tilde{K}\,(\nu-1)} = \mathbf{n}^{\tilde{K}}\cdot(\frac{-\mathbf{K(x)}}{\mu}\nabla p_s^{(\nu-1)}\cdot\mathbf{n}^{\tilde{K}})\ on\,\partial\tilde{K} \tag{1.55}$$

with $p_s^{(\nu-1)}$, the approximated multiscale pressure after a fixed number of smoothing steps (with smoothing operator such as line relaxation operator). Then the *correction basis* functions $\Phi_*^{\tilde{K}\,(\nu-1)}$ are determined with $r^{\tilde{K}\,(\nu-1)}$ as boundary condition. A new approximated multiscale pressure is obtained for next iteration $p^{msfv\,(\nu)}$which is smoothed again to get $p_s^{(\nu)}$. These steps are repeated for a prescribed number of iterations.

Two-phase flow and further improvements

The extension to two-phase flow is done introducing the total mobility $\lambda_t(S_w)$ as a function of the wetting saturation level S_w as a prefactor of $\mathbf{K}(\mathbf{x})$. A threshold is proposed (Jenny et al., 2005) in order to selectively update the basis functions and the correction functions to recompute at the new level. Indeed, updating these functions on the whole domain at every time step would be costly.

$$\frac{1}{1+\epsilon_\lambda} < \frac{\lambda^n}{\lambda^{n-1}} < 1+\epsilon_\lambda \tag{1.56}$$

The *MsFv* method has known many derivation based on those works. The latest derivation are based on the operator formulation of the method(Lunati and Lee, 2009). This leads to a preconditioner formulation that has even be extended to geomechanics (Wang et al., 2014; Castelletto et al., 2016).

Its use of *primal* and *dual* meshes make difficult its adaptation to unstructured meshes.

1.3.3 *Multiscale Restriction Smoothed Basis* (MsRSB)

In the same vein, the *Multiscale Restriction Smoothed Basis (MsRSB)* method(Møyner and Lie, 2016) has been designed, based on an extensive study of works on Algebraic MultiGrid methods (AMG)(Vaněk et al., 1996). It computes its basis function $\Phi_K^{(\nu=n)}$ iteratively on overlapped support, which are used as in *MsFv* to interpolate (or *prolongate*) its coarse pressure solution to the fine grid, and hence, constructing $p^{msrsb}(\mathbf{x})$, the multiscale approximate pressure. This computation is done using a classical Jacobi smoother. However, in order to keep a conservative resulting fields, some treatments are required on these overlaps; otherwise it spreads over the entire domain. Such a basis function is reproduced on Fig. 1.8(b).

On Fig. 1.7, the different supports on a Cartesian grid are presented. In order to introduce the steps of the algorithm, let us define three different areas associated with the basis functions computation. For a given coarse cell $K \in M_H$:

- the computational support I_K that extends outside of K,
- the overlap's boundary B_K,
- the global boundary inside the overlap region $G \cap I_K$ introducing G as the superposition of all the overlap's boundaries, $G = \bigcup_L B_L$.

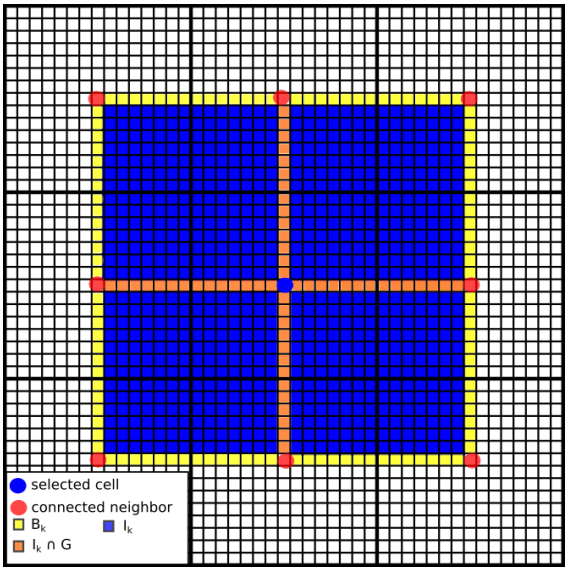

Figure 1.7: *MsRSB:* Definition of supports.

Let $M_h$denote the set of fine cells. For convenience, we identify in the following the domains I_K, B_K and G with their corresponding subsets of fine cells. Starting from the interpolator P_K , whose definition is:

$$\Phi_{i,K}^{(\nu=0)} = \begin{cases} 1 & i \in M_h, i \in M_K \\ 0 & elsewhere \end{cases} \tag{1.57}$$

The method uses successive smoothing iterations $\nu = 0, n$ that go through these steps:

1. Compute the relaxed Jacobi update with $\omega = 2/3$ optimal value for Poisson-like equation for I_K, for each area $K \in M_K$

$$\hat{d}_{i,K} = -\omega \sum_{j \in F} (D^{-1}A)_{i,j} \Phi_{j,K}^{\nu} \tag{1.58}$$

   with A the fine grid operator and D its diagonal.

2. Correct on the overlapping areas, introducing $H_i = \{k \,|\, i \in I_K\}$ collection of coarse cell owner's indexes of a fine cell $i \in G$

$$d_{i,K} = \begin{cases} \hat{d}_{i,K}, & i \in I_K \setminus G, \\ \dfrac{\hat{d}_{i,K} - \Phi_K^{\nu} \sum\limits_{k \in H_i} \hat{d}_{ik}}{1 + \sum\limits_{k \in H_i} \hat{d}_{ik}}, & i \in I_K \cap G, \\ 0, & i \notin I_K \end{cases} \tag{1.59}$$

3. Update $P_{i,K}^{\nu+1} = P_{i,K}^{\nu} + d_{i,K}$, $i \in F$, and evaluate the error $e_K = \underset{i \in I_K \setminus G}{max}(|\hat{d}_{i,K}|)$ on the internal support. Terminate if $e_K < tol$ and set $\Phi_{i,K} = \Phi_{i,K}^{\nu+1}, i \in F$.

The approximate multiscale pressure is then obtained as the following linear combination of the coarse cell pressures$\bar{p}_K, K \in M_H$

$$p^{msrsb}(\mathbf{x}) = \sum_{K \in M_H} \bar{p}_K \Phi_{i,K} \text{ for all } \mathbf{x} \in i,\ i \in M_K.$$

and the coarse scale system is obtained from the conservation equations in each coarse cell $K \in M_H$. As for the *MsFv, MsRSB* computes conservative coarse fluxes but has to add the same step to ensure local mass conservation.

Its framework is very flexible and allow to use unstructured meshes with single focus on the different support definition.

1.3.4 *Finite volume Mixed Hybrid Multiscale Method* (Fv-MHMM)

The *Finite volume Mixed Hybrid Multiscale Method* (*Fv-MHMM*)(Franc et al., 2017) has been proposed based on the formulation proposed by *Harder et al.*(Harder et al., 2013a, 2015). The primal hybrid formulation(Raviart and Thomas, 1977a) uses Lagrange multipliers λ to weakly ensure flux continuity through coarse element[1] interfaces. Its variational formulation is written as :

find $(p, \lambda) \in V \times \Lambda$ *such that*:

$$\begin{aligned} \int_\Omega \frac{-\mathbf{K}(\mathbf{x})}{\mu} \boldsymbol{\nabla} p \cdot \boldsymbol{\nabla} q \, d\mathbf{x} + \sum_{K \in M_H} \int_{\partial K} \lambda \mathbf{n} \cdot \mathbf{n}_K \, q|_K d\sigma \\ + \sum_{K \in M_H} \int_{\partial K} \mu \mathbf{n} \cdot \mathbf{n}_K q|_K d\sigma \\ = \int_\Omega f q d\mathbf{x} + \int_{\partial\Omega} \mu p_g d\sigma \quad \text{for all } (v, q) \in V \times \Lambda, \end{aligned} \tag{1.60}$$

where V is the broken Sobolev space $H^1(M_H)$ defined as:

$$H^1(M_H) = \{q \in L_2(\Omega) :\ q|_K \in H^1(K),\ K \in M_H\}, \tag{1.61}$$

[1]Raviart and Thomas works is formulated in the finite element method framework.

Λ stands for the following Lagrange multipliers space

$$\Lambda := \{\mu \in \prod_{K \in M_H} H^{-\frac{1}{2}}(\partial K) : \exists \boldsymbol{\sigma} \in H_{div}(\Omega) \text{ s.t. } \mu|_{\partial K} = \boldsymbol{\sigma} \cdot \mathbf{n}|_{\partial K},\ K \in M_H\}, \tag{1.62}$$

∇q is the broken gradient equal to $\nabla q|_K$ on each coarse cell $K \in M_H$, and $H^{-\frac{1}{2}}(\partial K)$ is the dual space of the space $H^{\frac{1}{2}}(\partial K)$ spanned by the traces on ∂K of functions in $H^1(K)$. $H_{div}(\Omega)$ is defined as:

$$H_{div}(\Omega) := \{\boldsymbol{\sigma} \in [L^2(\Omega)]^D : \boldsymbol{\nabla} \cdot \boldsymbol{\sigma} \in L^2(\Omega)\} \tag{1.63}$$

Core method

Let F_H be the set of coarse face σ of M_H. In order to construct a multiscale algorithm from Eq.1.60, let split the space V for pressure values into a direct sum of, on one hand, V_0, a cellwise constant polynomials on the coarse mesh and on the other hand a collection of subspace W_K of V with functions in $H^1(K)$ with zero mean values on K. Hence, the following orthogonal decomposition stands:

$$V = V_0 \oplus \bigoplus_{K \in M_H} W_K \tag{1.64}$$

It introduces a multiscale decomposition,

- on the coarse scale, a *global problem (GP)* has to be assembled and solved to find $(\bar{p}, \lambda) \in V_0 \times \Lambda$. As in the method presented above, $\bar{p}$ is a cellwise constant pressure level. The Lagrange multiplier λ can be here regarded as a coarse fluxes through the corresponding coarse face.

- on the fine scale, as previously a collection of coarse cell partitioned problems that provides us with basis functions.

An other decomposition between the *local lambda problems (LPL)* for Lagrange multipliers (or coarse fluxes) driven effects and the *local source problem* for source driven effects. They respectively reads,

Find $\Phi_K \in W_K$ *such that*:

$$\int_K -\frac{\mathbf{K}(\mathbf{x})}{\mu} \boldsymbol{\nabla} \Phi_K \cdot \boldsymbol{\nabla} \chi_K d\mathbf{x} + \int_{\partial K} \lambda \mathbf{n} \cdot \mathbf{n}_K \chi_K d\sigma = 0 \quad \text{for all } \chi_K \in W_K, \tag{1.65}$$

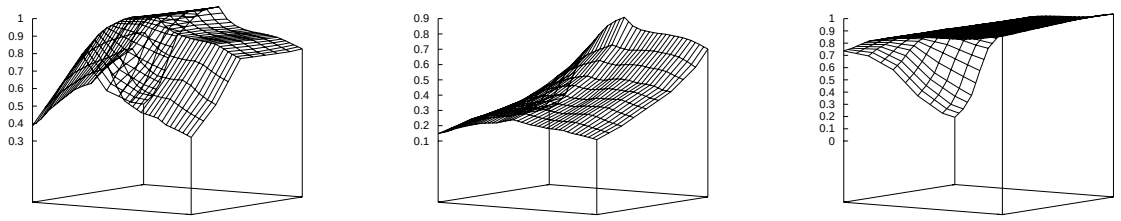

(a) *MsFv* basis (b) *MsRSB* basis (c) *FV-MHMM* basis

Figure 1.8: *MsFv, MsRSB* and *FV-MHMM* basis function on an heterogeneous permeability background

Find $\Phi_K^* \in W_K$ *such that*:

$$\int_K -\frac{\mathbf{K}(\mathbf{x})}{\mu}\boldsymbol{\nabla}\Phi_K^* \cdot \boldsymbol{\nabla}\chi_K^* d\mathbf{x} = \int_K f\chi_K^* d\mathbf{x} \quad \text{for all } \chi_K^* \in W_K, \tag{1.66}$$

setting $\Phi_K = T_K\lambda$ and $\Phi_K^* = \hat{T}_K f$.

Then then *global problem* is assemble using these basis functions :

Find $\bar{p}_K \in \mathbb{R}$, $K \in M_H$ *and* $\lambda \in \Lambda$ *such that:*

$$\begin{cases} \displaystyle\sum_{K\in M_H} \int_{\partial K} \lambda \mathbf{n}\cdot\mathbf{n}_K d\sigma = \int_K f d\mathbf{x} \quad \text{for all } K \in M_H, \\ \displaystyle\sum_{K\in M_H} \int_{\partial K} \mu \mathbf{n}\cdot\mathbf{n}_K(\bar{p}_K + T_K\lambda + \hat{T}_K f) d\sigma = \int_{\partial\Omega} \mu p_g \quad \text{for all } \mu \in \Lambda. \end{cases} \tag{1.67}$$

This is implemented using Two Point Flux Approximation (TPFA) for local problems on each coarse cell $K \in M_H$ and by approximating space Λ for Lagrange multipliers by a subspace Λ_H. Most of the time, the subspace Λ_H is chosen to be a vector space of polynomials $\mathbb{P}_l(\sigma)$ on each coarse face $\sigma \in F_H$, then denoted by $\Lambda_{l,l=0,1,2}$.As an illustration, a typical basis function is represented on Fig. 1.8(c).

It can be noted that *Fv-MHMM* is both locally and globally conservative as the conservative flux adjustment steps from *MsFv* and *MsRSB* is included directly in local problems (*LPL* and *LPS).*

Weighting schemes

Using such an algorithm on real case reveals that the construction of basis function should be fitted to the fine scale heterogeneities details. Indeed, in medium such as channelized medium that exhibits long correlation lengths with respect to the domain size, the error

level can be lowered by orders of magnitude (Franc et al., 2017). In order to adapt the basis function to its fine scale permeability support, two main weighting schemes are proposed as pre-processing step.

The less costly solution is to weight the function of $\mathbb{P}_l(\sigma)$ used to span the space Λ_l on each coarse face σ with respect to the fine scale transmissivities along the coarse faces. It provides us with a new space, which is piece-wisely adapted to the selected face. Let us then define the *transmissivity weighting scheme (tw)* for $\sigma \in F_H$:

- $F_{h,\sigma}$ denotes the set of fine faces of σ ,
- $T_e$denote the transmissivity of the fine face $e \in F_{h,\sigma}$.

Let the function λ_σ^{tw} be defined on σ such that

$$\lambda_\sigma^{tw}(\mathbf{x}) = \frac{T_e}{\sum_{e \in F_{h,\sigma}} T_e} \text{ for all } \mathbf{x} \in e,\ e \in F_{h,\sigma}. \tag{1.68}$$

Then the weighted space Λ_l is spanned on each coarse faceσ by $\lambda_\sigma \mathbb{P}_l(\sigma)$.

An alternative is the *multiscale two-point flux approximation (mstpfa)*(Møyner and Lie, 2014). It is also based on the construction of weighting space $\lambda_\sigma^{mstpfa}\mathbb{P}_l(\sigma)$, whose weighting function λ_σ^{mstpfa} is extracted from a cross-flow simulation across the coarse face $\sigma \in F_H$. The support $M_L \cup M_K$ used to perform this simulation is the fine cells that are included in the neighboring coarse cells $\mathcal{N}(\sigma) = \{K, L\}$. Then , the weighting scheme is defined as :

$$\lambda_\sigma(\mathbf{x}) = \frac{\phi(w_e)}{\sum_{e \in F_{h,\sigma}} \phi(w_e)} \text{ for all } \mathbf{x} \in e,\ e \in \overline{F_{h,\sigma}}, \tag{1.69}$$

$$\int_{K \cup L} \nabla \cdot (\mathbf{K}(\mathbf{x}) \nabla \cdot w_e) dx = 0$$

$$\begin{cases} w_e = p^d & if\ \mathbf{n}_\sigma^{\mathbf{K}} \cdot \mathbf{n}_{\partial(K \cup L)} > 0 \\ w_e = -p^d & if\ \mathbf{n}_\sigma^{\mathbf{K}} \cdot \mathbf{n}_{\partial(K \cup L)} < 0 \\ \boldsymbol{\nabla \cdot}(w_e) \cdot \mathbf{n} = 0 & elsewhere \end{cases} \tag{1.70}$$

$$\phi(w_e) = T_e(w_L - w_K).$$

Both these weighting schemes are illustrated on Fig. 6.1.

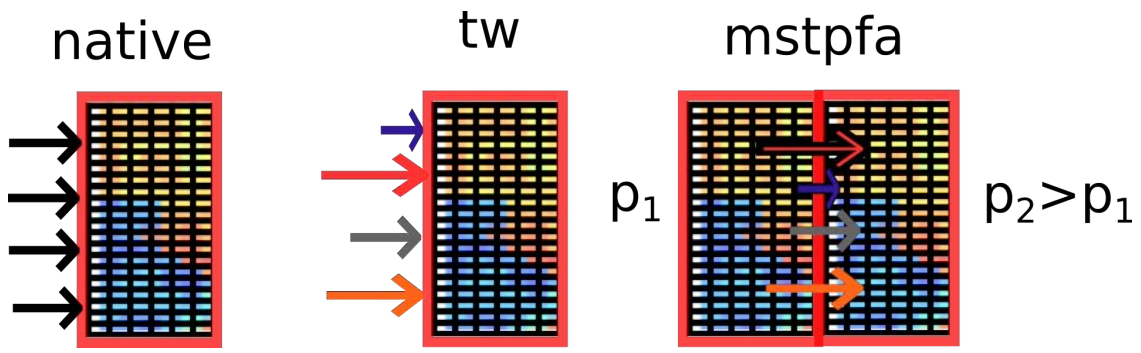

Figure 1.9: Illustration of different weighting schemes (*native, tw, mstpfa)*

References

Aarnes, J.: 2004, On the use of a mixed multiscale finite element method for greaterflexibility and increased speed or improved accuracy in reservoir simulation, *Multiscale Modeling & Simulation* .

Ababou, R.: 1994, Solution of stochastic groundwater flow by infinite series, and convergence of the one-dimensional expansion, *Stochastic Hydrology and Hydraulics* **8**(2), 139–155.

Ababou, R.: 1996, *Random porous media flow on large 3-D grids: numerics, performance, and application to homogenization*, Springer.

Ahmadi, A.: 1992, *Utilisation de propriétés équivalentes dans les modèles de reservoir: Cas des écoulements diphasiques incompressibles*, PhD thesis.

Ahmadi, A. and Quintard, M.: 1996, Large-scale properties for two-phase flow in random porous media, *Journal of hydrology* **183**(1), 69–99.

Arbogast, T.: 2000, Numerical subgrid upscaling of two-phase flow in porous media, *Numerical treatment of multiphase flows in porous media*, Springer, pp. 35–49.

Arbogast, T.: 2002a, Implementation of a locally conservative numerical subgrid upscaling scheme for two-phase darcy flow, *Computational Geosciences* **6**(3-4), 453–481.

Artus, V.: 2003, *Mise à l'échelle des écoulements diphasiques dans les milieux poreux hétérogènes*, PhD thesis, Paris 6.

Artus, V. and Noetinger, B.: 2004, Up-scaling two-phase flow in heterogeneous reservoirs: current trends, *Oil & gas science and technology* **59**(2), 185–195.

Audigane, P. and Blunt, M. J.: 2004, Dual mesh method for upscaling in waterflood simulation, *Transport in Porous Media* **55**(1), 71–89.

Aziz, K. et al.: 1993, Reservoir simulation grids: opportunities and problems, *Journal of Petroleum Technology* **45**(07), 658–663.

Babaei, M. and King, P. R.: 2012, A modified nested-gridding for upscaling–downscaling in reservoir simulation, *Transport in porous media* **93**(3), 753–775.

Barker, J. W., Thibeau, S. et al.: 1997, A critical review of the use of pseudorelative permeabilities for upscaling, *SPE Reservoir Engineering* **12**(02), 138–143.

Berkowitz, B. and Balberg, I.: 1993, Percolation theory and its application to groundwater hydrology, *Water Resources Research* **29**(4), 775–794.

Bøe, Ø.: 1994, Analysis of an upscaling method based on conservation of dissipation, *Transport in Porous Media* **17**(1), 77–86.

Bourgeat, A.: 1984, Homogenized behavior of two-phase flows in naturally fractured reservoirs with uniform fractures distribution, *Computer Methods in Applied Mechanics and Engineering* **47**(1), 205–216.

Bourgeat, A., Quintard, M. and Whitaker, S.: 1988, Elements de comparaison entre la methode d homogeneisation et la methode de prise de moyenne avec fermeture, *CRAS* .

Brooks, R. and Corey, A.: 1964, Hydraulic Properties of Porous Media, *Hydrol. Pap.*

Buckley, S. and Leverett, M.: 1942, Mechanism of fluid displacement in sands, *Trans. AIME* **146**, 107–116.

Cardwell Jr, W., Parsons, R. et al.: 1945, Average permeabilities of heterogeneous oil sands, *Transactions of the AIME* **160**(01), 34–42.

Castelletto, N., Hajibeygi, H. and Tchelepi, H. A.: 2016, Multiscale finite-element method for linear elastic geomechanics, *Journal of Computational Physics* .

Chen, T., Gerritsen, M. G., Lambers, J. V. and Durlofsky, L. J.: 2010, Global variable compact multipoint methods for accurate upscaling with full-tensor effects, *Computational Geosciences* **14**(1), 65–81.

Chen, Y. and Durlofsky, L. J.: 2006, Adaptive local–global upscaling for general flow scenarios in heterogeneous formations, *Transport in porous Media* **62**(2), 157–185.

Chen, Z. and Hou, T.: 2003b, A mixed multiscale finite element method for elliptic problems with oscillating coefficients, *Mathematics of Computation* .

Coats, K., Nielsen, R., Terhune, M. H., Weber, A. et al.: 1967, Simulation of three-dimensional, two-phase flow in oil and gas reservoirs, *Society of Petroleum Engineers Journal* **7**(04), 377–388.

Dagan, G.: 1979, Models of groundwater flow in statistically homogeneous porous formations, *Water Resources Research* **15**(1), 47–63.

Dagan, G.: 1982, Stochastic modeling of groundwater flow by unconditional and conditional probabilities: 1. conditional simulation and the direct problem, *Water Resources Research* **18**(4), 813–833.

Dake, L. P.: 1983, *Fundamentals of reservoir engineering*, Vol. 8, Elsevier.

De Marsily, G.: 1986, Quantitative hydrogeology, *Technical report*, Paris School of Mines, Fontainebleau.

Durlofsky, L. J., Jones, R. C. and Milliken, W. J.: 1997, A nonuniform coarsening approach for the scale-up of displacement processes in heterogeneous porous media, *Advances in Water Resources* **20**(5), 335–347.

Durlofsky, L. J. et al.: 1997, Use of higher moments for the description of upscaled, process independent relative permeabilities, *SPE Journal* **2**(04), 474–484.

Dykstra, H. and Parsons, R.: 1950, The prediction of oil recovery by waterflood, *Secondary Recovery of Oil in the United States* **2**, 160–174.

Efendiev, Y., Galvis, J. and Hou, T. Y.: 2013, Generalized multiscale finite element methods (gmsfem), *Journal of Computational Physics* .

Fadili, A.: 2001, *Ecoulements diphasiques en reservoirs petroliers heterogenes: homogeneisation stochastique*, PhD thesis, Toulouse, INPT.

Fayers, F. and Hewett, T.: 1992, A review of current trends in petroleum reservoir description and assessment of the impacts on oil recovery, *Advances in water resources* **15**(6), 341–365.

Fenton, G. A. and Griffiths, D.: 1993, Statistics of block conductivity through a simple bounded stochastic medium, *Water Resources Research* **29**(6), 1825–1830.

Franc, J., Jeannin, L., Debenest, G. and Masson, R.: 2017, Fv-mhmm methods for reservoir modeling, *Computational Geosciences* .

Freeze, R. A.: 1975, A stochastic-conceptual analysis of one-dimensional groundwater flow in nonuniform homogeneous media, *Water Resources Research* **11**(5), 725–741.

Gautier, Y., Blunt, M. J. and Christie, M. A.: 1999, Nested gridding and streamline-based simulation for fast reservoir performance prediction, *Computational Geosciences* **3**(3-4), 295–320.

Gelhar, L.: 1977, Effects of hydraulic conductivity variations on groundwater flows, *Hydraulic Problems Solved by Stochastic Methods* .

Gelhar, L. W. and Axness, C. L.: 1983, Three-dimensional stochastic analysis of macrodispersion in aquifers, *Water Resources Research* **19**(1), 161–180.

Gerritsen, M. and Lambers, J.: 2008, Integration of local–global upscaling and grid adaptivity for simulation of subsurface flow in heterogeneous formations, *Computational Geosciences* **12**(2), 193–208.

Gholami, V., Mohaghegh, S. D. et al.: 2009, Intelligent upscaling of static and dynamic reservoir properties, *SPE Annual Technical Conference and Exhibition*, Society of Petroleum Engineers.

Gomez-Hernandez, J. and Journel, A.: 1990, Stochastic characterization of grid-block permeabilities: from point values to block tensors, *ECMOR II-2nd European Conference on the Mathematics of Oil Recovery*.

Graham, W. and McLaughlin, D.: 1989, Stochastic analysis of nonstationary subsurface solute transport: 2. conditional moments, *Water Resources Research* **25**(11), 2331–2355.

Guibert, R., Horgue, P., Debenest, G. and Quintard, M.: 2015, A comparison of various methods for the numerical evaluation of porous media permeability tensors from pore-scale geometry, *Mathematical Geosciences* pp. 1–19.

Guyon, E., Hulin, J.-P. and Lenormand, R.: 1984, Application de la percolation à la physique des milieux poreux, *Annales des mines*, number 5-6, Dumas, pp. 17–40.

Guzman, R., Giordano, D., Fayers, F., Godi, A., Aziz, K. et al.: 1996, Evaluation of dynamic pseudo functions for reservoir simulation, *SPE Annual Technical Conference and Exhibition*, Society of Petroleum Engineers.

Hajibeygi, H., Bonfigli, G., Hesse, M. A. and Jenny, P.: 2008, Iterative multiscale finite-volume method, *Journal of Computational Physics* **227**(19), 8604–8621.

Hansen, A., Roux, S. R., Aharony, A., Feder, J., Jøssang, T. and Hardy, H.: 1997, Real-space renormalization estimates for two-phase flow in porous media, *Transport in porous media* **29**(3), 247–279.

Harder, C., Paredes, D. and Valentin, F.: 2013a, A family of multiscale hybrid-mixed finite element methods for the darcy equation with rough coefficients, *Journal of Computational Physics* **245**, 107–130.

Harder, C., Paredes, D. and Valentin, F.: 2013b, A family of multiscale hybrid-mixed finite element methods for the darcy equation with rough coefficients, *Journal of Computational Physics* .

Harder, C., Paredes, D. and Valentin, F.: 2015, On a multiscale hybrid-mixed method for advective-reactive dominated problems with heterogeneous coefficients, *Multiscale Modeling & Simulation* .

Hashin, Z. and Shtrikman, S.: 1963, Conductivity of polycrystals, *Physical Review* **130**(1), 129.

Henry, D.: 1856, *Les fontaines publiques de la ville de Dijon.*

Hernandez, J. G.: 1991, *A stochastic approach to the simulation of block conductivity fields conditioned upon data measured at a smaller scale*, University of California-Department of Earth Sciences.

Hewett, T. A. and Yamada, T.: 1997, Theory for the semi-analytical calculation of oil recovery and effective relative permeabilities using streamtubes, *Advances in Water resources* **20**(5), 279–292.

Hewett, T. and Behrens, R.: 1991, Scaling laws in reservoir simulation and their use in a hybrid finite difference/streamtube approach to simulation the effects of permeability heterogeneity, *Academic Press Inc., London* pp. 402–441.

Holden, L. and Lia, O.: 1992, A tensor estimator for the homogenization of absolute permeability, *Transport in porous media* **8**(1), 37–46.

Holden, L. and Nielsen, B. F.: 2000, Global upscaling of permeability in heterogeneous reservoirs; the output least squares (ols) method, *Transport in Porous Media* **40**(2), 115–143.

Horgue, P., Guibert, R., Gross, H., Creux, P. and Debenest, G.: 2015, Efficiency of a two-step upscaling method for permeability evaluation at darcy and pore scales, *Computational Geosciences* **19**(6), 1159.

Horgue, P., Soulaine, C., Franc, J., Guibert, R. and Debenest, G.: 2015, An open-source toolbox for multiphase flow in porous media, *Computer Physics Communications* **187**, 217–226.

Hou, T. and Wu, X.-H.: 1997, A multiscale finite element method for elliptic problems in composite materials and porous media, *Journal of computational physics* .

Hou, T. Y., Westhead, A. and Yang, D.: 2006, A framework for modeling subgrid effects for two-phase flows in porous media, *Multiscale Modeling & Simulation* **5**(4), 1087–1127.

Jacks, H. H., Smith, O. J., Mattax, C. et al.: 1973, The modeling of a three-dimensional reservoir with a two-dimensional reservoir simulator-the use of dynamic pseudo functions, *Society of Petroleum Engineers Journal* **13**(03), 175–185.

Jenny, P., Lee, S. H. and Tchelepi, H. A.: 2005, Adaptive multiscale finite-volume method for multiphase flow and transport in porous media, *Multiscale Modeling & Simulation* **3**(1), 50–64.

Jenny, P., Lee, S. and Tchelepi, H.: 2003, Multi-scale finite-volume method for elliptic problems in subsurface flow simulation, *Journal of Computational Physics* **187**(1), 47–67.

Jenny, P. and Lunati, I.: 2009, Modeling complex wells with the multi-scale finite-volume method, *Journal of Computational Physics* **228**(3), 687–702.

Jonoud, S. and Jackson, M. D.: 2008, New criteria for the validity of steady-state upscaling, *Transport in Porous Media* **71**(1), 53–73.

Journel, A., Deutsch, C., Desbarats, A. et al.: 1986, Power averaging for block effective permeability, *SPE California Regional Meeting*, Society of Petroleum Engineers.

Killough, J., Foster Jr, H. et al.: 1979, Reservoir simulation of the empire abo field: The use of pseudos in a multilayered system, *Society of Petroleum Engineers Journal* **19**(05), 279–288.

King, P.: 1989, The use of renormalization for calculating effective permeability, *Transport in porous media* **4**(1), 37–58.

King, P., Muggeridge, A. and Price, W.: 1993, Renormalization calculations of immiscible flow, *Transport in Porous Media* **12**(3), 237–260.

Kitanidis, P. K.: 1988, Prediction by the method of moments of transport in a heterogeneous formation, *Journal of Hydrology* **102**(1), 453–473.

Kruel Romeu, R.: 1994, *Ecoulement en milieux hétérogènes: prise de moyenne de perméabilité en régimes permanent et transitoire*, PhD thesis.

Kyte, J. R., Berry, D. et al.: 1975, New pseudo functions to control numerical dispersion, *Society of Petroleum Engineers Journal* **15**(04), 269–276.

Langlo, P. and Espedal, M. S.: 1994, Macrodispersion for two-phase, immiscible flow in porous media, *Advances in Water Resources* **17**(5), 297–316.

Le Floch, S., Merlin, F.-X., Guillerme, M., Dalmazzone, C. and Le Corre, P.: 1999, A field experimentation on bioremediation: bioren, *Environmental technology* **20**(8), 897–907.

Lenormand, R.: 1995, A stream tube model for miscible flow, *Transport in Porous Media* **18**(3), 245–261.

Lenormand, R. and Fenwick, D.: 1998, MDU: A Model For Dynamic Upscaling, *19th IEA collaborative project on enhanced oil recovery.*, Carmel, California, USA.

Lenormand, R. and Wang, B.: 1995, A stream tube model for miscible flow, *Transport in Porous Media* **18**(3), 263–282.

Lenormand, R. et al.: 1996, Transport equations for fluid displacements in stratified porous media: The mhd model, *SPE Journal* **1**(02), 179–190.

Leverett, M. C.: 1940, Capillary behavior in porous solids, *Trans. AIME* **142**(1), 152–169.

Lunati, I. and Jenny, P.: 2008, Multiscale finite-volume method for density-driven flow in porous media, *Computational Geosciences* **12**(3), 337–350.

Lunati, I. and Lee, S. H.: 2009, An operator formulation of the multiscale finite-volume method with correction function, *Multiscale modeling & simulation* **8**(1), 96–109.

Luo, H., Laouafa, F., Debenest, G. and Quintard, M.: 2015, Large scale cavity dissolution: From the physical problem to its numerical solution, *European Journal of Mechanics-B/Fluids* **52**, 131–146.

Matheron, G.: 1967, *Eléments pour une théorie des milieux poreux*, Masson.

Matheron, V.: 1968, Composition des perméabilités en milieux poreux hétérogène: critique de la règle de pondération géométrique, *rue* **23**(2).

Mattila, K., Puurtinen, T., Hyväluoma, J., Surmas, R., Myllys, M., Turpeinen, T., Robertsen, F., Westerholm, J. and Timonen, J.: 2016, A prospect for computing in porous materials research: Very large fluid flow simulations, *Journal of Computational Science* **12**, 62–76.

Møyner, O. and Lie, K.-A.: 2014, A multiscale two-point flux-approximation method, *Journal of Computational Physics* .

Møyner, O. and Lie, K.-A.: 2016, A multiscale restriction-smoothed basis method for high contrast porous media represented on unstructured grids, *Journal of Computational Physics* .

Muskat, M.: 1949, *Physical principles of oil production*, mcgraw-hil edn, New York.

Noetinger, B.: 1994, The effective permeability of a heterogeneous porous medium, *Transport in porous media* **15**, 99–127.

Nœtinger, B.: 2000, Computing the effective permeability of log-normal permeability fields using renormalization methods, *Comptes Rendus de l'Académie des Sciences-Series IIA-Earth and Planetary Science* **331**(5), 353–357.

Panfilov, M. and Floriat, S.: 2004, Nonlinear two-phase mixing in heterogeneous porous media, *Transport in porous media* **57**(3), 347–375.

Peaceman, D. W. et al.: 1996, Calculation of transmissibilities of gridblocks defined by arbitrary corner point geometry, Society of Petroleum Engineers.

Pickup, G. E. and Stephen, K. D.: 2000, An assessment of steady-state scale-up for small-scale geological models, *Petroleum Geoscience* **6**(3), 203–210.

Pickup, G., Stephen, K., Ma, J., Zhang, P. and Clark, J.: 2005, Multi-stage upscaling: selection of suitable methods, *Transport in porous media* **58**(1-2), 191–216.

Poley, A. D.: 1988, Effective permeability and dispersion in locally heterogeneous aquifers, *Water Resources Research* **24**(11), 1921–1926.

Ponting, D. K.: 1989, Corner point geometry in reservoir simulation, *ECMOR I-1st European Conference on the Mathematics of Oil Recovery*.

Portella, R., Hewett, T. et al.: 1997, Fast 3-d reservoir simulation and applications using streamlines, *Latin American and Caribbean Petroleum Engineering Conference*, Society of Petroleum Engineers.

Prevost, M., Edwards, M. G., Blunt, M. J. et al.: 2002, Streamline tracing on curvilinear structured and unstructured grids, *SPE Journal* **7**, Society of Petroleum Engineers.

Quintard, M. and Whitaker, S.: 1987, Ecoulement monophasique en milieu poreux: Effet des heterogeneites locales, *Journal de Mecanique Theorique Appliquee* **6**(5), 691–726.

Quintard, M. and Whitaker, S.: 1988, Two-phase flow in heterogeneous porous media: The method of large-scale averaging, *Transport in porous media* **3**(4), 357–413.

Quintard, M. and Whitaker, S.: 1994, Convection, dispersion, and interfacial transport of contaminants: Homogeneous porous media, *Advances in Water resources* **17**(4), 221–239.

Quintard, M. and Whitaker, S.: 1999, Fundamentals of transport equation formulation for two-phase flow in homogeneous and heterogeneous porous media, *Vadose Zone Hydrology: Cutting Across Disciplines: Cutting Across Disciplines* .

Raviart, P.-A. and Thomas, J.: 1977a, Primal hybrid finite element methods for 2nd order elliptic equations, *Mathematics of computation* .

Renard, P. and De Marsily, G.: 1997, Calculating equivalent permeability: a review, *Advances in water resources* **20**(5), 253–278.

Rubin, Y. and Gómez-Hernández, J. J.: 1990, A stochastic approach to the problem of upscaling of conductivity in disordered media: Theory and unconditional numerical simulations, *Water Resources Research* **26**(4), 691–701.

Saez, A., Otero, C. J. and Rusinek, I.: 1989, The effective homogeneous behavior of heterogeneous porous media, *Transport in Porous Media* **4**(3), 213–238.

Sagar, B.: 1978, Galerkin finite element procedure for analyzing flow through random media, *Water Resources Research* **14**(6), 1035–1044.

Sheldon, J. W., Zondek, B. and Cardwell, W. T.: 1959, One-dimensional, incompressible, non-capillary, two-phase fluid flow in a porous medium, *T. SPE. AIME* **216**, 290–296.

Stiles, W. E. et al.: 1949, Use of permeability distribution in water flood calculations, *Journal of Petroleum Technology* **1**(01), 9–13.

Stone, H. et al.: 1991, Rigorous black oil pseudo functions, *SPE Symposium on reservoir simulation*, Society of Petroleum Engineers.

Thiele, M. R.: 1994, *Modeling multiphase flow in heterogeneous media using streamtubes*, PhD thesis, stanford university.

Thiele, M. R., Batycky, R. P., Blunt, M., Orr Jr, F. et al.: 1996, Simulating flow in heterogeneous systems using streamtubes and streamlines, *SPE Reservoir Engineering* **11**(01), 5–12.

Van Genuchten, M. T.: 1980, A Closed-form Equation for Predicting the Hydraulic Conductivity of Unsaturated Soils1, *Soil Sci. Soc. Am. J.* **44**(5), 892.

Van Meurs, P.: 1956, The use of transparent three-dimensional models for studying the mechanism of flow processes in oil reservoirs, *Paper presented at Petroleum Branch Fall Meeting in Los Angeles*.

Vaněk, P., Mandel, J. and Brezina, M.: 1996, Algebraic multigrid by smoothed aggregation for second and fourth order elliptic problems, *Computing* .

Verdiere, S. and Vignal, M.: 1998, Numerical and theoretical study of a dual mesh method using finite volume schemes for two phase flow problems in porous media, *Numerische Mathematik* **80**(4), 601–639.

Wang, Y., Hajibeygi, H. and Tchelepi, H. A.: 2014, Algebraic multiscale solver for flow in heterogeneous porous media, *Journal of Computational Physics* .

Whitaker, S.: 1998, *The method of volume averaging*, Vol. 13, Springer Science & Business Media.

White, C., Horne, R. et al.: 1987, Computing absolute transmissibility in the presence of fine-scale heterogeneity, *SPE Symposium on Reservoir Simulation*, Society of Petroleum Engineers.

Winter, C. L., Newman, C. and Neuman, S. P.: 1984, A perturbation expansion for diffusion in a random velocity field, *SIAM Journal on Applied Mathematics* **44**(2), 411–424.

Wu, J.: 2013, A regional uplayering technique for preserving reservoir heterogeneities, *Mathematical Geosciences* **45**(3), 359–375.

Yokoyama, Y., Lake, L. W. et al.: 1981, The effects of capillary pressure on immiscible displacements in stratified porous media, *SPE Annual Technical Conference and Exhibition*, Society of Petroleum Engineers.

Zhang, P., Pickup, G. E., Christie, M. A. et al.: 2008, A new practical method for upscaling in highly heterogeneous reservoir models, *SPE Journal* **13**(01), 68–76.

Chapter 2

An open-source toolbox for multiphase flow in porous media

Contents

Résumé en français

Ce chapitre concerne l'implémentation de l'algorithme IMplicit Pressure Explicit Saturation (IMPES) dédié à la simulation d'écoulements darcéens sur la plateforme de calcul parallélisée OpenFOAM®. Cette plateforme favorise le développement d'algorithmes séquentiellement couplés, c'est donc naturellement que l'IMPES y est adapté. Les modèles classiques de *Brooks et Corey* et de *Van Genuchten* sont proposés pour modéliser la dépendance explicite des perméabilités relatives et de la pression capillaire à la saturation en fluide mouillant. De plus, une condition limite de couplage entre un flux imposé et son gradient de pression associé compatible avec la condition limite en saturation est aussi implémentée. La vérification du bon fonctionnement est faite pour les effets visqueux et gravitaire via la comparaison avec la résolution semi-analytique du cas de *Buckley Leverett ;* pour les effets capillaire et gravitaire, on se réfère à la solution stationnaire de l'équilibre capillaro-gravitaire.

Enfin, l'efficacité parallèle est testée sur un cas de digitation visqueuse. Un test de *scaling* est effectué et montre un comportement linéaire à super-linéaire pour 16 à 512 coeurs de calculs.

Ce chapitre a fait l'objet de la publication "*An open-source toolbox for multiphase flow in porous media"*(Horgue et al., 2015), dans la revue *Computer Physics Communications,* en Février 2015.

Multiphase flow in porous media provides a wide range of applications: from the environmental understanding (aquifer, site-pollution) to industrial process improvements (oil production, waste management). Modeling of such flows involves specific volume-averaged equations and therefore specific computational fluid dynamics (CFD) tools. In this work, we developed a toolbox for modeling multiphase flows in porous media with OpenFOAM®, an open-source platform for CFD. The underlying idea of this approach is to provide an easily adaptable tool that can be used in further studies to test new mathematical models or numerical methods. The package provides the most common effective properties models of the literature (relative permeability, capillary pressure) and specific boundary conditions related to porous media flows. To validate this package, two-phase flow solvers based on the IMPES method (IMplicit Pressure Explicit Saturation) are developed in the toolbox. The numerical validation is performed by comparison with analytical solutions on academic cases. Then, a satisfactory parallel efficiency of the solver is shown on a more complex configuration.

2.1 Introduction

Simulation of multiphase fluid flow in heterogeneous porous media is of great importance in many areas of science and engineering including:

- hydrology and groundwater flow,
- oil and gas reservoirs,
- gas-liquid contactors,
- waste management, biodegradation, and so on.

Objective of this work is to develop the basis of an open-source numerical tool easily adaptable to the wide variety of multiphase flows in porous medium. For that purpose, only the common features of these different flows are considered here, *i.e.* the simulation of an isothermal and incompressible two-phase flow with capillary effects. Others physical features such as phase change or compressible phase are not in the scope of this paper but are possible further developments of this toolbox. Due to the high complexity of the solid structure and large dimensions that the computational domain can reach, the common strategy consists of defining volume averaged balance equations with effective properties such as permeabilities, porosity, etc., which take into account the microscopic flow morphology of the problem studied. With such an approach, a cell of the grid contains both fluid and

solid. As usually done in the multiphase porous media modeling, the concept of "saturation" is defined as the volumetric filling rate of a fluid phase (gas or liquid) with the void space of this cell and all properties, phase velocities, phase pressures, etc. are considered homogeneous within the computational cell. Readers interested in the averaging process can be referred to Das and Hassanizadeh (Das and Hassanizadeh, 2005) where a state-of-the-art in modeling and experimental techniques to study multiphase flow phenomena in porous media has been done with a focus on upscaling.

In the last decade, several open-source simulators dedicated to porous media flows have been developed such as, for example, Dumu^x (Flemisch et al., 2011), MRST (Lie et al., 2012), OpenGeoSys (Kolditz et al., 2012) and PFlotran(Lichtner et al., 2013). The open-source platform used in this work, OpenFOAM®(Jasak, 1996; Weller et al., 1998), does not belong to this list since it has not been conceived as a specialized simulation tool but as a general toolbox for solving partial differential equations. However, with growing community and popularity , the use of OpenFOAM® to simulate flow through porous materials becomes more and more prevalent. In the usual OpenFOAM® solvers, porous medium flows are modeled by adding viscous and inertial resistance terms in the Navier-Stokes momentum equation to obtain, in the porous domain, the commonly called Darcy-Forchheimer law (Forchheimer, 1901). A mask function allows to define both "porous" areas with Darcy and Forchheimer coefficients, and "free" areas where the classical momentum equation is solved. The porous medium model is generic and can therefore easily be used to develop new OpenFOAM® solvers. It has been used, for example, to study compressible reacting flows (Piscaglia et al., 2010), mass transfer in solid oxide fuel cells (Novaresio et al., 2012) or interaction of waves and coastal porous structures (Higuera et al., 2014a,b). However, the current porous medium handling in OpenFOAM® does not allow to simulate the common features of multiphase flows in porous media, mainly because it lacks some essential elements to this modeling, such as, phase saturations, relative permeability models, capillarity models, and specific boundary conditions. With a large community of users and an efficiency demonstrated in various physical cases, it seems an appealing possibility to develop, in the OpenFOAM® standards, a dedicated toolbox that could serve as a basis for the study of multiphase flows in porous medium.

In this paper, we present a toolbox to simulate multiphase flows in porous media. Instead of solving a modified Navier-Stokes system, we solve the mass conservation equations for each fluid where the phase velocities are expressed using a generalization of Darcy's law (Muskat, 1949). Comprehensive reviews of the numerical methods available to solve this kind of problem can be found in the literature (see for example Aziz and Settari (Aziz and Settari, 1979), Gerritsen and Durlofsky (Gerritsen and Durlofsky, 2005) or Chen *et al.* (Chen et al.,

2006)). Two main methods can be retained to treat two-phase flow in porous media: *(i)* a sequential approach, IMplicit Pressure Explicit Saturation (IMPES) and *(ii)* a coupled approach, i.e. the "fully-implicit". The IMPES methodology treats all terms that depend on saturation, except the transient terms, as explicit functions of saturation. This allows saturation to be decoupled from the pressure, resulting in a smaller system of equations to be solved implicitly. This reduces significantly the computational effort. However, because IMPES involves some explicit terms, integration may be numerically unstable. As a result, the computational time saved by reducing the size of the system of nonlinear equations can be lost in small time stepping to solve saturations and could lead to numerical instabilities, or in some cases, to non-convergence. The "fully-implicit" approach solves the same equations as the IMPES method, except that it treats pressure and saturation variables implicitly. Thus, the "fully-implicit" method is unconditionally stable if composition or temperature does not vary in space and time. Then, other formulations exist to ensure stability even if composition and temperature vary with reactions, phase changes or other phenomena. One could refer to Cao (Cao, 2002) to have a large overview of the different formulations.

Given the sequential nature of OpenFOAM®, we have adopted the IMPES method to develop a dedicated toolbox for multiphase flows in porous media. This package, called *porousMultiphaseFoam*, includes two solvers *impesFoam* and *anisoImpesFoam* (for iso- and aniso-tropic porous medium, see Section 2.2.1), the most widely used porous multiphase models for relative permeabilities and capillarities and a new boundary condition to impose phase velocities.

The paper is organized as follows. In Section 2, we present the mathematical model and its implementation in OpenFOAM®. Then in Section 3, we describe the content of the *porousMultiphaseFoam* package. Finally, in Section 4 the toolbox is validated over several tests and the parallel performance is evaluated on a cluster.

2.2 Mathematical model

2.2.1 Mass-momentum conservation equations

When considering porous medium at the macro-scale, the flow is governed by volume averaged equations. Each computational cell contains both solid and void space (or pore-space) which is defined at the macro-scale as the porosity ε :

$$\varepsilon = \frac{V_{void}}{V_{cell}} \tag{2.1}$$

where V_{void} is the volume occupied by the void space and V_{cell} the volume of the cell. To deal with multiphase flows, we have to introduce the notion of saturation S_i defining the filling rate of the phase i within the pore-space of a computational cell:

$$S_i = \frac{V_i}{V_{void}} \tag{2.2}$$

where V_i represents the volume occupied by the i-phase within the computational cell. From their definitions, saturations vary in the range $[0; 1]$**.** In this work, we study the flow of a non-wetting phase a and wetting phase b through the porous medium. Saturations satisfy the following obvious relationship :

$$S_a + S_b = 1 \tag{2.3}$$

Considering an incompressible two-phase flow in a porous medium, the macro-scale mass balance equation for each phase i reads:

$$\varepsilon \frac{\partial S_i}{\partial t} + \nabla \cdot \mathbf{U}_i = q_i \tag{2.4}$$

where $\mathbf{U}_i$ stands for the superficial velocity and q_i is a source term, used for injection or extraction wells.

In the generalized Darcy's model (Muskat, 1949), the superficial velocity of each phase i is computed as

$$\mathbf{U}_i = -\frac{\mathbf{K}_i}{\mu_i} \cdot (\nabla p_i - \rho_i \mathbf{g}) \tag{2.5}$$

where the apparent permeability $\mathbf{K}_i$ is expressed as follows:

$$\mathbf{K}_i = \mathbf{K} k_{ri}(S_b) \tag{2.6}$$

$\mathbf{K}$ is the permeability tensor of the porous medium and $k_{ri}(S_b)$ is the relative permeability of the phase i, whose value between 0 and 1 depends on the local saturation of the wetting phase S_b. This modeling suggests that the presence of another fluid reduces the pore space available, and therefore, reduces the permeability. The two most widely used relative permeability correlations (Brooks and Corey (Brooks and Corey, 1964), Van Genuchten (Van Genuchten, 1980)) are detailed in the models presentation (see Section 2.2.4) and implemented in the library. Two solvers are developed in the toolbox depending on the porous medium considered, isotropic or anisotropic. In the numerical validation, the porous medium is considered as isotropic which means that the tensor $\mathbf{K}$ can be replaced by a scalar K. Note that in both case the permeability field can be heterogeneous, i.e. whose value vary

in space (the permeability is defined as a tensor field $\mathbf{K}$ or a scalar field K). Both solvers are useful as the isotropic solver requires less memory and computation time.

Due to capillary effects inside the porous medium, we do not have equality between averaged pressure fields of each phase. In classical multiphase porous medium approach, we generally define a macro-scale capillary pressure p_c depending on the saturation S_b (Leverett, 1940):

$$p_c(S_b) = p_a - p_b$$

The p_c values depending on the considered flow and porous medium properties are usually obtained experimentally and then correlated on a capillary pressure model. The three most widely used capillary pressure correlations (Brooks and Corey (Brooks and Corey, 1964), Van Genuchten (Van Genuchten, 1980) and linear model) are detailed in section 2.2.5 and implemented in the library. The capillary pressure correlation eliminates an unknown of the system and the mass conservation equations read :

$$-\varepsilon\frac{\partial S_b}{\partial t} + \nabla\cdot\left(-\frac{Kk_{ra}\left(S_b\right)}{\mu_a}\left(\nabla p_a - \rho_a\mathbf{g}\right)\right) = q_a \tag{2.7}$$

$$\varepsilon\frac{\partial S_b}{\partial t} + \nabla\cdot\left(-\frac{Kk_{rb}\left(S_b\right)}{\mu_b}\left(\nabla p_a - \rho_b\mathbf{g} - \nabla p_c(S_b)\right)\right) = q_b \tag{2.8}$$

with p_a and S_b the system variables.

2.2.2 The IMPES method

The system described by the mass conservation equations 2.7 and 2.8 has strong non-linearities due to relative permeabilities and capillary pressure correlations. Then, the resolution of the coupled system requires the use of non-linear solver (Newton-Raphson method for example) and consequently involves substantial computation time. As explained in the introduction, the IMPES algorithm used in this work and proposed first by Sheldon et al. (Sheldon et al., 1959) is an alternative method consisting in a segregated resolution of the coupled equations. This method needs a new model formulation detailed below.

Model formulation

The mass conservation equations are reformulated into a pressure-saturation system by summing equations 2.7 and 2.8. The system then reads :

$$\nabla \cdot \left(-\frac{K k_{ra}\left(S_b\right)}{\mu_a} \left(\nabla p_a - \rho_a \mathbf{g} \right) \right) + \nabla \cdot \left(-\frac{K k_{rb}\left(S_b\right)}{\mu_b} \left(\nabla p_a - \rho_b \mathbf{g} - \nabla p_c(S_b) \right) \right) = q_a + q_b \quad (2.9)$$

$$\varepsilon \frac{\partial S_b}{\partial t} + \nabla \cdot \mathbf{U}_b = q_b \quad (2.10)$$

The principle of this approach is to solve implicitly the global mass conservation, i.e. the pressure equation (2.9), while the saturation equation (2.10) is explicitly solved. The detailed algorithm as implemented in the toolbox is presented in Section 2.2.2.

To simplify the formulation, we define phase mobility M_i and gravitational contribution L_i as follows :

$$M_i = \frac{K k_{ri}\left(S_w\right)}{\mu_i} \quad (2.11)$$

$$L_i = \frac{K k_{ri}\left(S_w\right)}{\mu_i} \rho_i \quad (2.12)$$

Even if in the generalized Darcy's law the relation $L_i = \rho_i M_i$ is satisfied, we have found it convenient to separate each contribution. Indeed, it must be noted that more complex models involving viscous resistance terms between phases for instance ((Raats and Klute, 1968; Baveye and Sposito, 1984)) could be written using this generic formulation. Therefore, the same solver basis could be used for further investigations with more sophisticated two-phase flow models.

Moreover, reformulating the capillary term ∇p_c as

$$\nabla p_c = \frac{\partial p_c}{\partial S_b} \nabla S_b \quad (2.13)$$

allows to express the pressure equation (2.9) as a Poisson-type equation:

$$\nabla \cdot \left(\left(M_a + M_b \right) \nabla p_a \right) = - \left(L_a + L_b \right) \mathbf{g} - M_b \frac{\partial p_c}{\partial S_b} \nabla S_b + q_a + q_b \quad (2.14)$$

and the saturation equation reads:

$$\varepsilon \frac{\partial S_b}{\partial t} + \nabla \cdot \left(-M_b \nabla p_a + L_b \mathbf{g} + M_b \frac{\partial p_c}{\partial S_b} \nabla S_b \right) = q_b \quad (2.15)$$

To improve code readability, three fluxes depending on different contributions are defined on each face of the computational grid:

$$\phi_p = \left(M_{a,c\to f} + M_{b,c\to f}\right) \nabla p_a \cdot \mathbf{S}_f \tag{2.16}$$

$$\phi_g = \left(L_{a,c\to f} + L_{b,c\to f}\right) \mathbf{g} \cdot \mathbf{S}_f \tag{2.17}$$

$$\phi_{p_c} = M_{b,c\to f} \left(\frac{\partial p_c}{\partial S_b} \nabla S_b\right)_{c\to f} \cdot \mathbf{S}_f \tag{2.18}$$

where the operator $c \to f$ indicates that face-centered values are interpolated from cell-centered value using a numerical scheme detailed in section 2.2.2. The global flux is computed as follows:

$$\phi = \phi_p + \phi_g + \phi_{p_c} \tag{2.19}$$

and the flux of phase b can be expressed:

$$\phi_b = \frac{M_{b,c\to f}}{M_{a,c\to f} + M_{b,c\to f}} \phi_p + \frac{L_{b,c\to f}}{L_{a,c\to f} + L_{b,c\to f}} \phi_g + \phi_{p_c} \tag{2.20}$$

Time-step limitations

To determine the time step for pressure equation, two conditions can be used in the provided solver. The first limitation is directly inherited from the classical OpenFOAM® multiphase solvers (Jasak, 1996; Rusche, 2002) and is related to the Courant number C_o, defined for the incompressible phase i:

$$Co_i = max_{\forall cell} \left(0.5 \frac{\sum_{f=0}^{m} |\phi_i|}{V_{cell} \Delta t}\right) \Delta t \tag{2.21}$$

with m the number of neighbor faces f to the considered cell. The coefficient for time-step change is then expressed:

$$c_{\Delta t} = \frac{Co_{fixed}}{max\left(Co_a, Co_b\right)} \tag{2.22}$$

To avoid sudden and too large increases of the time-step which could lead to numerical instabilities, we define the time-step of pressure equation 2.9 as follows:

$$\Delta t_p^* = min\left(min\left(c_{\Delta t}, 1 + 0.1 c_{\Delta t}\right), 1.2\right) \Delta t_{last} \tag{2.23}$$

that limits to a maximum increase of 20%. Several tests show that it is necessary to impose $Co_{fixed} \leqq 0.1$ to ensure stability to the numerical simulations.

The second possible limitations for pressure equation, more commonly used in the IMPES method is the CFL condition discussed by various authors (Coats, 2003a,b; Preux and McKee, 2011), has been implemented in the provided toolbox and is defined as follows:

$$CFL = max_{\forall cell}\left[\frac{\Delta t}{\varepsilon V_{cell}}\left(2\frac{\partial p_c}{\partial S_b}\frac{M_a M_b}{M_a + M_b}\sum_{f=0}^{m} T_f + \frac{\partial F_b}{\partial S_b}\sum_{f=0}^{m}\phi\right)\right] \tag{2.24}$$

where F_b is the fractional flow:

$$F_b = \frac{\frac{k_{rb}}{\mu_b}}{\frac{k_{ra}}{\mu_a} + \frac{k_{rb}}{\mu_b}} \tag{2.25}$$

and T_f the transmissivitty of the face f:

$$T_f = \frac{K_f||\mathbf{S}_f||}{\Delta x_f} \tag{2.26}$$

whereΔx_f is the distance between the centers of two neighboring cells. The coefficient for time-step change, used in equation 2.23, is then expressed:

$$c_{\Delta t} = \frac{C_{CFL}}{CFL} \tag{2.27}$$

with $C_{CFL} < 1$. Note that to ensure stability for the various test cases provided in the toolbox, C_{CFL} is set to 0.75.

The stability for both conditions, CFL or Co, is not ensured if source/sink term are present since they are not take into account in these formulations. Moreover, if we consider further code developments in the conservation equations, stability will probably not be ensured. In anticipation of these potential changes, we added a limitation related to an user-defined maximal variation of saturation $\Delta S_{b,max}$. Then, the variation of S_b between two time steps should satisfy :

$$\Delta S_{b,n\rightarrow n+1} \leq \Delta S_{b,max} \tag{2.28}$$

which can be reformulated as follows:

$$\Delta t^*_{S_b} = min\left(\frac{V_c \Delta S_{b,max}}{\varepsilon\left(-\sum_{f=0}^{m}\mathbf{U}_b \cdot \mathbf{S}_f + V_c m_b\right)}\right) \tag{2.29}$$

Then, the global time-step for the next iteration is given by:

$$\Delta t_n = min\left(\Delta t^*_{S_b}, \Delta t^*_p\right) \tag{2.30}$$

Algorithm

1. Δt_{n+1} is computed from the two conditions (C_o or CFL and $\Delta S_{b,max}$).

2. Saturation S_b^{n+1} is explicitly computed using the last known flux field ϕ_b^n:

$$\varepsilon \frac{S_b^{n+1} - S_b^n}{\Delta t_{n+1}} + \nabla \cdot \phi_b^n = q_b \tag{2.31}$$

3. Properties depending on the saturation (M_a^{n+1}, M_b^{n+1}, L_a^{n+1}, L_b^{n+1} and $\left(\frac{\partial p_c}{\partial S_b}\nabla S_b\right)^{n+1}$) and related fluxes ($\phi_g^{n+1}$ and $\phi_{p_c}^{n+1}$) are updated.

4. Pressure field p^{n+1} is implicitly computed solving the pressure equation:

$$-\nabla \cdot \left(M_{a,c\to f}^{n+1} + M_{b,c\to f}^{n+1}\right) \nabla p^{n+1} + \nabla \cdot \phi_g^{n+1} + \nabla \cdot \phi_{p_c}^{n+1} = q_a + q_b \tag{2.32}$$

5. Then ϕ_p^{n+1} and, therefore, ϕ^{n+1} and ϕ_b^{n+1} can be updated for the next time step.

Numerical schemes

As the saturation has great influence on relative permeabilities and capillary pressure, it is necessary to use numerical schemes suitable to ensure robustness and stability to the segregated solver. In the provided solver *impesFoam*, each field (k_{ri}, K and $\frac{\partial p_c}{\partial S_b}$) has a user-defined interpolation scheme that can be modified in the simulation configuration files. In the following numerical validation of the solver (section 2.4), we use the classical numerical schemes of the IMPES method which are :

- Relative permeability k_{ri} : first order upwind scheme for stability in the presence of a saturation front.
- Intrinsic permeability K : harmonic average for high heterogeneities.
- Derivative of the capillary pressure $\frac{\partial p_c}{\partial S_b}$: linear interpolation.

We should note that the generic implementation of interpolated field in the *impesFoam* solver allows the use of all the numerical schemes proposed by OpenFOAM® (high order, TVD, NVD, etc. (Jasak, 1996; Weller et al., 1998; Rusche, 2002)).

2.2.3 Wellbore models

In this work, we do not focus on the wellbore modeling in porous media which is not trivial and has been discussed by several authors (Aziz and Settari, 1979; Peaceman, 1993). We set up a simple structure in the software to allow the subsequent development of more complex models. For that, we consider constant injection and extraction flow rates of wellbores in the developed solver. Two mask functions, defined in the domain, are used to set up the positions of injection and extraction points (1 indicates the presence of a wellbore, 0 the absence). The user-defined global flow rate is equally divided between all the computational cells occupied by the wellbores, depending on their volume. We consider that wellbores inject wetting phase and extract the two phases, depending on the mobility. Under these assumptions, the source-sink terms for each phase can be expressed:

$$q_a = -\frac{M_a}{M_a + M_b} Q_{extraction} \tag{2.33}$$

$$q_b = Q_{injection} - \frac{M_b}{M_a + M_b} Q_{extraction} \tag{2.34}$$

2.2.4 Relative permeability models

Two relative permeability models are provided in the developed library. Both involve the notion of effective saturation, which is a normalized saturation of the wetting phase. The effective saturation reads:

$$S_{b,eff} = \frac{S_b - S_{b,irr}}{1 - S_{a,irr} - S_{b,irr}} \tag{2.35}$$

where $S_{a,irr}$ and $S_{b,irr}$ is the irreducible (minimal) saturation of the phase a and b respectively.

Both correlations depend on the effective saturation $S_{b,eff}$, power coefficient m, and maximal relative permeabilities, k_{ra} and k_{rb} (set to 1 if not specified by the user).

Brooks and Corey Model (Brooks and Corey, 1964)

$$k_{ra}\left(S_{b,eff}\right) = k_{ra,max}\left(1 - S_{b,eff}\right)^m \tag{2.36}$$

$$k_{rb}\left(S_{b,eff}\right) = k_{rb,max} S_{b,eff}^m \tag{2.37}$$

Van Genuchten Model (Van Genuchten, 1980)

$$k_{ra}\left(S_{b,eff}\right) = k_{ra,max}\left(1 - S_{b,eff}\right)^{\frac{1}{2}} \left(1 - \left(S_{b,eff}\right)^{\frac{1}{m}}\right)^{2m} \tag{2.38}$$

$$k_{rb}\left(S_{b,eff}\right) = k_{rb,max} S_{b,eff}^{\frac{1}{2}} \left(1 - \left(1 - S_{b,eff}^{\frac{1}{m}}\right)^{m}\right)^{2} \tag{2.39}$$

2.2.5 The capillary pressure models

As for the relative permeability models, the capillary pressure correlations are based on the notion of effective saturation. However, the macro-scale capillary pressure tends to infinity when saturation S_b tends to $S_{b,irr}$ (and its derivative when S_b tends to $S_{b,max}$ in the Van Genuchten model). To accept irreducible and maximal saturations in numerical simulations, we define the p_c-effective saturation S_{b,p_c} as follows:

$$S_{b,p_c} = \frac{S_b - S_{p_c,irr}}{S_{p_c,max} - S_{p_c,irr}} \tag{2.40}$$

where the p_c-minimal $S_{p_c,irr}$ should satisfy:

$$S_{p_c,irr} < S_{b,irr} \tag{2.41}$$

For the Van Genuchten model, the p_c-maximal saturation $S_{p_c,max}$ should satisfy:

$$S_{p_c,max} > S_{b,max} \tag{2.42}$$

Brooks and Corey Model (Brooks and Corey, 1964) The correlation for capillary pressure reads:

$$p_c\left(S_{b,p_c}\right) = p_{c,0} S_{b,p_c}^{-\alpha} \tag{2.43}$$

where $p_{c,0}$ is the entry capillary pressure and $\frac{1}{\alpha}$ the pore-size distribution index. Deriving the equation (2.43), the capillary term in the pressure (2.14) and saturation (2.15) equations can be expressed:

$$\frac{\partial p_c}{\partial S_{b,p_c}}\left(S_{b,p_c}\right) = -\frac{\alpha p_{c,0}}{S_{p_c,max} - S_{p_c,irr}} S_{b,p_c}^{-\alpha} \tag{2.44}$$

Van Genuchten Model (Van Genuchten, 1980) The correlation for capillary pressure reads:

$$p_c\left(S_{b,p_c}\right) = p_{c,0}\left(\left(S_{b,p_c}\right)^{-\frac{1}{m}} - 1\right)^{\frac{1}{n}} \tag{2.45}$$

where $p_{c,0}$ is the entry capillary pressure and m the Van Genuchten coefficient. The coefficient n is generally correlated with m with the following relationship:

$$\frac{1}{n} = 1 - m \tag{2.46}$$

In the provided toolbox, this relationship is used to compute the n coefficient when it is not explicitly defined. Deriving the equation (2.45), the capillary term in the pressure (2.14) and saturation (2.15) equations can be expressed:

$$\frac{\partial p_c}{\partial S_{b,p_c}}\left(S_{b,p_c}\right) = -\frac{1-m}{m}\frac{p_{c,0}}{S_{p_c,max} - S_{p_c,irr}}\left(\left(S_{b,p_c}\right)^{-\frac{1}{m}} - 1\right)^{-m}\left(S_{b,p_c}\right)^{-\frac{1+m}{m}} \tag{2.47}$$

Linear Model The linear model is also available with:

$$p_c\left(S_{b,p_c}\right) = p_{c,0} + \left(1 - S_{b,p_c}\right)\left(p_{c,max} - p_{c,0}\right) \tag{2.48}$$

where $p_{c,0}$ and $p_{c,max}$ respectively the minimal and maximal capillary pressure. The capillary term in pressure and saturation equations is then given as follows:

$$\frac{\partial p_c}{\partial S_{b,p_c}}\left(S_{b,p_c}\right) = -\left(p_{c,max} - p_{c,0}\right) \tag{2.49}$$

2.2.6 "Darcy velocity" boundary condition

In the IMPES method, solving the pressure equation implies some limitations in terms of boundary conditions. For example, it is not straightforward to impose phase velocities on boundaries. To make it possible in the *impesFoam* solver, we developed a suitable Neumann boundary condition (called `darcyGradPressure` in the toolbox) for the pressure field. Assuming fixed phase velocities on the considered boundary, the total velocity can be expressed as follows:

$$\mathbf{U}_{fixed} = \mathbf{U}_{a,fixed} + \mathbf{U}_{b,fixed} = -\left(M_a + M_b\right)\nabla p_a + \left(L_a + L_b\right)\mathbf{g} + M_b\frac{\partial p_c}{\partial S_b}\nabla S_b \tag{2.50}$$

Then, we can expressed the Neumann boundary condition on the pressure field:

$$\mathbf{n}.\nabla p_a = -\mathbf{n}.\left[\left(M_a + M_b\right)^{-1}\left(\mathbf{U}_{fixed} - \left(L_a + L_b\right)\mathbf{g} - M_b\frac{\partial p_c}{\partial S_b}\nabla S_b\right)\right] \tag{2.51}$$

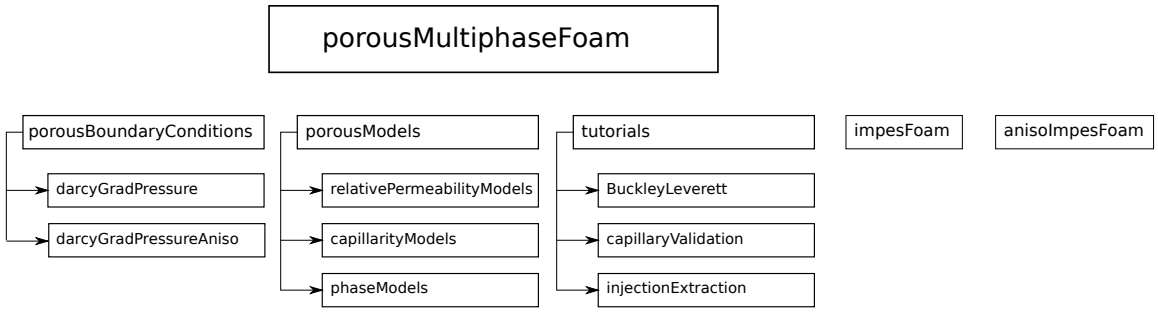

Figure 2.1: Structure of the OpenFOAM® porous multiphase toolbox.

where **n** denotes the normal to the face boundary. A similar boundary condition called `darcyGradPressureAniso` is defined for the *anisoImpesFoam* solver. Note that in that case, the tensor **K** needs to be invertible.

2.3 Description of software components

The global organization of the `porousMultiphaseFlowFoam` toolbox is depicted in figure 2.1.

The toolbox is divided in 4 parts: `porousModels`, `porousBoundaryConditions`, `impesFoam` and `tutorials`.

2.3.1 `porousModels`

This block compiles the `libporousModels.so` library containing the relative permeability, capillary pressure and phase models (see sections 2.2.4 and 2.2.5). Model parameters needed by the classes should be defined in the usual configuration file `transportProperties`. An example of a configuration file for a Brooks and Corey correlation is presented in Figure 2.2.

2.3.2 `porousBoundaryConditions`

This block compiles `libporousBoundaryConditions.so` library containing two new boundary conditions as detailed in section 2.2.6 and derived from the OpenFOAM® basic boundary condition `fixedGradientFvPatchField`. The boundary condition is called in the pressure file `p` as depicted in figure 2.3(left) while the velocities have usual Dirichlet boundary conditions (see an example of `Ub` file in Figure 2.3(right)).

```
phasea{
rho rho [1 -3 0 0 0 0 0] 1e0;
mu mu [1 -1 -1 0 0 0 0] 1.76e-5;
}

phaseb{
rho rho [1 -3 0 0 0 0 0] 1e3;
mu mu [1 -1 -1 0 0 0 0] 1e-3;
}

relativePermeabilityModel BrooksAndCorey;

capillarityModel BrooksAndCorey;

BrooksAndCoreyCoeffs{
m 3;
Sminpc Sminpc [0 0 0 0 0 0 0] 0;
Smaxpc Smaxpc [0 0 0 0 0 0 0] 1;
pc0 pc0 [1 -1 -2 0 0 0 0] 5;
alpha 0.2;
}
```

Figure 2.2: Example of a `transportProperties` file.

```
dimensions [1 -1 -2 0 0 0 0];

internalField uniform 0;

boundaryField {

boundaryExample{
type       darcyGradPressure;
}

}
```

```
dimensions [1 -1 0 0 0 0 0];

internalField uniform 0;

boundaryField {

boundaryExample{
type       fixedValue;
value      uniform (1e-5 0 0);
}

}
```

Figure 2.3: Example of pressure `p` file (left) and velocity `Ub` file (right) for `darcyGradPressure` boundary condition.

2.3.3 `impesFoam`

The solver *impesFoam* solves equations described in the section 2.2.2 considering isotropic porous medium (permeability K is a scalar field). This solver is used in the numerical validation of the developed library. It can be used as a development basis to integrate other features of multiphase flows in isotropic porous media.

2.3.4 `anisoImpesFoam`

The solver *anisoImpesFoam* solves same equations described as the *impesFoam* except that the intrinsic permeability $\mathbf{K}$ is a tensor field. Two injection cases are available in the provided toolbox. It can be used as a development basis to integrate other features of multiphase flows in anisotropic porous media.

2.3.5 `tutorials`

This block contains the validation tests presented in the section 2.4: Buckley-Leverett and capillary validation. An injection/extraction test case is also provided to ensure the proper implementation of the source/sink terms.

2.4 Numerical validations

The toolbox is validated using the solver *impesFoam*, i.e. the isotropic version of the IMPES method. However, numerical methods are the same for anisotropic solver and two injection test cases are provided in the `tutorials` to show an example of the use of the anisotropic solver *anisoImpesFoam*.

2.4.1 Buckley-Leverett

We consider the simplified case of Buckley-Leverett, i.e. a two-phase flow in a 1D domain (length $L = 1\,\mathrm{m}$, porosity $\varepsilon = 0.5$, intrinsic permeability $K = 1 \times 10^{-11}\,\mathrm{m}^2$, 400 computation cells) without capillary effects. This simplified case allows to develop a semi-analytical solution to get the shock saturation (saturation at the front), the front velocity and the saturation profile behind the front (Buckley and Leverett, 1942).

In the following tests, three fluids are considered (air, water and oil) whose properties are summarized in Table 2.1. The domain is initially fully saturated with the non-wetting fluid (air or oil depending in this case, $S_b = S_{b,irr}$ and $S_a = S_{a,max}$,) and we inject the wetting fluid (water) with a fixed constant velocity $U_b = 1 \times 10^{-5}\,\mathrm{m.s}^{-1}$.

(a)

fluid	ρ (kg.m^{-3})	μ (Pa.s)
air	1	$1.76.10^{-5}$
water	1000	1.10^{-3}
oil	800	1.10^{-1}

(b)

model	m
Brooks and Corey (Brooks and Corey, 1964)	3
Van Genuchten (Van Genuchten, 1980)	0.5

(c)

variable	value
p_a tolerance	10^{-12}
CFL	0.75
$\Delta S_{b,max}$	0.01

Table 2.1: Parameters for: (a) fluid, (b) model and (c) algorithm.

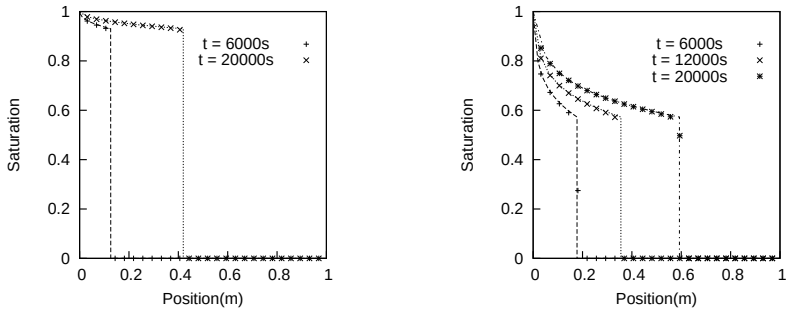

Figure 2.4: Saturation profiles for the Brooks and Corey model (left) and the Van Genuchten model (right). Dash lines are theoretical saturation profiles. .

The numerical validation is performed for the two relative permeabilities models, considering a water-air system for the Brooks and Corey model and a water-oil system for the Van Genuchten model. Model and algorithm parameters are summarized in Table 2.1. The comparison between numerical and semi-analytical results is shown in Figure 2.4. A good agreement is found with some minor numerical diffusion mainly due to the "upwind" scheme used for the relative permeability computation.

The case of the gravity regime is also studied, considering vertical injection of water in a air-saturated system for both models. Except the gravity contribution, the simulation parameters remain unchanged. In the gravity regime, i.e. when the flow rate injection is low, the front saturation is given by solving:

$$U_b - \frac{K k_{rb}(S_{b,front})}{\mu_b} \rho_b g_y = 0 \tag{2.52}$$

which gives $S_{b,front} = 0.467$ for Brooks and Corey model and $S_{b,front} = 0.754$ for the Van Genuchten model. The computed front velocities are respectively $4,28 \times 10^{-5}$ and $2,65 \times 10^{-5}$ m.s^{-1}. The good agreement between numerical and analytical results is shown in Figure 2.5.

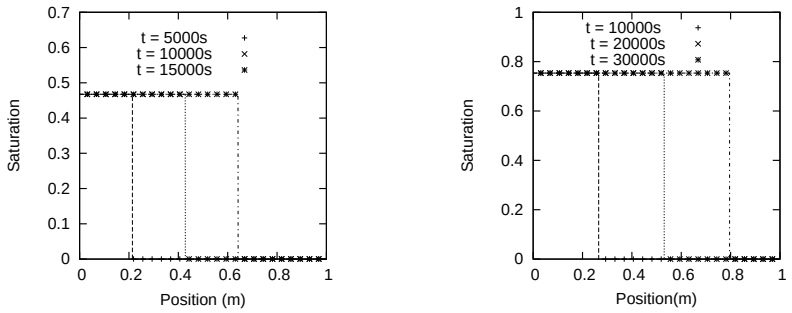

Figure 2.5: Saturation profiles in the gravity regime for the Brooks and Corey model (left) and the Van Genuchten model (right). Dash lines are theoretical saturation profiles. .

2.4.2 Capillaro-gravity equilibrium

We now consider a two-phase flow (air/water), with capillary pressure effects in a vertical 1D domain, similar to the previous section ($H = 1\,\mathrm{m}$). The bottom boundary condition is now a fixed wall ("Darcy velocity" boundary condition with $\mathbf{U}_a = \mathbf{U}_b = \mathbf{0}\,\mathrm{m/s}$) and the top boundary condition is a Dirichlet condition with fixed reference pressure $p = 0\,\mathrm{Pa}$ and irreducible saturation $S_b = S_{b,irr}$. We initialize the lower half of the domain with $S_b = 0.5$. Then we simulate the flow over a long period (2×10^6 seconds) to allow the establishment of a saturation profile along the vertical axis. When the stationary state is reached, we have:

$$U_a = U_b = 0 \tag{2.53}$$

and then we can write:

$$\frac{\partial p_a}{\partial y} = \rho_a g_y \tag{2.54}$$

$$\frac{\partial p_c}{\partial y} = \rho_b g_y - \frac{\partial p_a}{\partial y} \tag{2.55}$$

The capillary pressure gradient can be therefore simply expressed in term of gravity contribution:

$$\frac{\partial p_c}{\partial y} = (\rho_b - \rho_a) g_y \tag{2.56}$$

Therefore, the final saturation field should satisfy:

$$\frac{\partial S_b}{\partial y} = \frac{(\rho_b - \rho_a)\, g_y}{\frac{\partial p_c}{\partial S_b}(S_b)} \tag{2.57}$$

model	$p_{c,0}$	m	α
Brooks and Corey (Brooks and Corey, 1964)	1000		0.5
Van Genuchten (Van Genuchten, 1980)	100	0.5	

Table 2.2: Model parameters for capillary validation.

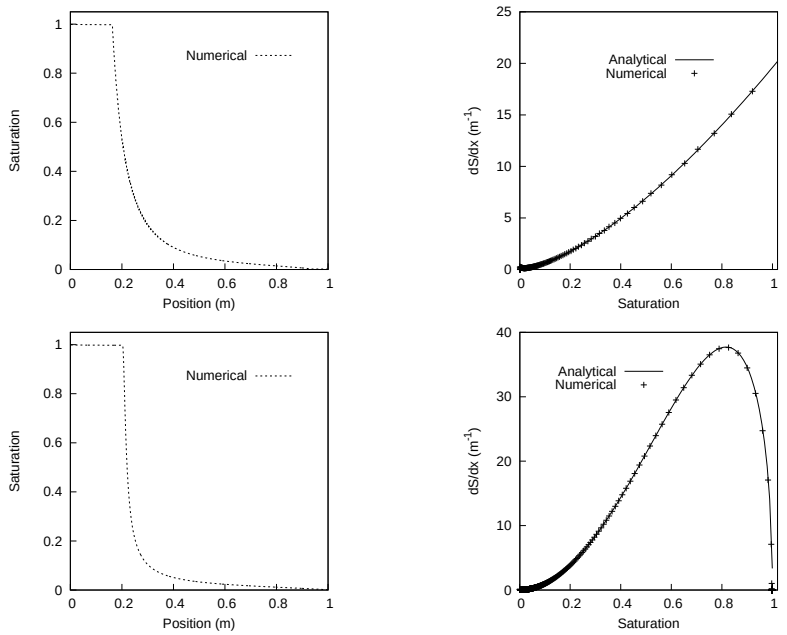

Figure 2.6: Saturation profiles (left) and gradients (right) depending on the capillary pressure model (top : Brooks and Corey, bottom : Van Genuchten).

where $\frac{\partial p_c}{\partial S_b}(S_b)$ follows a given correlation described in section 2.2.5. Algorithm parameters are identical to the previous test case (cf Table 2.1) and the model parameters are summarized in Table 2.2.

Saturation profiles at the capillary-gravity equilibrium are presented in the Figure 2.6(left). The comparison between theoretical and numerical evaluations of saturation gradients (depending on the saturation) validates the numerical implementation of the presented models (see Figure2.6).

2.4.3 Performance test: viscous fingering in a heavy oil reservoir

We now consider a water injection ($U_b = 1 \times 10^{-4}\,\mathrm{m.s^{-1}}$) in a horizontal oil saturated system (see fluid properties on Table 2.1). The size of the reservoir is $1 \times 0,4\ \mathrm{m}^2$ ($1,6 \times 10^6$ computation cells with a 2000×800 mesh). The permeability of the two-dimensional domain is heterogeneous by blocks with a value between 1×10^{-13} and $4 \times 10^{-13}\,\mathrm{m}^2$ (see Figure 2.7). The Van Genuchten model is used for relative permeability and capillary pressure with $m = 0,5$ and $p_{c,0} = 5\,\mathrm{Pa}$.

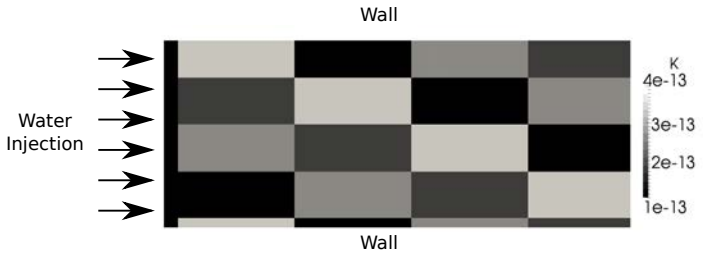

Figure 2.7: Heavy oil reservoir permeability field and boundary conditions.

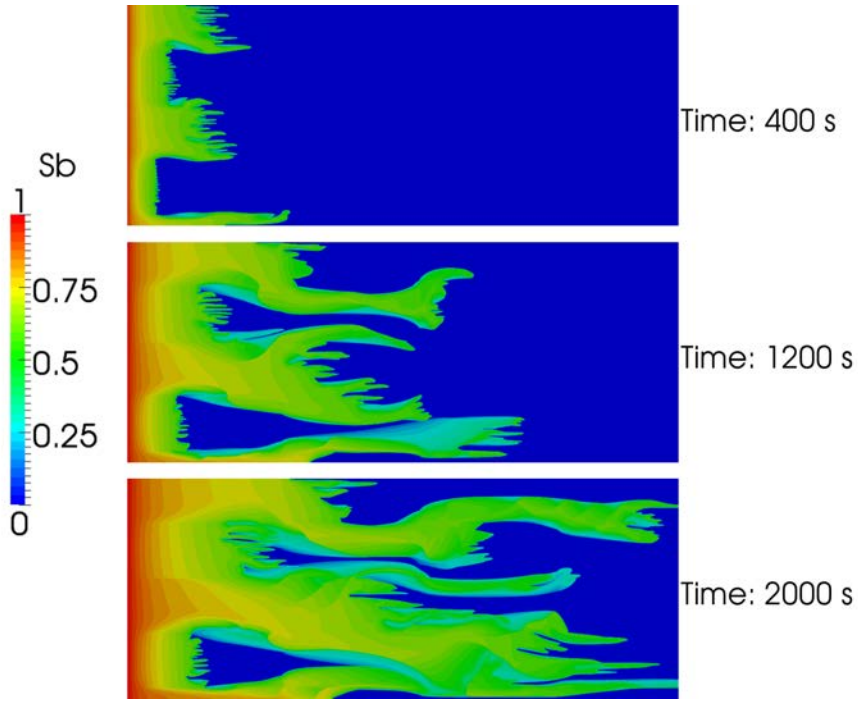

Figure 2.8: Viscous fingering in an heavy oil reservoir (Water saturation field S_b).

In this condition, we observe the emergence of multiple instabilities in the saturation front area (see Figure 2.8 a). The development of these instabilities leads to a so called "viscous fingering" (see Figure 2.8 b), a phenomenon due to the important viscosity ratio between the two fluids (Homsy, 1987).

The viscous fingering presents an important challenge to oil industry and needs to be accurately understood and modeled because theses instabilities decrease the efficiency of oil recovery processes. We do not focus in this study on these phenomena characterization and the reader interested could refer to previous experimental (Chen and Wilkinson, 1985; Homsy, 1987; Lenormand et al., 1988; Brock and Orr Jr., 1991; Doorwar and Mohanty, 2011) and numerical studies (Chen and Meiburg, 1998a,b; Riaz and Tchelepi, 2006; Ferrari and Lunati, 2013). Indeed, the number of "viscous fingers" depends on the reservoir properties but also on numerical parameters such as grid refinement and algorithm tolerance. Therefore,

the complete characterization would require a thorough study that is not in the scope of this paper. However, it is an interesting illustration of the possibilities of the solver by simulating a complex multiphase flow where the saturation front occupies almost the whole domain. A unique configuration is tested and used to evaluate the parallel performance of our solver.

In OpenFOAM®, the parallel algorithm is based on the domain decomposition method. Before the simulation, the whole domain is decomposed in n small domains, n being the number of computational cores used for the simulation. Then, each core solves a smaller linear system and information exchanges at boundaries between cores are done using the Message Passing Interface (MPI) communications protocol. Several decomposition methods are available in OpenFOAM® (*simple*, *scotch*, *manual*, etc.) and can be used independently of the considered solver. We use in our simulations the *simple* method which decomposes the domain in $n_x \times n_y \times n_z$ equal parts, where n_i are user-defined values. The pressure equation (2.14) is solved with the standard preconditioned conjugate gradient (PCG) solver with a fixed tolerance of 10^{-6}.

The "viscous fingering" phenomena is simulated on the Hyperion cluster which consists of 368 computation nodes of 2 quad-core Nehalem EX processors at 2.8 GHz with 8 MB of cache per processor. The MPI version installed on the cluster is the MPT-2.04, a specific version of MPI optimized for SGI clusters. Simulations were performed from 16 (the reference) to 1024 cores. The cluster was not empty during the simulations and allocates randomly computation nodes, whose 8 cores are fully dedicated to one task, to the request. The total simulation, i.e. 4000 s of physical time, takes around 700 hours of CPU time. The speedup σ for a simulation with n cores is computed as follows:

$$\sigma_n = \frac{T_{16}}{T_n} \tag{2.58}$$

where T_n is the computation time for n cores. The parallel efficiency ϵ_n is defined:

$$\epsilon_n = \frac{16}{n}\sigma_n \tag{2.59}$$

The results in term of speedup are presented in Figure 2.9. The numerical results show a super linear speedup until 256 cores ($\epsilon_{256} \approx 1,58$). This has already been observed on this software, see for example the study performed on a 3D cavity flow by the IT Center For Science CSC IT Center for Science. We assume that the explicit part of the resolution (saturation equation and the flow properties computation at each time step) can explain this observation. Indeed, increasing the number of processors decreases the number of computation cells and then RAM memory necessary for each processor. As the explicit

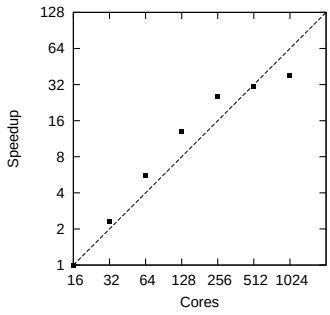

Figure 2.9: Log-log representation of the speedup with the *impesFoam* solver (reference is 16 cores)

treatment need low computation but high access memory (RAM and cache), this could lead to a parallel efficiency superior to 1. This effect decreases above 256 cores, because partial linear systems become smaller and the information exchange between cores takes relatively more computation time. A linear scaling is reached for 512 cores ($\epsilon_{512} \approx 0,97$). Then, the parallel efficiency for 1024 cores is low ($\epsilon_{1024} \approx 0,59$) because the linear system for each core become very small (only 1560 cells per core).

2.5 Conclusion

A toolbox for the simulation of multiphase flow in porous media has been developed using the standards of OpenFOAM®. This toolbox includes libraries for porous models (relative permeability, capillary pressure and phase model) and a specific porous boundary condition. A classical IMPES solver has been developed to validate the provided models by comparison with analytical solutions. A study on the parallel efficiency (up to 1024 cores) has also been performed on a complex multiphase flow. The presented solver shows a satisfactory speedup, provided to solve a sufficiently large problem. The provided solver can serve as a basis to develop other features, such as new multiphase or improved wellbore models. Moreover, the easily modifiable nature of the OpenFOAM® platform can be useful to test, for example, new numerical schemes or solving methods.

Acknowledgments

This work was granted access to the HPC resources of CALMIP under the allocation 2013-p13147. We are grateful to Dr Michel Quintard for interesting discussions.

References

Aziz, K. and Settari, A.: 1979, *Petroleum reservoir simulation*.

Baveye, P. and Sposito, G.: 1984, The operational significance of the continuum hypothesis in the theory of water movement through soils and aquifers, *Water Resour. Res.* **20**(5), 521–530.

Brock, D. and Orr Jr., F.: 1991, Flow visualization of viscous fingering in heterogeneous porous media, *SPE J.* **22614**, 211–217.

Brooks, R. and Corey, A.: 1964, Hydraulic Properties of Porous Media, *Hydrol. Pap.*

Buckley, S. and Leverett, M.: 1942, Mechanism of fluid displacement in sands, *Trans. AIME* **146**, 107–116.

Cao, H.: 2002, *Development of techniques for general purpose simulators*, PhD thesis, Stanford University.

Chen, C. and Meiburg, E.: 1998a, Miscible porous media displacements in the quarter five-spot configuration. Part 1. The homogeneous case, *J. Fluid Mech.* **371**, 233–268.

Chen, C. and Meiburg, E.: 1998b, Miscible porous media displacements in the quarter five-spot configuration. Part 2. Effects of heterogeneities, *J. Fluid Mech.* **371**, 269–299.

Chen, J. and Wilkinson, D.: 1985, Pore-scale viscous fingering in porous-media, *Phys. Rev. Lett.* **55**, 1892–1895.

Chen, Z., Huan, G. and Ma, Y.: 2006, *Computational Methods for Multiphase Flows in Porous Media*.

Coats, K.: 2003a, IMPES Stability: Selection of Stable Timesteps, *SPE J.* **8**(2), 181–187.

Coats, K.: 2003b, IMPES Stability: The CFL Limit, *SPE J.* **8**(3), 291–297.

CSC IT Center for Science: n.d., http://www.csc.fi/english/research/sciences/CFD/CFDsoftware/openfoa

Das, D. and Hassanizadeh, S.: 2005, *Upscaling multiphase flow in porous media : from pore to core and beyond*.

Doorwar, S. and Mohanty, K.: 2011, Viscous Fingering during Non-Thermal Heavy Oil Recovery, *SPE Annu. Tech. Conf. Exhib.*, Denver, Colorado, USA.

Ferrari, A. and Lunati, I.: 2013, Direct numerical simulations of interface dynamics to link capillary pressure and total surface energy, *Adv. Water Resour.* **57**, 19–31.

Flemisch, B., Darcis, M., Erbertseder, K., Faigle, B., Lauser, A., Mosthaf, K., Mthing, S., Nuske, P., Tatomir, A., Wolff, M. et al.: 2011, Dumu^x: Dune for multi-{phase, component, scale, physics, ...} flow and transport in porous media, *Advances in Water Resources* **34**(9), 1102–1112.

Forchheimer, P.: 1901, Wasserbewegung durch boden, *Z. Ver. Deutsch. Ing* .

Gerritsen, M. and Durlofsky, L.: 2005, Modeling fluid flow in oil reservoirs, *Annu. Rev. Fluid Mech.* **37**, 211–238.

Higuera, P., Lara, J. L. and Losada, I. J.: 2014a, Three-dimensional interaction of waves and porous coastal structures using OpenFOAM®. Part I: Formulation and validation, *Coast. Eng.* **83**, 243–258.

Higuera, P., Lara, J. and Losada, I.: 2014b, Three-dimensional interaction of waves and porous coastal structures using OpenFOAM®. Part II: Application, *Coast. Eng.* **83**, 259–270.

Homsy, G. M.: 1987, Viscous fingering in porous media, *Annu. Rev. Fluid Mech.* **19**, 271–311.

Horgue, P., Soulaine, C., Franc, J., Guibert, R. and Debenest, G.: 2015, An open-source toolbox for multiphase flow in porous media, *Computer Physics Communications* .

Jasak, H.: 1996, Error analysis and estimation for the finite volume method with applications to fluid flows.

Kolditz, O., Bauer, S., Bilke, L., Böttcher, N., Delfs, J., Fischer, T., Görke, U., Kalbacher, T., Kosakowski, G., McDermott, C., Park, C., Radu, F., Rink, K., Shao, H., Shao, H., Sun, F., Sun, Y., Singh, A., Taron, J., Walther, M., Wang, W., Watanabe, N., Wu, Y., Xie, M., Xu, W. and Zehner, B.: 2012, Opengeosys: an open-source initiative for numerical simulation of thermo-hydro-mechanical/chemical (thm/c) processes in porous media, *Environmental Earth Sciences* **67**(2), 589–599.

Lenormand, R., Touboul, E. and Zarcone, C.: 1988, Numerical models and experiments on immiscible displacements in porous media, *J. Fluid Mech.* **189**, 165–187.

Leverett, M. C.: 1940, Capillary behavior in porous solids, *Trans. AIME* **142**(1), 152–169.

Lichtner, P. C., Hammond, G. E., Lu, C., Karra, S., Bisht, G., Andre, B., Mills, R. T. and Kumar, J.: 2013, PFLOTRAN Web page. http://www.pflotran.org.

Lie, K., Krogstad, S., Ligaarden, I., Natvig, J., Nilsen, H. and Skaflestad, B.: 2012, Open-source matlab implementation of consistent discretisations on complex grids, *Computational Geosciences* **16**(2), 297–322.

Muskat, M.: 1949, *Physical principles of oil production*, mcgraw-hil edn, New York.

Novaresio, V., García-Camprubí, M., Izquierdo, S., Asinari, P. and Fueyo, N.: 2012, An open-source library for the numerical modeling of mass-transfer in solid oxide fuel cells, *Comput. Phys. Commun.* **183**(1), 125–146.

Peaceman, D.: 1993, Representation of a horizontal well in numerical reservoir simulation, *SPE Advanced Technology Series* **1**(1), 7–16.

Piscaglia, F., Montorfano, A. and Onorati, A.: 2010, Multi-dimensional computation of compressible reacting flows through porous media to apply to Internal Combustion Engine simulation, *Math. Comput. Model.* **52**(7-8), 1133–1142.

Preux, C. and McKee, F.: 2011, Study and Approximation of IMPES Stability: the CFL Criteria, *Finite Vol. Complex Appl. VI Probl. Perspect. Springer Proc. Math.* **4**, 713–721.

Raats, P. A. C. and Klute, A.: 1968, Transport in soils: The balance of momentum, *Soil Sci. Soc. Am. J.* **32**, 452–456.

Riaz, A. and Tchelepi, H. a.: 2006, Numerical simulation of immiscible two-phase flow in porous media, *Phys. Fluids* **18**(1), 014104.

Rusche, H.: 2002, *Computational fluid dynamics of dispersed two-phase flows at high phase fractions*, PhD thesis.

Sheldon, J. W., Zondek, B. and Cardwell, W. T.: 1959, One-dimensional, incompressible, non-capillary, two-phase fluid flow in a porous medium, *T. SPE. AIME* **216**, 290–296.

Van Genuchten, M. T.: 1980, A Closed-form Equation for Predicting the Hydraulic Conductivity of Unsaturated Soils1, *Soil Sci. Soc. Am. J.* **44**(5), 892.

Weller, H. G., Tabor, G., Jasak, H. and Fureby, C.: 1998, A tensorial approach to computational continuum mechanics using object-oriented techniques, *Computers in physics* **12**, 620.

Chapter 3

IMPES Algorithm and stability condition

Contents

Résumé français

Ce chapitre concerne l'étude des critères de stabilité pour un algorithme IMPES, en considérant un ajustement dynamique du pas de temps. En effet, l'IMPES propose un couplage séquentiel faible des équations de transport de la saturation (aussi appelée équation de saturation) et de l'équation de pression. De plus, l'algorithme admet une résolution explicite de l'équation de saturation, ce qui permet une moindre utilisation mémoire et une résolution plus rapide. Cependant, les nombreuses contraintes numériques qui pèsent sur la résolution (non-linéarités des coefficients, fortes hétérogénéités) ajoutées à la résolution explicite obligent à correctement borner la taille du pas de temps afin de garder une simulation stable.

Trois nombres CFL sont extraits de la littérature, nommément le nombre de Courant classique, le nombre de Coats et le nombre de Todd. Ils sont par la suite testés dans différentes configurations physiques : à dominante visqueuse, à dominante capillaire et à dominante gravitaire. La combinaison des effets est ensuite testée sur un cas classique du réservoir SPE 10. Il ressort des différents tests que, dans un cadre d'adaptation dynamique du pas de temps, la condition de Coats se révèle la plus optimale en garantissant la stabilité quelque soit la combinaison des effets physiques. Cependant, il s'avère aussi que la condition de Todd mène à des simulations stables et plus rapides dans le cas d'écoulement à forte dominante capillaire.

Ce chapitre est adapté de la publication "*Benchmark of different CFL conditions for IMPES / Comparaison de différentes conditions CFL pour l' IMPES*"*(Franc et al., 2016),* paru dans les *Comptes Rendus Mécaniques*, en Octobre 2016.

The IMplicit Pressure Explicit Saturation (IMPES) method is a prevalent way to simulate multiphase flows in porous media. The numerical stability of this sequential method implies limitations on time step which may differ depending on the flow regime studied. In this note, the three main stability criteria related to the IMPES method, that differ in their construction on the observed variables, are compared on homogeneous and heterogeneous configurations for different two-phase flow regimes (viscous/capillary/gravitational). This highlights that there is no single optimal criterion ensuring always both stability and efficiency. For capillary dominated flows, the Todd's condition is the most efficient while the standard Coat's condition in (C<1) should be preferred for viscous flows. When gravity effects are present, the Coat's condition must be restricted ($C < 0.25$) but remains more efficient than the Todd's condition.

3.1 Introduction

Among the possible numerical methods used to simulate two-phase flow in porous media (Aziz and Settari, 1979; Cao, 2002; Gerritsen and Durlofsky, 2005), the IMplicit Pressure Explicit Saturation (IMPES) method remains in use today (Mostaghimi et al., 2015; Negara et al., 2015). This sequential algorithm, originally proposed by Sheldon (Shewani et al., 2014), has the advantage to substantially reduce the size of linear systems to solve, compared to a fully implicit method. In return, the method is limited by important numerical stability restrictions on the time step size. Hybrid methods, Adaptive Implicit Methods (AIM), have also been proposed and consists in increasing implicitness in regions with high throughput ratio.(Russell et al., 1989).

The numerical instabilities are due to the non-linear effects involved in two-phase flow in porous media and mainly related to capillary pressure ans relative permeability laws. The explicit resolution of saturation requires the linearization of capillary and permeability laws which could lead to numerical instability. This can lead to erroneous calculations of the saturation field and, in the worst cases, to the end of the simulation (the computed saturation is out of the limits). The various laws and their complexity make stability even harder to predict and, therefore, different stability criteria have been studied and proposed. Todd (Todd et al., 1972) has first derived a condition based on averaged spatial and temporal saturation variation, which provides an increasing/decreasing factor for the time step. Coats Coats et al. (2003), through a proper Von Neumann analysis, has derived a CFL criteria based on mobility related terms, fluxes and capillary pressure. One can also use the classical CFL (Courant et al., 1928) condition to ensure stability. Other stability studies have been conducted focusing on upstream scheme (Sammon et al., 1988), on switching criteria for AIM

(Russell et al., 1989; Forsyth, 1989) or on extension to compositional and black-oil models (Wan et al., 2005). Even if the Coats' stability criterion is commonly used, it may be very restrictive in certain circumstances and is therefore not necessarily the optimum choice. To our knowledge, there is no study in the literature comparing these different stability criteria to highlight their effectiveness for different porous media flow regimes (viscous, capillary, gravitational).

This need for numerical stability is all the more important as two-phase flow in porous media are also often subject to physical instabilities. This class of instabilities can be caused by various configurations such as counter current flows and layered flows or by properties of the studied system (mobility ratio, viscosity ratio, permeability distribution). The most commonly known and studied instability is the viscous fingering phenomenon (Homsy, 1987). When one is interested in simulating this kind of physical instability, the numerical stability should be ensured to avoid the perturbation of the system by a numerical artifact.

In a recent work (Horgue et al., 2014), the IMPES method has been implemented and developed in the open-source framework OpenFOAM (Hrvoje, 1996; Weller et al., 1998). This open-source implementation has been successfully employed in various fields, such as two-phase flow in structured bed packing (Soulaine et al., 2014) or in waste management (Shewani et al., 2014).

The scope of the paper is the performance benchmark of existing criteria taken from the literature. A methodology is set up to compare their efficiency in terms of computational cost (number of linear solver iterations) for various cases. This study has been designed for helping IMPES users that struggle with stability issues in choosing the most suited criteria for their simulation. Its ambition is not to develop a new criteria but to gather user experiences on different configuration with different criteria. To our knowledge, there is no such gathering work in the literature. We proposed to cross-compare Todd, Coats and classical Courant-Friedrichs-Lewy criteria listed above, for different flow regimes (viscous/capillary/gravitational) and for homogeneous and heterogeneous permeability fields without singularities (e.g., no wellbore model). This note is organized in two parts. In the first one, two-phase flow equations for porous media are described, detailing the IMPES algorithm and presenting the three stability numbers investigated. We introduce mathematical formulation of the different criteria, stating which phenomena are included in the theoretical form. In the second part, numerical experiments are performed to explore the different stability conditions on three classical configurations, and define their efficiency.

3.2 Two-phase flow and stability numbers

3.2.1 Mathematical model

Two-phase flows under investigation are assumed incompressible, viscous and isothermal. The wetting and non-wetting phases are denoted w and n respectively. The mass conservation equation for each phase reads

$$\begin{aligned} \phi\frac{\partial S_w}{\partial t} + \boldsymbol{\nabla}\cdot\mathbf{u}_w &= q_w, \\ -\phi\frac{\partial S_w}{\partial t} + \boldsymbol{\nabla}\cdot\mathbf{u}_n &= q_n, \end{aligned} \tag{3.1}$$

with the obvious relationship

$$S_w + S_n = 1. \tag{3.2}$$

In these equations, S_α refers to the saturation, ϕ is porosity, q_α is the mass source/sink term and $\mathbf{u}_\alpha$ denotes the superficial velocity for each phase α. The latter are slow enough to be modeled by generalized Darcy's laws (Muskat, 1949),

$$\begin{aligned} \mathbf{u}_w &= -\boldsymbol{K}\cdot\lambda_w\left(\boldsymbol{\nabla}p_n - \rho_w\mathbf{g} - \boldsymbol{\nabla}p_c\right), \\ \mathbf{u}_n &= -\boldsymbol{K}\cdot\lambda_n\left(\boldsymbol{\nabla}p_n - \rho_n\mathbf{g}\right), \end{aligned} \tag{3.3}$$

where $\boldsymbol{K}$ is the permeability tensor intrinsic to the porous material, ρ_α is the fluid density and $\mathbf{g}$ the gravitational acceleration. The capillary pressure, p_c, i.e. the pressure difference between both phases depends on the saturation (Leverett et al., 1941) and reads,

$$p_c\left(S_w\right) = p_n - p_w. \tag{3.4}$$

The mobility λ_α is defined as

$$\lambda_\alpha = \left(\frac{k_{r,\alpha}(S_w)}{\mu_\alpha}\right)_{\alpha=w,n}, \tag{3.5}$$

where μ_α is the fluid viscosity and $k_{r,\alpha}$ is the relative permeability function.

Many models exist in the literature to represent the capillary pressure and the relative permeabilities according to the saturation (Leverett et al., 1941; Thomeer et al., 1960; Morel-Seytoux et al., 1996; Van Genuchten, 1980; Corey and Brooks, 1975). In the present study,

the well-established Brooks and Corey model (Corey and Brooks, 1975) is used. With such model, capillary pressure, p_c, and relative permeabilities, $k_{r,\alpha}$, read

$$\begin{aligned} p_c\left(S_w\right) &= p_{c,0}\, S_e^{-\frac{1}{m}} \\ k_{r,n}\left(S_w\right) &= k_{r,n_{max}}\left(1-S_e\right)^{\frac{3m+2}{m}} \\ k_{r,w}\left(S_w\right) &= k_{r,w_{max}} S_e^{\frac{3m+2}{m}}. \end{aligned} \tag{3.6}$$

where $p_{c,0}$, $k_{r,n_{max}}$ and $k_{r,w_{max}}$ are model parameters and the pore-size index, m, is a characteristic number of the porous medium considered: small for large range pore-size distribution, large for relatively uniform pore-size distribution. The reduced saturation,

$$S_e = \left(\frac{S_w - S_{w,irr}}{1 - S_{w,irr} - S_{n,res}}\right), \tag{3.7}$$

represents that amount of wetting phase that can flow. It depends on the irreducible wetting saturation, $S_{w,irr}$ and the residual non-wetting saturation, $S_{n,res}$.

3.2.2 IMPES algorithm

The chosen unknowns for the numerical implementation are the pressure of the non-wetting phase and the saturation of the wetting phase (p_n, S_w). The saturation S_w is governed by the wetting phase mass conservation Eq. (3.1) and the pressure p_n satisfies the global mass conservation,

$$\boldsymbol{\nabla}\cdot\left(-\boldsymbol{K}\cdot\lambda_t\boldsymbol{\nabla}p_n\right) - \boldsymbol{\nabla}\cdot\left(\boldsymbol{K}\cdot\Psi\left(\rho_w-\rho_n\right)\cdot\mathbf{g} - \boldsymbol{K}\cdot\Psi\frac{\partial p_c}{\partial S_w}\boldsymbol{\nabla}S_w\right) = q_t, \tag{3.8}$$

where $\lambda_t = \lambda_w + \lambda_n$ is the total mobility, $q_t = q_w + q_n$ is the total sink/source term and $\Psi = \frac{2\lambda_w\lambda_n}{\lambda_w+\lambda_n}$ is the harmonic average of mobilities.

The IMPES solution algorithm consists in solving implicitly the pressure equation (3.8) and explicitly the saturation equation (3.1). The details of the implemented algorithm can be found in a previous work (Horgue et al., 2014). In the following simulations, a first order upwind interpolation is used for mobility related terms and a backward Euler scheme is adopted for time discretization.

Linear solver used in the experiment is a conjugate gradient solver with a diagonal incomplete Cholesky preconditioner. It is a commonly used pair when dealing with symmetric matrices. Generalized geometric-algebraic multi-grid solver might be an appropriate alternative for solving this equation over large domains. As cases treated in the next section

remain simple in term of number of cells and considering that solver efficiency is not in the scope of this work, the choice of such a preconditioner-solver pair is not disadvantageous.

3.2.3 Stability criteria

In this section the three tested CFL conditions ensuring the stability of IMPES simulations are described: namely the classic Courant number condition (Co), the Todd's derived number condition (T) and the Coats' derived number condition (C). For each criterion, a time-step factor F, which gives the increase or decrease in the time-step size during the simulation, is defined.

Classic Courant number condition (Co)

This condition limits the Courant number of each phase α, by a user defined value, Co_{max}:

$$Co = \frac{1}{2} \max_{i,\alpha} \left(\frac{\sum\limits_{faces \subset i} |q_{\alpha,f}|}{V_i} \Delta t \right) < Co_{max} \qquad i = 1, N_{cells}. \tag{3.9}$$

This Courant number is a direct adaptation of the classical one extended to two-phase flows (Courant et al., 1928). It involves the sum of absolute values of fluxes in phase α through every faces of cell i (term $\sum\limits_{faces \subset i} |q_{\alpha,f}|$) and the volume V_i of the cell i. It is designed to ensure stability of the hyperbolic saturation equation but does not integrate coupling with pressure variation. The time-step factor F is defined as:

$$F = \frac{Co_{max}}{Co}. \tag{3.10}$$

Todd's number condition (T)

The first stability criterion dedicated to the IMPES algorithm (Todd et al., 1972) has been derived taking into account the discretized form of the pressure and saturation equations. It leads to a constraint on the time step, split into two time-step restrictions, regarding if capillary pressure p_c, or relative permeabilities k_r, are considered

$$\Delta t \leq \min_i \left[\Delta t_{p_c,i}, \Delta t_{k_r,i} \right] \qquad i = 1, N_{cells}. \tag{3.11}$$

Capillary restriction on time-step can be expressed as

$$\Delta t_{p_c,i} \leq \frac{\phi V_i}{|p'_c| \sum\limits_{faces \subset i} (T_f \Psi)} \qquad i = 1, N_{cells}. \tag{3.12}$$

where $T_f = ({}^{KA}/_{\Delta x})$ is the transmissivity of face f , whose area is noted A and whose distance to the cell center is noted Δx. Harmonic interpolation of K is chosen for computing the transmissivity T_f. Equation (3.12), reformulated as a CFL condition, reads :

$$CFL_{Todd,pc} = \Delta t_{p_c,i} \frac{|p'_c| \sum\limits_{faces \subset i} (T_f \Psi)}{\phi V_i} < CFL_{Todd,max}, \quad i = 1, N_{cells.} \tag{3.13}$$

which introduces a user-defined upper limit $CFL_{Todd,max}$.

Relative permeabilities restriction, formulated in terms of inter-cell fluxes, reads

$$\Delta t_{k_r,i} \leq \frac{\phi V_i}{f'_{w,i} \left(\sum\limits_{faces \subset i} |q_f| \right)} \qquad i = 1, N_{cells}, \tag{3.14}$$

with f'_w the derivative of the fractional flow $f_w = \frac{\lambda_w}{\lambda_t}$ with respect to the saturation of the wetting phase S_w and q_f the total flux through the f face. In terms of spatial and temporal saturation variation, a time step ratio can be used, with the 1/2 factor depending on the chosen spatial discretization scheme (e.g. here 1-pt upwind in 1D):

$$T = \frac{\Delta t^{n+1}_{k_r}}{\Delta t^{n}_{k_r}} = \frac{1}{2} \frac{\frac{1}{N_{cells}} \sum\limits_i |\Delta_{i,i+1} S_w|}{\max\limits_i (|\Delta_t S_w|)} \qquad i = 1, N_{cells}. \tag{3.15}$$

Here, the equation (3.15) defines directly a time step factor referred in the following as T number. The symbol $\Delta_{i,i+1} S_w$ stands for the difference between two neighbor cells and $\Delta_t S_w$ is the saturation difference between n and $n-1$ time state. The time-step factor F includes both part, capillary pressure and relative permeability, and is defined as:

$$F = min(T, \frac{CFL_{Todd,max}}{CFL_{Todd,pc}}). \tag{3.16}$$

Coats' number condition (C)

More recently, starting from inequality (3.12) and (3.14) using Neumann's stability analysis, a new stability number C has been developed (Coats et al., 2003):

$$C = \max_f \left[\frac{\Delta t}{\phi V_{i|f}} \left(\frac{\lambda_n}{\lambda_t \lambda_w} \left| q_{w,f} \right| \lambda'_w - \frac{\lambda_w}{\lambda_t \lambda_n} \left| q_{n,f} \right| \lambda'_n \right.\right.$$
$$\left.\left. + \left(T_f \Psi \right) \left(\left| \left(\frac{\partial p_c}{\partial S_w} \right)_f \right| \right) \right) \right] \leq C_{max} \qquad f = 1, N_{faces}, \quad (3.17)$$

where C_{max} is an user-defined limit. $V_{i|f}$ and $\left(\frac{\partial p_c}{\partial S_w}\right)_f$ are respectively the linear interpolated values of the neighbor cell's volume and derivative of capillary pressure with respect to wetting phase saturation S_w. The C number includes all considered phenomena (gravity and capillarity) and their spatial variations to better spot local effects that could results in instability. The time-step factor F is defined as:

$$F = \frac{C_{max}}{C}. \quad (3.18)$$

It can be noted that if capillary and gravity effects are neglected, Coats (C) and Todd (T) conditions reduce to the same restriction.This is in agreement with other analysis (Russell et al., 1989; Wan et al., 2005).

3.2.4 Time-step increasing factor management

In order to improve stability and avoid large time-step changes, the time step is computed as

$$\Delta t_{n+1} = \min \left(\min \left(F, 1 + 0.1F \right), 1.2 \right) \Delta t_n. \quad (3.19)$$

where F is the time step factor defined for each stability number (Courant, Coats or Todd).This approach is inherited from classical OpenFOAM solvers (Hrvoje, 1996) and limits the maximal increase to 20 %, and reduces the increase between $\sim$ 11 and 20 % as shown in Figure (3.1). Note that this heuristic management mainly occurs at the beginning of the simulations when saturation and pressure gradients are important. During simulations, the variation of stability numbers is small between time iterations and the upper bound of 1.10 % is rarely reached.

3.3 Numerical experiments

In order to highlight the differences between the above stability criteria, simulations on well-known test cases are performed. We first consider a classical Buckley-Leverett experiment (viscous and gravitational regimes), then a 1D capillary rise experiment (capillary regime)

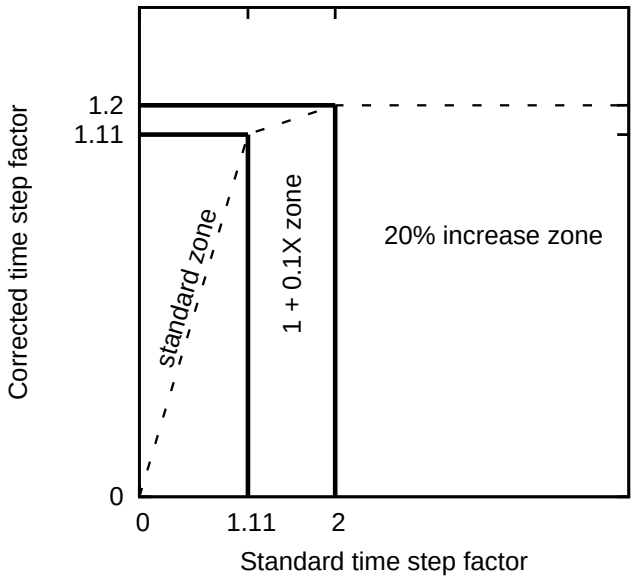

Figure 3.1: Time step evolution law.

and finally the 2D heterogeneous case (considering the three flow regimes) from (Christie et al., 2001). Without other mentions, simulations are run with $k_{r,w_{max}} = 1$ and $k_{r,n_{max}} = 1$. Saturation limits are set with $S_{w,irr} = S_{n,res} = 0.001$. Brooks and Corey's m parameter is equal to $m = 5$. To assess the efficiency of stability criteria, accumulated linear solver iterations are plotted as a function of physical time of the simulated phenomenon. Indeed, the sole time step size data cannot render if the resolution is more or less time consuming. Some criterion can return a bigger time step which leads to harder to solve system for the linear solver. That is why the accumulated sum of the linear solver iterations is chosen. It provides a better idea of whether the system is fast or long to solve whatever the size of the time step is because linear solver iterations are directly proportional to CPU-time needed to inverse the matrices.

Throughout the cases, ratio between viscous flux Φ_μ, gravitational flux $\Phi_{\mathbf{g}}$ and capillary flux Φ_{p_c} is given if relevant. The total flux Φ_t resulting from the pressure equation (3.8) is considered to be decomposed as:

$$\Phi_t = \Phi_\mu + \Phi_{\mathbf{g}} + \Phi_{p_c}, \tag{3.20}$$

highlighting the competition of the different phenomena driving the flow.

3.3.1 Buckley-Leverett experiments

Wetting phase is injected at $|u_{inj}| = 10^{-5}$ m.s^{-1} in the same direction as gravity acceleration with an absolute scalar permeability $K = 10^{-11}$ m^2. Gradient of capillary pressure is assumed

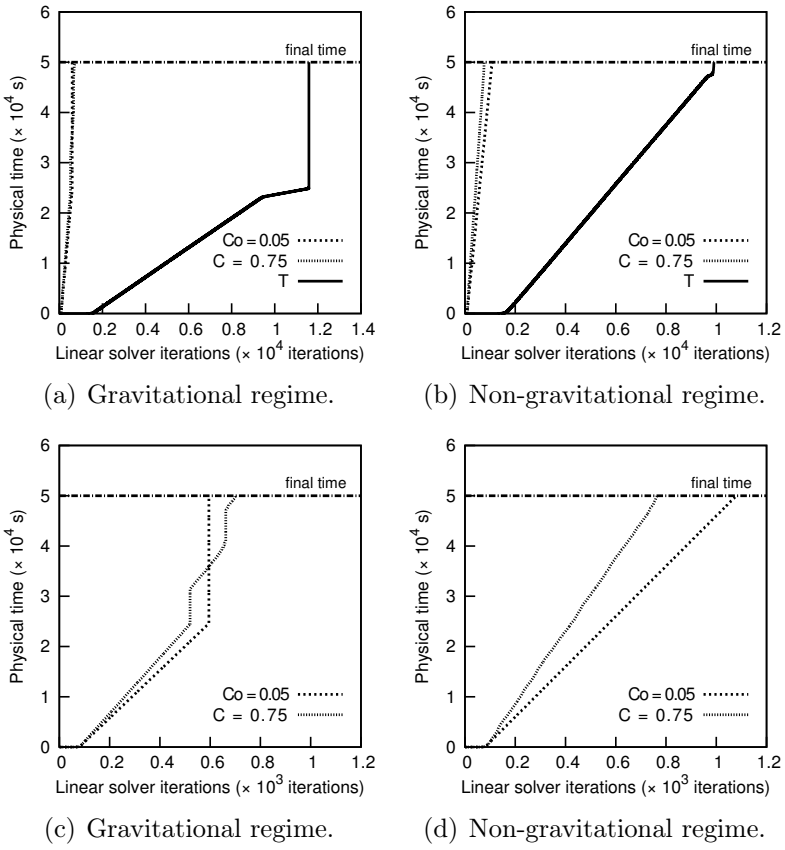

(a) Gravitational regime. (b) Non-gravitational regime.

(c) Gravitational regime. (d) Non-gravitational regime.

Figure 3.2: Evolution of the accumulated linear solver iterations for one-dimensional Buckley-Leverett experiment using the different stability criteria T , C and Co: (a,b) all stability criteria and (c,d) focusing C and Co criteria.

to be null. Depending on the regime, a semi-analytical solution can be calculated to predict the velocity and shape of the saturation front. This test highlights the relative permeability contribution to instability. In the gravitational case, the gravitational flux $\Phi_{\mathbf{g}}$ is 20 times greater than the viscous flux Φ_{μ}. The gravitational effects will set the front velocity.

Simulations have been checked to be in close agreement with semi-analytical results.The front velocity in gravitational or non-gravitational regime are close or equal to the theoretical values.

Figures 3.2(a)-3.2(b) plot the accumulated linear solver iterations necessary to reach the final physical time and highlight that the T factor is clearly too restrictive for the Buckley-Leverett case and requires between 10 and 50 times more iterations. Equation (3.15) gives too restrictive time steps for 1D cases which has been highlighted in (Todd et al., 1972). The criteria Co and C methods have similar time-steps (Figures 3.2(c)-3.2(d)) and involve almost the same computation time. However, we should note that contrary to

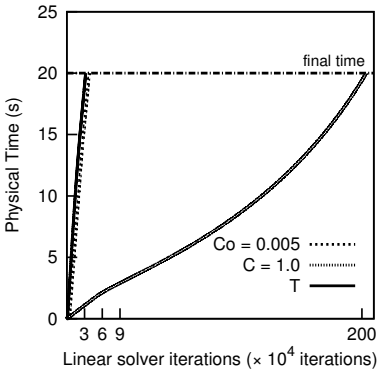

Figure 3.3: Evolution of the accumulated linear solver iterations for the capillary rise configuration.

the C factor, the Co method is case-dependent in the setting of its upper bound Co_{max} and therefore, several tests were necessary to get the optimized value.

3.3.2 Capillary-gravity equilibrium experiment

In order to test the capillary pressure contribution for the different criteria, we perform simulations on a 1D horizontal domain half-filled with water (of viscosity $\mu_w = 10^{-3} Pa \cdot s$ and density $\rho_w = 1000\, kg \cdot m^{-3}$). The other half is filled with air (of viscosity $\mu_w = 1.76\, 10^{-5} Pa \cdot s$ and density $\rho_n = 1\, kg \cdot m^{-3}$). The capillary pressure parameter, $p_{c,0} = 1000\, Pa$, has been tuned to balance gravity forces for this set of parameters. At the beginning of the simulation, the flow is mainly capillary-dominated due to high saturation gradients until the equilibrium state between capillary and gravity forces is reached. In this configuration, T based method efficiency is close to the Co based method(1.2 times faster) while the C method is 60 times slower with a upper bound $C_{max} = 1$(see Fig.(3.3)).

The maximum stable values of parameters Co_{max} and C_{max} for the tested cases and the related maximum time-step size reached during the simulations are reported in Table 3.1. It can be noticed that the Coats' criteria still ensures a stable simulation with values above the theoretical unit value ($C_{max} = 1$) as observed in (Coats et al., 2001, 2003). For gravitational Buckley-Leverett experiment,the saturation front is very sharp and leads to very restrictive criteria and maximum allowed time-step of similar size with Co criteria. The same remark can be derived from accumulated time steps Fig. 3.2(c). For capillary-gravity equilibrium simulation, even though maximal value of upper bound C_{max} is very high, the allowed time step is very restrictive. In such a configuration,Co and T criteria seem more appropriate.

	Co_{max}	C_{max}	$\Delta t_{Co,max}$	$\Delta t_{C,max}$	$\Delta t_{T,max}$
Non-gravitational Buckley-Leverett	0.15	1.19	37.49	65.25	0.18
Gravitational Buckley-Leverett	0.08	2.06	20	20.293	0.084
Capillary-gravity equilibrium	0.005	7.00	149.48	14.156	379.2

Table 3.1: Limits for Co_{max} and C_{max} parameters and maximum time-step allowed on Buckley-Leverett and Capillary rise cases.

3.3.3 SPE 10: 2D heterogeneous case

SPE 10th comparative solution project (Christie et al., 2001) proposed a two dimensional heterogeneous permeability field, a more realistic configuration than academic cases previously tested. The different stability numbers are tested out in non-gravitational, gravitational and capillary regime. Phase densities and viscosities are given by the authors ($\rho_{gas} = 1$ and $\rho_{oil} = 700$ kg.m^{-3}, $\mu_{gas} = 10^{-5}$ and $\mu_{oil} = 10^{-3}$ Pa.s). Relative permeabilities and capillary pressure follow a Brooks and Corey law with coefficient $m = 5$. The case is an injection-production scenario: gas is injected at the left side of the domain, oil and gas are produced at the right side. Without gravity (Figure 3.4, top) the gas injected pushes the oil towards the production wellbore, while including gravity effects (Figure 3.4, middle), oil and gas segregate because of the density difference and gas overlays oil present. Capillary effects taken into account with $p_{c,0} = 0.1$ bar, tend to smooth saturation values. In order to have easily readable representation of the prescribed domain, aspect ratio 0.2:2 is adopted. The accuracy of the numerical results are ensured by considering L_2-norm error with $Co_{max} = 5 \cdot 10^{-4}$ case as reference. The configurations tested present a maximal relative error below 0.5 %. Knowing that the discretization scheme used in 2D, the T prefactor should be set to 0.25. However, gravitational case is more challenging regarding stability and T prefactor should be reduced in order to ensure stability of the simulation as mentioned in (Todd et al., 1972). In the gravitational case, gravitational flux $\Phi_{\mathbf{g}}$is 100 times greater than viscous flux Φ_μ and in capillary dominated case $\Phi_{p_c}$is 500 times greater than Φ_μ.

The C method and the T method leads to similar computing time in the non gravitational case (cf. figure Fig. 3.5(a)), while Co leads to simulation 2.2 times slower.

In the gravitational case, the criterion Co leads to the fastest resolution (reported on Fig. 3.5(b)), more than 2 times faster than C criteria. This case illustrates what has been observed before in (Coats et al., 2003, 2001). C number could be either uniformly distributed throughout the domain and reaches its limit value only in one point (cf . Figure 3.6(a)) or has a more non uniform distribution with intermediate values and several points at the maximum value (cf. Figure 3.6(b)). In the first case , the stability is critical and C provides a good approximation of a suitable time step to keep the simulation stable. In the second

	Co_{max}	C_{max}	$\Delta t_{Co,max}$	$\Delta t_{C,max}$	$\Delta t_{T,max}$
Non gravitational	0.01	2.11	2445.3	27736	53290
Gravitational	0.01	0.56	2197	4925	7618
Capillary	0.01	3.63	2316	8583	49777
Capillary-gravity	0.003	0.36	667	1244	2512

Table 3.2: Limits for Co_{max} and C_{max} parameters and maximum time-step allowed on Buckley-Leverett and Capillary rise cases.

configuration, it is remarked that C is too restrictive and stability is still ensured for values beyond $C = 1$. Due to this change in distribution, C requires almost 8 more linear solver iterations to solve the problem. The T method behaves slightly better with a 1.75 times faster simulation.

Similarly to the one-dimensional test cases, the capillary driven case is the most difficult to achieve both stability and efficiency using C number because, without any other effects, it leads to unnecessary small time-steps. This is also the case for Co driven simulations because it requires to impose very low maximum limit (here 10^{-2}). Regarding efficiency, T is the best criterion as observed previously (Fig. 3.5(c)). Comparing the efficiency for this configuration, T is 4.25 times faster than Co and C is almost 6 times slower.

In the case where both capillary and gravitational effects are present, the T criteria and C criteria leads to similar performance while the Co produces a twice slower simulation (see Fig. 3.7.

As for homogeneous porous medium, the maximum stable values of criteria C and Co are gathered in Table 3.2. These results highlights that Coats number C allows the use of time-step from 2 to 10 times larger than those obtained with Co driven simulations. Non-gravitational cross-flow exhibits C_{max} larger than the similar Buckley-Leverett experiment (2.11 instead of 1.19) which can be explain because of the non-uniform distribution of maximum values of the criteria as shown in Fig. 3.6. This configuration also occurs for capillary dominated case. When gravitational effects are included, with or without capillary effects, $C_{max} = 1$ is no longer stable and should be reduced . Nonetheless, this criteria remains than Co driven simulation. The non-gravitational configuration is reported to be stable with value of $C_{max} = 2.0$ in (Coats et al., 2003).

For the challenging 2D cases that include gravity forces, Todd's criteria T had to be tuned to ensure stability, a prefactor δ is introduced as suggested in (Todd et al., 1972). The values of this factor are respectively $\delta = 1/16$ for gravity only case and $\delta = 1/32$ for the case in which all forces competed.

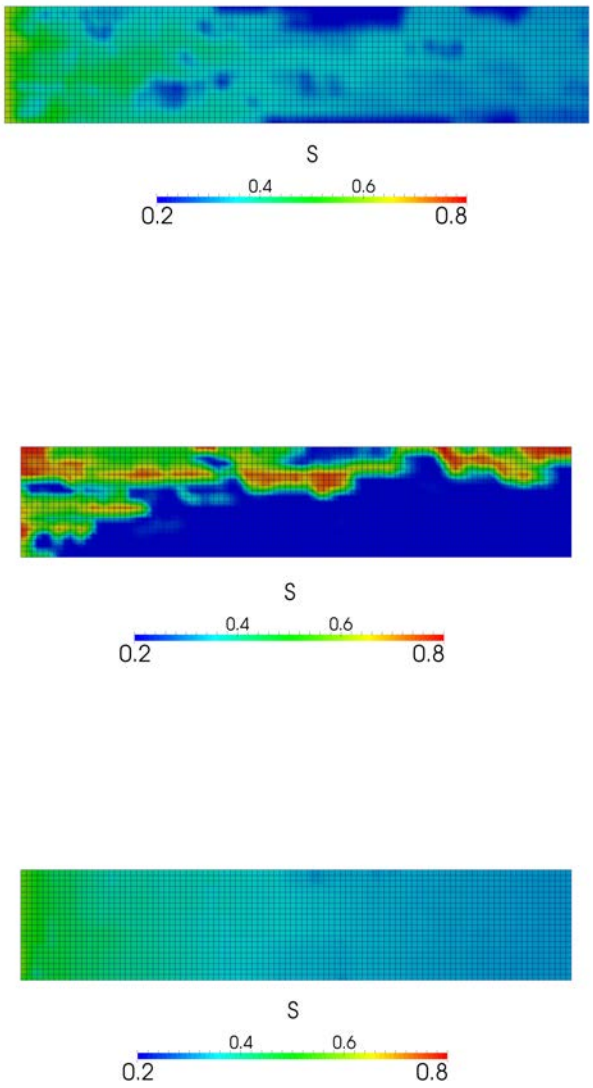

Figure 3.4: Gas saturation field 2D SPE 10 case for (top) non-gravitational, (middle) gravitational and (bottom) capillary regime.

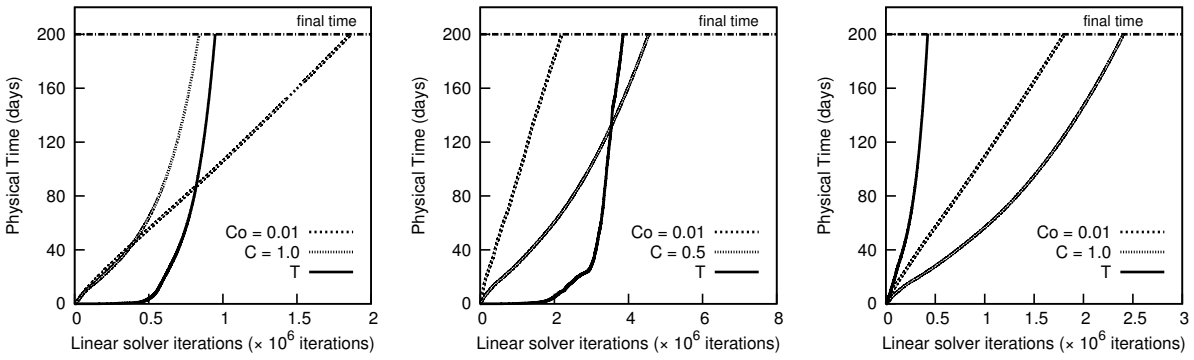

(a) Non-gravitational regime. (b) Gravitational regime. (c) Capillary regime.

Figure 3.5: Evolution of the accumulated linear solver iterations for the SPE 10 2D.

(a) Time 149 days. (b) Time 172 days.

Figure 3.6: Uniform and non uniform C number distribution in gravitational regime.

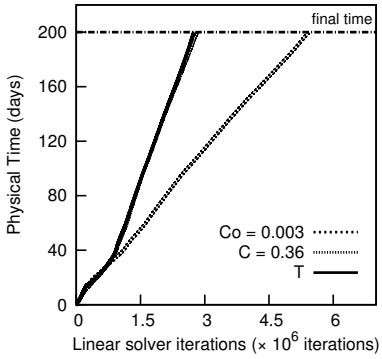

Figure 3.7: Evolution of the accumulated linear solver iterations for the SPE 10 2D in capillary-gravity regime.

3.4 Conclusion

IMPES algorithm and its sequential structure still represent an interesting alternative to coupled approaches when treating problems with challenging number of grid cells as required by highly detailed models. However, due to the specific form of conservative equations, the derivation of stability criterion more adapted than classic CFL condition is needed. Several contributions have tried to define more adapted saturation and pressure variation criterion (Todd et al., 1972) and still studying improvement on their formulation (Coats et al., 2003).

In this study, these various criteria have been compared with the classical Courant number in various conditions leading to the following observations. For homogeneous cases C method with limit set to $C_{max} = 1$ will ensure stability in every configuration. For 2D heterogeneous cases, the C method faces two configuration:

- When saturation front is diffuse, which is the case for capillary or viscous dominated flows, it is safe to use limit as $C_{max} = 1$. However, it can be noted that the T method offers an interesting alternative, leading to stable and fastest simulation.

- When saturation front is sharp, which is the case for gravity and capillary-gravity cases, phases are segregated and users have to limit criterion to $C_{max} = 0.25$, in order to keep simulation stable. In the capillary-gravity configuration, the T- method leads to similar performance as the C-method.

Even if Co driven simulations can give better results in some cases, it remains a condition too dependent on the considered case. Co_{max} limit to be imposed for ensuring stability can differ by a factor of 1000 and makes this criterion unreliable.

Acknowledgments

We thank ENGIE EPI and STORENGY for their financial support to J. Franc .

References

Aziz, K. and Settari, A.: 1979, *Petroleum reservoir simulation*, Applied Science Publishers London.

Cao, H.: 2002, *Development of techniques for general purpose simulators*, PhD thesis, Stanford University.

Christie, M., Blunt, M. et al.: 2001, Tenth spe comparative solution project: A comparison of upscaling techniques, *SPE Reservoir Evaluation & Engineering* .

Coats, K. et al.: 2001, Impes stability: The cfl limit, *SPE Reservoir Simulation Symposium*, Society of Petroleum Engineers.

Coats, K. et al.: 2003, Impes stability: selection of stable timesteps, *SPE Journal* .

Corey, A. and Brooks, R.: 1975, Drainage characteristics of soils, *Soil Science Society of America Journal* .

Courant, R., Friedrichs, K. and Lewy, H.: 1928, Uber die partiellen differenzengleichungen der mathematischen physik., *Math. Ann.* .

Forsyth, P.: 1989, Adaptive implicit criteria for two-phase flow with gravity and capillary pressure, *SIAM Journal on Scientific and Statistical Computing* .

Franc, J., Horgue, P., Guibert, R. and Debenest, G.: 2016, Benchmark of different cfl conditions for impes, *Comptes Rendus Mécanique* .

Gerritsen, M. and Durlofsky, L.: 2005, Modeling fluid flow in oil reservoirs, *Annu. Rev. Fluid Mech.* .

Homsy, G.: 1987, Viscous fingering in porous media, *Annual review of fluid mechanics* .

Horgue, P., Soulaine, C., Franc, J., Guibert, R. and Debenest, G.: 2014, An open-source toolbox for multiphase flow in porous media, *Computer Physics Communications* .

Hrvoje, J.: 1996, *Error Analysis and Estimation for the Finite Volume Method with Applications to Fluid Flows*, PhD thesis, Department of Mechanical Engineering Imperial College of Science, Technology and Medecine.

Leverett, M. et al.: 1941, Capillary behavior in porous solids, *Transactions of the AIME* .

Morel-Seytoux, H., Meyer, P., Nachabe, M., Tourna, J., Genuchten, M. v. and Lenhard, R.: 1996, Parameter equivalence for the brooks-corey and van genuchten soil characteristics: Preserving the effective capillary drive, *Water Resources Research* .

Mostaghimi, P., Percival, J., Pavlidis, D., Ferrier, R., Gomes, J., Gorman, G., Jackson, M., Neethling, S. and Pain, C.: 2015, Anisotropic mesh adaptivity and control volume finite element methods for numerical simulation of multiphase flow in porous media, *Mathematical Geosciences* .

Muskat, M.: 1949, Physical principles of oil production.

Negara, A., Salama, A. and Sun, S.: 2015, Multiphase flow simulation with gravity effect in anisotropic porous media using multipoint flux approximation, *Computers & Fluids* .

Russell, T. et al.: 1989, Stability analysis and switching criteria for adaptive implicit methods based on the cfl condition, *SPE Symposium on Reservoir Simulation*, Society of Petroleum Engineers.

Sammon, P. et al.: 1988, An analysis of upstream differencing, *SPE reservoir engineering* .

Shewani, A., Horgue, P., Pommier, S., Debenest, G., Lefebvre, X., Gandon, E. and Paul, E.: 2014, Assessment of percolation through a solid leach bed in dry batch anaerobic digestion processes, *Bioresource Technology* .

Soulaine, C., Horgue, P., Franc, J. and Quintard, M.: 2014, Gas-liquid flow modeling in columns equipped with structured packing, *AIChE Journal* .

Thomeer, J. et al.: 1960, Introduction of a pore geometrical factor defined by the capillary pressure curve, *Journal of Petroleum Technology* .

Todd, M., O'dell, P., Hirasaki, G. et al.: 1972, Methods for increased accuracy in numerical reservoir simulators, *Society of Petroleum Engineers Journal* .

Van Genuchten, M. T.: 1980, A closed-form equation for predicting the hydraulic conductivity of unsaturated soils, *Soil Science Society of America Journal* .

Wan, J., Sarma, P., Usadi, A., Beckner, B. et al.: 2005, General stability criteria for compositional and black-oil models, *SPE Reservoir Simulation Symposium*, Society of Petroleum Engineers.

Weller, H., Tabor, G., Jasak, H. and Fureby, C.: 1998, A tensorial approach to computational continuum mechanics using object-oriented techniques, *Computers In Physics* .

Chapter 4

FV-MHMM algorithm

Contents

Résumé en français

Ce chapitre concerne l'adaptation d'une méthode mixte hybride originellement formulée sous la forme d'une méthode aux éléments finis (Harder et al., 2013, 2015), en méthode volumes finis.On la nommera *FV-MHMM*, cela faisant référence à "Finite Volume- Mixed Hybrid Multiscale Model". A l'instar des méthodes mixtes hybrides, elle repose sur l'imposition faible de la contrainte de continuité entre les cellules via l'utilisation de multiplicateurs de *Lagrange*. Ce découpage permet alors d'envisager le sous-maillage à l'échelle fine (dans ces travaux l'échelle de Darcy) de blocs grossiers suscités. Un série de problèmes locaux est alors résolue sur les partitions de maillage fin ainsi découpées. Ces problèmes sont alors indépendants, ce qui ouvre la voie à une résolution parallélisée efficace. De ces problèmes locaux sont déduit des fonctions de bases qui sont utilisées une première fois pour l'assemblage d'un problème global, où la valeur des multiplicateurs de *Lagrange* est résolue. Dans un second temps, elles servent à construire sur la discrétisation fine, un champ de pression approximé par la méthode multiéchelle.

Ces méthodes multiéchelles ont, comme évoqué dans le Chapitre 1, l'avantage d'incorporer l'information des hétérogénéités de l'échelle fine à l'échelle supérieure et donc de contourner le problème des méthodes de changement d'échelle classique. De plus, l'aspect dynamique du couplage entre les échelles permet d'envisager une extension aux systèmes polyphasiques. La méthode *FV-MHMM*, décrite ici, hérite également du raffinement de l'espace des fonctions tests polynomiales pour gagner en précision.

Dans ces travaux, la formulation de la méthode est détaillée ; puis on s'attache à valider le caractère superconvergent de la méthode tout en se comparant à des solutions analytiques classiques(Carslaw and Jaeger, 1959). Plus précisément, les vérifications en comparaison avec une solution volumes finis à l'échelle fine, notamment sur les faciès chenalisés du test SPE 10, font apparaître la nécessité de pondérer les fonctions tests en les corrélant aux détails des hétérogénéités sous-jacentes. Enfin, l'algorithme est adapté et étendu aux écoulements monophasiques faiblement compressibles et diphasiques pour des cas simples.

Ce chapitre a fait l'objet de la publication "*FV-MHMM method for reservoir modeling" (Franc et al., 2016),* dans la revue *Computational Geosciences* en Avril 2017.

The present paper proposes a new family of multiscale finite volume methods. These methods usually deal with a dual mesh resolution, where the pressure field is solved on a coarse mesh, while the saturation fields, which may have discontinuities, are solved on a finer reservoir grid, on which petrophysical heterogeneities are defined. Unfortunately, the efficiency of dual mesh methods is strongly related to the definition of up-gridding and down-gridding steps, allowing defining accurately pressure and saturation fields on both fine and coarse meshes and the ability of the approach to be parallelized. In the new dual mesh formulation we developed, the pressure is solved on a coarse grid using a new hybrid formulation of the parabolic problem. This type of multiscale method for pressure equation called Multiscale Hybrid-Mixed method (MHMM) has been recently proposed for finite elements and mixed-finite element approach (Harder et al., 2013). We extend here the MH-Mixed Method to a Finite Volume discretization, in order to deal with large multiphase reservoir models. The pressure solution is obtained by solving a hybrid form of the pressure problem on the coarse mesh, for which unknowns are fluxes defined on the coarse mesh faces. Basis flux functions are defined through the resolution of a local finite volume problem, which accounts for local heterogeneity, whereas pressure continuity between cells is weakly imposed through flux basis functions, regarded as Lagrange multipliers. Such an approach is conservative both on the coarse and local scales and can be easily parallelized, which is an advantage compared to other existing finite volume multiscale approaches. It has also a high flexibility to refine the coarse discretization just by refinement of the Lagrange multiplier space defined on the coarse faces without changing nor the coarse nor the fine meshes. This refinement can also be done adaptively w.r.t. a posteriori error estimators. The method is applied to single phase (well-testing) and multiphase flow in heterogeneous porous media.

4.1 Introduction

Upscaling and scaling laws in science remain a challenge. Finding ways to deal with complex phenomena at a given scale and then, producing a mathematical model able to represent this physics, at the so-called macroscale, is difficult for many fields (hydrology, reservoir engineering, meteorology, etc...) (Wood, 2009).

For single-phase incompressible flows in porous media, pressure field obeys the following elliptic equation:

$$\begin{aligned} \boldsymbol{\nabla} \cdot (-K(\mathbf{x})\boldsymbol{\nabla} u) &= f \quad \text{in } \Omega, \\ u &= u_g \quad \text{on } \partial\Omega. \end{aligned} \tag{4.1}$$

where $K(\mathbf{x})$ is a symmetric and positive definite tensor defined at the Darcy's scale. The permeability distribution in space yields correlated structures that span several orders of magnitude. The link between the local scale, that is the Darcy-scale where $K(\mathbf{x})$ is locally varying, to a larger scale such as the reservoir scale was and continues to be the object of much attention in order to predict accurate fluid flows in porous media. When the medium is homogeneous or large enough for length scales to be separated , the problem is well understood and references are easy to find (see for instance (Renard and De Marsily, 1997)). However, when there is no length scale separation or when two-phase flow problems are studied (*i.e.* when pressure field is coupled with a saturation field strongly dependent on local heterogeneity), details of the permeability at the Darcy-scale must be kept in order to correctly describe flow in porous media.

Numerous multiscale algorithms are available to address this problem. Unlike traditional methods, multiscale approaches benefit from keeping information on the underlying details. Examples of these methods can be found in Multiscale Finite Element Methods (*MsFEM*) (Chen and Hou, 2003; Hou and Wu, 1997), numerical subgrid methods (*NSub*) (Arbogast, 2002) or the Multiscale Finite Volume Method (*MsFv*) (Jenny et al., 2003, 2005). All these methods address the problem by embedding Darcy-scale information from resolution of the sub-problems into the resolution of a reservoir-scale discretized problem. *MsFEM* (Chen and Hou, 2003; Hou and Wu, 1997) detailed and improved in (Aarnes, 2004), relies on the construction of a local basis function suited to the heterogeneities. Local velocity, ensuring mass conservation, is obtained using a mixed formulation. *NSub* proposes a different approach based on the decomposition of pressure into a coarse scale pressure and its subscale variation on fine scale. Coarse scale pressure is approximated using RT_0 (Raviart and Thomas, 1977) or BDM_1 (Brezzi et al., 1985) spaces while subscale variations use RT_0 spaces on the fine scale. Eventually *MsFv* formulates a method that obtains pressure as a linear combination of constructed coarse scale basis functions that embed fine scale variations. *MsFv* has to construct a dual grid in order to build its global system. Applying boundary conditions can be tedious (Dehkordi and Manzari, 2013). Moreover, it has been reported (Wang et al., 2014) that *MsFv*, without smoothing steps, can not solve some of the 10th SPE (Christie et al., 2001a) slices as it only resolves low frequency errors. It will be highlighted in the numerical tests.

This paper intends to develop a new finite volume multiscale method (*FV-MHMM*) derived from the Multiscale Hybrid-Mixed method (*MHMM*) formulated for finite elements and the mixed-finite element approach (Harder et al., 2013, 2015). The pressure equation is solved using a hybrid formulation on the coarse mesh, for which the unknowns are fluxes defined on the coarse mesh faces. Basis functions required for the construction of the

coarse-scale system (referred to as the global system) are obtained by solving two kinds of local problems, which account for heterogeneities in the permeability field but also for the treatment of the local source terms (*e.g.* wellbore pressure). The pressure continuity between coarse cells is then ensured by regarding flux basis functions as Lagrange multipliers. Such a method ensures mass conservation on both the local and global scales. It also offers the possibility of improving the coarse scale solution by refining the Lagrange multiplier space defined on coarse faces without changing either the coarse discretization or the fine mesh grid. This method offers the possibility of adaptive refinement with respect to *a posteriori* estimators.

The first section is dedicated to the mathematical formulation of the *FV-MHMM* method. The construction of the two kinds of local basis functions and the formulation of a global problem, including Lagrange multipliers as flux unknowns, are exposed. The second section presents selected numerical test cases. It is divided into three parts. The first part studies the convergence behavior of the method and gives the results on a heterogeneous permeability field. The second part presents the adaptation of the *FV-MHMM method* to slightly compressible flows and the third part extends this approach to two-phase flow, coupling the pressure equation with a fine scale updated equation of saturation.

4.2 Mathematical Development

4.2.1 Multiscale Hybrid-Mixed method

Let us define a polyhedral (polygonal in 2D) coarse mesh of the domain Ω by its set M_H of coarse cells $K \in M_H$ and its set of coarse planar faces (edges in 2D) F_H. On each coarse face of F_H, we define the unit normal vector $\mathbf{n}$ with a fixed orientation taking care to ensure that it is oriented outward on $\partial\Omega$. For each coarse cell $K \in M_H$, the unit normal vector on ∂K oriented outward to ∂K is denoted by $\mathbf{n}_K$.

The Multiscale Hybrid-Mixed method developed in (Harder et al., 2013, 2015) is based on the following primal hybrid variational formulation of (4.1) introduced in (Raviart and Thomas, 1977) which weakly enforces the continuity of the solution at the coarse faces F_H through the action of Lagrange multipliers:

find $(u,\lambda) \in V \times \Lambda$ *such that*:

$$\begin{aligned}\int_\Omega K(\mathbf{x})\boldsymbol{\nabla} u \cdot \boldsymbol{\nabla} v dx \;\; &+ \;\; \sum_{K\in M_H} \int_{\partial K} \lambda \mathbf{n}\cdot\mathbf{n}_K \, v|_K d\sigma \\ &+ \sum_{K\in M_H} \int_{\partial K} \mu \mathbf{n}\cdot\mathbf{n}_K u|_K d\sigma \\ &= \int_\Omega f v dx + \int_{\partial\Omega} \mu u_g d\sigma \quad \text{for all } (v,\mu) \in V\times\Lambda.\end{aligned} \tag{4.2}$$

where V is the broken Sobolev space $H^1(M_H)$ defined by

$$H^1(M_H) = \{v \in L_2(\Omega) :\; v|_K \in H^1(K),\, K \in M_H\},$$

Λ stands for the following Lagrange multipliers space

$$\Lambda := \{\mu \in \prod_{K\in M_H} H^{-\frac{1}{2}}(\partial K) : \exists \boldsymbol{\sigma} \in H_{div}(\Omega) \text{ s.t. } \mu|_{\partial K} = \boldsymbol{\sigma}\cdot\mathbf{n}|_{\partial K},\; K \in M_H\},$$

,∇v is the broken gradient equal to $\nabla v|_K$ on each coarse cell $K \in M_H$, $H_{div}(\Omega)$ is defined as:

$$H_{div}(\Omega) := \{\boldsymbol{\sigma} \in [L^2(\Omega)]^d : \boldsymbol{\nabla}\cdot\boldsymbol{\sigma} \in L^2(\Omega)\},$$

and $H^{-\frac{1}{2}}(\partial K)$ is the dual space of the space $H^{\frac{1}{2}}(\partial K)$ span by the traces on ∂K of functions in $H^1(K)$.

Let us denote by V_0 the space of cellwise constant functions in each coarse cell $K \in M_H$ and by W_K the set of functions in $H^1(K)$ with zero mean value on K. Then, $W := \Pi_{K\in M_H} W_K$ is a subspace of V such that we have the orthogonal decomposition

$$V = V_0 \oplus W = V_0 \oplus \bigoplus_{k\in M_H} W_K.$$

Following this decomposition, each $v \in V$ is uniquely decomposed as $v = v_{0,K} + \sum_{K\in M_H} \tilde{v}_K$ with $v_{0,K} \in V_0$ and $\tilde{v}_K \in W_K$ which leads to the splitting of the previous variational formulation as the sum of two local problems set on W_K for each coarse cell $K \in M_H$ and a global problem set on $V_0 \times \Lambda$.

For a given $\lambda \in \Lambda$, the first local problem, referred to as the *local lambda problem* (*LLP*) in the following, writes (see (Harder et al., 2015, 2013) for details): *Find* $\tilde{u}_K \in W_K$ *such that*:

$$\int_K K(\mathbf{x})\boldsymbol{\nabla}\tilde{u}_K \cdot \boldsymbol{\nabla}\tilde{v}_K dx + \int_{\partial K} \lambda\mathbf{n}\cdot\mathbf{n}_K \tilde{v}_K d\sigma = 0 \quad \text{for all } \tilde{v}_K \in W_K, \tag{4.3}$$

and we set $\tilde{u}_K = T_K\lambda$.

The second local problem dealing with the source term f and referred to as the *local source problem* (LSP) in the following, writes (see (Harder et al., 2013, 2015) for details): *Find* $\tilde{u}_K \in W_K$ *such that*:

$$\int_K K(\mathbf{x})\boldsymbol{\nabla}\tilde{u}_K \cdot \boldsymbol{\nabla}\tilde{v}_K dx = \int_K f\tilde{v}_K dx \quad \text{for all } \tilde{v}_K \in W_K, \tag{4.4}$$

and we set $\tilde{u}_K = \hat{T}_K f$.

The global problem solve the coarse conservation equations together with the trace continuity equations at the coarse interfaces (see (Harder et al., 2015, 2013) for a detailed analysis of this formulation): *find* $u_{0,K} \in \mathbb{R}, K \in M_H$ *and* $\lambda \in \Lambda$ *such that*:

$$\begin{cases} \displaystyle\sum_{K\in M_H} \int_{\partial K} \lambda\mathbf{n}\cdot\mathbf{n}_K d\sigma = \int_K f dx \quad \text{for all } K \in M_H, \\ \displaystyle\sum_{K\in M_H} \int_{\partial K} \mu\mathbf{n}\cdot\mathbf{n}_K(u_{0,K} + T_K\lambda + \hat{T}_K f)d\sigma = \int_{\partial\Omega} \mu u_g \quad \text{for all } \mu \in \Lambda. \end{cases} \tag{4.5}$$

The objective of the next subsection is to specify the MHM method when a Two Point Flux finite volume scheme is used to solve the local problems.

4.2.2 MHM method coupled with a Two Point Flux Approximation (TPFA) of the local problems

Each coarse cell K is submeshed with an orthogonal fine mesh and we denote by $M_{h,K}$ the set of sub-cells, by $F^{int}_{h,K}$ the set of interior faces and by $F^{ext}_{h,K}$ the set of boundary faces. The set of faces of the cell $X \in M_{h,K}$ is denoted by $F_X \subset F^{int}_{h,K} \cup F^{ext}_{h,K}$. The set of two cells sharing the interior face $\sigma \in F^{int}_{h,K}$ is denoted by $M_\sigma = \{X, Y\}$ and the notation $X|Y$ will also be used to denote the face σ at the interface between the two cells.

Let $V_{h,K}$ be the space of cellwise constant functions in each cell $X \in M_{h,K}$. For $u_{h,K} \in V_{h,K}$, we denote by u_X the value of $u_{h,K}$ in the cell X for all $X \in M_{h,K}$. V_h will denote the space of cell-wise constant functions on each cell $X \in M_h = \bigcup_{K\in M_H} M_{h,K}$ and for $u_h \in V_h$, $u_{h,K}$ denotes the restriction of u_h to the coarse cell K. Let us set

$$W_{h,K} = \{u_{h,K} \in V_{h,K} \,|\, \sum_{X\in M_{h,K}} |X|u_X = \int_K u_{h,K}(x)dx = 0\}.$$

Let us denote by $V_{h,\partial K} \subset L^2(\partial K)$ the set of piecewise constant functions on each face $\sigma \in F^{ext}_{h,K}$. For $u_{h,\partial K} \in V_{h,\partial K}$, we denote by $u_{K,\sigma}$ the value of $u_{h,\partial K}$ on the face $\sigma \in F^{ext}_{h,K}$.

The approximate solution in each coarse cell K and the approximate trace on ∂K , $K \in M_H$ will be denoted by $(u_{h,K}, u_{h,\partial K}) \in V_{h,K} \times V_{h,\partial K}$.

Let $(v_{h,K}, v_{h,\partial K}) \in V_{h,K} \times V_{h,\partial K}$, the TPFA at the face $\sigma \in F_X \cap F_{h,K}^{int}$ outward to the cell X is defined by

$$F_{X,Y}(v_X,v_Y) = F_{X,\sigma}(v_X,v_Y) = T_\sigma(v_X - v_Y), M_\sigma = \{X, Y\},$$

where T_σ is the transmissivity of the interior face σ, and the TPFA at the boundary face $\sigma \in F_X \cap F_{h,K}^{ext}$ outward to the cell X is given by

$$F_{X,\sigma}(v_X, v_{K,\sigma}) = T_{X,\sigma}(v_X - v_{K,\sigma}),$$

where $T_{X,\sigma}$ is the half transmissivity of the boundary face σ.

Let Λ_H denote a finite dimensional subspace of $L^2(F_H)$.

Local Problems

Using the finite volume scheme with TPFA, the discretization of the LLP local problem (4.3) is given by the following discrete variational formulation: given $\lambda \in \Lambda_H$, find $(u_{h,K}, u_{h,\partial K}) \in W_{h,K} \times V_{h,\partial K}$ such that for all $(v_{h,K}, v_{h,\partial K}) \in W_{h,K} \times V_{h,\partial K}$ one has

$$\begin{cases} \displaystyle\sum_{\sigma=X|Y\in F_{h,K}^{int}} T_\sigma(u_X - u_Y)(v_X - v_Y) \\ + \displaystyle\sum_{\sigma\in F_{h,K}^{ext}, \sigma\in F_X} T_{X,\sigma}(u_X - u_{K,\sigma})(v_X - v_{K,\sigma}) \\ + \displaystyle\sum_{\sigma\in F_{h,K}^{ext}} \int_\sigma v_{K,\sigma}\lambda\mathbf{n}\cdot\mathbf{n}_K d\sigma = 0. \end{cases}$$

Using a Lagrange multiplier to deal with the zero mean value constraint for the test functions in $W_{h,K}$, it is easy to show that this discrete variational formulation is equivalent to the following finite volume conservation equations: find $(u_{h,K}, u_{h,\partial K}) \in W_{h,K} \times V_{h,\partial K}$ such that

$$\sum_{\sigma=X|Y\in F_X\cap F_{h,K}^{int}} T_\sigma(u_X - u_Y) + \int_{\partial K\cap\partial X} \lambda\mathbf{n}\cdot\mathbf{n}_K d\sigma = \frac{|X|}{|K|}\int_{\partial K} \lambda\mathbf{n}\cdot\mathbf{n}_K d\sigma,$$

for all $X \in M_{h,K}$, and

$$F_{X,\sigma}(u_X, u_{K,\sigma}) = T_{X,\sigma}(u_X - u_{K,\sigma}) = \int_\sigma \lambda\mathbf{n}\cdot\mathbf{n}_K d\sigma,$$

at each face $\sigma \in F_{h,K}^{ext} \cap F_X$. Let us define the operators $(T_{h,K}, T_{h,\partial K})$ mapping Λ_H to $L^2(K) \times L^2(\partial K)$ and such that $(T_{h,K}\lambda, T_{h,\partial K}\lambda)$ is equal to the solution $(u_{h,K}, u_{h,\partial K})$ of the previous local problem.

Similarly, the functions $(\hat{T}_{h,K}f, \hat{T}_{h,\partial K}f)$ are defined for $f \in L^2(\Omega)$ by the solution $(u_{h,K}, u_{h,\partial K}) \in W_{h,K} \times V_{h,\partial K}$ of the finite volume conservation equations discretizing the LSP local problem (4.4):

$$\sum_{\sigma=X|Y\in F_X\cap F_{h,K}^{int}} T_\sigma(u_X - u_Y) = \int_X f dx - \frac{|X|}{|K|}\int_K f dx,$$

for all $X \in M_{h,K}$, and $u_{K,\sigma} = u_X$ for all $\sigma \in F_{h,K}^{ext} \cap F_X$.

Let us remark that we have for all $(\lambda, \mu) \in \Lambda_H \times \Lambda_H$

$$\left\{\begin{array}{l} \displaystyle\int_{\partial K} \mu \mathbf{n}\cdot\mathbf{n}_K T_{h,\partial K}\lambda d\sigma = \int_{\partial K} \lambda \mathbf{n}\cdot\mathbf{n}_K T_{h,\partial K}\mu d\sigma \\ \displaystyle = - \sum_{\sigma=X|Y\in F_{h,K}^{int}} T_\sigma(u_X - u_Y)(v_X - v_Y) \\ \displaystyle - \sum_{\sigma\in F_{h,K}^{ext}, \sigma\in F_X} T_{X,\sigma}(u_X - u_{K,\sigma})(v_X - v_{K,\sigma}), \end{array}\right.$$

with $(u_{h,K}, u_{h,\partial K}) = (T_{h,K}\lambda, T_{h,\partial K}\lambda)$, $(v_{h,K}, v_{h,\partial K}) = (T_{h,K}\mu, T_{h,\partial K}\mu)$ which implies that the bilinear form

$$a_{h,K}(\lambda, \mu) = -\int_{\partial K} \mu \mathbf{n}\cdot\mathbf{n}_K T_{h,\partial K}\lambda d\sigma,$$

on $\Lambda_H \times \Lambda_H$ is symmetric positive. The bilinear form $a_{h,K}$ is also definite if the restriction of the space Λ_H to ∂K is not "finer" than the space of piecewise constant functions on the fine faces of ∂K.

Global Problem

The discrete global problem is just obtained by replacing in (4.5) the vector space Λ by the discrete vector space Λ_H and the trace on ∂K of the continuous operators T_K and $\hat{T}_K$ by respectively the operators $T_{h,\partial K}$ and $\hat{T}_{h,\partial K}$ leading to the following set of discrete equations:

find $u_{0,K} \in \mathbb{R}, K \in M_H$ *and* $\lambda \in \Lambda_H$ *such that*:

$$\left\{ \begin{array}{l} \displaystyle\sum_{K \in M_H} \int_{\partial K} \lambda \mathbf{n} \cdot \mathbf{n}_K d\sigma = \int_K f dx \quad \text{for all } K \in M_H, \\ \displaystyle\sum_{K \in M_H} \int_{\partial K} \mu \mathbf{n} \cdot \mathbf{n}_K (T_{h,\partial K} \lambda + u_{0,K}) d\sigma = \int_{\partial \Omega} \mu u_g d\sigma \\ \displaystyle -\sum_{K \in M_H} \int_{\partial K} \mu \mathbf{n} \cdot \mathbf{n}_K \hat{T}_{h,\partial K} f d\sigma \quad \text{for all } \mu \in \Lambda_H. \end{array} \right. \tag{4.6}$$

The first equation is a direct transcription of coarse scale mass conservation while the second equation weakly enforces the trace continuity at coarse interfaces.

Roughly speaking, this mixed linear system (or saddle point problem) will be non singular if Λ_H contains, for each coarse face $\sigma \in F_H$, at least one function supported on σ with non zero mean value on σ, and if Λ_H is not *finer* than the space of piece-wise constant functions on the fine faces of F_H.

In the following 2D numerical test cases, the vector space Λ_H will be typically defined as the vector space of polynomials of degree l on each coarse face of F_H with $l = 0, 1, 2$. These choices of Λ_H will be denoted by Λ_l, $l = 0, 1, 2$ in the following.

Given a basis of Λ_H denoted by $\lambda_{\sigma,i}$ for all $\sigma \in F_H$, $i = 1, \cdots, n_\sigma$, the assembly of the global matrix can be done by computing on each coarse cell K the symmetric negative local rigidity matrix defined by

$$(A_K)^{\sigma_2,i_2}_{\sigma_1,i_1} = \int_{\partial K} \lambda_{\sigma_1,i_1} \mathbf{n} \cdot \mathbf{n}_K T_{h,\partial K} \lambda_{\sigma_2,i_2} d\sigma, \tag{4.7}$$

with $\sigma_1, \sigma_2 \in F_{h,K}$, $i_1 = 1, \cdots, n_{\sigma_1}$, $i_2 = 1, \cdots, n_{\sigma_2}$, as well as the local vector defined by

$$(B_K)_{\sigma,i} = \int_{\partial K} \lambda_{\sigma,i} \mathbf{n} \cdot \mathbf{n}_K \hat{T}_{h,\partial K} f d\sigma, \; \sigma \in F_{h,K}, \; i = 1, \cdots, n_\sigma. \tag{4.8}$$

and doing the global assembly in the finite element fashion.

In order to assess the amount of CPU workloads at each time step, a complexity analysis similar to the analysis of (Jenny et al., 2003) is reported in Appendix 4.4. The time spent in the global stage is indeed larger than in the *MsFv* method, but the overall process is found to be faster for constant($l = 0$) or linear($l = 1$) basis and as fast for quadratic ($l = 2$).

4.3 Numerical tests

In this section, numerical tests on different formulations of the *FV-MHMM* algorithm are performed. In the first subsection, convergence and heterogeneous test cases for incompressible formulation are presented. The second subsection shows how to adapt the algorithm to slightly compressible flows and presents a basic example of a production wellbore in a bounded reservoir. In the last subsection, a two-phase case permits to present the adaptation of the method to multiphase flow and allows comparisons with well-known Buckley-Leverett solution.

4.3.1 Incompressible algorithm

Incompressible formulation of the method is now tested in various configurations. Firstly, the convergence characteristic behavior of the method is assessed for two simple cases. The convergence study on the piecewise constant coarse cell unknown $u_{0,K}$ is reported to be h^2-convergent independently of case treated or Λ_l considered. The analysis for a homogeneous permeability field is chosen (see on Fig.4.1). The independence of $u_{0,K}$ convergence rate to the polynomial functions' subspace Λ_l chosen is also denoted in (Harder et al., 2013).

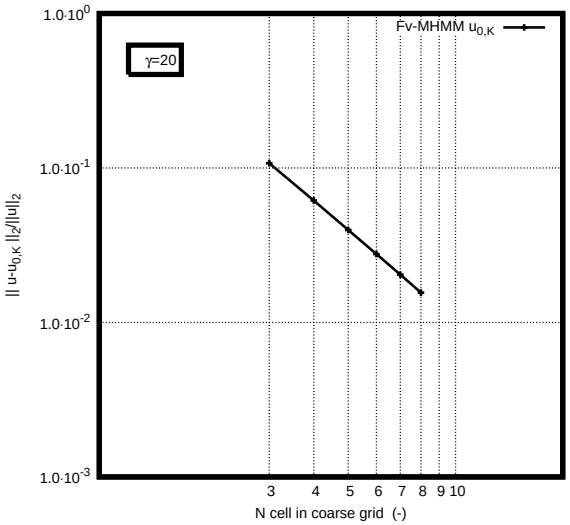

Figure 4.1: Convergence behavior of $u_{0,K}$ with respect to coarse grid refinement for homogeneous permeability field.

Convergence on a homogeneous permeability field

Simulations are performed solving (4.1) with an isotropic permeability field, reducing the tensor $K(\mathbf{x})$ to the scalar parameter $K = 1$. For the first test, the source term value is

$f(x, y) = 1$ throughout the whole square domain of extend $a = 1$. On the boundaries of the global domain, unknown is weakly imposed to $u_g = 0$. Meshgrids are uniformly discretized with the same number of cells along each direction. Let us then define γ as the number of fine cells embedded in a coarse cell along one direction. Convergence study is performed keeping γ constant (see on Fig. 4.2).

The error is measured as L_2-norm of the relative error between reconstructed field $u_h = u_{0,K} + \tilde{u}_\lambda + \tilde{u}_f$ to a semi-analytical solution taken from (Carslaw and Jaeger, 1959). The solution is expressed as an infinite sum which is truncated for the study at $n = 200$:

$$u(x, y) = \frac{(a^2 - x^2)}{2} - \frac{16\, a^2}{\pi^3} \sum_{n=0}^{\infty} \frac{(-1)^n \cos\left({}^{(2n+1)\pi x}/_{2a}\right) \cosh\left({}^{(2n+1)\pi y}/_{2a}\right)}{(2n+1)^3 \cosh\left({}^{(2n+1)\pi}/_{2}\right)}. \tag{4.9}$$

Convergence rate with respect to the coarse grid discretization depends on the Λ_l space chosen. Refining Λ_l space ensures lower error levels for the same coarse grid discretization as reported in (Harder et al., 2013) (see on Fig. 4.2).

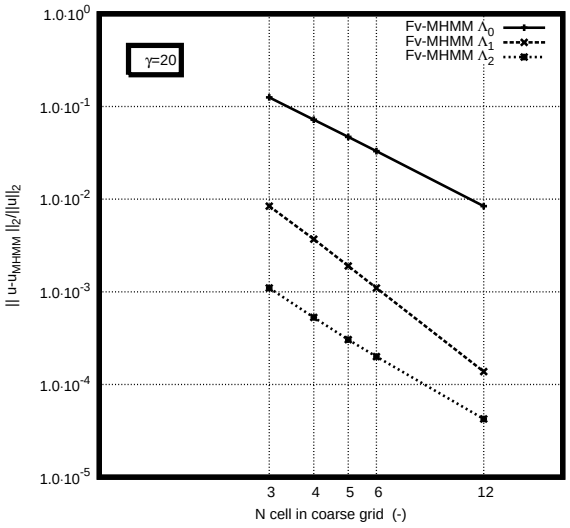

Figure 4.2: Convergence for different Λ_l space on a homogeneous Laplacian case.

Convergence including sinusoidal source term

For the second test, the same problem as the previous case is performed, but including spatially varying source term. We impose the unknown to be null on the boundaries and the source term is modeled as a sinusoidal term following:

$$f(x, y) = 8\pi^2 sin(2\pi x) sin(2\pi y) \tag{4.10}$$

Same remarks as previously can be drawn from figure Fig. 4.3. The convergence behavior obtained for u_h is h^{l+2}-convergence on $\Lambda_l, l \in \{0, 1, 2\}$. This is comparable to the results of (Harder et al., 2013).

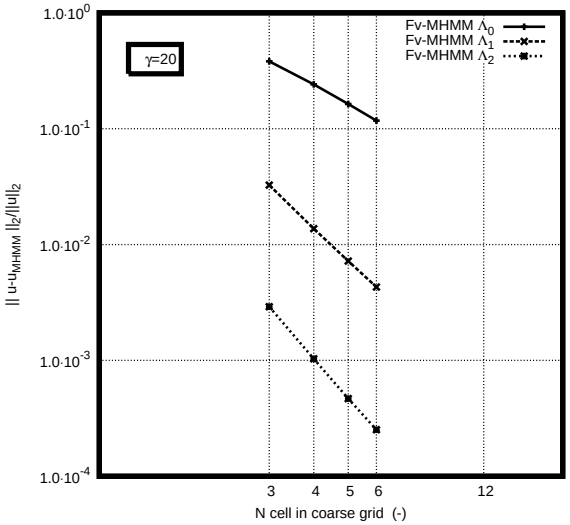

Figure 4.3: Convergence for different Λ_l space with sinusoidal source term.

Study of heterogeneous sample

The next example is based on the 83th and the 13th slices proposed in the 10th SPE comparative solution project (Christie et al., 2001a). The former is a highly contrasted channelized permeability field typical of fluvial media, while the latter is heterogeneous typical of prograding near-shore environment. The domain is $370 \times 670 m^2$. It is gridded using uniform Cartesian cells (60x220) as prescribed by the data set values for permeability. It is characterized respectively by a mean permeability value of $\mu(K) = 5.38\,10^{-10} m^2$ and highly variable permeability background of variance $\sigma(ln(K)) = 12.17$ for the channelized medium. The 13th slice is characterized by a mean permeability value of $\mu(K) = 6.07\,10^{-10} m^2$ and mildly variable permeability background of variance $\sigma(ln(K)) = 6.01$. Their logarithmic map are shown on Fig. 4.4. We impose a constant pressure drop, $\Delta u = 1\ Pa$, between opposite faces in the y-direction. A no-flux condition is imposed on the other boundaries. A reference finite volume solution is obtained on the fine grid and reported on Fig. 4.5. Software used is an OpenFOAM developed code (Horgue et al., 2015). Performances of $\Lambda_l,\ l \in \{1, 2\}$ spaces are evaluated on a coarse grid of 10x11 cells.

Let us consider first the case of a channelized permeability. As expected, increasing the order of polynomial space Λ_l allows us to capture more details of the channelized flow. However, the L_2-norm error level for Λ_2 remains high as reported on table Tab. 4.1.

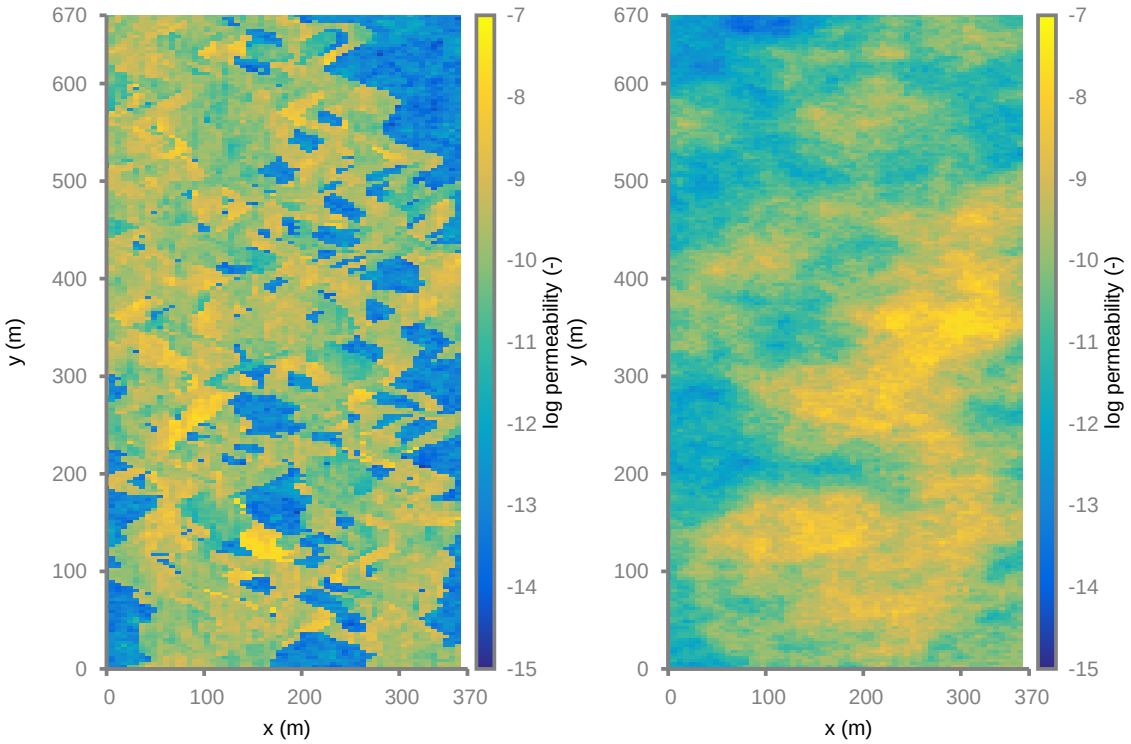

Figure 4.4: Map of log permeability of a fluvial and near-shore typed slices of the 10th SPE case.

It is then important to optimize the choice of test functions used in the local problems (*LLP* and *LSP*). To this effect, a fine scale transmissivity weighted method can be used in the local *LLP* and global problems construction in the spirit of (Verdiere and Vignal, 1998). This consists in weighting the basis functions of the space Λ_l at each coarse face according to the fine faces transmissivities leading to a weighted choice of the Lagrange multiplier space Λ_H.

To be more specific, let us denote by $\sigma \in F_H$ a given coarse face. Let $F_{h,\sigma}$ denote the set of fine faces of the coarse face σ and T_e denote the transmissivity of the fine face e. The new basis functions of Λ_H are defined on each coarse face σ by

$$\lambda_{\sigma,i}(s) = s^i \frac{T_e}{\sum_{e \in F_{h,\sigma}} T_e}, i = 0, \cdots, l,$$

where l is the polynomial degree of the space and s the coordinate along the 1D face σ. This choice of the basis functions emphasizes high permeability areas over low permeability areas. It eases the flow to follow channel paths.

From Tab. 4.1, readers can observe that including a weighting scheme improves strongly the scheme convergence compared to unweighted basic approach. Indeed, the weighted

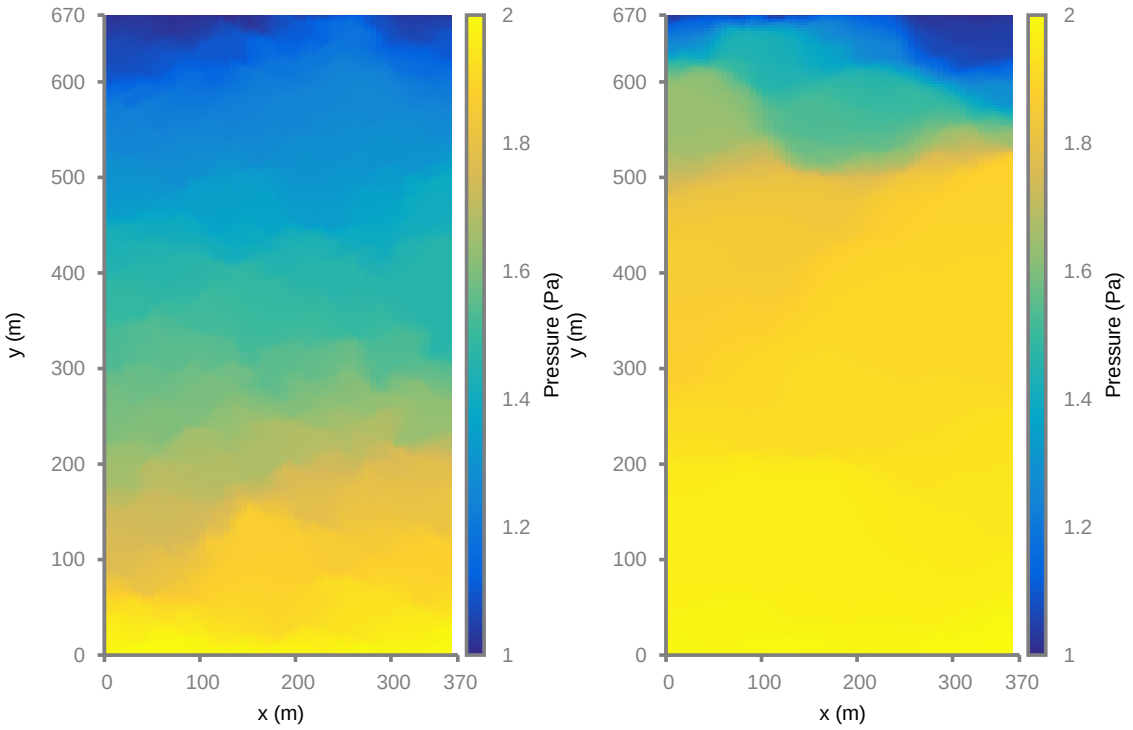

Figure 4.5: Finite volume reference solutions of a fluvial and near-shore typed slices of the 10th SPE case.

	basic	$transmissivity - weighted$
Λ_1	0.033	0.0063
Λ_2	0.022	0.0047

Table 4.1: Relative $norm - L_2$ error level refining Λ_l for a channelized SPE slice.

scheme avoids trapping fluids in regions of low permeability and does not show the numerical artifacts present in the unweighted basic approach. The L_2-norm error is then reduced more than 10 times using transmissivity-based weights.

As an example, we plot on Fig. 4.6 the pressure fields on the slice 73 comparing the basic and weighted schemes. This illustrates the ability of the modified model to treat the local heterogeneities related to high variations of the permeability fields. Consequently, when dealing with highly contrasted heterogeneous media, it is required to use the corrected *FV-MHMM* rather than the basic scheme.

Concerning the near-shore typed medium, *FV-MHMM* is efficient in its original formulation and errors between the two formulations of the same magnitude as reported in Tab. 4.2.

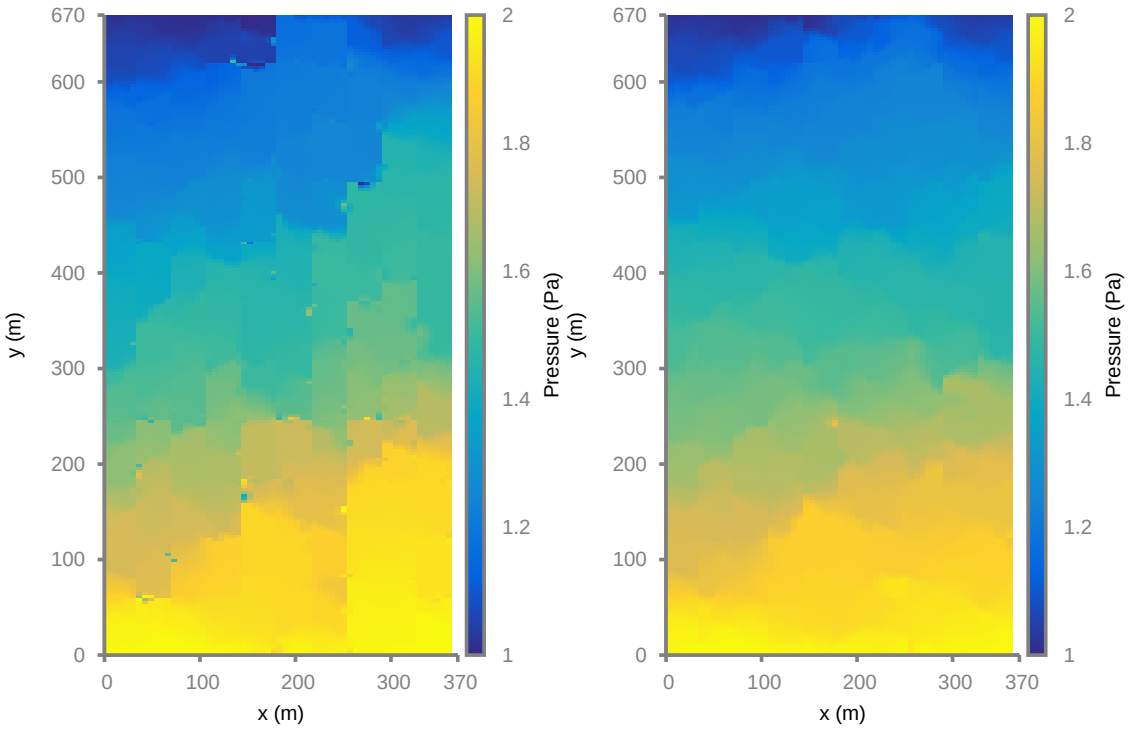

Figure 4.6: Result of incompressible single phase flow with basic and transmissivity weighted basis functions for Λ_1 on SPE slice with channelized medium (*i.e.* fluvial typed).

	basic	$transmissivity - weighted$
Λ_1	0.0031	0.0010
Λ_2	0.0017	$5.9\,10^{-4}$

Table 4.2: Relative $norm - L_2$ error level refining Λ_l for a near-shore typed SPE slice.

To conclude this section on heterogeneous fields, simulations has been performed on several of the 10th SPE heterogeneous slices comparing *FV-MHMM* with *MsFv* algorithm as it is implemented in *MRST2016a* (Lie, 2014). *MsFv* is here considered as a stand-alone multiscale solver and no iterations are used in the reported results. Relative $L_2 - norm$ errors with respect to the fine scale finite volume solution for the Λ_1 space are plotted on Fig. 4.7. The two main remarks developed above are highlighted in that graph. In representation of prograding near-shore porous medium (slice from number 1 to number 35), basic and weighted schemes for deriving local basis functions produce errors of the same order of magnitude. However, if a channelized medium is considered, typical of fluvial environment (slice from number 36 to number 85), transmissivity weighted scheme improves significantly the accuracy. *MsFv* error reported on Fig. 4.7 are truncated as the method struggles to find

a solution on some slices. As a comparable situation, the reader can refer to (Wang et al., 2014).

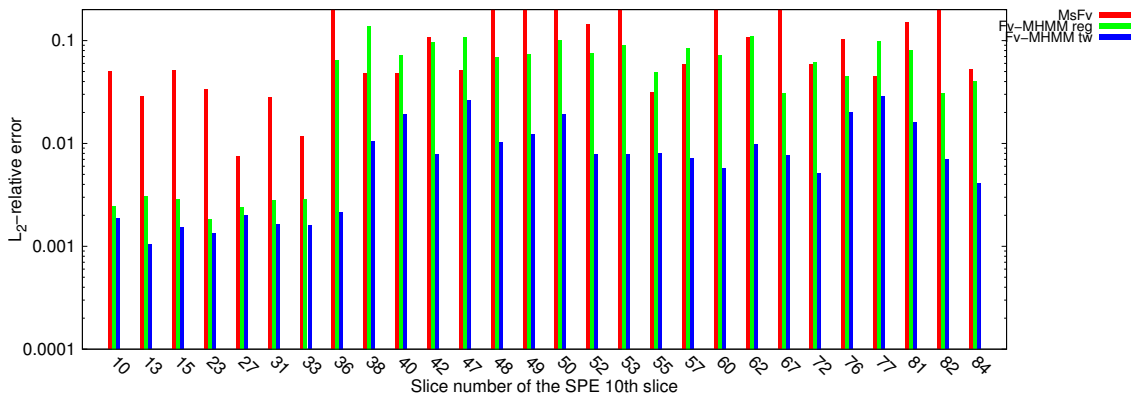

Figure 4.7: L_2 relative errors of the pressure fields while solving incompressible single phase flow using *MsFv*, basic weighted and transmissivity weighted basis functions for Λ_1 on several of the SPE slices.

For the sake of completeness, Tab. 4.3 reports the mean value (and standard deviation) of the errors, considering slices by faciès as if they were several equivalent realizations of an heterogeneous permeability field. On the Tarbert faciès, weighted and unweighted formulations produce error of the same order of magnitude, but ten times smaller than *MsFv*. They also produce less discrepancy between the slices. The difficulties for *MsFv* to find a solution on some of the Upper-Ness faciès are highlighted by a higher standard deviation values.

	Tarbert faciès	Upper-Ness faciès
MsFv	0.03(0.017)	0.438(0.589)
FV-MHMM-$\Lambda_2(reg)$	$2.61(0.41) \cdot 10^{-3}$	0.072(0.029)
FV-MHMM-$\Lambda_2(tw)$	$1.57(0.31) \cdot 10^{-3}$	0.011(0.007)

Table 4.3: Means and standard deviation of L_2-norm error w.r.t the type of heterogeneities

However, the latest development in the MsFv method proposed an algebraic version of the algorithm (Castelletto et al., 2016). The method is then considered as a parallelizable preconditioner to a fine grid solver such as GMRES (Manea et al., 2015). With this algebraic approach, convergence is reached on all of the 10th SPE slices.

4.3.2 Slightly compressible algorithm

The *FV-MHMM* method can be adapted to slightly compressible flows (Harder et al., 2015). Introducing a compressibility parameter c such as $\frac{d\rho}{\rho} = c\, du$, the porosity ϕ and the viscosity μ, the elliptic system of (4.1) turns into the following parabolic equation:

$$\begin{aligned} \boldsymbol{\nabla} \cdot (\frac{-K(\mathbf{x})}{\mu} \boldsymbol{\nabla} u(\mathbf{x},t)) + \phi c \frac{\partial u(\mathbf{x},t)}{\partial t} &= f(\mathbf{x},t) \quad \forall (\mathbf{x},t) \in \Omega \times \mathbb{R}^+, \\ \frac{-K(\mathbf{x})}{\mu} \boldsymbol{\nabla} u \cdot \mathbf{n} &= 0 \quad \forall (\mathbf{x},t) \in \partial\Omega \times \mathbb{R}^+, \\ u(\mathbf{x},0) &= 0 \quad \forall \mathbf{x} \in \Omega. \end{aligned} \tag{4.11}$$

Following (Harder et al., 2015), the *FV-MHMM* algorithm can be adapted to solve such a parabolic problem based on the new orthogonal decomposition of the space V:

$$V = \bigoplus_{K \in M_H} V_K$$

with $V_K = H^1(K)$.

The *Local Lambda Problem* and *Local Source Problem* can be rewritten in each coarse cell $K \in M_H$ after an Euler implicit time discretization (with time step Δt) and the TPFA discretization in space as follows:

$$\begin{cases} \displaystyle\sum_{\sigma = X|Y \in F_X \cap F_{h,K}^{int}} T_\sigma (u_X - u_Y) + \int_X {}^{\phi c}/_{\Delta t} u_X dx \\ + \displaystyle\int_{\partial K \cap \partial X} \lambda \mathbf{n} \cdot \mathbf{n}_K d\sigma = 0, \text{ for all } X \in M_{h,K}, \\ \displaystyle\sum_{\sigma = X|Y \in F_X \cap F_{h,K}^{int}} T_\sigma (u_X - u_Y) + \int_X {}^{\phi c}/_{\Delta t} u_X dx = \\ \displaystyle\int_X (f + {}^{c}/_{\Delta t}\, u_X^{n-1}) dx, \text{ for all } X \in M_{h,K}, \end{cases} \tag{4.12}$$

in which u_X^{n-1} stands for the pressure solution at the previous time step.

The previous time step solution on the right hand side of the local source-problem makes the solution of this local source-problem time dependent. Moreover, if dynamic time-stepping strategy is adopted, the basis functions of the Local lambda problems need also to be updated at each time step for which Δt is modified.

As a validation test, a comparison between the fine scale finite volume method and *FV-MHMM* is given in figure Fig. 4.8. The test case is a centered wellbore with a constant rate of discharge $q_0 = -4.5 \cdot 10^{-5}\ m^3 \cdot s^{-1}$ embedded in a square field of dimension $a = 3500\ m$. The fine-mesh discretization is 81×81 cells. The boundary conditions are considered to be homogeneous Neumann as stated in (4.11). The wellbore is active in the central cell. The homogeneous background permeability field is taken as equal to $K = 5 \cdot 10^{-13}\ m^2$ throughout

the whole domain. The compressibility is set at $3.9\,10^{-10}\ Pa^{-1}$ with viscosity $\mu = 10^{-3} Pa \cdot s$ and porosity $\phi = 0.25$.

We clearly note the accordance between the two solutions.

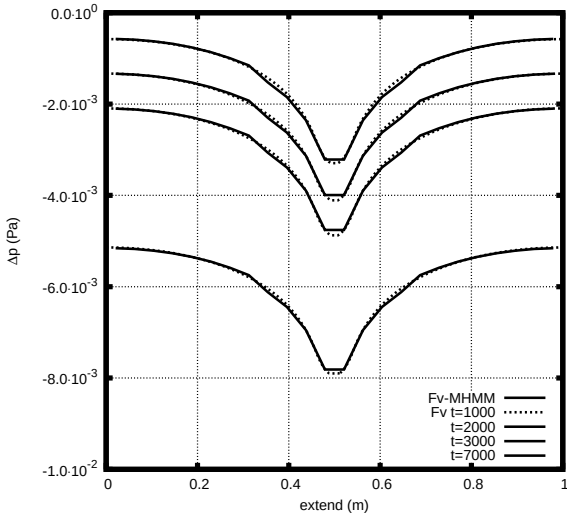

Figure 4.8: Comparison between finite volume and *FV-MHMM* on injection case.

4.3.3 Two phase flow model

We generalized, in this section, the approach to incompressible immiscible two-phase flow. The saturations of the wetting and non-wetting phases are respectively referred to as S_w and S_n. We also introduce phases mobilities $\lambda_w(S_w)$ and $\lambda_n(S_n)$ as:

$$\begin{aligned} \lambda_w(S_w) &= \frac{kr_w(S_w)}{\mu_w} \\ \lambda_w(S_w) &= \frac{kr_n(S_w)}{\mu_n} \end{aligned} \tag{4.13}$$

in which $kr_w(S_w)$ and $kr_n(S_w)$ denote the relative permeabilities respectively of the wetting and non-wetting phase. The dynamic viscosities of the wetting and non-wetting phases are introduced as μ_w and μ_n.

Let us introduce the generalized Darcy laws for the non-wetting phase, noted with subscript n, and for the wetting phase, noted with the subscript w, as :

$$\begin{aligned} \mathbf{v_w} &= -K(\mathbf{x})\lambda_w(S_w)\boldsymbol{\nabla} u, \\ \mathbf{v_n} &= -K(\mathbf{x})\lambda_n(S_w)\boldsymbol{\nabla} u. \end{aligned} \tag{4.14}$$

The total Darcy velocity is defined as:

$$\mathbf{v} = -K(\mathbf{x})\lambda_t(S_w)\boldsymbol{\nabla} u. \tag{4.15}$$

Here the capillary pressure has been neglected, *i.e.* the wetting and non-wetting phase pressure are equal. From the continuity equation of total flow and the mass balance in the wetting phase, a two-phase flow system is derived coupling an hyperbolic saturation equation with a parabolic pressure equation :

$$\begin{aligned}
\boldsymbol{\nabla} \cdot (-K(\mathbf{x})\lambda_t(S_w)\boldsymbol{\nabla} u) &= f \quad \text{in } \Omega, \\
u &= u_g \quad \text{on } \partial\Omega_D, \\
\mathbf{v} \cdot \mathbf{n} &= q_0 \quad \text{on } \partial\Omega_N \\
\phi \frac{\partial S_w}{\partial t} + \boldsymbol{\nabla} \cdot (f_w(S_w)\, \mathbf{v}) &= 0 \quad \text{in } \Omega, \\
\mathbf{v_w} \cdot \mathbf{n} &= q_{w,0} \quad \text{on } \partial\Omega_N.
\end{aligned} \tag{4.16}$$

in which the fractional flow of the wetting phase $f_w(S_w) = {}^{\lambda_w(S_w)}/_{\lambda_t(S_w)}$ is defined.

Brooks and Corey models (Brooks and Corey, 1964) for mobilities $\lambda_w(S_w)$, $\lambda_n(S_w)$ and $\lambda_t(S_w)$ are adopted here. They are written as:

$$\begin{aligned}
\lambda_w(S_w) &= \frac{1}{\mu_w}\left(\frac{S_w - S_{n,res}}{1 - S_{w,c} - S_{n,res}}\right)^2, \\
\lambda_n(S_w) &= \tfrac{1}{\mu_n} \left(\frac{1 - S_w - S_{n,res}}{1 - S_{w,c} - S_{n,res}}\right)^2, \\
\lambda_t(S_w) &= \lambda_n(S_w) + \lambda_n(S_w).
\end{aligned} \tag{4.17}$$

introducing the saturation parameters, $S_{n,res}$ and $S_{w,c}$ respectively residual non-wetting phase saturation and connate wetting phase saturation.

FV-MHMM algorithm is used to solve the pressure equation of the two-phase flow system (4.16), introducing transmissivity terms depending on the saturation $T_\sigma(S_w^{n+1})$. The hyperbolic saturation equation is solved using a first order upwind scheme. The two equations are coupled sequentially in the spirit of IMPES algorithm (Sheldon et al., 1959).

In order to validate two-phase flow implementation, we perform a Buckley Leverett test (Buckley et al., 1942). From this equation, front position and saturation are determined. The viscosity ratio is set to ${}^{\mu_w}/_{\mu_n} = 1$ and the injection rate is set at $q_0 = q_{w,0} = 2 \cdot 10^{-3}\ m^3 \cdot s^{-1}$. Mobility parameters are defined as $S_{n,res} = S_{w,c} = 0$. The porosity is set to

$\phi = 0.5$. On Figure Fig. 4.9, the comparisons between front positions determined using the semi-analytical and from two phase flow *FV-MHMM* are reported. Here, a 6×1 coarse grid is used overlaying a 48×1 fine discretization. There is no loss of accuracy as shown on the right plot of figure Fig. 4.9, when compared to a finite volume simulation run on the fine grid discretization.

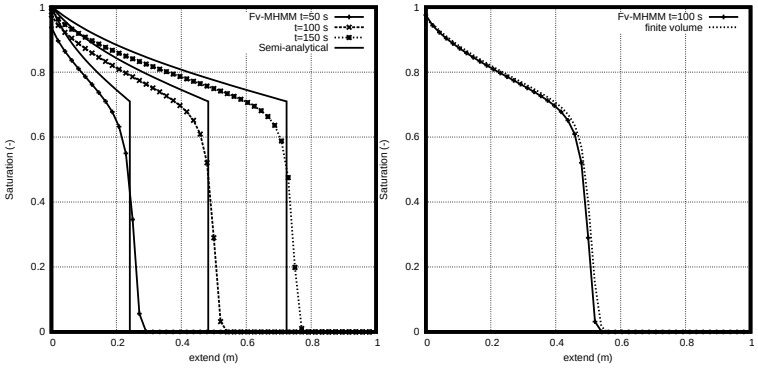

Figure 4.9: Compared Buckley-Leverett: on the left, saturation front from semi-analytical and *FV-MHMM*; on the right, finite volume solutions and two-phase *FV-MHMM*.

Next case involves a random permeability field through which a cross flow is performed. The porosity and Brooks and Corey parameters are kept at the previous values. Injection rate is set at $q_0 = 2\ 10^{-4}\ m^3 \cdot s^{-1}$. The injection of fluid with the same viscosity $\mu_w = \mu_n = 10^{-3}\, Pa \cdot s$ is studied. The overlaying coarse grid is kept at a 6×1 discretization level, while the fine grid is changed to a 48×4 discretization. A randomly generated permeability field is defined with $\mu(K) = 4.97 \cdot 10^{-10} m^2$ with values ranging from $1.2 \cdot 10^{-11} m^2$ to $9.97 \cdot 10^{-10} m^2$. The reference is the fine grid solution obtained using OpenFOAM finite volume solver (Horgue et al., 2015). On Fig. 4.10, this solution is plotted on the left side. The saturation front is solely perturbed by local heterogeneities in permeability values. This reference is compared to Λ_1, in the middle of Fig. 4.10, and Λ_2, on the right side of Fig. 4.10, solution from two-phase *FV-MHMM* for $t = 34\, s$.

From Fig. 4.10, it can be noted again that refining Λ_l spaces switching from $l = 1$ to $l = 2$ allows us to capture more and more details of the solution. It provides us a new way of improving the solution without neither refining any meshes nor reducing time-step size.

4.4 Conclusion

In this paper, a new multiscale *FV-MHMM* method has been introduced for the resolution of the problem (4.1). This approach is based on a hybrid formulation of the pressure problem, where main unknowns are fluxes on the faces of a coarse mesh. Two kinds of local

problems are involved: a local lambda problem (LLP) and a local source problem (LSP) in order to build the global problem. Each of these problems embeds local heterogeneity details. Considering flux basis functions as Lagrange multipliers, pressure continuity is weakly imposed on the coarse mesh. The mathematical formulation of this method has been presented and convergence has been tested on various test cases. Extensions of the *FV-MHMM* to slightly compressible cases and two-phase cases have been introduced.

FV-MHMM method is a promising method. Local problems are indeed entirely localized and could be run on different processors. Moreover, unlike classical finite volume methods, *FV-MHMM* offers possible degrees of refinement in the educated choice for the tests functions μ defined in spaces of polynomial functions Λ_l. Including *a posteriori* error estimators offers the possibility of local and adapted refinement of the Λ_l space.

Eventually, further works will focus on dealing with highly heterogeneous media and with cross-comparison with the main existing methods such as *MsFv* (Jenny et al., 2003, 2005), *MsFEM* (Aarnes, 2004; Hou and Wu, 1997), GMsFEM (Efendiev et al., 2013) or numerical subgrid methods (Arbogast, 2002).

This work was supported by STORENGY and ENGIE EPI. We would also like to thank Egermann Patrick and Ababou Rachid for their helpful comments and remarks on this work.

References

Aarnes, J.: 2004, On the use of a mixed multiscale finite element method for greaterflexibility and increased speed or improved accuracy in reservoir simulation, *Multiscale Modeling & Simulation* .

Arbogast, T.: 2002, Implementation of a locally conservative numerical subgrid upscaling scheme for two-phase darcy flow, *Computational Geosciences* .

Brezzi, F., Douglas Jr, J. and Marini, L. D.: 1985, Two families of mixed finite elements for second order elliptic problems, *Numerische Mathematik* .

Brooks, R. and Corey, A.: 1964, Hydraulic properties of porous media and their relation to drainage design, *Transactions of the ASAE* .

Buckley, S., Leverett, M. et al.: 1942, Mechanism of fluid displacement in sands, *Transactions of the AIME* .

Carslaw, H. and Jaeger, J.: 1959, Conduction of heat in solids, *Oxford: Clarendon Press, 1959, 2nd ed.* .

Castelletto, N., Hajibeygi, H. and Tchelepi, H. A.: 2016, Multiscale finite-element method for linear elastic geomechanics, *Journal of Computational Physics* .

Chen, Z. and Hou, T.: 2003, A mixed multiscale finite element method for elliptic problems with oscillating coefficients, *Mathematics of Computation* .

Christie, M., Blunt, M. et al.: 2001a, Tenth spe comparative solution project: A comparison of upscaling techniques, *SPE Reservoir Simulation Symposium*, Society of Petroleum Engineers.

Dehkordi, M. M. and Manzari, M. T.: 2013, Effects of using altered coarse grids on the implementation and computa tional cost of the multiscale finite volume method, *Advances in Water Resources* .

Efendiev, Y., Galvis, J. and Hou, T. Y.: 2013, Generalized multiscale finite element methods (gmsfem), *Journal of Computational Physics* .

Franc, J., Jeannin, L., Debenest, G. and Masson, R.: 2016, Fv-mhmm methods for reservoir modeling, *Computational Geosciences* .

Harder, C., Paredes, D. and Valentin, F.: 2013, A family of multiscale hybrid-mixed finite element methods for the darcy equation with rough coefficients, *Journal of Computational Physics* .

Harder, C., Paredes, D. and Valentin, F.: 2015, On a multiscale hybrid-mixed method for advective-reactive dominated problems with heterogeneous coefficients, *Multiscale Modeling & Simulation* .

Horgue, P., Soulaine, C., Franc, J., Guibert, R. and Debenest, G.: 2015, An open-source toolbox for multiphase flow in porous media, *Computer Physics Communications* .

Hou, T. and Wu, X.-H.: 1997, A multiscale finite element method for elliptic problems in composite materials and porous media, *Journal of computational physics* .

Jenny, P., Lee, S. and Tchelepi, H.: 2003, Multi-scale finite-volume method for elliptic problems in subsurface flow simulation, *Journal of Computational Physics* .

Jenny, P., Lee, S. and Tchelepi, H.: 2005, Adaptive multiscale finite-volume method for multiphase flow and transport in porous media, *Multiscale Modeling & Simulation* .

Lie, K.-A.: 2014, An introduction to reservoir simulation using matlab, *SINTEF ICT* .

Manea, A., Sewall, J., Tchelepi, H. et al.: 2015, Parallel multiscale linear solver for highly detailed reservoir models, *SPE Reservoir Simulation Symposium*, Society of Petroleum Engineers.

Raviart, P.-A. and Thomas, J.: 1977, Primal hybrid finite element methods for 2nd order elliptic equations, *Mathematics of computation* .

Renard, P. and De Marsily, G.: 1997, Calculating equivalent permeability: a review, *Advances in water resources* .

Sheldon, J., Cardwell Jr, W. et al.: 1959, One-dimensional, incompressible, noncapillary, two-phase fluid flow in a porous medium.

Verdiere, S. and Vignal, M.: 1998, Numerical and theoretical study of a dual mesh method using finite volume schemes for two phase flow problems in porous media, *Numerische Mathematik* .

Wang, Y., Hajibeygi, H. and Tchelepi, H. A.: 2014, Algebraic multiscale solver for flow in heterogeneous porous media, *Journal of Computational Physics* .

Wood, B.: 2009, The role of scaling laws in upscaling, *Advances in Water Resources* .

Appendix A : Complexity analysis

(Jenny et al., 2003) proposed a complexity analysis of their *MsFv* algorithm. Following their example, we will here remind their results and apply such an analysis on *FV-MHMM* to be able to compare the two approaches. The notations that will be used are introduced in Tab. 4.4.

n_v	number of volumes in the fine grid
N_v	number of volumes in the coarse grid
N_n	number of nodes in the coarse grid
N_f	number of faces in the coarse grid
γ	coarsening ratio $\sim {}^{n_v}/_{N_v}$
a_n	number of adjacent coarse volume to a coarse node
a_v	number of adjacent coarse volume to a coarse volume
$t_1(n)$	time to solve a linear system with n unknowns

Table 4.4: Notations for complexity analysis

Assuming that $t_1(n) \sim ct_m n^\alpha$ where t_m is the time spend for one multiplication, c and α constant depending on the solver. This complexity analysis neglects time spent in the reconstruction of the pressure and the fluxes leading to the following time by steps:

$$\begin{aligned} t_I &\approx N_n a_n c t_m \gamma^\alpha, \\ t_{II} &\approx N_v (a_v + 1) c t_m \gamma^\alpha \\ t_{III} &\approx c t_m N_v^\alpha. \end{aligned}$$

with the step I identified as construction of equivalent transmissivities for coarse scale fluxes, the step II as the construction of basis functions sets Φ on the primal grid and the step III as the solution on the coarse grid.

In the same manner FV-MHMM can be analyzed as:

$$\begin{aligned} t_{LLP} &\approx 2d(l+1) N_v c t_m \gamma^\alpha, \\ t_{LSP} &\approx N_v c t_m \gamma^\alpha, \\ t_{GP} &\approx c t_m [N_v + (l+1) N_f]^\alpha. \end{aligned}$$

where d is the dimension number, l the order of the polynomial space used to approximate Λ_H as introduced in the paper. The step LLP is the local problem in terms of Lambda, the

step *LSP* is the local problem in terms of source contribution and *GP* is the global problem also as introduced in the paper.

Considering an average number of coarse faces as $N_f \approx d(N_v^{1/d}+1)\prod_{i=1}^{d-1} N_v^{1/d}$ with the parameters of Tab. 4.5, time used in term of t_m for each steps of both algorithms are represented on Fig. 4.11. It can be noticed that increasing polynomial order of approximation of Λ_H increases the computational cost for solving *LLP* and *GP*.

n_v	N_v	N_n	d	a_v	a_n	α	c
8100	9	12	2	8	4	1.5	10

Table 4.5: Parameters of comparison.

Increasing the order $l \in \{0,1,2\}$ of the polynomial space that approximated Λ_H, the speed up of *FV-MHMM* versus the *MsFv* method is respectively of 2.86, 1.59 and 1.10.

Moreover the step I and step III are reported to be parallelizable for the *MsFv* method (Jenny et al., 2003). As for the *FV-MHMM*, all the *local problems lambda (LLP)* and *local problems source (LSP)* are independent from each other and therefore embarrassingly parallel. Moreover, the TPFA matrix for a selected coarse cell has to be generated only one time and can be used for solving both *LLP* and *LSP* associated with this coarse cell.

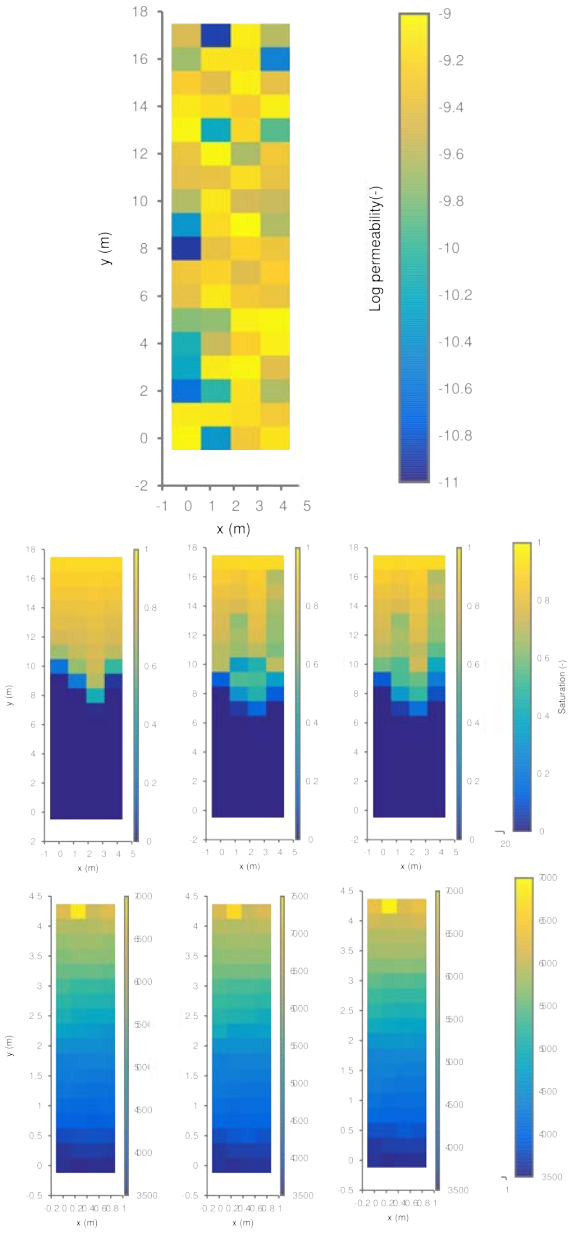

Figure 4.10: Detail of the comparison on a multiphase flow situation using FV-MHMM method at different orders and fine grid finite volume solution. Respectively, on the top logarithmic map of the permeability, on the bottom; from left to right, finite volume solution, two-phase *FV-MHMM* solution Λ_1 and Λ_2 for saturation and related pressure fields.

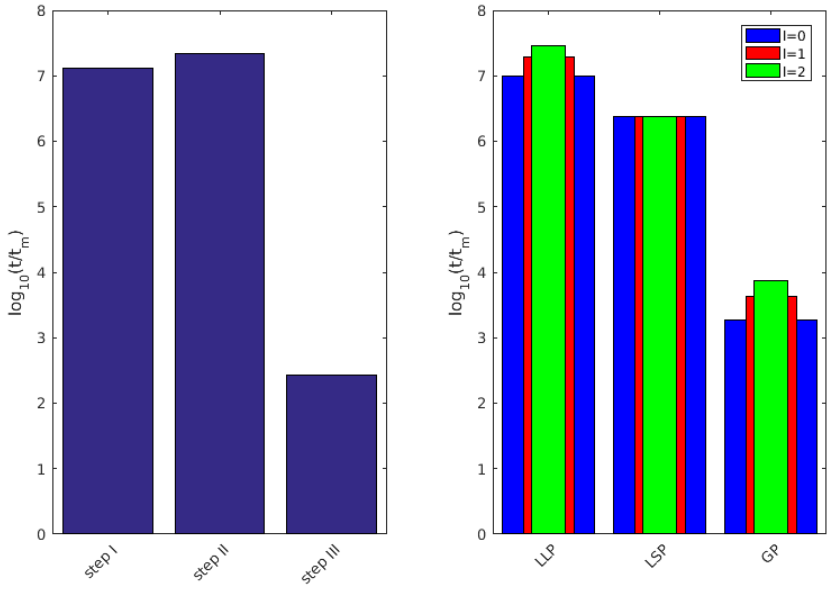

Figure 4.11: Time spent for the *MsFv* and the *FV-MHMM* in terms of operations.

Chapter 5

Comparisons of FV-MHMM with other Finite Volume Multiscale Methods

Contents

Résumé de chapitre

Ce chapitre concerne la comparaison de diverses méthodes utilisées en ingénierie réservoir pour traiter le problème de l'écoulement par méthode multiéchelle dans des milieux fortement hétérogènes. Nous partirons du problème à l'échelle géologique, *i.e.* l'échelle de Darcy, et nous la considérerons comme notre échelle fine. Cela veut dire qu'un premier changement d'échelle a été réalisé pour obtenir les valeurs de la perméabilité en tous points du maillage à l'échelle géologique. En se focalisant sur des méthodes types volumes finis, telles que *MsFv* (Jenny et al., 2003), *MsRSB* (Møyner and Lie, 2016) et *FV-MHMM* (Franc, Jeannin, Debenest and Masson, 2016), on cherchera d'abord à les décrire en unifiant les formulations mathématiques des problèmes. Puis, on intercomparera les méthodes sur des cas tests provenant de la littérature du domaine (Christie et al., 2001) en les utilisant dans une formulation dite native. Par la suite, certaines améliorations des schémas de base seront analysées afin de déterminer les performances relatives de chacune. En particulier, on mettra en avant l'intérêt de la mise en place des schémas itératifs pour la *MsFv* et la *MsRSB,* tandis que l'on pourra monter en ordre sur les fonctions de base tout en mettant en place des schémas de pondération pour la *FV-MHMM.*

Sur l'ensemble des cas réalisés et sur les deux types de faciès (coupes 1-35 type Tarbert, coupes 36-85 type chenal), les performances des méthodes sont comparées en termes d'erreur. Les mêmes discrétisations, grossières et fines, sont imposées. Les résultats démontrent que les méthodes améliorées sont bien plus performantes que les méthodes natives, permettant ainsi de réduire les erreurs relatives observées en atteignant des niveaux proches de 10^{-5} en norme L_2 si l'on se réfère à la solution fine pour les pressions.

In fine, on teste ces trois méthodes sur un cas où l'on a des bandes alternées de grandes et faibles perméabilités non alignées avec la grille cartésienne. Ce cas est excessivement complexe et permet de bien vérifier l'intérêt de corriger les versions natives des méthodes pour une bien meilleure précision. Une reconstruction des flux est comparée avec la solution fine. Cela démontre la capacité des méthodes itératives *MsFv* et *MsRSB* à reproduire les effets locaux, et à bien prendre en compte les variations de propriétés.

Ce chapitre, mis en forme dans le format requis par *Transport in Porous Media*, est la base d'un article soumis en septembre 2017.

Upscaling and multiscale algorithms both serve the same aim of defining models that are able to capture global trends of the flow properties on a larger scale than the reference scale, referred to as the fine-scale. However, *upscaling* and *multiscale methods* differ when it comes to the treatment of the fine-scale. *Upscaling* techniques, once they have averaged the flow properties, produce an upscaled equivalent model and deal with it at the large-scale. On the other hand, *multiscale methods* are designed to keep the fine scale information as they consider that a good accuracy can not be achieved without it. Then, they will couple scales thanks to upgridding and downgridding steps.

For the methods that are in use in this study, the Darcy-to-Field scale upscaling will be considered. The generalized Darcy's law is considered as the fine scale model. This will give us the reference solution. *Multiscale algorithm*s have been extensively studied, starting from the works of Hou and Wu on Multiscale Finite Elements (Hou and Wu, 1997) for Darcy like equations.

On one hand, the finite elements methods have known important developments with Multiscale Finite Element Methods (MsFEM)(Arbogast et al., 2000), numerical subgrid methods(Arbogast, 2002; Arbogast et al., 2007) and more recently Generalized Multiscale Finite Element Methods (GMsFEM) (Efendiev et al., 2013). These relie on the construction of local basis function that fits the underlying heterogeneities. Numerical subgrid methods are rather solving for averaged pressure values on the coarse scale and for its variation on subgrid scale.

On the other hand, the Multiscale Finite volume methods (*MsFv* (Jenny et al., 2003)) have been derived and designed to be locally and globally conservative. This work has been extended by introducing iterative algorithm to smooth multiscale approximate solutions (Hajibeygi et al., 2008). Later works have introduced other features to model density driven flows or flows with capillary forces by using correction functions (Lunati and Lee, 2009). . More recently, an algebraic formulation of the method has been developed (Wang et al., 2014). Its use as a preconditioner for Krylov-type iterative solvers has been investigated (Castelletto et al., 2016). On another branch, the Multiscale Restriction Smoothed Basis (*MsRSB* (Møyner and Lie, 2016)) has been developed. It takes its inspiration from extensive studies of *MsFv* algorithm and algebraic multigrid solvers (Vaněk et al., 1996) introducing multiple time Jacobi smoothing on overlapping supports to construct its basis functions. An alternative method, Finite volume-Multiscale Hybrid Mixed Method (*FV-MHMM* (Franc, Jeannin, Debenest and Masson, 2016)) has been proposed. It is based on the family of multiscale hybrid-mixed finite element methods introduced in (Harder et al., 2013) which has been adapted to finite volume formulation.

This paper intends to cross-compare the above-mentioned finite volume multiscale methods, *i.e.* the multiscale finite volume method (*MsFv*), the multiscale restriction smoothed basis method (*MsRSB*) and the finite volume multiscale hybrid mixed method (*FV-MHMM*). The first section will give more details about the considered three methods. In a second section, the performance of each method on 2D layers of the 10th SPE (Christie et al., 2001) test case will be compared. As a last test case, a slanted permeability field will be considered.

5.1 Methods Description

In this section, we describe briefly the three finite volume methods used to study multiscale problems for fluid flow in heterogeneous media. For single-phase incompressible flows, pressure field equation over the domain Ω follows the Darcy's equation:

$$\boldsymbol{\nabla} \cdot (-K(\mathbf{x})\boldsymbol{\nabla} p) = \mathrm{f} \text{ in } \Omega, \tag{5.1}$$

where, $K(\mathbf{x})$ stands for the permeability field which is heterogeneously distributed over Ω, and f a general source term. Boundary conditions are needed and are defined according to the following equations.

$$\begin{aligned} (-K(\mathbf{x})\boldsymbol{\nabla} p) \cdot \mathbf{n}_{\partial\Omega} &= g \text{ on } \partial\Omega_{\mathrm{N}}, \\ p &= p^g \text{ on } \partial\Omega_{\mathrm{D}}, \end{aligned}$$

where $\mathbf{n}_{\partial\Omega}$ stands for the unit normal vector to the boundary $\partial\Omega$ outward to Ω, and $\overline{\partial\Omega}_D \cup \overline{\partial\Omega}_N = \overline{\partial\Omega}$, $\partial\Omega_D \cap \partial\Omega_N = \emptyset$. The first equation is a classical Neumann boundary condition with prescribed flux g on $\partial\Omega_N$, whereas the second one is a Dirichlet boundary condition with imposed pressure p^g on $\partial\Omega_D$.

Herein, we focus on the finite volume methods available and we briefly recall the systems of equations to be solved in each of them.

5.1.1 *FV-MHMM*

Let M_H be the set of coarse cells K partitioning the domain Ω, F_H be the set of coarse faces, and ∂K denote the boundary of a coarse cell K with its unit normal vector $\mathbf{n}_K$ oriented outward to K.

Starting from the primal hybrid formulation of Raviart and Thomas (Raviart and Thomas, 1977b,a), Harder *et al.* (Harder et al., 2013, 2015) explain how to construct a multiscale

method sharing the same idea that flux continuity between cells (here coarse scale cells) can be enforced weakly using Lagrange multipliers λ. It is formulated as :

find $(p, \lambda) \in V \times \Lambda$ *such that*:

$$\begin{aligned}\int_\Omega K(\mathbf{x})\boldsymbol{\nabla} p \cdot \boldsymbol{\nabla} q d\mathbf{x} + \sum_{K\in M_H} \int_{\partial K} \lambda \mathbf{n}\cdot\mathbf{n}_K\, q|_K d\sigma \\ + \sum_{K\in M_H} \int_{\partial K} \mu \mathbf{n}\cdot\mathbf{n}_K p|_K d\sigma \quad \text{for all } (q,\mu)\in V\times\Lambda, \\ = \int_\Omega f v d\mathbf{x} + \int_{\partial\Omega} \mu p^g d\sigma\end{aligned} \tag{5.2}$$

where V is the broken Sobolev space $H^1(M_H)$ defined as:

$$H^1(M_H) = \{v \in L_2(\Omega) :\ v|_K \in H^1(K),\ K \in M_H\}, \tag{5.3}$$

Λ stands for the following Lagrange multipliers space

$$\Lambda := \{\mu \in \prod_{K\in M_H} H^{-\frac{1}{2}}(\partial K) : \exists \boldsymbol{\sigma} \in H_{div}(\Omega) \text{ s.t. } \mu|_{\partial K} = \boldsymbol{\sigma}\cdot\mathbf{n}|_{\partial K},\ K \in M_H\}, \tag{5.4}$$

∇v is the broken gradient equal to $\nabla v|_K$ on each coarse cell $K \in M_H$, and $H^{-\frac{1}{2}}(\partial K)$ is the dual space of the space $H^{\frac{1}{2}}(\partial K)$ spanned by the traces on ∂K of functions in $H^1(K)$.

Let then split the space V orthogonally as :

$$V = V_0 \oplus \Pi_{K\in M_H} W_K,$$

where V_0 is the space of piecewise constant functions on each coarse cell $K \in M_H$ and W_K is the subset of null mean function over $H^1(K)$. This definition introduces the two-scale modeling scheme.

At fixed Lagrange multiplier λ, the fine scale solution in W_K defined by Eq. (5.2) decouples. It is obtained by superposition of the solutions of two local problems, a *local lambda problem* for Lagrange multipliers driven effects and a *local source problem* for source driven effects. They respectively read:

Find $\tilde{p}_K \in W_K$ *such that*:

$$\int_K K(\mathbf{x})\boldsymbol{\nabla}\tilde{p}_K \cdot \boldsymbol{\nabla}\tilde{q}_K d\mathbf{x} + \int_{\partial K} \lambda \mathbf{n}\cdot\mathbf{n}_K \tilde{q}_K d\sigma = 0 \quad \text{for all } \tilde{v}_K \in W_K, \tag{5.5}$$

Find $\tilde{p}_K \in W_K$ *such that*:

$$\int_K K(\mathbf{x})\boldsymbol{\nabla}\tilde{p}_K \cdot \boldsymbol{\nabla}\tilde{q}_K d\mathbf{x} = \int_K f\tilde{q}_K d\mathbf{x} \quad \text{for all } \tilde{v}_K \in W_K, \tag{5.6}$$

setting $\tilde{p}_K = T_K\lambda$ and $\tilde{p}_K = \hat{T}_K f$.

The coupling of the local fine scale solutions is obtained using Eq. (5.2) with test functions in $V_0 \times \Lambda$ to compute the Lagrange multiplier λ and the mean values in the coarse cells. It is formulated as follows using the previous solutions of the *local* problems $T_K\lambda$ and $\hat{T}_K f$ for all coarse cells $K \in M_H$:

Find $p_{0,K} \in \mathbb{R}, K \in M_H$ *and* $\lambda \in \Lambda$ *such that*:

$$\begin{cases} \displaystyle\sum_{K\in M_H} \int_{\partial K} \lambda\mathbf{n}\cdot\mathbf{n}_K d\sigma = \int_K f d\mathbf{x} \quad \text{for all } K \in M_H, \\ \displaystyle\sum_{K\in M_H} \int_{\partial K} \mu\mathbf{n}\cdot\mathbf{n}_K (p_{0,K} + T_K\lambda + \hat{T}_K f) d\sigma = \int_{\partial\Omega} \mu u_g \quad \text{for all } \mu \in \Lambda. \end{cases} \tag{5.7}$$

This multiscale algorithm is here implemented using a *TPFA* scheme for the local problems on each coarse cell K and by replacing the space Λ by a subspace Λ_H. In the following test cases, the vector space Λ_H will be typically defined as the vector space of polynomials $\mathbb{P}_l(\sigma)$ of degree l on each coarse face $\sigma \in F_H$. These choices of Λ_H will be denoted by Λ_l, $l = 0, 1, 2$ in the following sections. These polynomial spaces can also be weighted using harmonic averaging of the permeability field on each fine face of F_H as described in the following section. Readers can refer to (Franc, Jeannin, Debenest and Masson, 2016) for further details.

As an illustration, a typical basis function is reported respectively on Fig.5.3.

Once these basis functions are computed and the global system Eq. (5.7) solved, the approximate fine scale pressure $p^{fv-mhmm}(x)$ is interpolated as a linear combination of the coarse cell pressures as follows

$$p(\mathbf{x}) \approx p^{fv-mhmm}(\mathbf{x}) = \sum_{K\in M_H} \left[p_{0,K} + \sum_{\sigma\in F_{H,K}} (T_K\lambda + \hat{T}_K f) \right] \tag{5.8}$$

Now, we will briefly recall the *MsFv* method.

5.1.2 *MsFv*

The multiscale method *Multiscale Finite Volume (MsFv)* (Jenny et al., 2003) is constructed using two different meshes. A primal coarse grid is defined by partitioning a fine grid as

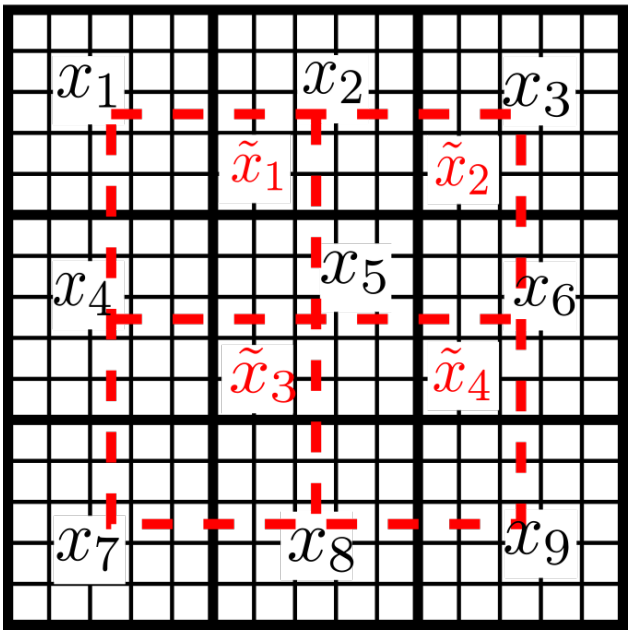

Figure 5.1: *MsFv*: primal grid (full lines) dual grid (dashed lines)

usual in multiscale methods (solid line on Fig.5.1). Then a dual coarse grid is constructed, joining the cell centers of the primal grid (dashed lines on Fig. 5.1). The basis functions will be evaluated on this staggered dual grid. Those basis functions are useful to calculate equivalent transmissivities (see Fig. 5.3). Those meshes are superimposed to a fine mesh grid, capturing the details of the fine scale properties.

We now briefly recall the first three steps of the construction regarding the calculation of the coarse pressure. A remaining step deals with conservative fine-scale velocity field reconstruction which is required to couple the flow with a transport equation.

Let us consider a *primal coarse grid* denoted by M_H with coarse cells $K \in M_H$ of cell center $\mathbf{x}_K$. At each vertex $\mathbf{x}_{\widetilde{K}}$ of the primal grid, a dual coarse cell denoted by $\widetilde{K}$ is built joining the neighboring cell centers $\mathbf{x}_K$, $K \in M_{\widetilde{K}}$, where $M_{\widetilde{K}}$ denote the set of primal coarse cells sharing the vertex $\mathbf{x}_{\widetilde{K}}$. This defines the *dual coarse grid* $\widetilde{M}_H$ as the set of dual coarse cells $\widetilde{K} \in \widetilde{M}_H$. Let us also denote by $\mathbf{x}_{\widetilde{K}}$, $\widetilde{K} \in \widetilde{M}_K$ the vertices of the cell K.

The first step is to build the basis functions $\tilde{\Phi}_K^{\widetilde{K}}$, $K \in M_{\widetilde{K}}$ (Fig. 5.3) on each dual coarse cell $\widetilde{K}$. The second step is the computation of the correction functions $\tilde{\Phi}_*^{\widetilde{K}}$ for all $\widetilde{K} \in \widetilde{M}_H$. Both sets of basis functions are used to interpolate the pressure as a linear combination of the primal coarse cell pressures $\bar{p}_K, K \in M_H$. This allows to express the fluxes on the primal coarse cell faces as linear combinations of the primal coarse cell pressures. Then, in the third

step, the linear system for the primal coarse cell pressures is obtained from the conservation equations written on the primal coarse cells.

For each $\widetilde{K} \in \widetilde{M}_H$, the basis functions $\Phi_K^{\widetilde{K}}$, $K \in M_{\widetilde{K}}$ are solutions of the following equations set on the dual coarse cell $\widetilde{K}$ with value $\delta_{K,L}$ at the vertices $\mathbf{x}_L$, $L \in M_{\widetilde{K}}$ of the dual coarse cell $\widetilde{K}$:

$$\begin{cases} \boldsymbol{\nabla}\cdot\mathbf{K}(\mathbf{x})\boldsymbol{\nabla}\Phi_K^{\widetilde{K}} & = 0 \qquad in\ \widetilde{K}, \\ \boldsymbol{\nabla}_\perp \cdot \mathbf{K}(\mathbf{x})\boldsymbol{\nabla}\Phi_K^{\widetilde{K}} & = 0 \qquad on\ \partial\widetilde{K}, \\ \Phi_K^{\widetilde{K}}(\mathbf{x}_L) & = \delta_{K,L}, \quad L \in M_{\widetilde{K}}. \end{cases} \tag{5.9}$$

The addition of a second kind of basis functions, *correction basis functions*, is set to model inhomogeneous part of the multiscale approximation of the fine scale pressure, introducing $\Phi_*^{\widetilde{K}}$ whose definition reads :

$$\begin{cases} \boldsymbol{\nabla}\cdot\mathbf{K}(\mathbf{x})\boldsymbol{\nabla}\Phi_*^{\widetilde{K}} & = f \qquad in\ \widetilde{K}, \\ \boldsymbol{\nabla}_\perp \cdot \mathbf{K}(\mathbf{x})\boldsymbol{\nabla}\tilde{\Phi}_*^{\widetilde{K}} & = 0 \qquad on\ \partial\widetilde{K}, \\ \Phi_*^{\widetilde{K}}(\mathbf{x}_L) & = 0, \quad L \in M_{\widetilde{K}}. \end{cases} \tag{5.10}$$

Once these basis functions are computed, the approximate fine scale pressure $p^{msfv}(x)$ is interpolated as a linear combination of the primal coarse cell pressures as follows :

$$p(\mathbf{x}) \approx p^{msfv}(\mathbf{x}) = \sum_{K \in M_H} \bar{p}_K \left[\sum_{\widetilde{K} \in \widetilde{M}_K} \Phi_K^{\widetilde{K}}(\mathbf{x}) \right] + \sum_{\widetilde{K} \in \widetilde{M}_H} \Phi_*^{\widetilde{K}}(\mathbf{x}) \tag{5.11}$$

and the primal coarse cell pressures $\bar{p}_K$, $K \in M_H$ are obtained from the conservation equations in each primal coarse cell K defining the set of linear coarse scale equations.

If one would like to add, sink terms, gravity or capillary effects, new basis functions have to be defined, denoted as correction functions in the system of basis functions calculations (see (Lunati and Jenny, 2008) or (Jenny and Lunati, 2009)). An iterative scheme can also be applied in order to reduce the error which happened at *dual* coarse cells' boundaries. For multiphase flow, a conservative fine-scale velocity field is required and an extra step is then needed to ensure that p^{msfv} fulfills this requirement.

As a last method, we choose to report one of the most recent multiscale method *MsRSB*.

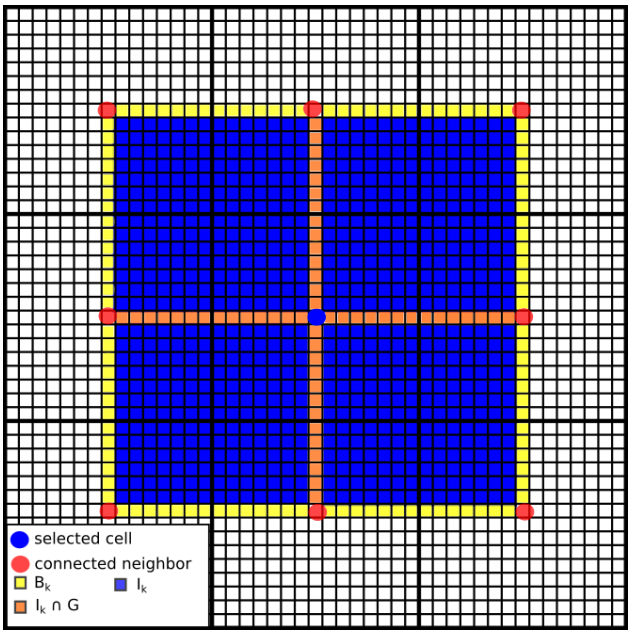

Figure 5.2: *MsRSB*: Definition of mesh elements, different areas, and boundaries used.

5.1.3 *MsRSB*

MsRSB method is inspired from the work on AMG solver (Vaněk et al., 1996). It takes advantages of overlapping areas between coarse cells to compute the needed basis functions (see Fig. 5.2). However, a particular treatment has to be done during smoothing iterative process for the fine cells included in these overlapping regions.This will enforce the partition of unity, and it will allow to build a conservative operator (see Fig. 5.3). Let us define three different areas for defining the basis functions computation associated to a given coarse cell $K \in M_H$: I_K the overlap support, the overlap's boundaryB_K and the global boundary inside the overlap region $G \cap I_K$ introducing G as the superposition of all the overlaps' boundaries, $G = \bigcup_K B_K$ (see Fig. 5.2).

Let F denote the set of fine cells. For convenience, we identify in the following the domains K, I_K, B_K and G with their corresponding subsets of fine cells. Starting from the prolongation operator defined for all fine cells $i \in F$ as $P^1_{i,K} = 1,\ i \in K$ and $P^1_{i,K} = 0,\ i \notin K$ and smoothing it using n relaxed Jacobi iterations, the algorithm then reads for $\nu = 1, n$:

Starting from the prolongation operator defined for all fine cells $i \in F$ as $P^1_{i,K} = 1,\ i \in K$ and $P^1_{i,K} = 0,\ i \notin K$ and smoothing it using n relaxed Jacobi iterations, the algorithm then reads for $\nu = 1, n$:

1. Compute the relaxed Jacobi update with $\omega = 2/3$ optimal value for Poisson-like equation for I_K, for each area K

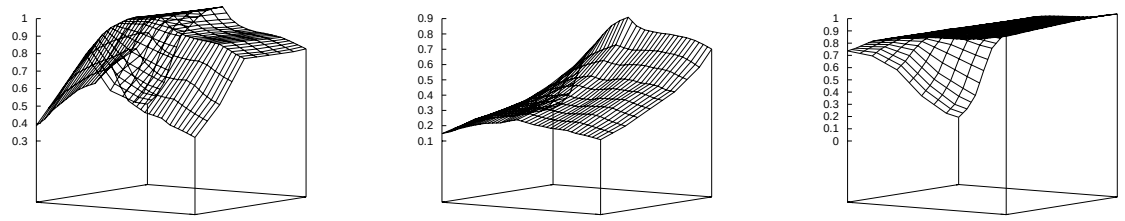

(a) *MsFv* (b) *MsRSB* (c) *FV-MHMM*

Figure 5.3: Illustration of basis function for *(a)MsFv, (b)MsRSB and (c)FV-MHMM.*

$$\hat{d}_{i,K} = -\omega \sum_{j \in F} (D^{-1}(A - D))_{i,j} P^{\nu}_{j,K} \tag{5.12}$$

with A the fine grid operator and D its diagonal.

2. Correct on the overlapping areas, introducing $H_i = \{K \,|\, i \in I_K\}$ collection of coarse owner's indexes of a fine cell $i \in G$

$$d_{i,K} = \begin{cases} \hat{d}_{i,K}, & i \in I_K \setminus G, \\ \dfrac{\hat{d}_{i,K} - P^{\nu}_{i,K} \sum\limits_{k \in H_i} \hat{d}_{ik}}{1 + \sum\limits_{k \in H_i} \hat{d}_{ik}}, & i \in I_K \cap G, \\ 0, & i \notin I_K \end{cases} \tag{5.13}$$

3. Update $P^{\nu+1}_{i,K} = P^{\nu}_{i,K} + d_{i,K}$, $i \in F$, and evaluate the error $e_K = \max\limits_{i \in I_K \setminus G} (|\hat{d}_{i,K}|)$ on the internal support. Terminate if $e_K < tol$ and set $P_{i,K} = P^{\nu+1}_{i,K}, i \in F$.

The fine scale approximate pressure is then obtained as the following linear combination of the coarse cell pressures $\bar{p}_K, K \in M_H$

$$p^{MsRSB}(\mathbf{x}) = \sum_{K \in M_H} \bar{p}_K P_{i,K} \text{ for all } \mathbf{x} \in i,\ i \in F.$$

and the coarse scale system is obtained from the conservation equations in each coarse cell $K \in M_H$.

5.2 Methods improvement

Dealing with highly heterogeneous permeability fields exhibiting higly connected path is problematic for such methods. Both *MsFv* and *MsRSB* methods have known significant improvements since they were derived (Hajibeygi et al., 2008, 2010; Hajibeygi and Jenny, 2011; Lunati and Jenny, 2008; Wang et al., 2014). One of the most notable is to use several cycles successively smoothing and solving via-multiscale methods to converge to the fine scale results.

The *FV-MHMM* does not implement such a technique. But, two types of weighting schemes are proposed in this section in order to enhance its solution accuracy.

Let p_{ms} denote the approximation of the fine scale pressure and p_c be the coarse scale solution obtained by the multiscale method (without mention of the multiscale method). Let us introduce the operator notation of Eq. (5.1) as

$$Ap = b \tag{5.14}$$

$$A_c p_c = Rb \tag{5.15}$$

With P the prolongation operator based on the basis function computed in *MsFv* or *MsRSB* and R the restriction operator as described in (Møyner and Lie, 2016). The coarse scale operator A_c is then related to the fine scale operator A, in such a way as :

$$R(Ap_{ms}) = RA(Pp_c) = A_c p_c \tag{5.16}$$

5.2.1 MsFv and MsRSB iterative formulation

Both *MsFv* and *MsRSB* can be used in smoother-multiscale cycle as mentionned in Alg. 5.1.

Let us denote the *multiscale residuals* $R_{ms}^{\nu-1} = b - Ap_{ms}^{\nu-1}$, which measures the discrepancy from the reconstruted multiscale solution p_{ms} to the finite volume solution $A^{-1}b$.

with $f_{smooth}(z)$ implementing either a Jacobi smoother or an ILU_0 factorization with 0-level of fill in. The use of different smoothing functions leads both *MsFv* and *MsRSB* to different convergence behavior. The cases reported on Fig. 5.4 are simulations over the two type of facies found in the layers in 10th SPE case. They are performed setting a tolerance stopping criteria on the residuals to 10^{-12} and a 10×11 coarses cells onto the 60×220 fine cells discretization.

On Fig.5.4(a), for the log-normally distributed facies, the convergence of the Jacobi and ILU_0 smoothers are comparable but allows lower error reduction with respect to the number of iterations.

Algorithm 5.1 Smoother-multiscale solution cycle description.

Let be $f_{c2f}(z) = P(A_c^{-1}Rz)$ and $f_{smooth}(z)$.

1. Construct a first multiscale approximation of the fine scale pressure using:

$$p_{ms}^0 = f_{c2f}(b)$$

2. if [iterations are demanded and a smoother is provided], for ν iterations times (or before if residual is small enough w.r.t tolerance)

   (a) apply one iteration of smoothing of the multiscale residual

$$p_{ms}^{\nu-1} = f_{smooth}(R_{ms}^{\nu-1})$$

   (b) update $p_{ms}^{\nu}$by solving such as,

$$p_{ms}^{\nu} = p_{ms}^{\nu-1} + f_{c2f}(R_{ms}^{\nu-1})$$

On Fig.5.4(b), it can be seen, as reported in (Møyner and Lie, 2016; Wang et al., 2014), that the *MsFv* methods can struggle to find a solution on such channelized medium. It can be corrected choosing larger blocks to fit more heterogeneous features into the coarse blocks. Switching to a 5×11 coarse discretization allows to find a converged *MsFv* solution but implies a lower accuracy for the *MsRSB* solution. This configuration is reported on Fig. 5.4(c). Jacobi is then limited as the fine scale operator has important off-diagonal coefficients. As in (Møyner and Lie, 2016; Wang et al., 2014), the ILU_0 smoother will be chosen when operating smoother-multiscale solution cycles with these methods.

5.2.2 FV-MHMM Weighting schemes

The definition of a weighting schemes is crucial for the *FV-MHMM* as previously described in (Franc, Jeannin, Debenest and Masson, 2016). It allows to adapt the basis functions to the underlying heterogeneities and leads to a 5 times lower error level. Indeed, such a weighting schemes will ease the flow in the highly permeable media and will stop it in the barrier regions.

Transmissivity weighting (tw) scheme

For the *FV-MHMM*, according to (Franc, Jeannin, Debenest and Masson, 2016), we can weight the functions of $\mathbb{P}_l(\sigma)$ to produce a new space that is piecewisely adapted to the

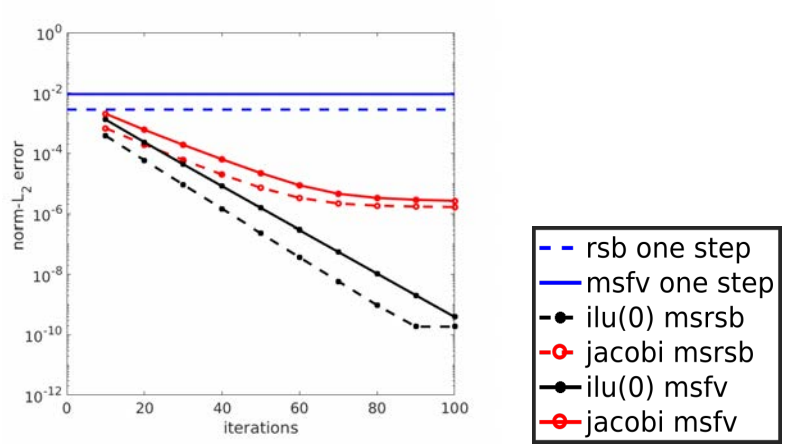

(a)

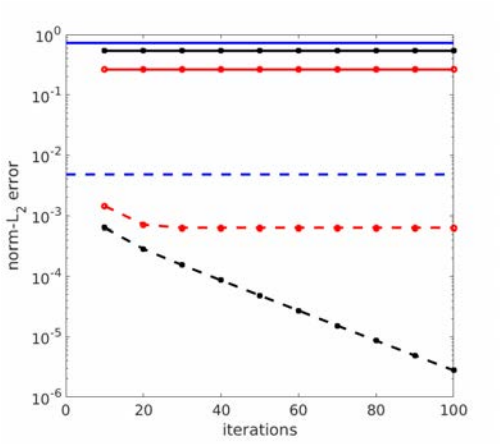

(b)

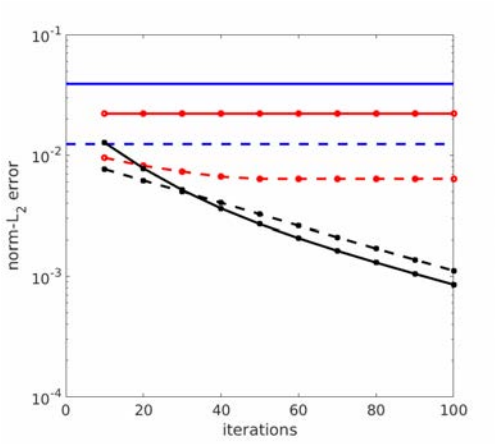

(c)

Figure 5.4: Convergence behavior considering Jacobi or ILU_0 smoother. Dotted lines stand for *MsRSB* method; solid lines are for *MsFv* method. Behavior (a) for the 13^{th} SPE10 test case with a 10×11 coarse mesh, (b) for the 84^{th} SPE10 test case with a 10×11 coarse mesh and (c) for a 5×11 coarse mesh. Blue lines represent for each multiscale methods, the error level, as if they are considered as a single stage multiscale solver (corresponding to step 1 in Alg. 5.1).

neighbor transmissivities of the selected coarse face. Let us define the transmissivity weighting scheme (tw) for $\sigma \in F_H$:

- $F_{h,\sigma}$ denotes the set of fine faces of σ
- T_e denote the transmissivity of the fine face $e \in F_{h,\sigma}$.

Let the function λ_σ be defined on σ such that

$$\lambda_\sigma(\mathbf{x}) = \frac{T_e}{\sum_{e \in F_{h,\sigma}} T_e} \text{ for all } \mathbf{x} \in e,\ e \in F_{h,\sigma}.$$

Then the weighted space Λ_l is spanned on each coarse faceσ by $\lambda_\sigma \mathbb{P}_l(\sigma)$.

MultiScale Two Point Flux Approximation (mstpfa) scheme

Another adaptation can be inspired from (Møyner and Lie, 2014; Aarnes, 2004b). Performing a local simulation of an imposed flux through the coarse face, the heterogeneous fine scale fluxes along the coarse face can be used to build a weighting scheme. Let us define a multiscale two point flux approximation weighting scheme (*mstpfa)* for $\sigma \in \overline{F_H}$, $\overline{F_H} \cap \partial\Omega = \varnothing$:

- $F_{h,\sigma}$ denotes the set of fine faces of σ
- ϕ_e denote the flux of the fine face $e \in F_{h,\sigma}$.

Let the function λ_σ be defined on σ such that

$$\lambda_\sigma(\mathbf{x}) = \frac{\phi_e}{\sum_{e \in F_{h,\sigma}} \phi_e} \text{ for all } \mathbf{x} \in e,\ e \in F_{h,\sigma}.$$

Then the weighted space Λ_l is spanned on each coarse faceσ by $\lambda_\sigma \mathbb{P}_l(\sigma)$.

In the next section, a focus will be done on the accuracy of each method compared to different facies. As an indicator, we will compare the fine scale solution to the multiscale ones. The accuracy with respect to the fine grid finite volume solution will be assessed using the following error measures:

$$\epsilon_{L_2} = \frac{||p_{ms} - p_{ref}||_2}{||p_{ref}||_2} \tag{5.17}$$

$$\epsilon_1(\mathbf{x}) = \frac{|p_{ms}(\mathbf{x}) - p_{ref}(\mathbf{x})|}{p_{ref}^{max} - p_{ref}^{min}},\ \mathbf{x} \in \Omega. \tag{5.18}$$

The first indicates the overall level of error while the second plotted in colormap mode will allow us to correlate the errors with the mesh and/or the permeability field features.

physics dim.	$1200ft \times 2200ft$
fine grid	$60 \times 220\, cells$
coarse grids	$(5, 10) \times 11\, cells$
boundary cdt	$\Delta p = 1\, Pa$

Table 5.1: Simulation conditions for SPE 10^{th} test case.

Whether use of weighted version or native of *FV-MHMM*, quadratic polynomial space will be used to approximate Λ_H (*i.e.* use of Λ_2). An ILU_0 smoother will be use when dealing with smoother-multiscale methods cycle implementation , denoted as improved version for *MsFv* and *MsRSB*. In the next section, *MRST2016* Toolbox (Lie, 2014) will be used when considering tests for both *MsFv* and *MsRSB* methods.

5.3 The 10^{th} SPE Case

The first test involves 2D layers of the 3D heterogeneous permeability field that has been generated for the 10^{th} SPE benchmark (see (Christie et al., 2001)). It is a well known test case that produces two main facies characteristics. On the 35 first layers, Tarbert formation types have been generated. Those layers are characterized by correlated log-normally distributed permeability values with high contrasts but moderate correlation lengths with respect to the size of the domain. On the remaining 50 layers, a fluvial Upper-Ness type has been generated. Those are channelized, *i.e.* the correlation length is of the size of the global domain extent. It produces very challenging permeability fields to perform upscaling on, as the scale separation assumption is not fulfilled. In a first step, native version of each multiscale method will be tested on different layers. In a second step, some improvement techniques will be taken into account and the error levels reported.

The two layers we select to perform this study are the 13^{th} layer, for the top layers, and 84^{th} layer , for the bottom layers. Once again they are chosen because they correspond respectively to two different permeability backgrounds, with different correlation lengths. Their log permeability maps are reported on Fig.5.5.

Dealing with the channelized typed layers, *MsFv* struggles to converge as explained in (Møyner and Lie, 2016; Wang et al., 2014). Nonetheless a converged result can be obtained coarsening the coarse mesh, including more heterogeneous features in the same coarse cell. It is then decided to run tests with a 5×11 and 10×11 coarse meshes. Such a coarsening will result in a loss of accuracy for both *MsFv* and *FV-MHMM*. The coarse discretization 5×11 is chosen when reporting $\epsilon_1(\mathbf{x})$ as colormap.

For the numerical test cases, we define the following conditions reported in Tab.5.1.

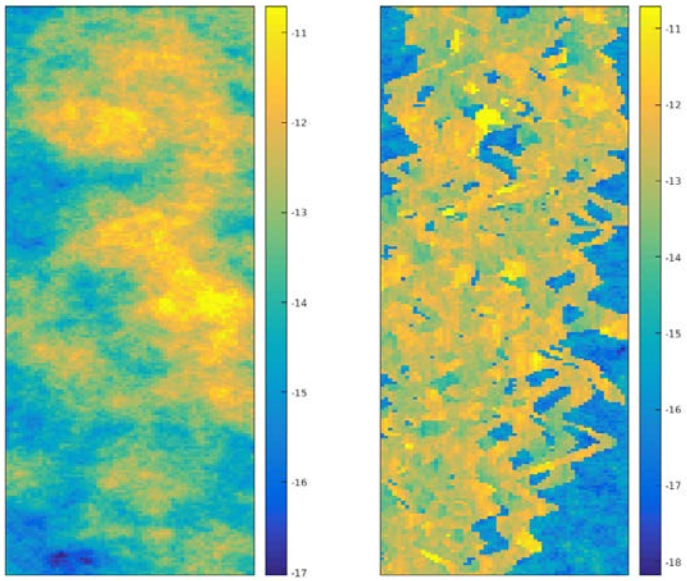

Figure 5.5: Log-permeability field on the 13^{th} and 84^{th} layers.

5.3.1 Native versions of multiscale solvers

In this section, all the methods are used as direct solver. That is to say, with considering only the first stage of the Alg. 5.1 for *MsFv* and *MsRSB*. For *FV-MHMM*, it excludes any weighting schemes.

From Fig. 5.6(a), the reader can notice that all methods localized their error peaks in the impermeable area at the top of the layer. From the $L_2 - norm$ error reported in Tab. 5.1(a), it can be observed that the *FV-MHMM* in this configuration produce one order of magnitude lower error.

Switching to the channelized 84^{th} layer, as the *MsFv* produces locally $\epsilon_1(\mathbf{x})$ error measures greater than 1, the scale is limited to the second largest value (which is obtained for *FV-MHMM*). From Fig. 5.6(b), it can be observed that each methods produces their maximum errors, where impermeable features appear in the highly permeable channels. As confirmed by the the $L_2 - norm$ error report in Tab. 5.1(b), *MsRSB* produces the most accurate result on that facies with 5 times lower error level.

Repeating these tests on several layers along the 10^{th} SPE test case, ϵ_{L_2} measures are represented on Fig. 5.7, while statistical report per facies is reported on Tab. 5.3. The same observation can be generalized. *MsRSB* is the most accurate method for channelized media, as it can benefit from the overlapping definitions in its basis functions construc-

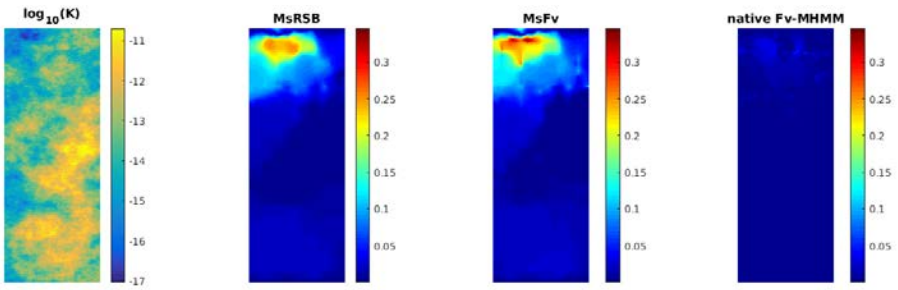

(a) 13^{th} slice

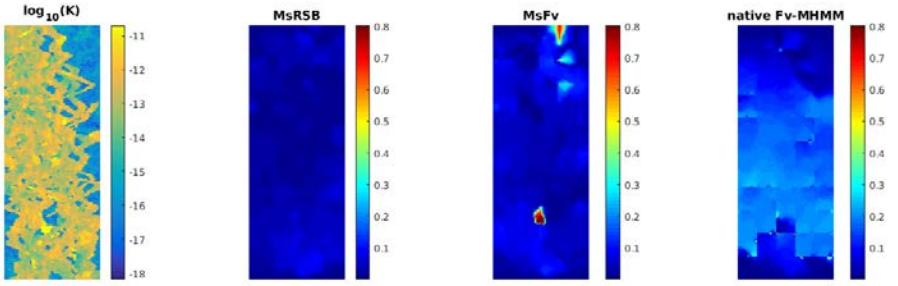

(b) 84^{th} slice

Figure 5.6: Native methods: Normalized error $\epsilon_1(\mathbf{x})$ for the 13^{th} and 84^{th} SPE layer.

tion. It includes more effects from the highly connected paths, whereas *FV-MHMM*, which has independently constructed basis functions, is then limited by its definition of effective boundary condition to apply to its *local problem lambda* and *local problem source.* Indeed, the space Λ_l is spanned by $\mathbb{P}_l(\sigma)$ on each coarse face $\sigma \in F_H$, independently from the fine scale information, hence , the introduction of weighting scheme for the space Λ_l. In order to better fit the heterogeneous media, we can modify the native version of each algorithm. *MsFv* can make the use of smoothing steps in order to converge to the desired fine scale solution. Based on the native *MsFv*, the neglected fluxes from the localization assumption can be estimated from the residual.

5.3.2 Improved implementations versions of the multiscale algorithms

On Fig. 5.8 is reported $\epsilon_1(\mathbf{x})$ for *MsRSB* and *MsFv* with 25 cycles and 100 cycles of smoother-multiscale solution. The $\epsilon_1(\mathbf{x})$ levels for transmissivity weighted (*tw*) and multiscale two point flux approximation (*mstpfa*) *FV-MHMM* are also reported.

On the 13^{th}layers (Fig. 5.8(a)), the smoothing cycles significantly improved the accuracy of the solution. Similarly, noticing the scales, we can verify that *tw* and *mstpfa* weighting

(a) Native methods: ϵ_{L_2} error report for 13^{th} layer

	MsFv	*MsRSB*	native *Fv-MHMM*
mesh 10×11	0.0216	0.0209	0.00249
mesh 5×11	0.0236	0.0220	0.00226

(b) Native methods: ϵ_{L_2} error report for 84^{th} layer

	MsFv	*MsRSB*	native *Fv-MHMM*
mesh 10×11	NC	0.0111	0.0322
mesh 5×11	0.0390	0.0124	0.0585

Table 5.2: Native methods: $L_2 - norm$ error report for native methods (*i.e.* single stage *MsFv* or *MsRSB* and *Fv-MHMM* without weighing scheme). NC stands for non converged solution.

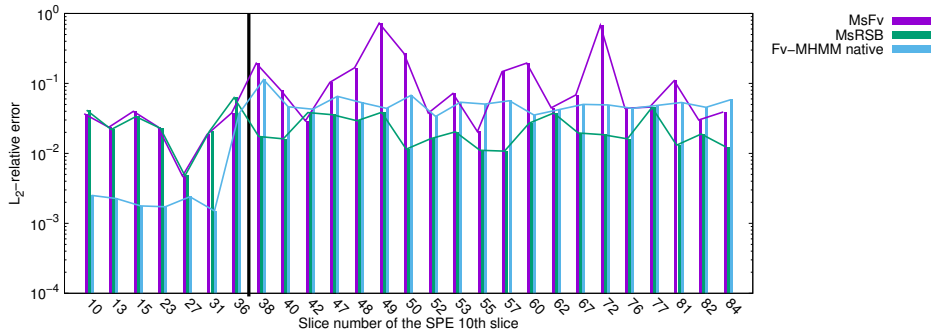

Figure 5.7: Native methods: Relative $L_2 - norm$ errors for all the SPE layers.

	Top layers	Bottom layers
MsFv	0.0246(0.0128)	0.150(0.196)
MsRSB	0.0242(0.0125)	0.0246(0.0138)
native Fv-MHMM	$2.03(0.41) \cdot 10^{-3}$	0.0520(0.0166)

Table 5.3: Native methods: $L_2 - norm$ statistics *per facies*. Values are presented as *mean (standard deviation)*.

(a) Improved methods: ϵ_{L_2} error report for 13^{th} layer

	MsFv	*MsRSB*	*tw FV-MHMM*	*mstpfa FV-MHMM*
mesh 10×11	$3.21 \cdot 10^{-5}$	$2.55 \cdot 10^{-5}$	$1.14 \cdot 10^{-3}$	$9.30 \cdot 10^{-4}$
mesh 5×11	$2.11 \cdot 10^{-4}$	$1.58 \cdot 10^{-4}$	$1.46 \cdot 10^{-3}$	$8.53 \cdot 10^{-4}$

(b) Improved methods: ϵ_{L_2} error report for 84^{th} layer

	MsFv	*MsRSB*	*tw FV-MHMM*	*mstpfa FV-MHMM*
mesh 10×11	NC	$4.72 \cdot 10^{-4}$	$3.25 \cdot 10^{-3}$	$3.24 \cdot 10^{-3}$
mesh 5×11	$8.55 \cdot 10^{-4}$	$1.11 \cdot 10^{-3}$	$4.73 \cdot 10^{-3}$	$3.67 \cdot 10^{-3}$

Table 5.4: Improved methods: $L_2 - norm$ error report for improved methods (*i.e.* 100 smoother-multiscale solution cycles for *MsFv* or *MsRSB* and *FV-MHMM* with *tw* and *mstpfa* weighting schemes). NC stands for non converged solution.

	Top layers	Bottom layers
MsFv	$1.82(1.02) \cdot 10^{-4}$	0.255(0.347)
MsRSB	$2.35(1.47) \cdot 10^{-4}$	$6.78(7.82) \cdot 10^{-3}$
tw Fv-MHMM	$2.03(0.47) \cdot 10^{-3}$	$6.56(2.68) \cdot 10^{-3}$
mstpfa Fv-MHMM	$9.30(4.17) \cdot 10^{-4}$	$7.56(6.28) \cdot 10^{-3}$

Table 5.5: Improved methods: $L_2 - norm$ statistics *per facies*. Values are presented as *mean (standard deviation).*

schemes have positive impact on the accuracy. This result is supported by the report on $L_2 - norm$ error synthesized in Tab. 5.3(a). A hundred cycles drop the error levels by two orders of magnitude, while weighting scheme produce between one and half to two times less error.

On the 84^{th} layer (Fig. 5.8(b)), *MsFv* and *MsRSB* efficiently smooth out their errors, while weighting schemes for *FV-MHMM* allow to reduce the error in better representing the flow at the boundaries when computing basis functions. Looking at the report on Tab. 5.3(b), the cycles significantly improves the accuracy of the multiscale approximation, especially for *MsFv*. Regarding, the weighting schemes effects, it can be noticed that *mstpfa* scheme is more efficient on 5×11 coarse discretization than on 10×11 discretization. It can be explained by the fact that it includes more details of the flow by considering larger neighboring coarse cells in its computation.

From the summary plot Fig. 5.9 and statistical report Tab. 5.5, we can observe that on the top layers, the smoother-multiscale solution cycles for *MsFv* and *MsRSB* result in error levels one order of magnitude smaller than what can be achieved with *tw* and *mstpfa FV-MHMM*. On the channelized medium, *MsRSB* cycled and weighted formulations achieved to reach the same accuracy, when comparing their $L_2 - norm$ error levels.

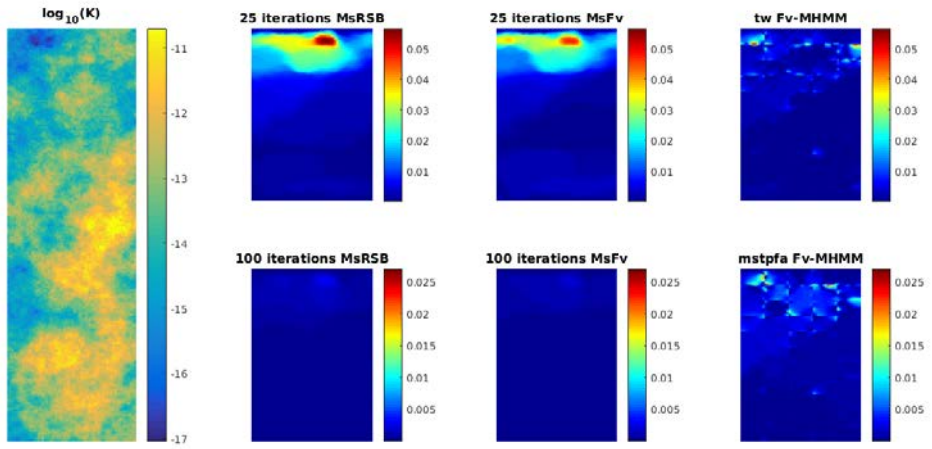

(a) 13^{th} slice

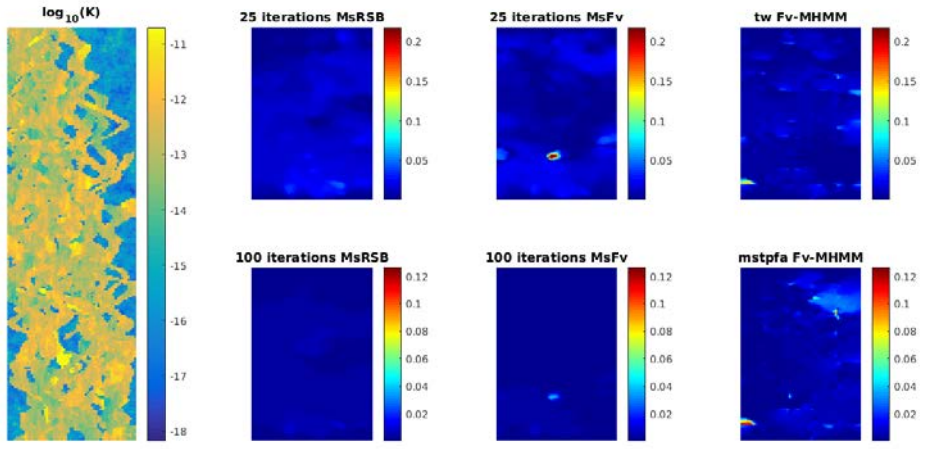

(b) 84^{th} slice

Figure 5.8: Improved methods: Normalized error $\epsilon_1(\mathbf{x})$ for the 13^{th} and 84^{th} SPE layer.

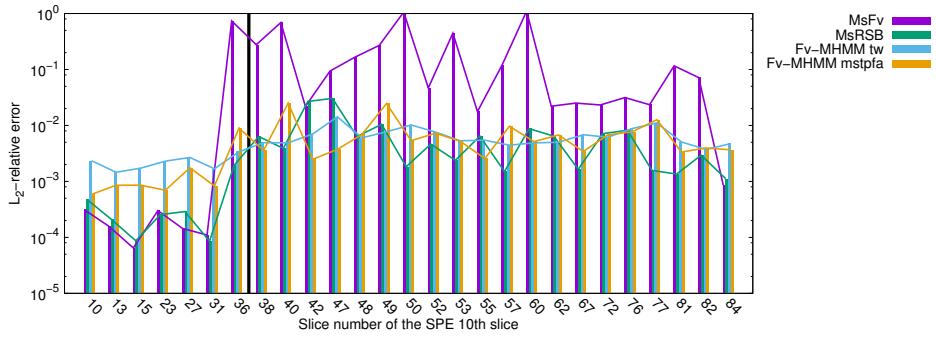

Figure 5.9: Improved methods: Relative $L_2 - norm$ errors for all the SPE layers.

physical dimensions of the slanted test case	$75ft \times 5ft$
fine grid : number of cells (x,y)	$256 \times 64\, cells$
coarse grid : number of cells (x,y)	$32 \times 16\, cells / 8 \times 4\, cells$
pressure drop imposed in y-direction	$\Delta p = 1\, Pa$

Table 5.6: Simulation conditions for the slanted test case.

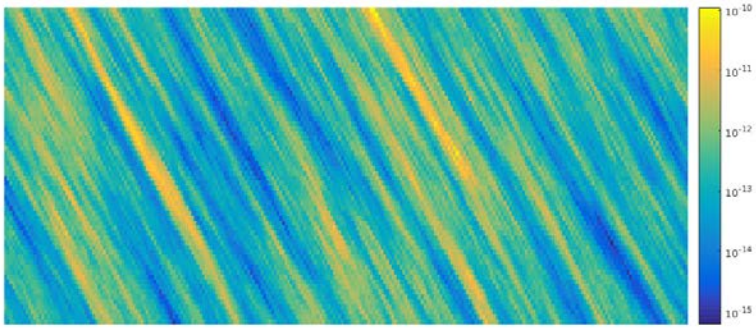

Figure 5.10: Example of a log-permeability field map in the slanted case.

5.4 The slanted case study

The second test case is a bottom to top cross flow performed on a $75ft$ by $5ft$ slanted permeability field. The main feature of this case is the stripes of low and high permeable regions which are non aligned with the cartesian grids. Ten realizations have been drawn with the two non-dimensional correlation lengths $\lambda_1 = 0.5$ and $\lambda_2 = 0.02$. The variance of K is set such as $\sigma(\log(k)) = 3.0$. An example of such a realization is given on Fig. 5.10.

As before, error levels are reported in terms of mean and standard deviations in Tab. 5.7. From these data, the reader can observe that on *native* formulations, both *MsFv* and *MsRSB* have their error level reduce when considering a refined coarse discretization. Switching to the improved version of algorithm, it can be noticed that too fine coarse mesh for *MsFv* deteriorates the accuracy as it includes less details about the surrounding flows. Apart from that, the cycles are once again efficient in dropping the error level up to two orders of magnitude. On the FV-MHMM side, weighting schemes are counterproductive. The slanted heterogeneous features induce a corner flow which is badly estimates by both schemes. It results in less accurate solution. Considering this analysis of the results on the slanted case, an alternative approach for the FV-MHMM method (different of *tw* or *mstpfa* approaches) will be needed to obtain results comparable to other methods. For example, a possibility we are exploring is to build an adaptive formulation of the FV-MHMM formulation, in the same vein as adaptive finite elements, which could be combined with *tw* or *mstpfa* weighting schemes approaches.

(a) Native methods

	8×4	32×16
MsFv	0.0576(0.0224)	0.0526(0.0202)
MsRSB	0.0365(0.00457)	0.0180(0.00257)
native FV-MHMM	0.0164(0.00325)	$5.73(1.51) \cdot 10^{-3}$

(b) Improved methods

	8×4	32×16
MsFv	$3.62(1.31) \cdot 10^{-3}$	$4.42(1.12) \cdot 10^{-2}$
MsRSB	$4.10(1.37) \cdot 10^{-3}$	$9.24(3.97) \cdot 10^{-5}$
tw FV-MHMM	$2.15(0.167) \cdot 10^{-2}$	$1.79(0.156) \cdot 10^{-2}$
mstpfa FV-MHMM	$8.39(2.09) \cdot 10^{-3}$	$8.75(0.625) \cdot 10^{-3}$

Table 5.7: $L_2 - norm$ statistics on slanted realizations. Values are presented as *mean (standard deviation).*

Conclusion

In this paper, three different multiscale methods *FV-MHMM*, *MsFv* and *MsRSB* have been tested using several different configurations. The *MsFv* and *MsRSB* methods are currently the most widely used in the reservoir simulation community(Moyner et al., 2015; Lunati et al., 2009). Their performances have been cross-compared. On log-normally distributed facies of the 10^{th} SPE test case, *MsFv* and *MsRSB* share the same accuracy which is improved by two order of magnitude after few smoother-multiscale solution cycles. *FV-MHMM* has in-between performance in terms of accuracy and can improve slightly its results by the use of weighting schemes (*tw* or *mstpfa).* The channelized type of medium challenges more the multiscale methods tested. *MsFv* has to work with a coarse enough mesh to be sure to find a solution on all layers as already mentioned in (Wang et al., 2014; Møyner and Lie, 2016). Considered as a single stage multiscale solver, *MsRSB* finds solution with one order of magnitude lower error than the native form of FV-MHMM. If few cycles for *MsRSB* and weighting scheme for *FV-MHMM* are used, the error levels are lowered by one order of magnitude.

In a last part, a slanted permeability case was studied : with this type of heterogeneity, the *FV-MHMM*struggles to correctly reproduce fine scale fluxes. On the other hand, *MsRSB* and *MsFv*, respectively in their cycled version, correctly reproduce the fine scale details, as their solutions converge to the fine scale solution. This slanted permeability test highlights a limitation of *FV-MHMM*, which has to do with the proper definition of effective boundary conditions for its basis functions. Indeed, either *MsFv* by its dual-primal mesh definition

which leads to a multiple point coarse stencil, or *MsRSB* by its definition of overlapping areas, include more details of the surrounding flow when computing their basis functions.

The construction of the weighting schemes for the *FV-MHMM* aims at enhancing this boundary condition to better fit the surrounding flow. In the slanted test case, since the weighting schemes do not improve the solution accuracy, another idea would be to develop an adaptive formulation of the *FV-MHMM* by analogy with adaptive finite elements. This work is ongoing.

On the other hand, *MsRSB* and *MsFv* methods have been enriched by many improvements. They have already been used to treat 3D cases with more elaborate fluid models(Møyner et al., 2017; Hilden et al., 2016). For instance, capillary and gravity effects, black oil model and fractured medium, have all been implemented (Møyner et al., 2016; Bosma et al., 2017; Shah et al., 2016; Lunati and Jenny, 2008). *MsRSB* is also adapted to unstructured meshes (Møyner, 2014). Furthermore, after having been reformulated as algebraic solvers, *MsRSB* and *MsFv* are now considered in most recent work as a non-symmetric preconditioner for the fine-scale problem using GMRES solvers (Møyner, 2014; Manea et al., 2015). Once formulated in its algebraic form, *FV-MHMM* could be used as a preconditioning technique, in the same fashion as in the work of (Lunati and Lee, 2009). This will be a forthcoming line of research.

Acknowledgements

The authors would like to thank ENGIE and STORENGY for the financial support of J.Franc. INP Toulouse is also acknowledged for the travel grant, BQR SMI, of J.Franc. We also thank Prof. Margot Gerritsen, ICME-Stanford, for all the advices and discussions on the multiscale finite volume methods.

Aarnes, J. E.: 2004b, On the use of a mixed multiscale finite element method for greaterflexibility and increased speed or improved accuracy in reservoir simulation, *Multiscale Modeling & Simulation* .

Arbogast, T.: 2002, Implementation of a locally conservative numerical subgrid upscaling scheme for two-phase darcy flow, *Computational Geosciences* **6**(3-4), 453–481.

Arbogast, T., Cowsar, L. C., Wheeler, M. F. and Yotov, I.: 2000, Mixed finite element methods on nonmatching multiblock grids, *SIAM Journal on Numerical Analysis* **37**(4), 1295–1315.

Arbogast, T., Pencheva, G., Wheeler, M. F. and Yotov, I.: 2007, A multiscale mortar mixed finite element method, *Multiscale Modeling & Simulation* **6**(1), 319–346.

Bosma, S., Hajibeygi, H., Tene, M. and Tchelepi, H. A.: 2017, Multiscale finite volume method for discrete fracture modeling on unstructured grids (ms-dfm), *Journal of Computational Physics* **351**, 145–164.

Castelletto, N., Hajibeygi, H. and Tchelepi, H. A.: 2016, Multiscale finite-element method for linear elastic geomechanics, *Journal of Computational Physics* .

Christie, M., Blunt, M. et al.: 2001, Tenth spe comparative solution project: A comparison of upscaling techniques, *SPE Reservoir Simulation Symposium*, Society of Petroleum Engineers.

Efendiev, Y., Galvis, J. and Hou, T. Y.: 2013, Generalized multiscale finite element methods (gmsfem), *Journal of Computational Physics* **251**, 116–135.

Franc, J., Jeannin, L., Debenest, G. and Masson, R.: 2016, Fv-mhmm methods for reservoir modeling, *Computational Geosciences* .

Hajibeygi, H., Bonfigli, G., Hesse, M. A. and Jenny, P.: 2008, Iterative multiscale finite-volume method, *Journal of Computational Physics* .

Hajibeygi, H. and Jenny, P.: 2011, Adaptive iterative multiscale finite volume method, *Journal of Computational Physics* .

Hajibeygi, H., Lunati, I. and Lee, S. H.: 2010, Error estimate and control in the msfv method for multiphase flow in porous media, *Proceedings of XVIII International Conference on Computational Methods in Water Resources (CMWR XVIII), Barcelona, Spain*.

Harder, C., Paredes, D. and Valentin, F.: 2013, A family of multiscale hybrid-mixed finite element methods for the darcy equation with rough coefficients, *Journal of Computational Physics* .

Harder, C., Paredes, D. and Valentin, F.: 2015, On a multiscale hybrid-mixed method for advective-reactive dominated problems with heterogeneous coefficients, *Multiscale Modeling & Simulation* .

Hilden, S. T., Møyner, O., Lie, K.-A. and Bao, K.: 2016, Multiscale simulation of polymer flooding with shear effects, *Transport in Porous Media* **113**(1), 111–135.

Hou, T. Y. and Wu, X.-H.: 1997, A multiscale finite element method for elliptic problems in composite materials and porous media, *Journal of computational physics* .

Jenny, P., Lee, S. and Tchelepi, H.: 2003, Multi-scale finite-volume method for elliptic problems in subsurface flow simulation, *Journal of Computational Physics* .

Jenny, P. and Lunati, I.: 2009, Modeling complex wells with the multi-scale finite-volume method, *Journal of Computational Physics* **228**(3), 687–702.

Lie, K.-A.: 2014, An introduction to reservoir simulation using matlab: user guide for the matlab reservoir simulation toolbox (mrst). sintef ict.

Lunati, I. and Jenny, P.: 2008, Multiscale finite-volume method for density-driven flow in porous media, *Computational Geosciences* **12**(3), 337–350.

Lunati, I. and Lee, S. H.: 2009, An operator formulation of the multiscale finite-volume method with correction function, *Multiscale modeling & simulation* .

Lunati, I., Tyagi, M. and Lee, S.: 2009, Multiscale finite volume method for reservoir simulation.

Manea, A., Sewall, J., Tchelepi, H. et al.: 2015, Parallel multiscale linear solver for highly detailed reservoir models, *SPE Reservoir Simulation Symposium*, Society of Petroleum Engineers.

Møyner, O.: 2014, Construction of multiscale preconditioners on stratigraphic grids, *ECMOR XIV-14th European Conference on the Mathematics of Oil Recovery*.

Møyner, O. and Lie, K.-A.: 2014, A multiscale two-point flux-approximation method, *Journal of Computational Physics* .

Møyner, O. and Lie, K.-A.: 2016, A multiscale restriction-smoothed basis method for high contrast porous media represented on unstructured grids, *Journal of Computational Physics* .

Møyner, O., Lie, K.-A. et al.: 2016, A multiscale restriction-smoothed basis method for compressible black-oil models, *SPE Journal* **21**(06), 2–079.

Moyner, O., Lie, K. and Natvig, J.: 2015, Adaptive multiscale multi-fidelity reservoir simulation.

Møyner, O., Tchelepi, H. et al.: 2017, A multiscale restriction-smoothed basis method for compositional models, *SPE Reservoir Simulation Conference*, Society of Petroleum Engineers.

Raviart, P.-A. and Thomas, J.: 1977a, Primal hybrid finite element methods for 2nd order elliptic equations, *Mathematics of computation* .

Raviart, P. and Thomas, J.: 1977b, A mixed finite element method for 2-nd order elliptic problems, *Mathematical aspects of finite element methods* pp. 292–315.

Shah, S., Møyner, O., Tene, M., Lie, K.-A. and Hajibeygi, H.: 2016, The multiscale restriction smoothed basis method for fractured porous media (f-msrsb), *Journal of Computational Physics* **318**, 36–57.

Vaněk, P., Mandel, J. and Brezina, M.: 1996, Algebraic multigrid by smoothed aggregation for second and fourth order elliptic problems, *Computing* .

Wang, Y., Hajibeygi, H. and Tchelepi, H. A.: 2014, Algebraic multiscale solver for flow in heterogeneous porous media, *Journal of Computational Physics* .

n_v	Number of volumes in the fine grid
N_v	Number of volumes in the coarse grid
N_n	Number of nodes in the coarse grid
N_f	Number of faces in the coarse grid
γ	Coarsening ratio $\sim n_v/N_v$
a_n	Number of coarse volumes adjacent to a coarse node
a_v	Number of coarse volumes adjacent to a coarse volume
n_{it}	Number of iterations spent in smoothing basis function for *MsRSB*
$t_1(n)$	Time to invert a linear system with n unknowns

N_v	n_v	γ	d	a_v	a_n	N_n	n_{it}
9	3600	400	2	8	4	12	100

Table 5.8: Parameters

5.A Complexity comparison

Following the steps which are written in (Jenny et al., 2003) for complexity analysis of *MsFv* multiscale algorithm, we remind here the results for *FV-MHMM(Franc, Jeannin, Debenest and Masson, 2016)* and proposed the same kind of analysis for *MsRSB*. The notations introduced are presented in Tab. 5.8.

Assuming that $t_1(n) \sim ct_m n^\alpha$ where t_m is the time spent for one multiplication, c and α are constants depending on the solvers. This complexity analysis neglects time spent in the reconstruction of the pressure and the fluxes. For *MsFv,* reproducing the analysis of (Jenny et al., 2003), it leads to :

$$
\begin{aligned}
t_{MsFv1} &\approx N_n a_n c t_m \gamma^\alpha, \\
t_{MsFv2} &\approx N_v (a_v + 1) c t_m \gamma^\alpha, \\
t_{MsFv3} &\approx c t_m N_v^\alpha
\end{aligned}
$$

with the step $MsFv1$, the time spent in constructing the basis function on the dual grid; $MsFv2$, the time spent building coarse scale equivalent transmissivities on the coarse grid and $MsFv3$, the time needed to invert the coarse system.

In the same manner, *FV-MHMM* can be cast into three main steps :

$$
\begin{aligned}
t_{LLP} &\approx 2d(l+1) N_v c t_m \gamma^\alpha, \\
t_{LSP} &\approx N_v c t_m \gamma^\alpha, \\
t_{GP} &\approx c t_m [N_v + (l+1) N_f]^\alpha
\end{aligned}
$$

where d is the dimension number, l the order of the polynomial space used to approximate Λ_H and considering an average number of faces as $N_f \approx d(N_v^{1/d}+1)\prod_{i=1}^{d-1} N_v^{1/d}$. The LLP step denotes the time spent in the construction of Lagrange multipliers related basis functions; LSP, the time spent in the construction of source term related basis functions and GP the time spent inverting the global problem.

For the *MsRSB,* it has to be noted that its basis functions computations do not require inverting any operator. Indeed, in the Jacobi smoother formulation, only diagonal preconditioner D^{-1} is required, which is trivially inverted. It left us with :

$$
\begin{aligned}
t_{MsRSB1} &\approx n_{it}(\gamma_{overlap}+\gamma)N_v t_m \\
t_{MsRSB2} &\approx n_{it}\gamma_{overlap} N_v t_m \\
t_{MsRSB3} &\approx c t_m N_v^{\alpha}
\end{aligned}
$$

with the step $MsRSB1$ stands for the time spent in smoothing the basis functions on the overlapping supports; $MsRSB2$ represents the time spent restricting the spreading of the basis functions to ensure mass conservation and, as in *MsFv,* $MsRSB3$, the time needed to invert the coarse system. Estimating the overlap size is done counting nodes nu_n, edges nu_e and faces nu_f of a coarse cell depending on d (see. Tab. 5.9). To define $\gamma_{overlap}$, let us introduce $\overline{nc}$ the mean number of fine cells per dimension embedded in a coarse cell, that is do say $\overline{nc} \approx \gamma^{1/d}$.Then, the overlapping area is counted as :

$$
\begin{aligned}
\gamma_{overlap} = {} & nu_f \overline{nc}^{(d-1)}(\frac{\overline{nc}}{2})+ \\
& nu_e \overline{nc}^{(d-2)}(\frac{\overline{nc}}{2})^2+ \\
& nu_n(\frac{\overline{nc}}{2})^d
\end{aligned}
$$

Moreover, the step $MsFv1$ and step $MsFv2$ are reported to be parallelizable for the *MsFv* method (Jenny et al., 2003). As for the *FV-MHMM*, all the local problems lambda (LLP) and local problems source (LSP) are independent from each others and therefore can be parallely. Moreover, the TPFA matrix for a selected coarse cell has to be generated only one time and can be used for solving both LLP and LSP associated with this coarse cell.

	$d=1$	$d=2$	$d=3$
nu_f	2	4	6
nu_e	0	0	12
nu_n	0	4	8

Table 5.9: Counting for *MsRSB* overlap.

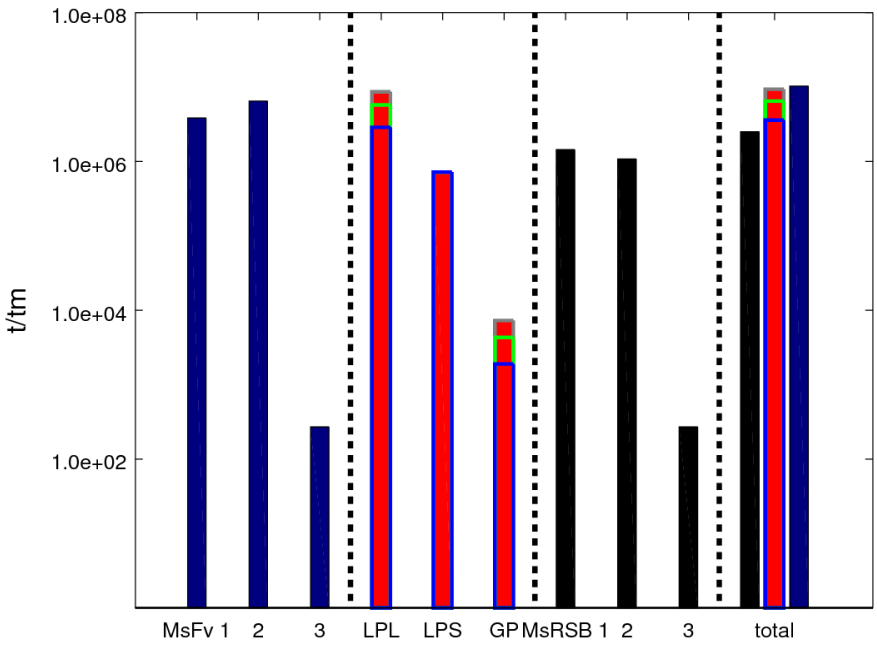

Figure 5.11: Complexity plot for Tab. 5.8 parameters. From left to right, the first region stands for *MsFv*, the second for *FV-MHMM*, the third for *MsRSB*. The right most region represents the total amount of computational time spent for each method.

Chapter 6

A posteriori estimator

Contents

Résumé en français

Ce chapitre développe l'utilisation de méthodes permettant d'adaptation aux champs de perméabilités hétérogènes pour la méthode *FV-MHMM*. Même si l'on avait pu démontrer que des fonctions de type pondération apportaient un gain en terme de précision, dans ce chapitre, un estimateur *a posteriori* pour guider le raffinement automatique du maillage grossier est décrit. Celui-ci permet l'insertion de nouveaux degrés de liberté sur les faces grossières (*i.e.* la subdivision d'une face grossière en plusieurs faces grossières) ce qui permet d'attendre des gains en précision. C'est notamment le cas lorsqu'une structure très perméable (resp. imperméable) dans un fond très imperméable (resp. perméable) traverse la face grossière. En effet, dans ce cas de figure, le multiplicateur de Lagrange associé, qui peut également être vu comme un flux grossier, doit retranscrire, à la fois les dynamiques de l'avancée rapide dans le substrat très perméable et du front figé ou ralenti dans la zone imperméable. Le redécoupage adéquat de la face va donc mieux correspondre à la physique du problème. Cependant, il faut pour cela un estimateur de l'écart de la pression approximée, par la méthode multiéchelle sur la discrétisation fine, à la solution que l'on obtiendrait par la résolution du même système à l'échelle fine, sans toutefois avoir accès à cette solution de référence. La méthode *FV-MHMM* s'appuie sur des multiplicateurs de Lagrange pour assurer la continuité de pression entre les cellules grossières. Il est possible de caractériser la qualité de la solution en évaluant les sauts présents à ces interfaces. On construit alors un estimateur *a posteriori* qui va guider la division des faces grossières. Cette technique n'étant pas incompatible avec l'utilisation de schémas de pondération, les deux mécanismes seront donc utilisés conjointement.

Les travaux réalisés sont présentés de manière graduelle. Tout d'abord, on traitera le cas d'une simple inclusion ce qui permet de vérifier l'efficacité de ce raffinement par estimateur *a posteriori*. Ensuite, sur un cas plus complexe de perméabilités hétérogènes distribuées de façon log-normale, on établit la bonne corrélation entre l'erreur relative déterminée cellule par cellule obtenue en comparant la solution fine et la solution approximée par la méthode multiéchelle et les valeurs de l'estimateur *a posteriori* aux faces. L'action des différents schémas de pondération menant à différentes sélections de faces à raffiner y est aussi détaillée. Ensuite, une étude sur 10 réalisations statistiquement équivalentes est entreprise. Les différents couples "schéma de pondération-méthode *a posteriori*" y sont testés. Il en ressort que l'option la plus optimale, c'est-à -dire celle qui nécessite le moins d'ajout de degrés de liberté tout en assurant une meilleure précision, est celle qui utilise le couple $\Lambda_0 - mstpfa$ et plusieurs itérations du mécanisme *a posteriori*. Un test ultérieur sur les deux types de milieux du réservoir type SPE 10 vient confirmer cette observation. Il souligne aussi, dans le cas d'un milieu fortement chenalisé, l'importance d'utiliser des schémas de

pondération. Ceux-ci permettent de gagner plusieurs ordres de grandeurs sur l'erreur tout en considérant le même espace polynomial pour les multiplicateurs de *Lagrange*. Enfin, une extension au diphasique est proposée. En effet, une telle technique peut permettre d'utiliser un maillage plus grossièrement discrétisé à l'échelle réservoir tout en raffinant localement les faces grossières au passage du front, *i.e.* quand la contrainte est la plus forte, et en rétablissant la discrétisation originelle une fois le front passé.

Ce chapitre est un projet d'article destiné à être soumis prochainement.

Multiscale methods for simulating groundwater flow and for predicting reservoir production have known significant breakthrough over the last decades. While their formulations are efficient as they include lots of fine scale effects through their constructions, they can benefit from efficiency mechanisms that avoid systematic updates, *e.g.* selective updates for two-phase flow in active areas. This Chapter introduces an adaptive mechanism driven by an *a posteriori* error estimator which triggers coarse face division and, hence, degree of freedom addition. As it is not incompatible with the use of the previously introduced weighting schemes, a benchmark study is carried out. The already presented *transmissivity weighting* (*tw*) scheme is used along with a new scheme, the *multiscale two point flux approximation (mstpfa).*

6.1 Introduction

Underground flow simulation is of prime importance for prediction in oil and gas industries but also for environmental remediation. As the underground permeability is most of the time highly heterogeneously distributed, it makes simulations more complex. Furthermore, the progress in data capture techniques and technologies produces more and more detailed inputs for models which can no longer be used for implementing stochastic workflow. The multiscale methods are then designed to upgrid parts of the data and then reduce this computational cost associated to make it manageable. They proceed in including fine scale variations in coarse scale operators as upscaling methods do, but without requiring a scale separation.

Multiscale methods for solving flows in heterogeneous media has been at first developed in a finite element formulation. Multiscale Finite Element Methods (MsFEM)(Hou and Wu, 1997), numerical subgrid methods(Arbogast, 2002) and Generalized Multiscale Finite Element Methods (GMsFEM)(Efendiev et al., 2013) are representative examples of these finite element methods. They rely on the construction of local basis functions that fit the underlying heterogeneities. Numerical subgrid methods are rather solving for averaged pressure values on the coarse scale approximated with RT_0 or BDM_1 elements and for their variations on subgrid scale approximated by RT_0 elements. Once the first mixed formulation derived, the reservoir engineering industries initiated their transpositions into the finite volume framework. Initial step was made with the Multiscale Finite Volume Method (*MsFv*)(Jenny et al., 2003b; Hajibeygi et al., 2008b; Lunati and Lee, 2009). Later come the Multiscale Restriction Smoothed Basis (*MsRSB*)(Møyner and Lie, 2016) and the Finite Volume Mixed Hybrid Multiscale Method (*FV-MHMM*)(Franc, Jeannin, Debenest and Masson, 2016). The *MsFv* method constructs a dual staggered grid to build its coarse scale pressure system. The basis functions are found on this dual grid and used to construct

equivalent transmissivities on the primal grid. The *MsRSB* is designed from work on Algebraic Multigrid Methods(Vaněk et al., 1996). On overlapping supports, it constructs basis function which are iteratively smoothed and restricted to ensure partition of the unity and thus mass conservation. The *FV-MHMM* is based on mixed hybrid formulation (Harder et al., 2013, 2015). It uses Lagrange multipliers unknowns that can be regarded as coarse face fluxes to ensure the continuity between coarse computational cells.

Different weighting schemes improve the accuracy of *FV-MHMM* when simulating over highly heterogeneous permeability field with correlated features such as channelized layers. They are designed to weight the test functions that are used in local computation of basis function in accordance with the underlying fine-scale transmissivities. The Transmissivitty Weighting scheme (tw) and the MultiScale Two Point Flux Approximation (mstpfa) are introduced in this paper. They are either based on the weighting according to underlying permeabilities or to the fluxes resulting from a simple cross flow in the neighborhood as described in (Møyner and Lie, 2014).

Another mechanism to improve the quality of the fine-scale mapped solution is to adapt the distribution of the degrees of freedom according to a local estimate of the error. Such an *a posteriori* estimate is designed and tested in the paper adapted from (Harder et al., 2015).

In the first section of this paper, *FV-MHMM*'s derivation is briefly introduced. Then, its weighting scheme and *a posteriori* estimator are explained. In the second section, numerical experiments are presented. The first case is a simple proof of concept of the *a posteriori* estimator on an inclusion case allowing error reduction. Afterwards, we combine weighting schemes and adaptive mechanism on log-normal permeability distribution. Equivalent realizations of log-normally distributed permeability field and one top-one bottom layer from the 10th SPE CSP (Christie et al., 2001) are then treated. Lastly, a two-phase flow test case involving such corrections is shown.

6.2 Materials and methods

6.2.1 *FV-MHMM*

Let M_H be the set of coarse cells K partitioning the domain Ω, F_H be the set of coarse faces, and ∂K denote the boundary of a coarse cell K with its unit normal vector $\mathbf{n}_K$ oriented outward to K.

Starting from the primal hybrid formulation of Raviart and Thomas (Raviart and Thomas, 1977a,b), Harder *et al.* (Harder et al., 2013, 2015) explain how to construct a multiscale

method sharing the same idea that flux continuity between cells (here coarse scale cells) can be enforced weakly using Lagrange multipliers λ. It is formulated as :

find $(u, \lambda) \in V \times \Lambda$ *such that*:

$$\begin{aligned} \int_\Omega \mathbf{K}(\mathbf{x})\boldsymbol{\nabla} u \cdot \boldsymbol{\nabla} v d\mathbf{x} \quad &+ \quad \sum_{K \in M_H} \int_{\partial K} \lambda \mathbf{n} \cdot \mathbf{n}_K \, v|_K d\sigma \\ &+ \quad \sum_{K \in M_H} \int_{\partial K} \mu \mathbf{n} \cdot \mathbf{n}_K u|_K d\sigma \\ &= \quad \int_\Omega f v d\mathbf{x} + \int_{\partial\Omega} \mu u_g d\sigma \quad \text{ for all } (v, \mu) \in V \times \Lambda, \end{aligned} \tag{6.1}$$

where V is the broken Sobolev space $H^1(M_H)$ defined as:

$$H^1(M_H) = \{v \in L_2(\Omega) : \; v|_K \in H^1(K), \, K \in M_H\},$$

Λ stands for the following Lagrange multipliers space

$$\Lambda := \{\mu \in \prod_{K \in M_H} H^{-\frac{1}{2}}(\partial K) : \exists \boldsymbol{\sigma} \in H_{div}(\Omega) \text{ s.t. } \mu|_{\partial K} = \boldsymbol{\sigma} \cdot \mathbf{n}|_{\partial K}, \; K \in M_H\},$$

∇v is the broken gradient equal to $\nabla v|_K$ on each coarse cell $K \in M_H$, and $H^{-\frac{1}{2}}(\partial K)$ is the dual space of the space $H^{\frac{1}{2}}(\partial K)$ spanned by the traces on ∂K of functions in $H^1(K)$.

Let then split the space V orthogonally as :

$$V = V_0 \oplus \Pi_{K \in M_H} W_K,$$

where V_0 is the space of piecewise constant functions on each coarse cell $K \in M_H$ and W_K is the subset of null mean function over $H^1(K)$. This definition introduces the two-scale modeling scheme.

At fixed Lagrange multiplier λ, the fine scale solution in W_K defined by Eq. (6.1) decouples. It is obtained by superposition of the solutions of two local problems, a *local lambda problem* for Lagrange multipliers driven effects and a *local source problem* for source driven effects. They respectively read:

Find $\tilde{u}_K \in W_K$ *such that*:

$$\int_K \mathbf{K}(\mathbf{x})\boldsymbol{\nabla} \tilde{u}_K \cdot \boldsymbol{\nabla} \tilde{v}_K d\mathbf{x} + \int_{\partial K} \lambda \mathbf{n} \cdot \mathbf{n}_K \tilde{v}_K d\sigma = 0 \quad \text{ for all } \tilde{v}_K \in W_K, \tag{6.2}$$

Find $\tilde{u}_K \in W_K$ *such that*:

$$\int_K \mathbf{K}(\mathbf{x})\boldsymbol{\nabla}\tilde{u}_K \cdot \boldsymbol{\nabla}\tilde{v}_K d\mathbf{x} = \int_K f\tilde{v}_K d\mathbf{x} \quad \text{for all } \tilde{v}_K \in W_K, \tag{6.3}$$

setting $\tilde{u}_K = T_K\lambda$ and $\tilde{u}_K = \hat{T}_K f$.

The coupling of the local fine scale solutions is obtained using Eq. (6.1) with test functions in $V_0 \times \Lambda$ to compute the Lagrange multiplier λ and the mean values in the coarse cells. It is formulated as follows using the previous solutions of the *local* problems $T_K\lambda$ and $\hat{T}_K f$ for all coarse cells $K \in M_H$:

find $u_{0,K} \in \mathbb{R}$, $K \in M_H$ *and* $\lambda \in \Lambda$ *such that:*

$$\begin{cases} \sum_{K\in M_H} \int_{\partial K} \lambda\mathbf{n}\cdot\mathbf{n}_K d\sigma = & \int_K f d\mathbf{x} \quad \text{for all } K \in M_H, \\ \sum_{K\in M_H} \int_{\partial K} \mu\mathbf{n}\cdot\mathbf{n}_K(u_{0,K} + T_K\lambda + \hat{T}_K f)d\sigma = & \int_{\partial\Omega} \mu u_g \quad \text{for all } \mu \in \Lambda. \end{cases} \tag{6.4}$$

This multiscale algorithm is here implemented using a *TPFA* scheme for the local problems on each coarse cell K and by replacing the space Λ by a subspace Λ_H. In the following test cases, the vector space Λ_H will be typically defined as the vector space of polynomials $\mathbb{P}_l(\sigma)$ of degree l on each coarse face $\sigma \in F_H$. These choices of Λ_H will be denoted by Λ_l, $l = 0, 1, 2$ in the following sections. These polynomial spaces can also be weighted using harmonic averaging of the permeability field on each fine face of F_H as described in the following section. Readers can refer to (Franc, Jeannin, Debenest and Masson, 2016) for further details.

6.2.2 Weighting scheme

Using the formulation presented above experiences a loss of accuracy when dealing with heterogeneous permeability field. This is particularly important where the permeability field has both high contrast in the values in a short distance range and long correlated features whose characteristic lengths are larger than the size of a coarse cell. In such a case, a weighting scheme which can better include heterogeneities details into the test function μ is helpful. Two of them are described in the following subsections.

Transmissivity weighting scheme (tw)

The first idea tested (referred to as *tw* scheme hereafter), is to weight the test functions $\mu \in \Lambda_l$ along the coarse face with the neighboring transmissivity defined on the fine grid .

Denoting $F_{h,\sigma}$the set of fine faces of coarse face σ and $T_e$the transmissivity of the fine face $e \in F_{h,\sigma}$, it reads:

$$\lambda_\sigma(\mathbf{x}) = \frac{T_e}{\sum_{e \in F_{h,\sigma}} T_e} \text{ for all } \mathbf{x} \in e,\ e \in F_{h,\sigma}. \tag{6.5}$$

This will ease the flow in areas which are the most permeable around the coarse face σ and hold it on low permeable region as underlined in (Franc, Jeannin, Debenest and Masson, 2016).

Local Resolution weighting scheme (mstpfa)

The second weighting scheme (then referred to as the *mstpfa* scheme) involves the simulation of several local test-flow problems around the coarse faces to construct the set of weights (Møyner and Lie, 2014). Let us denote by $\mathcal{N}(\sigma) = \{K, L\}$, the set of the two coarse cells neighboring the internal coarse face $\sigma \in \overline{F}_H$, where $\overline{F_H}$ referred to the set of internal coarse faces of M_H. Then , the weighting scheme is defined as :

$$\lambda_\sigma(\mathbf{x}) = \frac{\phi(w_e)}{\sum_{e \in F_{h,\sigma}} \phi(w_e)} \text{ for all } \mathbf{x} \in e,\ e \in \overline{F_{h,\sigma}}. \tag{6.6}$$

$$\int_{K \cup L} \nabla \cdot (\mathbf{K}(\mathbf{x}) \nabla \cdot w_e) dx = 0$$

$$\begin{cases} w_e = p^d & if\ \mathbf{n}_\sigma^{\mathbf{K}} \cdot \mathbf{n}_{\partial(K \cup L)} > 0 \\ w_e = -p^d & if\ \mathbf{n}_\sigma^{\mathbf{K}} \cdot \mathbf{n}_{\partial(K \cup L)} < 0 \\ \phi(w_e) \cdot \mathbf{n} = 0 & elsewhere \end{cases}$$

$$\phi(w_e) = T_e(w_L - w_K).$$

All these preprocessing weighting schemes are illustrated on Fig. 6.1.

Even if it produces an overhead cost at the preprocessing stage, it allows to reveal the embedded features and specific flow behavior. On the other hand, the *tw* scheme is less expensive to construct as it only deals with permeability values in the neighboring of the coarse face.

6.2.3 *A posteriori* error estimator

In order to enhance the solution in areas which need higher precision due to heterogeneities in the permeability field or coupling between flow equation and a transport equation (*e.g.*

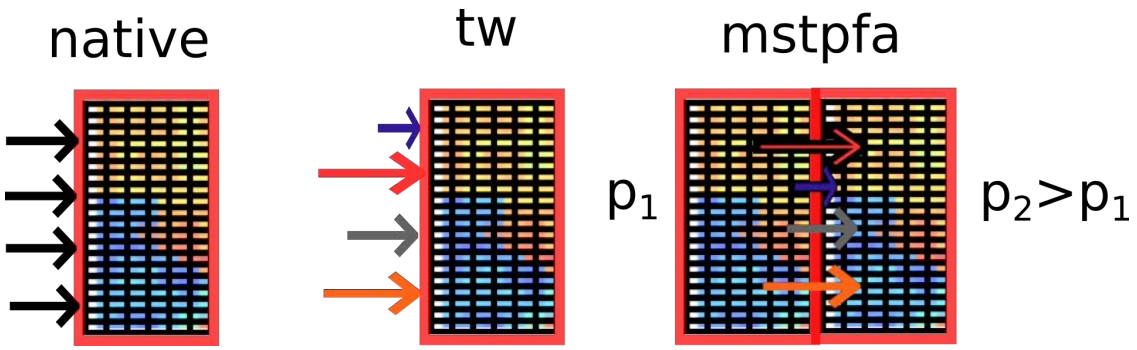

Figure 6.1: Illustration of different weighting schemes (*native, tw, mstpfa)*

for multiphase flow) , an *a posteriori* error estimator is derived. It measures the jump between coarse cells K in $p^{ms}|_{\partial K}$, whose definition is :

$$p^{ms}|_{\partial K} = u_{0,K} + T_{\partial K}\lambda + \hat{T}_{\partial K} f \tag{6.7}$$

Let us then define, $R_{\tilde{F}_H}(F_H)$, an estimator which reads as :

$$R_{\tilde{F}_H}(\sigma) = \begin{cases} -\frac{1}{2}[\![p^{ms}]\!], & \sigma \in \overline{F_H} \\ 0, & o.w. \end{cases} \tag{6.8}$$

where for $\sigma = \partial K \cap \partial L \in \overline{F_H}$ of neighbors $\mathcal{N}(\sigma) = \{K, L\}$

$$[\![p^{ms}]\!] = p^{ms}|_{\sigma}^{K} \mathbf{n}_{\sigma}^{\mathbf{K}} + p^{ms}|_{\sigma}^{L} \mathbf{n}_{\sigma}^{\mathbf{L}} \tag{6.9}$$

Then, an *a posteriori* estimator is defined as:

$$\eta_{\tilde{F_H}}(\sigma) = C||R_{\tilde{F}_H}(\sigma)||_2 \tag{6.10}$$

And the refinement process splits each coarse face σ that is such as :

$$\eta_{\tilde{F_H}}(\sigma) > \theta \eta_{F_{H,max}}, \tag{6.11}$$

into two new coarse faces, where $\eta_{F_{H,max}}$is the maximum value of the estimator on the initial set of coarse faces $\overline{F_H}$ and θ a setting factor (here taken as $\theta = 0.75$).

In the next part of the paper, we will perform several numerical tests in order to demonstrate the possible improvement that can be achieved using such an estimator. Using this *a posteriori* estimator, it is also possible to combine it with the use of the different weighting schemes. Both mechanisms will be in use in the following tests.

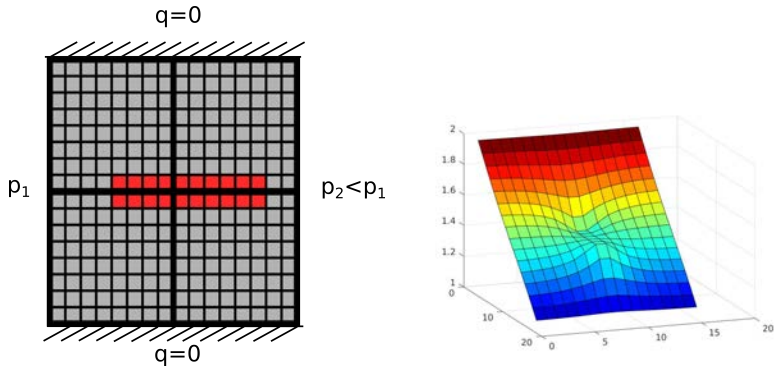

(a) (b)

Figure 6.2: Inclusion case: (a) log permeability set-up and (b) fine finite volume solution.

6.3 Numerical tests and applications

The first test involves only a basic inclusion that lies at the coarse cell's boundaries. This configuration is known to bring numerical errors to *FV-MHMM*. In a second step, the estimator is used on a 2D one-phase flow problem using a set of statistically equivalent layers with a log-normally distributed permeability. Error levels are reported through the iterations. The two faciès type of SPE are also tested in similar conditions. To conclude and extend the use of such a method, precision improvement on a two-phase flow heterogeneous test case will be observed.

6.3.1 Proof of concept

A posteriori estimator

The operating conditions of the first test case are reported on Fig. 6.2. This test consists in a block inclusion of high permeability $k_i = 2000\ mD$ into a constant permeability background of value $k_b = 1\ mD$. A constant pressure drop is applied along the x-direction while boundaries along the y-direction are kept as walls. The difficulty of such a case is that the inclusion extends across coarse block faces. Moreover, the jump in permeability values between the two regions is important. Consequently, it is difficult for *FV-MHMM* to compute a unique *Lagrange multiplier* on the central coarse faces. Indeed, it has to describe both the flow into the highly permeable inclusion and the impermeable background. The adaptive algorithm will split those coarse faces into smaller ones, introducing a new coarse face, and thus, add a new degree of freedom. It goes on until there is no more jump or if there is as many degrees of freedom as on the fine mesh.

	$\nu = 0$	$\nu = 1$	$\nu = 4$
d.o.f added	12	14	18
$\|\|p - p_{ref}\|\|_2$	0.0358	0.0261	$3 \cdot 10^{-4}$

Table 6.1: Inclusion case: L_2-norm error w.r.t the *a posteriori* iterations

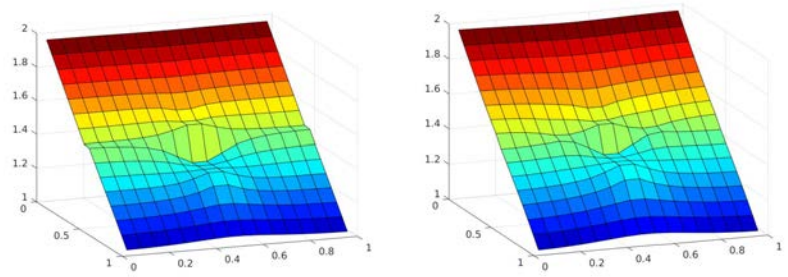

Figure 6.3: Inclusion case: Pressure values after zero iteration, $\nu = 1$ iterations and $\nu = 4$ iterations of *a posteriori* scheme.

The solution iteratively converges towards the finite volume solution (see Fig. 6.3) and the error is reduced up to a factor 100 as reported on Tab. 6.1. Nonetheless, this operation has a cost in terms of number of degrees of freedom on the coarse discretization. Consequently, the number of non-zeros elements in the global matrix to invert increases.

Weighting schemes and *a posteriori* combined

In this section, we will combine the different weighting schemes and the *a posteriori* error estimator. Those two correction methods are compatible with each other. We perform the analysis on a 2D layer using a log-normal distributed permeability realization given on Fig 6.4. The discretization adopted are 50×50 fine cells and 5×5 superimposed coarse cells. As before, a cross-flow driven by Dirichlet boundary condition for pressure is performed from the lower bound to the upper bound of the domain.

First of all, readers may wonder, in spite that the $R_{\widetilde{F}_H}$ function leads to an improvement of the solution, is it selective in the area that are refined ? In other words, is the *a posteriori* estimator well correlated with areas which exhibit the maximum error when the multiscale pressure is compared to the fine finite volume solution ?

To answer to this question, on the bottom of Fig. 6.5(b) the second adaptive iteration $\nu = 2$ on a log-normally distributed permeability layer is reported for each weighting schemes. On the background using an adapted color-map, the error is measured (as $L_1 - norm$) with respect to the fine scale finite volume solution. On the superimposed coarse mesh, red-circles

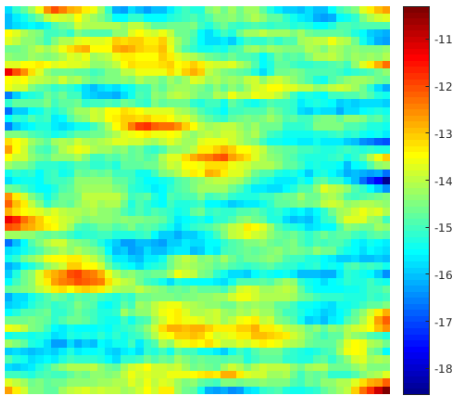

Figure 6.4: Log-permeability map of the permeability distribution.

are plotted on each coarse faces if $\eta_{F_H}(\sigma) > \eta^{native}_{F_{H,max}}$ (*i.e* if the value triggers the splitting criterion). The estimator exhibits a good correlation with the error reported as L_1-norm.

On the other hand, it can be noted that the combination of the *a posteriori* scheme and the weighting scheme results in different coarse faces refinement while going through the iterations. We report on the top of the Fig. 6.5 the results of the adaptive refinement respectively without any weighting scheme, with *tw* scheme and with *mstpfa* scheme after few iterations. Three zones are highlighted on Fig.6.5(a) to exhibit both the advantages but also the limits of the different combinations. The log-permeability values are reported in the form of a background colormap to allow the reader to correlate degree of freedom addition and heterogeneous features in the permeability field.It is important to point out that we keep the threshold value $\eta^{native}_{F_{H,max}}$ obtained without any weighting scheme, for all the combinations. Indeed, the weighting schemes improves the accuracy of the solution (as reported on Tab. 6.2) and thus it lowers the threshold factor $\eta_{F_{H,max}}$ determined on the initial iteration $\nu = 0$. So, for instance, the threshold value set for *mstpfa* weighted *FV-MHMM* $\eta^{mstpfa}_{F_{H,max}}$ would lead to the selection of coarse faces that would not be selected for $\eta^{native}_{F_{H,max}}$. The comparison would then have a bias.

- The red square highlights an area where coarse cells embedded high or low permeability inclusion. As it is away from coarse face's neighboring fine cells, the *tw* scheme can not detect them and it results in face selection (and refinement) for both native and *tw* weighted schemes.

- The blue square highlights an area where both *tw* and *mstpfa* schemes are efficient and avoid refinement. In this configuration, the permeability variations are in the neighborhood of the face and are then captured by both schemes.

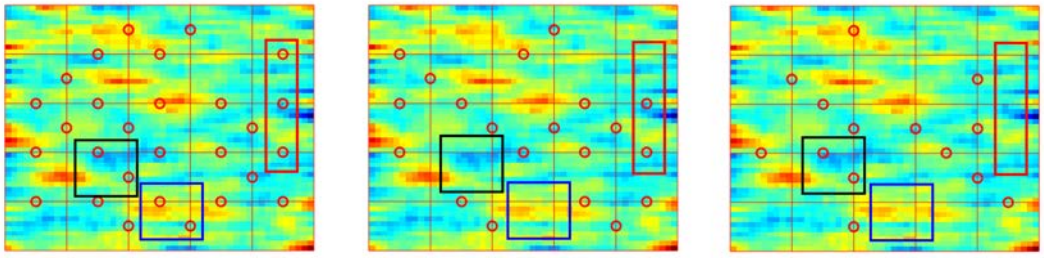

(a) Effects of weighting schemes on a posteriori estimate

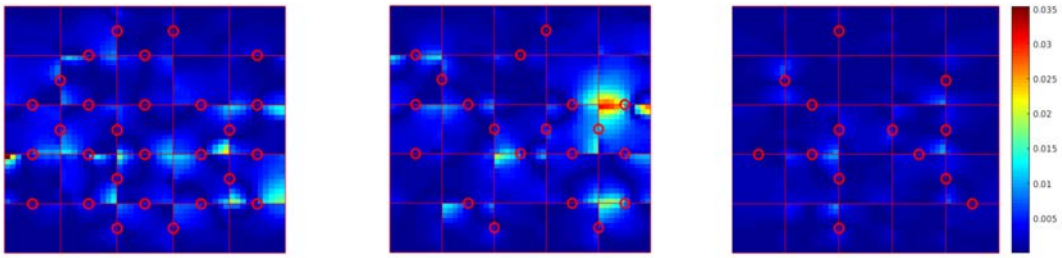

(b) L_1-norm error maps

Figure 6.5: Weighting scheme and adaptation combined.(resp. without scheme, *tw* scheme and *mstpfa* scheme)

	native	*tw*	*mstpfa*
without iterations	$4.51\,10^{-2}$	$3.46\,10^{-2}$	$1.5\,10^{-2}$
after $\nu = 1$ iterations	$1.06\,10^{-3}$	$9.60\,10^{-4}$	$7.31\,10^{-4}$

Table 6.2: L_2-norm for the different weighting schemes.

- The black square stresses a limitation of *mstpfa* scheme. Indeed, in this case, a low permeability barrier is spreading around the vertex shared by a group of four cells. This is ill-captured by the *mstpfa* scheme as it processes by cross flow simulation along faces'normal direction. It can not capture the corner phenomenon.

Once the set-up of the *a posteriori* scheme is tested and its combination with the weighting schemes is analyzed, let us switch to more elaborate test cases. The first one-phase flow case is to draw 10 statistically equivalent realizations of a log-permeability field.

6.3.2 Single phase flow test case

Log normal distributed realizations

The following test case consists in the study of 10 realizations of layers with a log-normally distributed permeability with $\sigma(log(K)) = 0.75$ as depicted on Fig. 6.6. The discretization

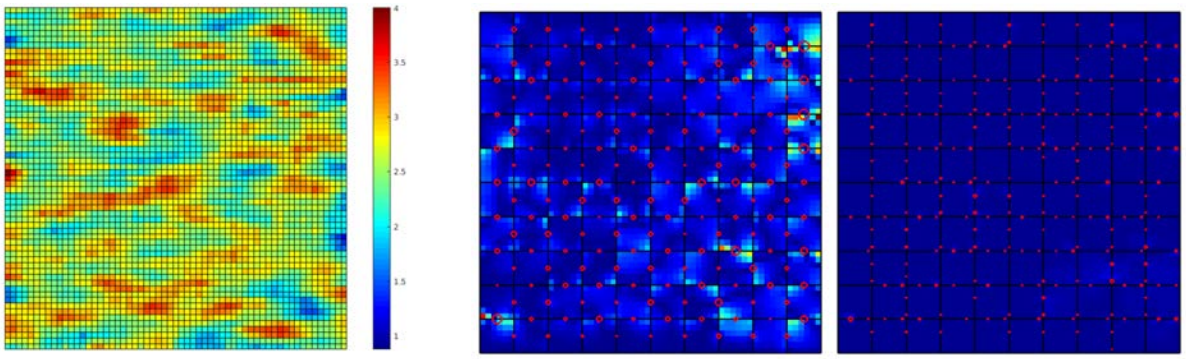

(a) (b)

Figure 6.6: Log-normal case: (a) example of the log-permeability map of a realization and (b) error level and *a posteriori* estimator values through iterations.

chosen is 100×100 for the fine mesh and 10×10 for the coarse mesh. The flow conditions are kept as a pressure-driven flow from the bottom to the top.

On the Fig. 6.6, the L_1- error map and levels of $R_{\tilde{F_H}}$ for the first and the second iteration of the *a posteriori* algorithm are reported. As above, red dots represent coarse faces but here all faces are represented and the radius of the circle is proportional to the value $||\eta_{\tilde{F}_H}||$. The cellwise error is represented as the background colormap. The reader can once again observed that the estimator is well correlated to the error level and also that iterations imply both error and estimator's value drops. As there is no more faces selected for refinement (red circles are all small), the *a posteriori* loop will end.

The next step is to study the *a posteriori* estimator effect on several realizations of a log-normally distributed permeability field. In order to reflect the accuracy-efficiency trade-off , the error reports are plotted as a function of addition of degrees of freedom (see Fig. 6.7). Readers can notice that the best choice is a few times iterated *a posteriori* version of the weighted *FV-MHMM* using *mstpfa* weighting scheme.

10th SPE layers

In order to get to a more realistic case, two layers of the 10th SPE test case (Christie et al., 2001) are selected. The simulation parameters are gathered in Tab. 6.3. One from the upper Tarbert-typed part (layer number 13) and another from the lower fluvial-typed part (layer number 85). They can be seen on Fig. 6.8. From the log-permeability maps, it can be noticed that even if the upper-layer has a wide range of permeability values, but the variations in each direction are smooth, while for the fluvial type, variations of permeability values are stiff.

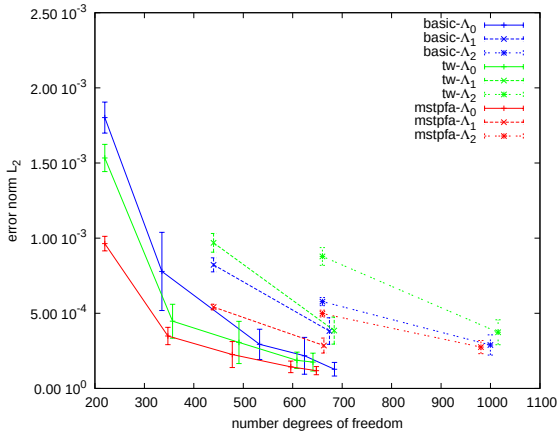

Figure 6.7: Log-normal case: $Norm - L_2$ error in function of the cost in terms of degrees of freedom.

coarse mesh size	10×11
fine mesh size	60×220
domain size	$370m \times 670m$
Δp (bottom to top)	1 Pa

Table 6.3: 10th SPE simulation parameters.

On Fig. 6.8 are also represented black circles that mark coarse faces selected for division after few iterations of *a posteriori* scheme. On the 13th layer, adaptive refinement takes place mainly in the lower bottom where low permeable blocks are present. As it has been observed before (Møyner and Lie, 2016; Wang et al., 2014), the error is focused on this inclusion for all multiscale methods. On the 85th layer, black circles are more widespread along the channels and appear on each coarse faces that neighbor a coarse cell in which either an inclusion of low permeability or a frontier between high and low permeable media is embedded. The fact that there is more black circles on the 13th layer than on the 85th means that in this configuration the error is more homogeneously widespread, while on the 85th layer, the error level is locally high.

Looking at the error plot on Fig. 6.9, readers can notice that, as before, from a complexity point of view, the better accuracy-efficiency trade-off is reached using $\Lambda_0 - mstpfa$ and iterating few times.

On the other hand, it can be seen that the weighting schemes have a moderate effect on Tarbert-typed layer, while on channelized type, they have a critical effect in improving the solution. This can be explained by the fact that, in such a kind of bi-modal distribution, there is no physical ground for equivalent distribution of the flux along a crossing coarse face. Thus, the details of the underlying heterogeneities have to be included.

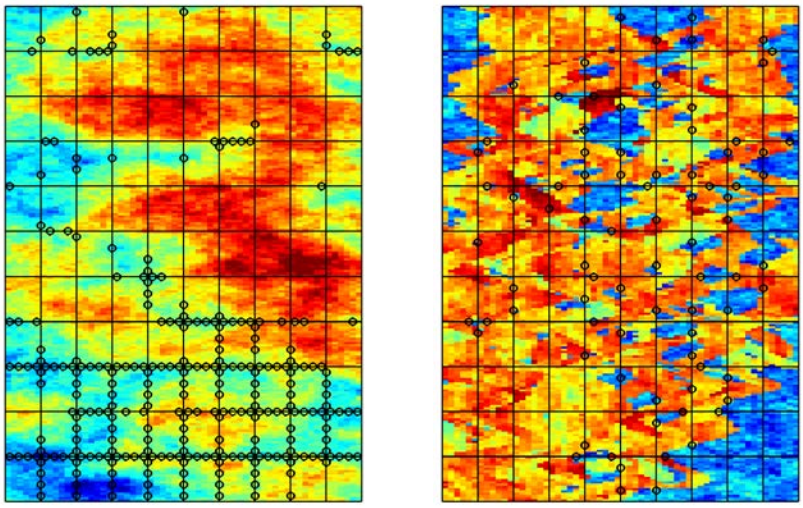

(a) (b)

Figure 6.8: SPE case : log-permeability maps of (a) 13th layer and (b) 85th layer.

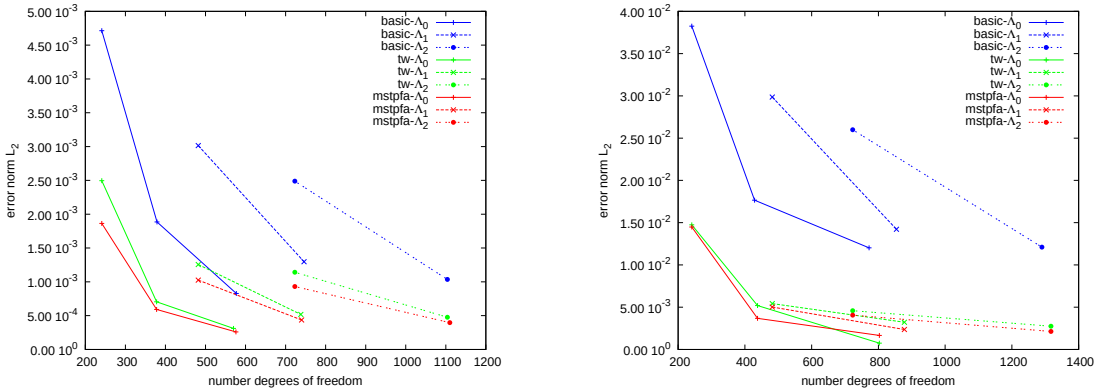

(a) (b)

Figure 6.9: SPE case: $Norm - L_2$ error in function of the cost in terms of degrees of freedom for (a) 13th layer and (b) 85th layer.

The ability to add degree of freedom can also be an interesting asset when considering the extension to the two-phase flow problem. It allows using coarse discretization and the use of local refinement as the saturation front goes through tricky areas. The coarse mesh is then reset to its original discretization once the front is away from the area.

6.3.3 Two-phase flow problems

This *a posteriori* scheme can also be used to treat two phase flow situations at the reservoir scale. This two-phase immiscible incompressible flow system is modeled using total mobility, defined as $\lambda_t(s_w) = \lambda_w(s_w) + \lambda_g(s_w)$. This mobility is used as a weighting prefactor of transmissivity. It reflects that the different phases are competing to go through the medium. A coupled pression-saturation (p_g, S_w) system is then derived using a classical hyperbolic transport equation for modeling water saturation transport phenomenon. It reads:

$$\begin{cases} -\nabla \cdot (K(\mathbf{x})\lambda_t(s_w)\,\nabla p_g) = 0 \\ \epsilon \frac{\partial s_w}{\partial t} + \nabla \cdot (-K(\mathbf{x})\lambda_w(s_w)\,\nabla p_w) = 0 \end{cases} \qquad \forall \mathbf{x} \in \Omega,$$

$$\begin{cases} -K(\mathbf{x})\lambda_t(s_w)\,\nabla p_g = q^w_{inj} \\ s_w = 1.0 \end{cases} \qquad \forall \mathbf{x} \in \partial\Omega_{N,} \tag{6.12}$$

$$p_g = p^{ref} \qquad \forall \mathbf{x} \in \partial\Omega_D$$

These equations are sequentially solved with an implicit formulation for elliptic pressure equation followed by an explicit update of the saturation as in IMPES formulation. The pressure equation is solved on the coarse scale using the multiscale method and the saturation equation is update on the fine scale. For the sake of the simplicity, at every new time step, the original coarse grid is restored. This allows us to avoid dealing with the definition of a merge criterion. A $\Lambda_0 - FV\text{-}MHMM$ formulation is used with the different weighting schemes. A simple log-normal permeability map as reported on Fig. 6.10 is considered. It is $1\,m$ long and $0.1\,m$ large for a 16×4 fine discretization partitioned by a 4×2 coarse mesh. The physical configuration is injection of water (denoted by w hereafter) from the left hand side, which results in the gas (denoted by g) drain towards the right end side. All the physical parameters are reported on Tab. 6.4. Brooks and Corey models(Corey and Brooks, 1975) for water mobilities $\lambda_w(s_w)$ and for gas mobilities $\lambda_g(s_w)$ are also reported as functions of the water saturation s_w. At the outlet face, the reference pressure is set to p^{ref} value.

As before, we report hereafter $norm - L_2$ error variation for all the weighting schemes at the last *a posteriori* iteration w.r.t the time. On the same plot using a left ordinate axis, we

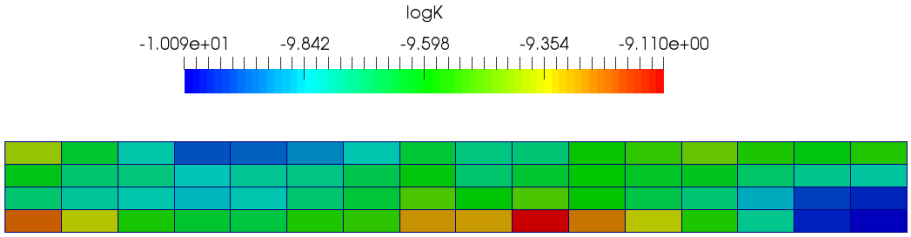

Figure 6.10: Log-permeability map of heterogeneous porous media.

μ_w	$1.0\,10^{-3}\,Pa\,s$
μ_g	$1.76 \cdot 10^{-5}\,Pa\,s$
q^w_{inj}	$10^{-6}\,m \cdot s^{-1}$
p^{ref}	$2.5\,Pa$
$\lambda_w(s_w)$	$\frac{s^2}{\mu_w}$
$\lambda_g(s_w)$	$\frac{(1-s)^2}{\mu_g}$

Table 6.4: Physical parameters for injection scenario.

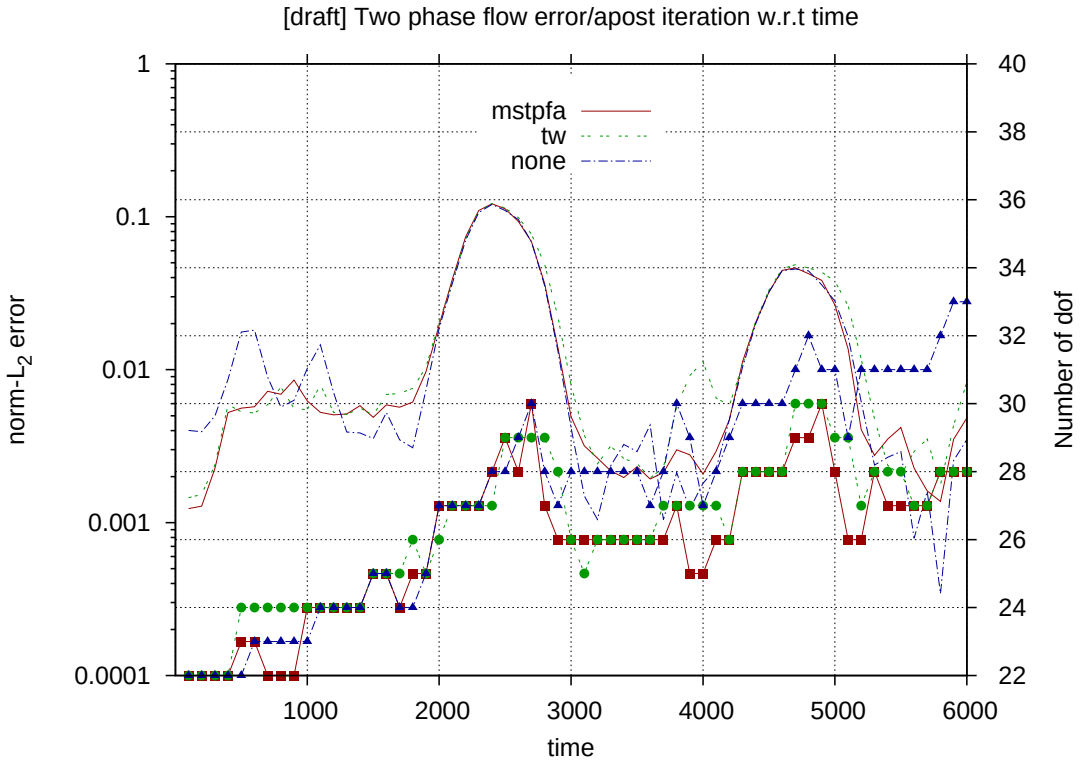

Figure 6.11: Two phase flow: $norm - L_2$ error variation and cost w.r.t time.

report the degrees of freedom used by each schemes noting that the original configuration has 22 degrees of freedom and the maximum allowed is 40 degrees of freedom (as the boundary are not taken into account in the adaptive refinement process). On Fig. 6.11, the reader can notice that around $t = 2500\,s$ and at $t = 4500\,s$, all weighting schemes experience large error levels. That is the time when the front is respectively crossing the first barrier to the flow and then an highly permeable inclusion. It can also be highlighted that an intensive and always increasing use of degrees of freedom addition allows the none weighted formulation to be more accurate than the weighted ones. However, as previously stated, the *mstpfa* weighted formulation appears to be the best efficiency-accuracy trade. Indeed, it reaches the lower error level with the fewer degrees of freedom.

Conclusion

In this chapter, an *a posteriori* mechanism for FV-MHMM is introduced and illustrated to drive coarse face refinement. It is tested along with two weighting schemes (*tw* and *mstpfa*) on academic and more realistic heterogeneous porous media. It is shown that, eventhough these weighting schemes introduce some overhead costs as preprocessing step, they also

greatly improve the accuracy when dealing with highly heterogeneous porous medium with long correlated feature as it is the case for channelized medium.

Combined with these weighting schemes, an *a posteriori* mechanism , which selects a set of coarse faces for splitting based on a threshold criteria, is designed. Its efficiency and its correlation with $norm - L_1$ error level are shown on simple example. Then it is used on more complex heterogeneous permeability fields. An analysis of cost versus error reduction indicates that the best configuration is a *mstpfa*-Λ_0 as Lagrange multiplier space and few iterations of the *a posteriori* mechanism to insert degrees of freedom where it lacks information. This numerical recipe is then extended to a two phase flow model where it allows using coarser discretization and locally refine where the saturation front is. The best compromise for efficiency-accuracy is found to be the *mstpfa*-Λ_0 combination, which keeps the degree of freedom addition moderate.

References

Arbogast, T.: 2002, Implementation of a locally conservative numerical subgrid upscaling scheme for two-phase darcy flow, *Computational Geosciences* .

Christie, M., Blunt, M. et al.: 2001, Tenth spe comparative solution project: A comparison of upscaling techniques, *SPE Reservoir Simulation Symposium*, Society of Petroleum Engineers.

Corey, A. and Brooks, R.: 1975, Drainage characteristics of soils, *Soil Science Society of America Journal* **39**(2), 251–255.

Efendiev, Y., Galvis, J. and Hou, T. Y.: 2013, Generalized multiscale finite element methods (gmsfem), *Journal of Computational Physics* .

Franc, J., Jeannin, L., Debenest, G. and Masson, R.: 2016, Fv-mhmm methods for reservoir modeling, *Computational Geosciences* .

Hajibeygi, H., Bonfigli, G., Hesse, M. A. and Jenny, P.: 2008b, Iterative multiscale finite-volume method, *Journal of Computational Physics* .

Harder, C., Paredes, D. and Valentin, F.: 2013, A family of multiscale hybrid-mixed finite element methods for the darcy equation with rough coefficients, *Journal of Computational Physics* .

Harder, C., Paredes, D. and Valentin, F.: 2015, On a multiscale hybrid-mixed method for advective-reactive dominated problems with heterogeneous coefficients, *Multiscale Modeling & Simulation* .

Hou, T. Y. and Wu, X.-H.: 1997, A multiscale finite element method for elliptic problems in composite materials and porous media, *Journal of computational physics* .

Jenny, P., Lee, S. and Tchelepi, H.: 2003b, Multi-scale finite-volume method for elliptic problems in subsurface flow simulation, *Journal of Computational Physics* .

Lunati, I. and Lee, S. H.: 2009, An operator formulation of the multiscale finite-volume method with correction function, *Multiscale modeling & simulation* .

Møyner, O. and Lie, K.-A.: 2014, A multiscale two-point flux-approximation method, *Journal of Computational Physics* .

Møyner, O. and Lie, K.-A.: 2016, A multiscale restriction-smoothed basis method for high contrast porous media represented on unstructured grids, *Journal of Computational Physics* .

Raviart, P.-A. and Thomas, J.: 1977a, Primal hybrid finite element methods for 2nd order elliptic equations, *Mathematics of computation* **31**(138), 391–413.

Raviart, P. and Thomas, J.: 1977b, A mixed finite element method for 2-nd order elliptic problems, *Mathematical aspects of finite element methods* pp. 292–315.

Vaněk, P., Mandel, J. and Brezina, M.: 1996, Algebraic multigrid by smoothed aggregation for second and fourth order elliptic problems, *Computing* .

Wang, Y., Hajibeygi, H. and Tchelepi, H. A.: 2014, Algebraic multiscale solver for flow in heterogeneous porous media, *Journal of Computational Physics* .

Conclusion

In this thesis, the theoretical basis and development of a new type of multiscale method, Finite Volume - Multiscale Hybrid Mixed Method (*FV-MHMM*), for reservoir modeling is described. Nonetheless, the first step when aiming to apply *upscaling* techniques to two-phase flows is to get acquainted with the previous works on single phase flow. The first studies on how to upscale a heterogeneous permeability background led to defined simple bounds to an effective permeability. Then, the homogenization theory and its derivatives achieved to derive homogenized permeabilities under a set of restricting assumptions (periodicity, definition of a representative elementary volume, flow regime). They linked the large scale derived problem to fine scale data thanks to a closure problem. Though these frameworks tend to highlight other dependencies that are not included in usual large scale modeling, the first steps towards an usable *upscaled* permeability was made.

However, extending to two-phase flow brings out new questions. Indeed, the equations are much more complex because they exhibit non linear coupling between pressure and saturation unknowns. Then, there is two views of upscaling: the numerical upscaling and the physical upscaling. The physical upscaling is performed using the same method as the single phase upscaling. It gives a rise to new coupling terms that are not present in the original fine scale system. The reservoir engineers have still grown interest in applicable block upscaling. In developing renormalization techniques and pseudo functions, they constructed sets of ready-to-use techniques which are able to reproduce averaged behavior of the fine scale phenomenon. They also initiated the transposition of these techniques to two-phase flow, while considering several saturation distributions as several single phase problem with the fine scale intrinsic permeability tweaked by the relative permeabilities. This mechanism allows constructing pseudo two-phase flow properties at large scale, which are nevertheless dependent on the flow regime and on the injection scenario considered. As it comes clear that some areas will never satisfy the conditions necessary to apply these methods, the idea of dynamic mesh adaptation emerged. The *upscalable* areas are computing their upscaled properties using localized flow simulation while active areas are treated at the fine scale. This idea is the starting point of the multiscale method in the porous media community. As

such local simulations can provide block upscaled properties, why not keeping the fine scale we aim to upscale from, and partition it with a coarse discretization ? Why not make them continuously communicate to model dynamic behavior ?

A starting work is to develop Darcy scale (also referred to as fine scale) which will be used as a reference solution when assessing the accuracy of the multiscale methods results. This is done developing an open-source toolbox dedicated to multiphase flow in porous medium using the OpenFOAM. *impesFoam* includes the main Brooks and Corey model and Van Genuchten model for modeling the relative permeabilities and capillary pressure. An IMplicit Pressure Explicit Saturation (IMPES) scheme is chosen to sequentially couple saturation and pressure. IMPES is often opposed to Full Implicit Methods (FIM). The explicit treatments of the saturation allows indeed to lower the size of the system to invert and lead to faster time iterations. Nonetheless, such a weak sequential coupling in a non-linear two-phase flow is constrained by a small time-step to ensure stability of the simulation. A *CFL* condition has thus to be studied, in order to perform stable simulations but not constrained by an overly small time step . *impesFoam* implements also a power low bounded mechanism to dynamically adapt its time-step, inherited from OpenFOAM. The study of the CFL condition for the IMPES algorithm select three criteria for a comparative study : the classical Courant number, the Coats and the Todd number. The benchmark is done considering both the stability and the performance while the time step size is changing dynamically. While the Coats number ensures stability whatever the physics provided that the upper limit is lowered when including capillary and gravity effects, Todd's number is found to be an interesting alternative when capillary phenomenon is dominant.

The core study of the thesis is the development of a Finite Volume Multiscale algorithm based on the works of *Harder et al.* . These type of method uses a fine grid (here discretized at the geological scale) on which a coarse grid (discretized at the reservoir scale) is superimposed. This mixed hybrid formulation shares the idea from *Raviart and Thomas* to ensure continuity between coarse cells thanks to Lagrange multipliers. These multipliers can also be regarded as coarse fluxes through the coarse faces. The multiscale nature leads to subgrid these coarse cells by partitioning the fine grid by the coarse grid, to solve local problems on it and to get basis functions. The final step is the assembly of a global coarse scale matrix that is inverted to find Lagrange multipliers value and hence reconstruct an approximation of the fine scale pressure. It can be noted that these local problems, which include details of the heterogeneities into their solution, are independent from each other. It can then be concurrently implemented. *FV-MHMM* offers also an other degree of refinement in considering polynomial function space to find the Lagrange multipliers unknowns. Consequently, unlike common finite volume implementation, it allows

increasing the accuracy by increasing the polynomial order of this function space. The first tests on channelized medium highlighted that if the heterogeneous features have long extent with respect to the coarse cell size, it is necessary to tune the above mentioned polynomial function space for Lagrange multipliers. The *transmissivity weighting* scheme is then proposed. It weights locally the polynomial test function by the local value of transmissivity. This operation results in an increased accuracy, as it favors the flow in area that are highly permeable and hinder it in impermeable area.

The *FV-MHMM* is then compared with the most widely used finite volume multiscale methods, *MsFv* and *MsRSB*. The focus on each type of faciès in the 10th SPE case, log-normally distributed and channelized, reveals that it achieves similar accuracy level to the common methods with few iterations. On the most difficult channelized layers, it provides slightly less accurate solutions than *MsRSB*, which benefits from its smoothing and overlapping structure. On such layers, the preprocessing step of adaptation of the polynomial space for Lagrange multipliers allows us to greatly improves the accuracy. As a second case, a statistical analysis is performed on a slanted permeability background, which exhibits tilted and heterogeneous stripes of heterogeneous values. Eventhough the *FV-MHMM* benefits from weighting schemes and the increase in polynomial order, the fact that these permeability features are not aligned with the Cartesian mesh makes it troublesome. A weighting scheme, which can input information about local flow, is then required. It is named the *multiscale two-point flux approximation* scheme (mstpfa). It consists in a local (and fine-scale) cross flow simulation around each coarse internal faces, which takes the two neighboring coarse cells as the support. It allows us to evaluate locally the fluxes across the coarse face and build a weighting scheme from it.

The last study develops an *a posteriori* estimator to drive local coarse face adaptation. This estimator constructs a measure of the jump across the coarse face that results from the weakly enforcement of inter cells continuity. Its correlation with the norm-L_1 error when comparing the multiscale solution with the fine grid solution is investigated. Once knowing that it selects coarse faces where the error is maximal, a threshold value is set with respect to its initial value. New degrees of freedom are subsequently iteratively added on the selected set of coarse faces. As this kind of mechanism still allows the use of weighting schemes, its performance is reported with and without it. It appears after some tests on the 10th SPE layers, that the weighting schemes spare some degrees of freedom additions. The efficiency-accuracy optimal is often to use the piecewise constant polynomial space with the weighting scheme *mstpfa* ($\Lambda_0 - mstpfa$) , which already captures main flow feature while increasing polynomial order provides us with a small gain.

Further development The extension to the two-phase flow has already been initiated. It consists in an extension of the algorithm described before. As initially done for the *MsFv*, the saturation and pressure unknowns are sequentially coupled through an IMPES-like algorithm, in which the hyperbolic saturation/transport equation is updated on the fine mesh. In order to gain efficiency, a threshold factor is set to trigger the update of the basis functions in the coarse cells whether they are active or not. They should reduce significantly the work load in the case of stable front . An interesting point is that, as stressed describing the algorithm, the solution is both locally and globally conservative. It can then be noted that the Lagrangian multipliers directly provides the divergence-free fluxes at the coarse cell interfaces. The addition of other physical phenomenon such as gravity or capillary terms can be included using the source basis functions.

An other possible improvement of the algorithm is to implement a cost-control degrees of freedom additions in the *a posteriori* driven algorithm. It is a direct result from the efficiency-accuracy analysis. As the *a posteriori* algorithm is now designed, it tends to add most of its new degrees of freedom on the first iterations. This is a typical bottleneck scenario when considering memory and CPU usage. If we managed to control the number of additions, we can produce a better workload balanced algorithm. Further developments can even investigate, as in adaptive mesh refinement, a threshold criteria that triggers the coarse face merger to spare some degrees of freedom.

Lastly, the natural further development will be to make a reformulation of this algorithm as a preconditioner to a fine scale system, as it has been done for *MsFv* and *MsRSB.* Their multiscale structure makes them suitable for being adapted as a preconditioner to a fine grid solver, such as a GMRES solver. It is indeed a formulation that is easy to integrate in any industrial or widely deployed finite volume solver.

Conclusion

Au cours de cette thèse, les bases théoriques d'une nouvelle méthode multiéchelle pour l'étude des écoulements en réservoir, à savoir la méthode mixte hybride multiéchelle en volumes finis (*FV-MHMM*), ont été proposées. Cependant, la première étape, dès lors qu'on s'intéresse au changement d'échelle pour les systèmes diphasiques, est de porter son attention sur les travaux antérieurs. Les premières études sur le changement d'échelle en milieu saturé, dans le cas d'un milieu où le champ de perméabilité est hétérogène, ont essayé de définir des estimateurs simples tels que des bornes pour déterminer une perméabilité équivalente. Après cela, l'homogénéisation et ses théories dérivées ont réussi à définir des perméabilités homogénéisées dans le cadre restreint de certaines hypothèses (périodicité, définition d'un volume représentatif élémentaire, régime d'écoulement). Elles procèdent en reliant les grandeurs à la grande échelle aux variations à la petite échelle au moyen d'un problème de fermeture. Bien que ces études tendent à démontrer que la dépendance des lois à la grande échelle nécessite des équations plus complexes que celles suggérées par le mimétisme formel des lois à la petite échelle, le premier pas vers une perméabilité *upscalée* était fait.

Cependant, les problèmes liés à l'upscaling multiphasique adressent de nouvelles questions . Le système d'équations est bien plus complexe car il présente un couplage entre pression et saturation avec des paramètres de transport non linéaires. Dès lors, deux perspectives d'étude étaient possibles : l'upscaling numérique ou l'upscaling physique. L'upscaling physique est réalisé par les mêmes méthodes qu'en monophasique, et font apparaître des termes supplémentaires suggérant des couplages supplémentaires qui ne s'expliquent pas par la simple transposition des équations d'une échelle à l'autre. Les ingénieurs réservoirs ont tout de même développé un intérêt pour un changement d'échelle par blocs, plus utilisable. Par le développement de la renormalisation et des techniques de pseudo-fonctions, ils ont construit un ensemble de méthodes prêtes à l'emploi pour une utilisation en ingénierie, qui sont capables de reproduire les comportements moyens homogénéisés, des phénomènes à la petite échelle. Ils ont également initié la transposition de ces méthodes aux systèmes diphasiques, en considérant différentes distributions de saturation comme autant de problèmes saturés

avec une perméabilité intrinsèque hétérogène modulée par les perméabilités relatives. Ce procédé permet alors la construction de pseudo propriétés diphasiques à la grande échelle, qui sont néanmoins dépendantes des conditions de simulation dans lesquelles elles ont été obtenues (régime d'écoulement, débits injection/production). Comme il est clair que certaines zones ne pourront jamais satisfaire aux conditions établies par ces méthodes, l'idée d'adapter dynamiquement le maillage est apparue. Les valeurs équivalentes sont calculées sur les régions où *l'upscaling* est possible à l'aide de simulations locales à la petite échelle tandis que les régions *actives* sont traitées avec la discrétisation fine. Cette idée est aussi le point de départ des méthodes multiéchelles dans la communauté milieux poreux. Comme ces simulations locales réussissent à fournir des propriétés à la grande échelle, pourquoi ne pas garder l'échelle fine de laquelle on veut partir et découper en blocs notre domaine ? Pourquoi ne pas faire communiquer, via ces blocs, nos deux échelles ?

La première étape a été le développement d'un outil à l'échelle de Darcy (aussi appelé échelle fine ici) qui sera utilisé en tant que solution de référence quand il faudra juger de la qualité des solutions obtenues par les méthodes multiéchelles. Ces développements ont amené à la création d'une suite de programmes libres dédiés à l'étude des milieux poreux *impesFoam* en utilisant la plateforme libre de développement OpenFOAM. *impesFoam* inclut les principaux modèles *Brooks et Corey* et *Van Genuchten* pour ce qui est de modéliser les perméabilités relatives et pression capillaire. Un couplage de type *IMplicit Pressure Explicit Saturation (IMPES)* est choisi pour lier les variations de saturation à celles de la pression. L'IMPES est souvent opposé aux méthodes complètement implicites telles que le *Full Implicit Model (FIM)*. Le traitement explicite des saturations permet une économie tant sur l'utilisation mémoire que sur le temps d'inversion du système linéaire en pression. Ceci permet d'être normalement plus efficace sur la résolution d'un système linéaire moins important. Néanmoins, un tel couplage faible et séquentiel, associé à un modèle diphasique non-linéaire est nécessairement contraint par un pas de temps de taille réduite pour assurer la stabilité de la simulation. Une condition CFL a été étudiée dans l'optique de réussir à mener des simulations avec un pas de temps suffisamment petit pour garantir la stabilité mais pas inutilement petit. L'*impesFoam* dispose également une loi de changement dynamique du pas de temps basé sur une loi en puissance et hérité de l'implémentation classique d'OpenFOAM. On sélectionne alors trois critères de stabilité pour une étude comparative : le nombre de Courant classique, le nombre de Coats et le nombre de Todd. Une comparaison est alors menée en terme de stabilité et d'efficacité numérique tout en ajustant continuellement les pas de temps. On constate que le nombre de Coats assure la stabilité quelque soit la physique du problème, mais le nombre de Todd offre une alternative adaptée lorsque la capillarité est dominante.

Le coeur de ces travaux concerne le développement d'une méthode multiéchelle en formulation volumes finis basé sur les travaux de *Harder et al.* Cette classe de méthode fait coexister deux discrétisations : l'une à l'échelle fine (ou géologique dans notre cas), l'autre à l'échelle grossière (celle du réservoir). Cette forme mixte hybride repose sur la même idée que les travaux de *Raviart et Thomas* pour assurer la continuité entre les blocs grossiers à l'aide de multiplicateurs de Lagrange. Ces multiplicateurs peuvent aussi être interprétés comme des flux grossiers à travers les faces du maillage grossier. La nature multiéchelle implique de sous-mailler ces cellules grossières en partitionnant le maillage fin à l'aide du maillage grossier, de résoudre sur celles-ci des problèmes locaux pour en tirer des fonctions de bases. L'étape finale consiste à assembler une matrice globale à la grande échelle qui devra être inversée pour trouver la valeur des multiplicateurs de Lagrange. Cela permet de construire une pression approximée par la méthode multiéchelle, à l'échelle fine. On peut noter que ces problèmes locaux, qui incluent plus de détails des hétérogénéités dans leur solution, sont indépendants les uns des autres. Ils peuvent donc être implémentés pour être résolus de façon parallèle. La méthode *FV-MHMM* offre aussi un autre degré de raffinement en considérant un espace de fonctions polynomiales pour ces multiplicateurs. Ainsi, contrairement aux méthodes volumes finis classiques, une nouvelle façon d'améliorer la précision du résultat est d'augmenter le degré du polynôme choisi pour l'approximation des multiplicateurs. Les premiers tests sont menés sur des milieux chenalisés, soulignant que si les structures hétérogènes sont d'étendue longue par rapport à la taille caractéristique d'un bloc grossier, il est alors nécessaire d'adapter l'espace polynomial de fonctions pour les multiplicateurs de Lagrange. Le *schéma de pondération en transmissivité* est donc proposé. Il repose sur la pondération locale des fonctions tests polynomiales par la valeur de la transmissivité. Ce processus permet d'atteindre une précision supérieure car il favorise l'écoulement dans les zones très perméables et l'empêche dans les zones peu perméables.

La *FV-MHMM* est ensuite comparée avec les méthodes multiéchelles volumes finis couramment employées dans l'ingénierie réservoir, à savoir les méthodes *MsFv* et *MsRSB.* L'attention est portée sur chacun des types de faciès du cas SPE 10, à savoir des coupes de perméabilités hétérogènes distribuées de façon log-normale et des coupes chenalisées. L'étude révèle alors que la *FV-MHMM* atteint les mêmes niveaux de précision que les méthodes classiques. Sur les cas complexes chenalisés, elle fournit une solution un peu moins précise que celle fournie par la méthode *MsRSB,* qui elle bénéficie de son mécanisme de lissage et de sa construction par recouvrement. Sur de tels champs, l'étape de préprocessing que constitue l'adaptation de l'espace des fonctions polynomiales pour les multiplicateurs de Lagrange (schéma de pondération) permet d'améliorer la précision de façon notable. Afin de comparer sur un autre type de champs, on a choisi de réaliser une étude sur 10

réalisations statistiquement équivalentes de champ de perméabilité où une succession de bandes alternativement perméables et imperméables sont inclinées par rapport aux mailles cartésiennes. Malgré la pondération et les polynômes d'ordre élevé, la méthode *FV-MHMM* a des difficultés à obtenir une bonne précision en raison de l'inclinaison des structures. Un schéma de pondération qui pourrait retranscrire ces informations à propos des écoulements locaux sera nécessaire. On le nomme le *schéma d'approximation à deux point multiéchelle* (mstpfa). Il consiste en une simulation locale (à l'échelle fine) d'un flux imposé selon l'axe de la normale à une face grossière sélectionnée. Le domaine utilisé est celui formé par ces deux cellules grossières adjacentes à la face. Cela permet l'évaluation locale des flux à travers la face et la construction d'un schéma de pondération.

Enfin, une étude relative au mécanisme de raffinement automatique des faces grossières dirigé par un estimateur *a posteriori* est réalisée. L'estimateur permet de mesurer le saut en pression aux faces grossières du à l'imposition faible de la contrainte de continuité. Sa corrélation avec l'erreur en norme L_1, quand on compare la pression obtenue par la résolution du système fin et la pression approximée par la méthode multiéchelle, est vérifiée. Une fois établi que les faces grossières sont sélectionnées en cohérence avec l'erreur en norme L_1, une valeur seuil est fixée lors de la première évaluation du saut. De nouveaux degrés de liberté sont alors ajoutés en subdivisant les faces grossières dont la valeur de l'estimateur est supérieure au seuil fixé. Comme ce type de démarche n'est pas incompatible avec l'utilisation des schémas de pondération, les deux sont utilisés conjointement pour étudier leur performance. Il ressort après des tests sur les coupes SPE 10 que les schémas de pondération permettent l'économie de certains degrés de liberté. Le couple schéma de pondération-méthode *a posteriori* qui est le plus optimal, si l'on considère le critère 'coût en nombre de degrés de liberté - précision', est le choix de polynômes constants par morceaux pondérés par un schéma de pondération *mstpfa* ($\Lambda_0 - mstfa$) auquel on applique quelques itérations de la méthode *a posteriori.* L'augmentation de l'ordre du polynôme permet de capturer plus de détail de l'écoulement fin mais se révèle coûteuse.

Développements futurs

La transposition au modèle diphasique a déjà été entreprise. Elle consiste en une extension de l'algorithme précédemment décrit. Comme fait avant dans le cas de la *MsFv,* les inconnues de saturation et de pression sont couplées séquentiellement au moyen d'un algorithme de type *IMPES*, dans lequel l'équation hyperbolique de transport/saturation est mise à jour sur le maillage fin. Pour gagner en efficacité, un mécanisme de seuil est utilisé pour déclencher la mise à jour des fonctions de bases par cellules grossières, selon qu'elles soient actives ou non. Cela réduit considérablement la charge de travail dans le cas de front stable. Un autre point

d'intérêt, comme souligné dans la description de la méthode multiéchelle, est que celle-ci est à la fois conservative localement et globalement. Il apparaît alors que les multiplicateurs de Lagrange fournissent directement les flux conservatifs au travers des faces grossières. L'ajout d'autres phénomènes physiques tels que la gravité ou encore la pression capillaire peut donc être fait en utilisant les fonctions de bases sources.

Un autre point sur lequel il convient d'avancer est le développement d'un raffinement adaptatif à coût contrôlé. Il sera basé sur l'estimateur *a posteriori* proposé. Dans son développement actuel, l'estimateur décide un ajout massif de degrés de liberté sur sa première itération. Ceci peut être identifié comme un scénario de goulot d'étranglement en termes de ressources numériques (CPU, mémoire). Si nous parvenons à contrôler le nombre de degrés de liberté ajoutés, nous produirons une méthode adaptative plus équilibrée en charge de travail. Des travaux ultérieurs pourront porter, comme dans le cas de méthodes à maillage adaptatif, sur la détermination d'un critère commandant la fusion de degré de liberté.

Enfin, le développement naturel lié aux méthodes multiéchelles est la reformulation de l'algorithme en tant que préconditionneur à un système fin résolu par exemple par un solveur GMRES. Cette formulation permettrait en effet une intégration plus simple aux solveurs volumes finis industriels efficaces qui travaillent à l'échelle fine (ou géologique ici).

Title: Two-Phase flow properties upscaling in heterogeneous porous media

Abstract:

The groundwater specialists and the reservoir engineers share the same interest in simulating multiphase flow in soil with heterogeneous intrinsic properties. They also both face the challenge of going from a well-modeled micrometer scale to the reservoir scale with a controlled loss of information. This *upscaling* process is indeed worthy to make simulation over an entire reservoir manageable a stochastically repeatable.

Two *upscaling* steps can be defined: one from the micrometer scale to the *Darcy* scale, and, another from the *Darcy* scale to the reservoir scale. In this thesis, a new second upscaling multiscale algorithm *Finite Volume Mixed Hybrid Multiscale Methods (Fv-MHMM)* is investigated. Extension to a two-phase flow system is done by weakly sequentially coupling saturation and pressure via IMPES-like method.

Keywords: Upscaling - Multiscale method - Two Phase Flow - IMPES - Heterogeneous porous media

Auteur : FRANC Jacques

Titre : Mise à l'échelle des propriétés polyphasiques d'écoulement en milieux poreux hétérogènes

Directeur de thèse : Pr. DEBENEST Gérald

Lieu et Date de la soutenance : IMFT, Allée du Pr. Camille Soula, 31400 Toulouse; le 18/01/2018

RESUME en français :

L'étude des écoulements souterrains et l'ingénierie réservoir partagent le même intérêt pour la simulation d'écoulement multiphasique dans des sols aux propriétés intrinsèquement hétérogènes. Elles rencontrent également les mêmes défis pour construire un modèle à l'échelle réservoir en partant de données micrométriques tout en contrôlant la perte d'informations. Ce procédé d'*upscaling* est utile pour rendre les simulations faisables et répétables dans un cadre stochastique.

Deux processus de mise à l'échelle sont définis : l'un depuis l'échelle micrométrique jusqu'à l'échelle de *Darcy,* et, un autre depuis l'échelle de *Darcy* vers l'échelle du réservoir. Dans cette thèse, un nouvel algorithme traitant du second *upscaling Finite Volume Mixed Hybrid Multiscale Method (FV-MHMM)* est étudié. L'extension au diphasique est faite au moyen d'un couplage séquentiel faible entre saturation et pression grâce à une méthode de type IMPES.

Mots-clés : Mise à l'échelle - Méthodes multiéchelles - Diphasique - IMPES - Milieux poreux hétérogènes

---

Discipline Administrative : Surfaces et interfaces continentales, Hydrologie

---

Intitulé et Adresse de l'U.F.R. ou du laboratoire : UMR-5502 IMFT - Institut de Mécanique des Fluides de Toulouse